

Innovative Nanoparticles for the Photodynamic Therapy of Lung Cancer

Zoë Rachael Goddard

School of Pharmacy
University of East Anglia
May 2020

Thesis submitted in partial fulfilment of the requirements for the degree of
Doctor of Philosophy of the University of East Anglia.

© This copy of the thesis has been supplied on condition that anyone who consults it is understood to recognise that its copyright rests with the author and that use of any information derived therefrom must be in accordance with current UK Copyright Law. In addition, any quotation or extract must include full attribution.

Declaration

This thesis has been submitted to the University of East Anglia for the degree of Doctor of Philosophy and is, to the best of my knowledge, original except where stated, referenced and acknowledged.

Zoë Goddard

Abstract

Photodynamic therapy (PDT) involves the use of a photosensitiser drug which, when activated by visible light, causes the formation of cytotoxic singlet oxygen and subsequent cell death. Photosensitisers are hydrophobic and notoriously hard to deliver intravenously, but their attachment to gold nanoparticles has been found to overcome this issue. These nanoparticles can also be functionalised with directing ligands which can actively target the photosensitisers to lung cancers.

Herein, we investigate three classes of targeting moieties for the delivery of gold nanoparticles (AuNPs) functionalised with a zinc phthalocyanine photosensitiser (C11Pc) and polyethylene glycol (PEG) to lung cancers: peptides, antibodies and small molecules.

Two epidermal growth factor receptor (EGFR) targeting peptides were investigated as targeting moieties, with the composition of the peptide, coupling agents and solvent systems found to effect the singlet oxygen production and phototoxicity of the resulting nanoparticles. Excitingly, targeted phototoxicity was observed in EGFR overexpressing cell lines for one of these constructs, with 7% cell viability observed at 200 nM.

An investigation into the most efficient conjugation strategies for the addition of either an anti-EGFR or anti-HER2 antibody to C11Pc-PEG-AuNPs led to the exploration of both random chemical and protein based site-specific antibody conjugation. While no phototoxicity was observed, this led to the exploration of Fc binding peptides for site-specific antibody conjugation to gold nanoparticles.

Folic acid was investigated for the delivery of C11Pc-PEG-AuNPs to folate receptor alpha expressing lung cancers. Folic acid is a known quencher of singlet oxygen so steps towards a protease cleavable sequence were undertaken to allow for the cleavage of this directing ligand intracellularly, allowing for the switch on of the photodynamic activity in lung cancer cells.

Access Condition and Agreement

Each deposit in UEA Digital Repository is protected by copyright and other intellectual property rights, and duplication or sale of all or part of any of the Data Collections is not permitted, except that material may be duplicated by you for your research use or for educational purposes in electronic or print form. You must obtain permission from the copyright holder, usually the author, for any other use. Exceptions only apply where a deposit may be explicitly provided under a stated licence, such as a Creative Commons licence or Open Government licence.

Electronic or print copies may not be offered, whether for sale or otherwise to anyone, unless explicitly stated under a Creative Commons or Open Government license. Unauthorised reproduction, editing or reformatting for resale purposes is explicitly prohibited (except where approved by the copyright holder themselves) and UEA reserves the right to take immediate 'take down' action on behalf of the copyright and/or rights holder if this Access condition of the UEA Digital Repository is breached. Any material in this database has been supplied on the understanding that it is copyright material and that no quotation from the material may be published without proper acknowledgement.

Contents

Declaration	ii
Abstract	iii
Contents	iv
Abbreviations	x
Acknowledgements	xii
Chapter One Introduction	1
1.1 Photodynamic therapy	2
1.1.1 Photosensitisers for PDT	3
1.1.2 Non-small cell lung cancer and PDT	7
1.2 Nanomedicine and cancer therapeutics	9
1.3 Gold nanoparticles as drug carriers	10
1.4 Active targeting of gold nanoparticles for cancer therapeutics	12
1.4.1 Antibody directed gold nanoparticles	12
1.4.1.1 IgG antibodies	12
1.4.1.2 Antibody fragments and nanobodies	17
1.4.2 Protein directed gold nanoparticles	18
1.4.3 Peptide directed gold nanoparticles	20
1.4.4 Aptamer directed gold nanoparticles	24
1.4.5 Carbohydrate directed gold nanoparticles	27
1.4.6 Small molecule directed gold nanoparticles	29
1.4.7 Gold nanoparticles with multiple targeting modalities	33
1.5 Conclusion and future outlook	34
1.6 Thesis outline	38
1.7 References	39
Chapter Two Design, Synthesis and Biological Evaluation of Peptide Directed Phthalocyanine-Gold Nanocarriers	52
2.1 Introduction	53
2.1.1 The overexpression of receptors in cancer	53
2.1.2 The epidermal growth factor receptor	53
2.1.3 Targeting the EGFR	54

2.1.4	Peptides as targeting agents.....	57
2.1.5	Peptides for targeting the EGFR.....	59
2.2	Summary and chapter aims	61
2.3	Results and discussion.....	62
2.3.1	Peptide selection and synthesis.....	62
2.3.2	Determination of receptor presence on cell lines.....	68
2.3.3	Confirmation of peptide binding	70
2.3.4	Cell viability assays	71
2.3.5	Synthesis of a scrambled peptide to confirm targeting effect of AEYLRK	72
2.3.6	Nanoparticle synthesis and characterisation.....	73
2.3.6.1	Synthesis of peptide directed phthalocyanine-gold nanoparticles	73
2.3.6.2	Synthesis of control nanoparticles	77
2.3.6.3	Singlet oxygen production	81
2.3.6.4	Solvent variation.....	83
2.3.6.5	Coupling agent investigation	87
2.3.7	Phototoxicity of AuNPs.....	91
2.3.7.1	Phototoxicity of peptide-conjugated C11Pc-PEG-AuNPs	91
2.3.7.2	Phototoxicity of control AuNPs.....	93
2.3.8	Nanoparticle binding by fluorescent microscopy.....	94
2.4	Conclusion and future work	95
2.5	References.....	97

Chapter Three Investigations into Antibody Conjugation for the Development of Antibody Directed Phthalocyanine-Gold Nanocarriers 107

3.1	Introduction.....	108
3.1.1	Antibodies	108
3.1.2	Non-covalent antibody conjugation.....	109
3.1.3	Covalent antibody conjugation.....	110
3.1.3.1	Conjugation through amines	111
3.1.3.2	Conjugation through thiols.....	113
3.1.3.3	Conjugation through cross-linkers	115
3.1.3.4	Conjugation through click chemistry	117
3.1.4	Protein-based antibody conjugation.....	119
3.1.4.1	Biotin-(strept)avidin for bioconjugation.....	120
3.1.4.2	Fc binding proteins for bioconjugation	121

3.2	Summary and chapter aims	122
3.3	Results and discussion.....	124
3.3.1	Functionalisation of C11Pc-PEG-AuNPs with anti-EGFR antibodies. 124	
3.3.1.1	Antibody functionalisation through EDC/NHS chemistry	125
3.3.1.2	Antibody functionalisation through maleimide chemistry.....	129
3.3.2	Determination of antibody functionalisation.....	131
3.3.3	Antibody binding to EGFR receptors.....	133
3.3.4	Analysis of the singlet oxygen production of the anti-EGFR antibody conjugates.....	134
3.3.5	Phototoxicity of antibody conjugated C11Pc-PEG-AuNPs.....	135
3.3.6	Determination of antibody binding post conjugation	136
3.3.7	Site-Specific antibody conjugation – using the Fc region	137
3.3.7.1	Protein G for site specific antibody conjugation.....	137
3.3.7.2	Peptide mimics of protein A/G – Fc-III	141
3.4	Conclusions and future work.....	144
3.5	References.....	147

Chapter Four Towards Protease Cleavable Sequences to ‘Turn on’ the Photodynamic Activity of Folate Directed Phthalocyanine-Gold Nanocarriers 154

4.1	Introduction.....	155
4.1.1	Small molecules as targeting agents	155
4.1.2	Folic acid and its uptake in the human body.....	155
4.1.3	The significance of folic acid in NSCLC	156
4.1.4	Folic acid as a targeting agent.....	157
4.1.4.1	Folic acid conjugated small molecule therapies	158
4.1.4.2	Folic acid and PDT.....	160
4.1.4.3	Cleavable folate therapies.....	162
4.1.5	Proteases and their significance in cancer.....	163
4.1.6	Cathepsin B substrates and cleavable therapies	164
4.2	Summary and chapter aims	166
4.3	Results and discussion.....	167
4.3.1	Folic acid conjugation.....	167
4.3.2	Synthesis of folate ligand 2-aminoethylfolic acid.....	171
4.3.3	Determination of the presence of FR α and cytotoxicity of 4.6.....	175
4.3.4	Functionalisation of C11Pc-PEG-AuNPs with 2-aminoethylfolic acid. 177	
4.3.5	Singlet oxygen production	178

4.3.6	Towards a cathepsin B cleavable linker	179
4.3.6.1	Development of an amine cross-linker for the solid phase	179
4.3.6.2	Employment of 4.36 to synthesise a cathepsin B cleavable folate linker	182
4.4	Conclusions and future work.....	187
4.5	References.....	189
Chapter Five Experimental		198
5.1	General procedures	199
5.1.1	Materials and solvents.....	199
5.1.2	Instrumental techniques	199
5.1.3	Solid phase peptide synthesis.....	201
5.1.4	Cell culture, passage and count	201
5.1.5	Flow cytometry.....	202
5.1.6	Preparation of buffers.....	202
5.2	Design, synthesis and biological evaluation of peptide directed phthalocyanine-gold nanocarriers.....	203
5.2.1	Synthesis of FITC- β AAEYLRK (2.16).....	203
5.2.2	Synthesis of FITC- β ALARLLTK (2.17).....	203
5.2.3	Fluorescence microscopy for peptide binding determination	204
5.2.4	Flow cytometry.....	204
5.2.5	Assessment of peptide cytotoxicity	204
5.2.6	Synthesis of FITC- β ARALELK (2.26)	204
5.2.7	Synthesis of HS-PEG-peptides (2.27 and 2.28).....	205
5.2.8	Synthesis of peptide-C11Pc-PEG-AuNPs (2.29 and 2.30)	205
5.2.9	Synthesis of C11Pc-PEG-AuNPs.....	205
5.2.10	Synthesis of PEG-AuNPs.....	206
5.2.11	Synthesis of 5-(3-(3-aminopropyl)thioureido)-2-(6-hydroxy-3-oxo-3H- xanthen-9-yl) benzoic acid (2.34).....	206
5.2.12	Synthesis of FITC-PEG	207
5.2.13	Synthesis of FITC-PEG-AuNPs (2.31)	207
5.2.14	Synthesis of FITC-C11Pc-PEG-AuNPs (2.33)	207
5.2.15	Singlet oxygen production	208
5.2.16	Optimised solvent system for peptide-nanoparticle synthesis.....	208
5.2.17	Variation of coupling agent.....	209
5.2.18	Phototoxicity of 2.29	210

5.2.19	Phototoxicity of control AuNPs.....	210
5.3	Investigations into antibody conjugation for the development of antibody directed phthalocyanine-gold nanocarriers.....	210
5.3.1	Synthesis of C11Pc-PEG-AuNPs.....	210
5.3.2	FITC-tagging of antibodies (3.7).....	210
5.3.3	Conjugation of 5-FAM to antibody (3.8).....	211
5.3.4	Conjugation of 2.34 to C11Pc-PEG-AuNPs (3.9).....	211
5.3.5	Antibody functionalisation of C11Pc-PEG-AuNPs via EDC/NHS (3.10 and 3.15).....	211
5.3.6	Functionalisation of C11Pc-PEG-AuNPs with PDEA.....	212
5.3.7	Antibody functionalisation of C11Pc-PEG-AuNPs via maleimide (3.12, 3.13, 3.16).....	212
5.3.8	Reduction of antibody disulphides and functionalisation of 3.12 (3.14 and 3.17).....	212
5.3.9	Flow cytometry.....	213
5.3.10	Singlet oxygen production.....	213
5.3.11	SDS-PAGE for determining antibody binding to AuNPs.....	213
5.3.12	Anti-EGFR antibody functionalisation of 2.31.....	214
5.3.13	Fluorescence microscopy for the internalisation of antibody-AuNPs... ..	214
5.3.14	Synthesis of PEG-AuNPs.....	214
5.3.15	Synthesis of protein G-PEG-AuNPs (3.19).....	214
5.3.16	Non-covalent binding of anti-HER2 antibody to 3.19 (3.20).....	214
5.3.17	Cross-linking of anti-HER2 antibody to 3.19 (3.21).....	215
5.3.18	SDS-PAGE of protein G-AuNPs.....	215
5.3.19	Gly-Fc-III-Bpa (3.22) and FITC-Fc-III-Bpa (3.23) synthesis.....	215
5.3.20	UV crosslinking of 3.22 to an anti-EGFR antibody.....	216
5.3.21	SDS-PAGE for 3.22 binding to an anti-EGFR antibody.....	216
5.3.22	UV crosslinking of 3.23 to an anti-EGFR antibody.....	216
5.3.23	SDS-PAGE for 3.23 binding to an anti-EGFR antibody.....	217
5.4	Towards protease cleavable sequences to ‘turn on’ the photodynamic activity of folate directed phthalocyanine-gold nanocarriers.....	217
5.4.1	Synthesis of FA-Lys (4.12) on the solid phase.....	217
5.4.2	Temperature controlled synthesis of 4.12 on the solid phase.....	218
5.4.3	Synthesis of 3-dimethylaminopropylfolic acid (4.13) via temperature control.....	218
5.4.4	Synthesis of 4.13 via NHS-ester.....	219

5.4.5	Synthesis of $N^{2,10}$ -Bis(trifluoroacetyl)pyrofolinic acid/anhydride (4.14 and 4.15)	220
5.4.6	Synthesis of N^{10} -(trifluoroacetyl)pyrofolinic acid (4.16)	220
5.4.7	Synthesis of pteroyl hydrazide (4.17)	221
5.4.8	Synthesis of pteroyl azide (4.18)	221
5.4.9	Synthesis of tetramethylguanadium <i>L</i> -methyl folate (4.19)	222
5.4.10	Synthesis of 2-aminoethylfolinic acid (4.6)	222
5.4.11	4.6 cytotoxicity assessment	223
5.4.12	Synthesis of polyethylene Glycol-2-aminoethylfolinic acid (4.29)	223
5.4.13	Synthesis of 4.6 functionalised C11Pc-PEG-AuNPs (4.30)	224
5.4.14	Variation of 4.29 concentration on AuNPs (4.31, 4.32 and 4.33)	224
5.4.15	Singlet oxygen production	224
5.4.16	Synthesis of 5-(2,5-dioxopyrrolidin-1-yl)oxy-5-oxopentanoic acid (4.36)	225
5.4.17	Malachite green test for carboxylic acids on resin	225
5.4.18	Synthesis of peptide 4.41 (4.6-4.36-Lys)	225
5.4.19	Synthesis of peptide 4.43 (4.6-4.36-V-Cit-PABA-K)	226
5.4.20	4.36 addition screen	226
5.4.20.1	4.36-Val (4.44)	226
5.4.20.2	4.36-Trp	227
5.4.20.3	4.36-Ala	227
5.4.20.4	4.36-Leu	227
5.4.20.5	4.36-Phe	227
5.4.20.6	4.36-Glu	228
5.4.20.7	4.36-Arg	228
5.4.20.8	4.36-Lys	228
5.5	References	229

Abbreviations

ABMA	9,10-anthracenediyl-bis(methylene) dimalonic acid
ADC	Antibody drug conjugate
AuNPs	Gold nanoparticles
AuNRs	Gold nanorods
AuNSs	Gold nanostars
BCA	Bicinchoninic acid
Bpa	<i>para</i> -benzoylphenylalanine
C11Pc	1,1',4,4',8,8',15,15',18,18',22,22'-tetradecakisdecyl-25,25'-(11,11'dithiodiundecyl) diphthalocyanine zinc
CatB	Cathepsin B
CDI	Carbonyldiimidazole
DCC	<i>N,N'</i> -dicyclohexylcarbodiimide
DIC	<i>N,N'</i> -diisocarbodiimide
DMEM	Dulbecco's Modified Eagle Medium
DMP	Dimethyl pimelimidate dihydrochloride
Dox	Doxorubicin
DTT	Dithiothreitol
EDC	1-ethyl-3-(3-dimethylaminopropyl)carbodiimide hydrochloride
EGFR	Epidermal growth factor receptor
EPR	Enhanced permeability and retention
Fab	Variable region of an antibody
Fc	Constant region of an antibody
FCS	Foetal calf serum
FITC	Fluorescein isothiocyanate
FRα	Folate receptor alpha
HATU	<i>N</i> -[(Dimethylamino)-1 <i>H</i> -1,2,3-triazolo-[4,5- <i>b</i>]pyridin-1-ylmethylene]- <i>N</i> -methylmethanaminium hexafluorophosphate <i>N</i> -oxide
HBTU	<i>N,N,N',N'</i> -Tetramethyl- <i>O</i> -(1 <i>H</i> -benzotriazol-1-yl)uronium hexafluorophosphate
HER2	Human epidermal growth factor receptor 2

HOBt	1-hydroxybenzotriazole hydrate
Ig	Immunoglobulin
MES	2-(<i>N</i> -morpholino)ethanesulphonic acid
MOPS	3-(<i>N</i> -morpholino)propanesulphonic acid
MTS	3-(4,5-dimethylthiazol-2-yl)-5-(3-carboxymethoxyphenyl)-2-(4-sulfophenyl)-2H-tetrazolium
MWCO	Molecular weight cut off
NHS	<i>N</i> -hydroxysuccinimide
NMM	<i>N</i> -methylmorpholine
NSCLC	Non-small cell lung cancer
PABA	<i>para</i> -amino benzoic acid
PBS	Phosphate buffered saline
PDC	Peptide drug conjugate
PDEA	Pyridine dithioethylamine hydrochloride
PDT	Photodynamic therapy
PEG	Polyethylene glycol
PES	Polyethersulphone
PTT	Photothermal therapy
PyBOP	(Benzotriazol-1-yloxy)tripyrrolidinophosphonium hexafluorophosphate
RPMI	Roswell Park Memorial Institute 1640 Medium
SDS	Sodium dodecyl sulphate
SDS-PAGE	Sodium dodecyl sulphate polyacrylamide gel electrophoresis
s-NHS	<i>N</i> -hydroxysulfosuccinimide
SPAAC	Strain promoted azide alkyne cycloaddition
SPDP	Succinimidyl 3-(2-pyridyldithio)propionate
SPR	Surface plasmon resonance
TBTU	2-(1H-benzotriazole-1-yl)-1,1,3,3-tetramethylammonium tetrafluoroborate
TCEP	Tris(2-carboxyethyl)phosphine
TIPS	Triisopropylsilane
TKI	Tyrosine kinase inhibitor

Acknowledgements

I'd like to thank my supervisors Prof. Mark Searcey, Prof. David Russell and Dr María Marín for all their support and guidance throughout my PhD. Thanks for the opportunities you provided me with, for challenging me to be a better scientist and for believing in me.

I'd also like to thank the Searcey group, past and present, for making working in the lab for the past three years such a good experience. A special thanks goes to Dr. Andrew Beekman and Dr. Marco Comminetti for their day to day advice and support on the days when it felt like everything was going wrong. Thank you to Prof. Maria O'Connell for all your help with the cell culture performed throughout my PhD.

If I were to thank everyone at UEA who's helped or supported me throughout my PhD, the list would be endless. You know who you are and thank you for your help, friendships and for making UEA such an enjoyable place to work.

Thanks to all my friends outside of the lab for their support and welcome breaks from science when I needed them.

Last, but by no means least, I'd like to thank my family. Thanks for your support throughout my life and for pushing me to strive to be the best I can be.

Chapter One

Introduction

1.1 Photodynamic therapy

Photodynamic therapy (PDT) for cancer involves the combination of a photosensitiser and light to produce singlet oxygen within cancerous cells, which ultimately leads to cell death. A photosensitiser is a molecule that mediates a reaction to light, and in the case of PDT this is the conversion of molecular triplet oxygen ($^3\text{O}_2$) into highly reactive singlet oxygen ($^1\text{O}_2$) *via* the promotion of an electron. The overall aims of PDT are to produce a cancer treatment that is minimally invasive, has few side effects (the only side effect being photosensitivity), has no lifetime dose limitations and kills cancerous cells within one treatment.^{1,2}

During the photodynamic process, light of a specific wavelength is absorbed by a photosensitiser, exciting the molecule from the ground state, S_0 (^1PS), to an excited state, S_1 ($^1\text{PS}^*$). The lifetime of $^1\text{PS}^*$ is in the nanosecond range, meaning there is limited time for quenching to occur when the molecule is in this state.³ The molecule can leave this excited state *via* three pathways; a radiative path where the excess energy is lost as fluorescence, through internal conversion to the ground state or through intersystem crossing (ISC) to the excited triplet state, $^3\text{PS}^*$. Photosensitisers have high ISC quantum yields and therefore many of the molecules cross from $^1\text{PS}^*$ to $^3\text{PS}^*$. While molecules can leave this excited state through radiative decay (phosphorescence), the excited triplet state has a lifetime in the range of micro- to milliseconds which gives enough time for quenching and chemical interactions to occur.⁴ From this point two pathways can be followed, both ultimately leading to cell death. For a type I reaction, the photosensitiser excited state is quenched *via* electron transfer or physical deactivation by oxygen, forming free radicals and reactive oxygen species by oxidising organic substrates in the immediate vicinity. This generally occurs when there is a high concentration of photosensitiser or when the cell is hypoxic.² Type II reactions occur *via* energy transfer to $^3\text{O}_2$ which then causes the excitation of oxygen, producing the $^1\text{O}_2$ excited state.⁵ A simplified Jablonski diagram of the photodynamic process can be seen in **Figure 1.1**. Type I and II reactions will occur simultaneously, and the ratio depends on the photosensitiser, the oxygen concentration, the substrates present and the subcellular localisation of the photosensitiser. Generally, type II reactions are responsible for the majority of the phototoxicity in PDT.⁵

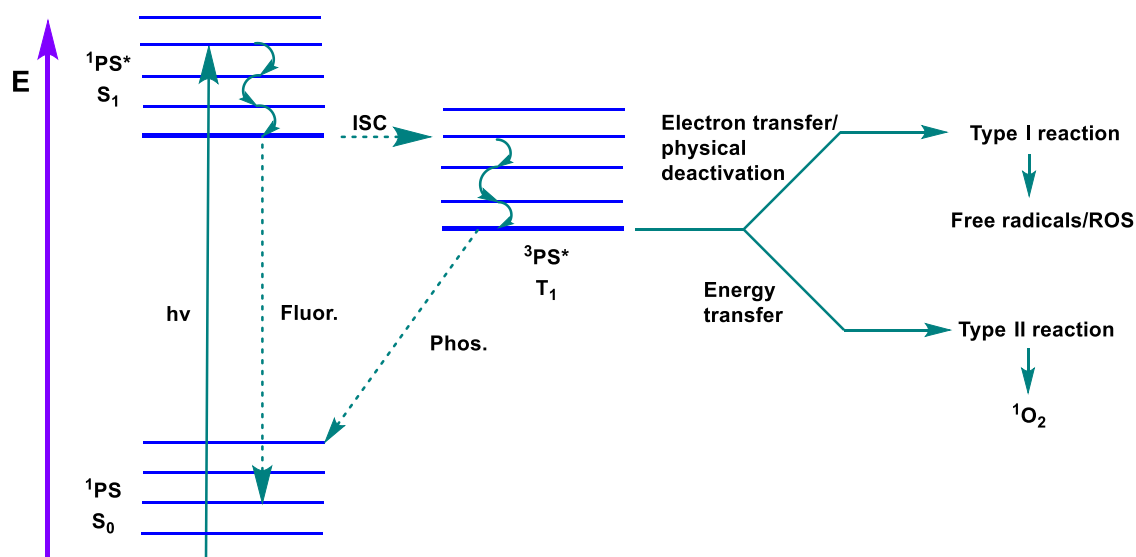


Figure 1.1: Simplified Jablonski diagram of the photodynamic process. Fluor. = fluorescence, Phos. = phosphorescence, ISC = intersystem crossing

$^1\text{O}_2$ is extremely reactive and damages subcellular organelles, stimulating the apoptotic and necrotic pathways which cause cell death.⁶ Photosensitisers can also accumulate within blood vessels and cause vascular damage during PDT treatment which leads to tumour hypoxia and subsequent cell death.⁷ Singlet oxygen has a lifetime of under 0.04 μs and a radius of action of less than 0.02 μm .⁸ Human cells have a diameter of 10-100 μm , meaning $^1\text{O}_2$ cannot diffuse more than a cells length. This means PDT has the potential to be a very specific cancer treatment if cancer cells can be preferentially targeted over normal healthy cells.

1.1.1 Photosensitisers for PDT

Ideal photosensitisers for PDT are isomerically pure, have good stability, have a high molar extinction coefficient between 650-800 nm, have a high quantum yield for singlet oxygen, have no dark toxicity, interact preferentially with cancer cells and clear relatively quickly from normal tissue.^{9,10} The majority of reported photosensitisers are hydrophobic aromatics as they fulfil many of these criteria.

The wavelength at which photosensitisers absorb is very important for the efficacy of the treatment. Below 650 nm, haemoglobin and other naturally occurring chromophores in the body absorb strongly and would interfere with the absorbance of the photosensitiser.¹¹ The penetration of light through the body also increases with increasing wavelength so photosensitisers with higher absorption maxima can be used to treat cancer

at lower depths. However, above 800 nm, the photosensitiser may no longer have the energy to convert triplet oxygen to singlet oxygen; the conversion requires approximately 92 kJ/mol which is equivalent to a wavelength of 1274 nm.¹²

First-generation photosensitisers are derived from hematoporphyrin derivative (HpD), a mixture of partially unidentified monomeric, dimeric and oligomeric porphyrin structures.¹³ HpD is not isomerically pure, meaning it is not an ideal photosensitiser. Photofrin[®] (**Figure 1.2**), was developed from partially purified HpD, resulting in an isomerically pure first-generation photosensitiser which is approved for clinical use.^{14,15}

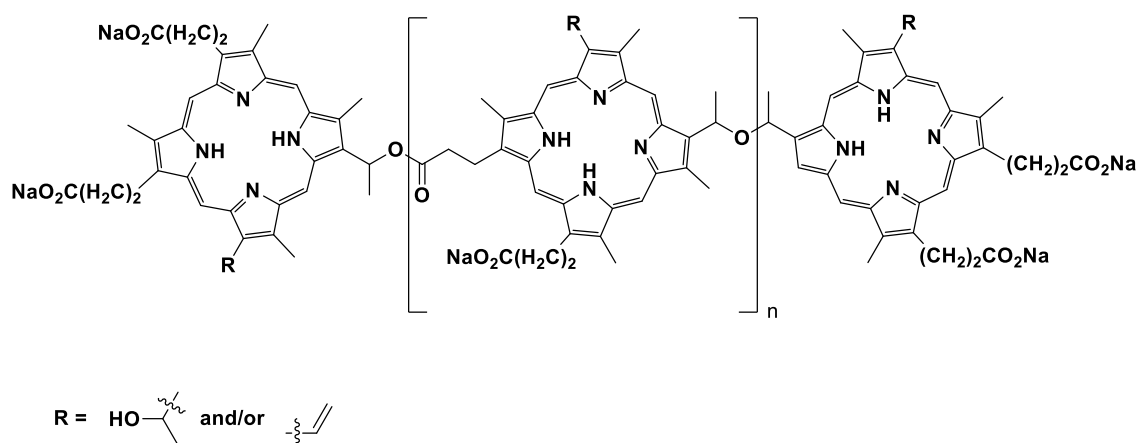


Figure 1.2: Structure of Photofrin[®], a mixture of polymerised porphyrins. $n = 0-6$ repeating units

Photofrin[®] is a mixture of polymerised porphyrins that are water soluble, which leads to ease of administration. Photofrin[®] exhibits high efficacy for tumour destruction and negligible dark toxicity.¹⁶ Another well-known first-generation photosensitiser approved for clinical use is protoporphyrin IX (PpIX, **Figure 1.3**), generally administered through treatment with 5-aminolaevulanic acid (ALA), a precursor in the biosynthetic pathway for the formation of PPIX, itself a precursor to haem.¹⁷

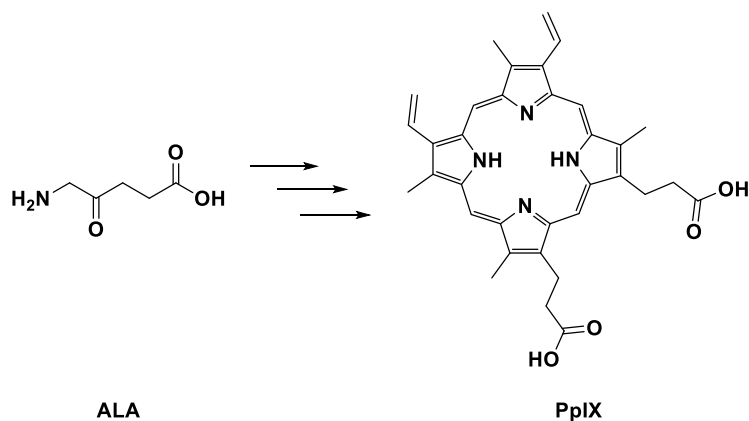


Figure 1.3: The structure of ALA and its conversion to PpIX

While these compounds possess interesting properties, the main issue with first generation photosensitisers is their retention time within the body. Photofrin[®] is retained in the body for 6-8 weeks post injection, and the prolonged light sensitivity is undesirable as it effects quality of life. Furthermore, first generation photosensitisers exhibit poor selectivity, so large doses are required for effective treatment, alongside relatively low extinction coefficients, which means prolonged light exposure is required for effective treatment.^{18,19} The peak absorbance of both PPIX and Photofrin[®], and thus their activation wavelength, is at *ca.* 630 nm²⁰ which largely overlaps with sunlight, increasing the chances of an adverse reaction if the patient were to be exposed to light. The low wavelength for excitation also means that there is low penetration into human tissue; Photofrin[®] is only effective to a depth of 0.5 cm with ALA restricted to a depth of 0.2 cm.²¹ These issues led to the development of second-generation photosensitisers with the aim of improving these adverse characteristics.

Second-generation photosensitisers are generally based on substituted porphyrins, chlorins and phthalocyanines, the structures of which are shown in **Figure 1.4**. These structures absorb intensely at higher wavelengths than first generation photosensitisers, have higher selectivity, are well characterised with high purity, are retained by the body for a shorter period of time and generally have a higher singlet oxygen quantum yield.

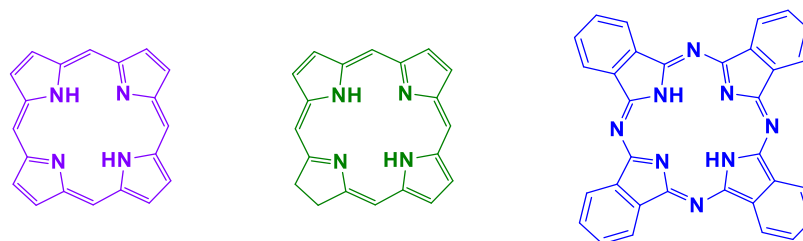


Figure 1.4: Core structures of a porphyrin (purple), a chlorin (green) and a phthalocyanine (blue)

Second generation porphyrins tend to be substituted with groups that increase the molar extinction coefficient and move the absorption peak of the molecule to higher wavelengths. An example of these substituted porphyrins is *meta*-tetrahydroxyphenylporphyrin (*m*THPP, **Figure 1.5a**). *m*THPP shows a higher singlet oxygen quantum yield than Photofrin[®] and therefore is seen to be 25-30 times as effective as this first-generation photosensitiser. Its molar extinction coefficient is an order of magnitude higher than that of unsubstituted porphyrins and it absorbs at a slightly higher wavelength of 650 nm.²²

Chlorin photosensitisers include chlorin e_6 (Ce6, **Figure 1.5c**) and *meta*-tetrahydroxyphenylchlorin (*m*THPC, **Figure 1.5b**). Ce6 shows an absorbance maximum at 662 nm, a high molar extinction and is rapidly eliminated from the body.²³ *m*THPC is a synthetic chlorin clinically approved for PDT that absorbs light at 652 nm. It differs from *m*THPP by the reduction of a double bond within the porphyrin structure. This reduction causes a red shift in the absorption and increases the strength of this absorbance. *m*THPC has a high singlet oxygen quantum yield and is retained within the body for up to two weeks.^{21,22}

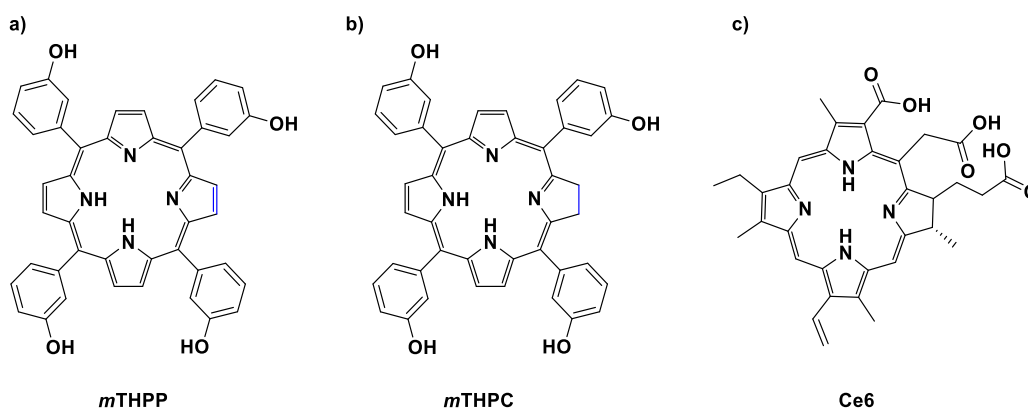


Figure 1.5: The structures of a) *m*THPP, b) *m*THPC and c) Ce6. The reduced double bond that differs the structure of *m*THPP and *m*THPC is highlighted in blue

Phthalocyanines are attractive photosensitisers due to their high extinction coefficient, in general two orders of magnitude higher than that of Photofrin[®]. Many phthalocyanines applied to PDT also contain a central diamagnetic metal, such as Zn²⁺ or Al³⁺, which greatly increases the singlet oxygen quantum yield.²⁴ A range of phthalocyanines are currently undergoing clinical trials for applications as second generation photosensitisers including a silicon(IV) phthalocyanine known as Pc4 (**Figure 1.6a**) and zinc(II) phthalocyanines (ZnPcs, **Figure 1.6b**). Pc4 absorbs very strongly at 670 nm and ZnPcs have strong absorptions around 700 nm. A mixture of sulphonated aluminium phthalocyanines, known as Photosens[®] (**Figure 1.6c**), is approved in Russia for the treatment of a variety of cancers including skin, stomach and breast cancers.^{25,26} Photosens[®] is a rare example of a hydrophilic photosensitiser. Generally, the best photosensitisers for PDT are hydrophobic as they tend to show higher singlet oxygen quantum yields and the hydrophobicity leads to an accumulation in the hydrophobic regions of cells, assisting with their uptake from the blood stream. Hydrophobic photosensitisers also tend to have better selectivity; they show a ratio of 7:1 tumour:normal cell accumulation compared to a 2:1 ratio seen for hydrophilic photosensitisers.^{12,27}

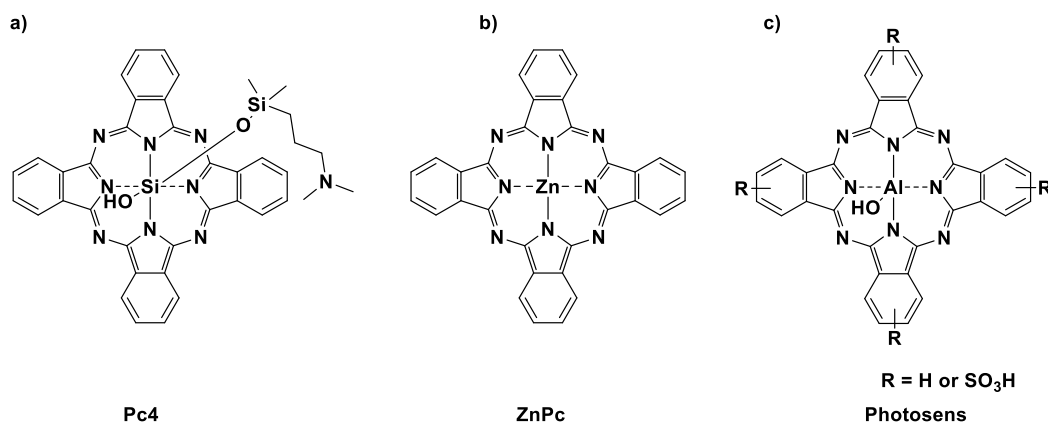


Figure 1.6: The structures of a) Pc4, b) ZnPc and c) Photosens[®]

1.1.2 Non-small cell lung cancer and PDT

Lung cancer as a whole is the third most common cancer in the UK and the most common cause of cancer related death. In 2018, 1.7 million deaths were attributed to lung cancer worldwide.²⁸ Survival rates for lung cancer are shockingly low, with only 32% of patients surviving for one or more years, 10% for five or more years and only 5% survive for ten years or more.²⁹ Lung cancer has two main subtypes: small-cell lung cancer (SSLC)

and non-small cell lung cancer (NSCLC). Approximately 85% of lung cancer cases within the UK are NSCLC, which can be further divided into four groups; squamous cell carcinoma, adenocarcinoma, large-cell carcinoma and 'others'. Adenocarcinoma and squamous cell carcinoma are by far the most common types of NSCLC, making up *ca.* 40% and 25% of all lung cancer cases, respectively.³⁰

The high mortality rates for lung cancer have two main contributing factors: it is hard to diagnose at an early stage, with many cases being discovered after the cancer has metastasised, and the fragility of the lungs makes surgical resection of the tumour difficult. Currently the most common treatment for lung cancer is surgical resection,³¹ yet many patients are not able to undergo this procedure as it compromises lung function. If a lung carcinoma is in a position where it compromises breathing itself, it is too dangerous to undergo surgery. Any patient with reduced lung function cannot have surgery as it will cause the loss of too much lung function and result in a very poor quality of life; thus, leaving chemotherapy and radiotherapy as the main viable treatment options.³²

Photodynamic therapy is preferable to surgery, chemotherapy and radiotherapy as it results in less collateral damage. PDT was first applied to NSCLC in 1982 by *Hayata et al.* using hematoporphyrin derivative.³³ Photofrin[®] has since become the main photosensitiser approved for lung cancer treatment. Early-stage lung cancers have been treated with Photofrin[®] with complete response rates in *ca.* 78% of cases.³⁴⁻³⁶ It was observed that the response rate was related to the size of the tumour; patients with tumours smaller than 0.5 cm showed a 94% complete response rate, tumours 1-2 cm in size had an 80% complete response rate, and tumours larger than 2 cm had a much lower complete response rate of 44%.³⁵ These results are not unexpected as the efficacy of PDT depends on the ability of light to penetrate the tumour, and the light necessary to activate Photofrin[®] (630 nm) can only penetrate approximately 0.5 cm through human tissue.²¹ While promising results have been obtained using Photofrin[®], significant side effects such as erythema, fibrosis and cicatricial stenosis, the narrowing of ducts due to the build-up of scar tissue,^{34,35} have been observed due to the lack of selectivity of this first generation photosensitiser. As second-generation photosensitisers have been seen to increase the selectivity of PDT, an investigation into other photosensitisers may reduce these side effects, while providing a significant response rate. Second-generation photosensitisers, however, are notoriously hydrophobic and so their delivery to NSCLC is challenging. To counter this, a water-soluble delivery system is required and recent advances in

nanotechnology have highlighted nanoparticles as highly efficient and selective delivery vehicles for photosensitisers.

1.2 Nanomedicine and cancer therapeutics

Over 100 years ago, Paul Ehrlich described the concept of a ‘magic bullet’ for chemotherapy, in which drugs can be delivered directly to their desired target, removing devastating off-target effects.³⁷ While there are many ways to go about the development of a ‘magic bullet’, one such method is that of nanotechnology and nanomedicine, an emerging field of cancer therapeutics involving sub-micrometre delivery vehicles (1-100 nm) to transport the desired therapeutic to its target. Nanomedicine involves the use of nanoparticles, with their nanoscale size providing significantly altered physical, chemical and biological properties from that of the bulk material, with these altered properties favourable for their use as delivery vehicles.

Nanoparticles have been shown to display passive targeting towards tumours through the enhanced permeability and retention (EPR) effect (**Figure 1.7**).³⁸ The EPR effect occurs due to the fact that tumours have a high demand for blood flow to provide the necessary nutrients and oxygen for their uncontrolled cell growth. As they rapidly expand in size, tumours form new blood vessels to provide for this excess need, and these blood vessels tend to be poorly formed and ‘leaky’. As nanoparticles are relatively large in size compared to natural small molecules and growth factors, they rarely pass through the walls of properly formed blood vessels in normal tissue. The leaky vasculature in tumours, however, allows for the passage of nanoparticles through their walls and leads to an accumulation of nanoparticles in the tumour. Tumours also display poor lymphatic drainage meaning that the nanoparticles that pass through into the tumour *via* the leaky blood vessels are not carried away as efficiently from cancerous tissue as from normal tissue, increasing this accumulation in tumours. This passive accumulation of nanoparticles in cancerous tissues highlights their ability to act as ‘magic bullets’.

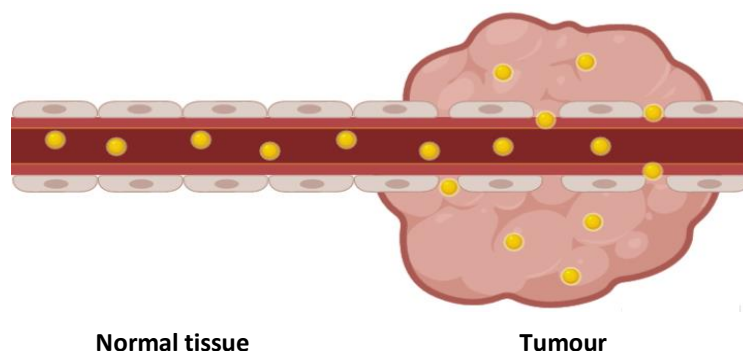


Figure 1.7: The passive targeting of nanoparticles towards tumours through the EPR effect. The small size of nanoparticles means they cannot pass through the walls of blood vessels in healthy tissue, but the 'leaky' vasculature in tumours allows for nanoparticles to penetrate through the blood vessels and to accumulate in the tumour

A second benefit of nanoparticles is their large surface area to volume ratio, meaning that one nanoparticle can carry a large quantity of a payload to their target, providing a very attractive method for drug delivery. This large surface area also allows for the attachment of multiple different payloads to one nanoparticle, allowing for their co-delivery to a target, which has many therapeutic benefits. Diagnostic tools can also be attached to nanoparticles alongside payloads to elicit a theranostic effect, where the nanoparticle system can be used to diagnose and treat cancers simultaneously.^{39,40} Nanoparticles have been seen to improve stability, solubility and circulatory half-lives of drugs, along with improved drug efficacy.^{41–43} They have also been designed to release their payload upon internalisation into cancerous cells due to an internal stimulus such as pH or a reducing environment, restricting drug release to within cancer cells and improving the pharmacokinetics of a drug.^{44,45} The benefits of nanoparticle delivery systems highlight their applicability for the delivery of payloads to cancers.

1.3 Gold nanoparticles as drug carriers

Many types of nanoparticle have been developed for drug delivery, including liposomes, polymeric nanoparticles, quantum dots, carbon dots, upconverting nanoparticles and inorganic nanoparticles. Inorganic structures include gold, silver, silica, iron oxide and copper sulphide nanoparticles. While these all have their benefits, gold nanoparticles (AuNPs) highlight themselves as ideal drug carriers; they are chemically inert and minimally toxic, meaning they can pass through the body without eliciting any adverse reactions.^{46,47} For intravenous use as drug carriers, AuNPs are often coated in a layer of

polyethylene glycol (PEG) ligands. PEG is clinically approved for intravenous use and its amphiphilic nature stabilises nanoparticles within biological media, making AuNPs dispersible within aqueous environments. PEG also increases the circulatory half-life of AuNPs by blocking the adsorption of opsonins and serum proteins, which enable the uptake and clearance of nanoparticles through the reticuloendothelial system.

The surface of AuNPs is easily functionalised through the formation of strong gold-sulphur (Au-S) bonds that will spontaneously form through thiol surface adsorption. Au-S bonds are non-labile and results in AuNPs that are stable to physiologically relevant pH and salt concentrations.⁴⁸ The synthesis of AuNPs involves the reduction of Au(III) to Au(0), which initiates the nucleation of AuNPs. Tight control over the reaction conditions means that the size and shape of AuNPs can be selected and varied to fit the desired purpose. Different nanostructures are beneficial for different purposes, and their uptake and potential therapeutic properties vary from shape to shape. The ability to form these different structures is a benefit of AuNPs and this is not possible with other nanosystems. The synthesis of AuNPs of differing shapes, such as nanosquares, nanostars (AuNSs) and nanorods (AuNRs, **Figure 1.8**) is usually completed through a seeded growth method. Here, small AuNPs are synthesised, generally 4-5 nm in size, and the addition of these seeds to Au(III) solutions containing different reducing and capping agents can influence the shape of the nucleated nanosystems.⁴⁹

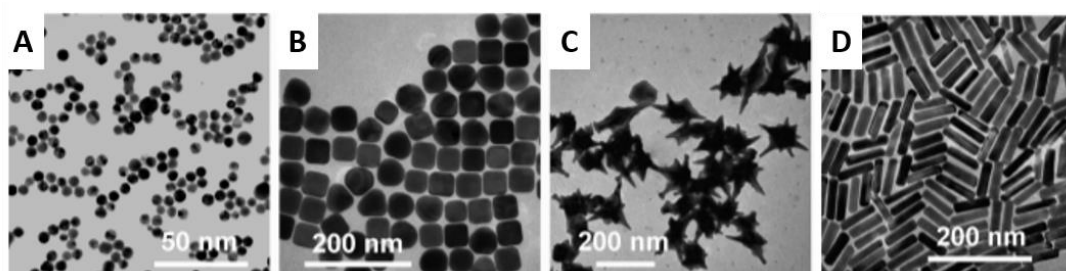


Figure 1.8: Examples of AuNPs shapes. *a*) nanospheres or nanoparticles (AuNPs), *b*) nanosquares, *c*) nanobranched or nanostars (AuNSs), and *d*) nanorods (AuNRs) [adapted from ref. 50]

The strength of the reducing agent has a strong influence on the size of the AuNPs produced. For example, the use of a strong reducing agent such as sodium borohydride (NaBH_4) results in sub-10 nm AuNPs, whereas for larger AuNPs a milder reducing agent such as trisodium citrate is commonly used. The synthesis of AuNPs also relies on the presence of a stabilising agent, and the choice of stabilising agent can influence the size and shape of the resulting AuNPs through steric hindrance, and reduce the polydispersity

of the synthesised AuNPs.^{51–53} For example, the addition of thiolated ligands upon reduction of Au(III) leads to the formation of strong Au-S bonds that cap the nanoparticles at a small and relatively monodisperse size, but control over the gold:ligand ratio determines the exact size of the AuNPs synthesised.⁵⁴

AuNPs display a strong surface plasmon resonance (SPR) due to the oscillation of electrons upon exposure to light. AuNPs absorb visible light with extinction coefficients orders of magnitude higher than those of many strongly absorbing organic dyes, and this SPR band is dependent on the size and shape of the AuNPs.⁵⁵ This provides a unique property to AuNPs as the strong absorption of light means that the nanoparticle itself can be used as a therapeutic agent. When AuNPs are irradiated with light matching the wavelength of their SPR band they rapidly heat and can destroy cells through photothermal ablation, known as photothermal therapy (PTT).⁵⁶

The biocompatibility, lack of cytotoxicity, stability, ease of synthesis and functionalisation, passive targeting and the unique SPR properties of AuNPs highlight their potential as delivery systems for cancer therapeutics.

1.4 Active targeting of gold nanoparticles for cancer therapeutics

While passive targeting of AuNPs relying on the EPR effect has been extensively explored, as the interest in personalised medicine has grown in recent years, the focus has turned towards the active targeting of gold nanoparticles to a particular site. Active targeting of AuNPs involves the attachment of a targeting moiety, specific towards a desired surface receptor, onto the nanoparticle surface, alongside the payload. In cancer, the targeting moiety used often recognises a receptor that is overexpressed by tumour cells, but examples also exist of AuNPs targeted towards receptors that are cryptic or not expressed on healthy cells. A plethora of targeting moieties have been explored and these can be split into the general categories of antibodies, proteins, peptides, aptamers, carbohydrates and small molecules.

1.4.1 Antibody directed gold nanoparticles

1.4.1.1 IgG antibodies

When the idea of actively targeting nanoparticles towards a known oncogene was first imagined, antibodies presented themselves as an ideal targeting moiety. Antibodies are

highly specific towards a receptor, to which they display an extremely high affinity. While there are many types of antibodies, most antibodies used for therapeutics are IgG antibodies. IgG antibodies have a Y-shaped structure consisting of a constant (Fc) region that is unchanged in all IgG antibodies and a variable (Fab) region that is unique to each antibody. This Fab region contains two antigen recognition sites, as shown in **Figure 1.9**. Antibodies are usually produced in animal models and therefore they can elicit an immune response within the human body, however the high affinity of antibodies towards a very specific target has resulted in an extensive interest in using them as targeting moieties for AuNPs.

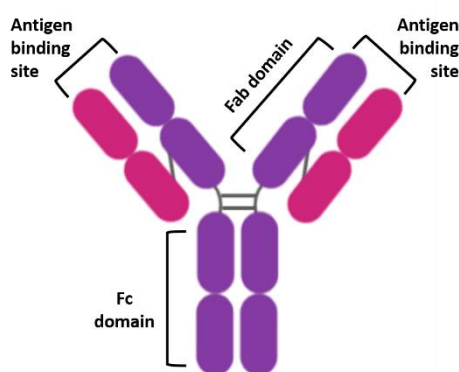


Figure 1.9: Structure of an IgG antibody, showing the heavy (purple) and light (pink) chains, the variable Fab domain, the constant Fc domain and the antigen binding sites

The development of antibodies as clinically approved therapeutics in their own right may have encouraged the development of antibody-AuNPs. The antibodies trastuzumab and cetuximab have been clinically approved to target HER2 overexpressing breast cancers⁵⁷ and EGFR overexpressing colorectal cancer respectively.⁵⁸ As these antibodies are clinically approved, their affinity to their target has already been validated and therefore they have both been extensively investigated for the targeted delivery of AuNPs. For example, cetuximab and trastuzumab have been used to direct AuNPs towards cancers for enhanced radiotherapy.^{59–61} AuNPs can act as radiosensitisers, increasing the effect of radiation therapy on tumours as they release photoelectrons and Auger electrons upon irradiation with X-ray and near-IR radiation.⁶² Along with these clinically approved antibodies, a number of other antibodies have been used to deliver AuNP-conjugated radiosensitisers to a range of different targets. Antibody functionalised AuNPs have also been extensively studied for targeted PTT of a multitude of cancers.^{63–65} Consistently, increased cytotoxicity and selective uptake of these targeted AuNPs is observed.

Antibody-functionalised AuNPs were first used for the targeted delivery of anticancer agents in 2008, when gemcitabine (Gem) was delivered to pancreatic adenocarcinoma by cetuximab-functionalised AuNPs with increased cytotoxicity observed over non-targeted Gem-AuNPs.⁶⁶ Since then, AuNPs have been used to deliver chemotherapeutic drugs such as doxorubicin (Dox) and oxaliplatin. These chemotherapeutic drugs are either bound to the AuNP core *via* reversible Au-N bonds, adsorbed to the core through hydrophobic interactions or are conjugated onto PEG ligands (**Figure 1.10**) to form a mixed monolayer on the nanoparticle surface alongside the antibody. Chemotherapeutic drugs have also been adsorbed into the AuNP core itself.^{67–69}

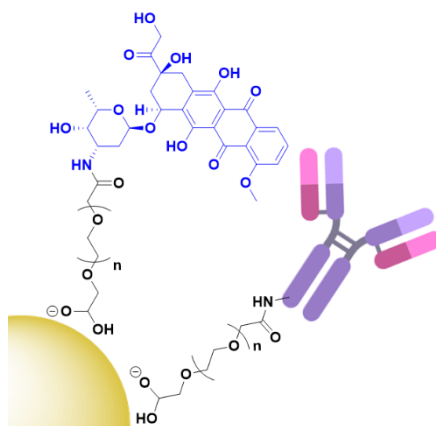


Figure 1.10: Structure of Ab directed Dox (blue) AuNPs, with both the payload and antibody conjugated through a PEG (black) linker [adapted from ref. 67]

Few examples exist of conjugating the delivered drug onto the antibody itself, potentially due to the relative fragility of antibodies and the relative ease of conjugating payloads to the nanoparticle over the antibody. One example of this is the addition of the radionuclide ^{131}I to cetuximab post-conjugation of this antibody onto AuNPs for radioimmunotherapy.⁷⁰ The decision to radiolabel the antibody itself likely stems from the fact that radiolabelled cetuximab has been extensively investigated as an agent for radioimmunotherapy. These AuNPs were seen to display a targeted decrease in cell viability of A549 cells, with this cytotoxicity higher than that of ^{131}I at the same dosage,⁷⁰ highlighting the ability of AuNPs to increase the potency of a payload.

While many different antibody conjugated AuNP systems have been reported, the vast majority of them rely on common chemistry for the addition of the antibody to the nanoparticle system. Firstly, most of these nanosystems are stabilised with a thiolated linker such as a PEG chain, which is highly water soluble and approved for medical use.

These PEG chains are often terminated with a carboxylic acid or activated succinimidyl ester for the addition of an antibody through the formation of random amide bonds with free amine residues on the surface of the antibody. While many variants of these linkers exist, summarised in **Table 1.1**, the chemistry of the antibody conjugation is identical.

Table 1.1: Summary of coupling agents used to conjugate antibodies onto AuNPs

Coupling agent(s)	Linker	Notes
EDC/NHS or sulfo-NHS	HS-PEG-COOH ^{61,71-76}	NHS and sulfo-NHS vary in water solubility, but the conjugation chemistry is identical. (sulfo)-NHS acts to stabilise the activated carboxylic acid formed by EDC, before random amide bonds are formed with antibody amines
	HOOC-PEG-COOH ⁶⁷	
	11-mercaptoundecanoic acid ⁷⁷	
EDC	DSPE-PEG-COOH ⁶⁹	No stabilising ester formed but forms the same random amide bonds as EDC/NHS
Succinimidyl valerate (SVA)	Orthopyridyl disulphide (OPSS)-PEG-SVA ^{59,60,78}	OPSS is a disulphide that reacts with the Au core. SVA contains an NHS-ester, forming random amide bonds
Succinimidyl ester	<i>N</i> -succinimidyl-S-acetylthiopropionate ^{68,70}	NHS ester linkage to form random amide bonds. Acetylthiopropionate can then be reduced for thiol addition to AuNP
Bis(sulfosuccinimidyl)suberate (BS3)	HS-amine polymer ⁷⁹	Linker with two sulfo-NHS termini to link amines. Random amide bonds formed to antibody
Hydrazide	(HS) ₂ -PEG-hydrazide ⁸⁰	Hydrazide reacts with activated COOH to give hydrazine. Reactivity is random towards carbonyls on antibody
pH adjustment	None ⁶⁴	pH reduced below isoelectric point of Ab to encourage electrostatic interactions

This ubiquity of functionalisation chemistry, while concentrations of both coupling agents and antibody may need to be varied depending on the desired system, perhaps highlights the versatility of antibodies as targeting agents for AuNPs. It can be imagined that, if the same process is used for antibody conjugation time and time again, antibodies can be switched in and out to target the same system to any oncogene required. While most conjugates in the literature use some variation of this amide bond formation involving lysines on the antibody, a PEG linker terminated in a hydrazide can be used,

which allows for the cross-linking of AuNPs with carboxylic acids on the surface of antibodies.⁸⁰ This chemistry, while utilising different residues on the antibody is still completely random and may lead to even more variations as there are on average more carboxylic acids present on antibodies than amines.⁸¹

The uptake of antibodies into cells often relies on receptor mediated endocytosis. This process provides a target-specific internalisation mechanism for Ab-AuNPs; however the conjugation of antibodies is notorious for altering their pharmacokinetics. It has been observed that the endocytosis of cetuximab-AuNPs is in fact accelerated from that of free cetuximab, and the mechanism by which this endocytosis occurs is altered upon conjugation. This altered internalisation mechanism leads to differing subcellular localisation between cetuximab and its resulting gold nanoconjugate.⁸² It is also observed that not all antibodies are internalised upon receptor binding. It is still under debate whether trastuzumab is internalised upon binding to HER2,^{83,84} however it has been shown that the internalisation of trastuzumab is increased upon cross-linking, possibly due to multivalent binding. HER2 overexpressing cells show increased internalisation of trastuzumab-AuNPs compared to non-conjugated trastuzumab at the same concentration.⁷⁸ These reports highlight a key consideration for the synthesis of antibody-AuNPs; the kinetics and uptake of the antibody is likely to be altered upon conjugation. While in the reported examples these alterations appear to be beneficial for increased uptake, this may not always be the case and the pharmacokinetics of conjugated antibodies may warrant further investigation to help select the best antibodies possible for delivering AuNPs to the corresponding target.

While antibodies display high affinity towards their target, this affinity relies on the antigen binding sites remaining non-functionalised and unhindered. The majority of reports of antibody functionalised AuNPs rely on completely random amide bond formation for the addition of the antibody, which may result in some of the active sites of the antibody being in or near the nanoparticle surface and thus, reducing the binding ability of these conjugates. It has been shown that protein G, an Fc region binding protein, can be used to control the orientation of an antibody on the AuNP surface and therefore to maintain optimal activity.⁸⁵ While no comparison is made to AuNPs conjugated with antibody without the presence of protein G, there is increased uptake of these EGFR targeted AuNPs compared to a non-targeted control and selective PTT is observed.^{66,85} This perhaps provides a sensible alternative to commonly used antibody

functionalisation techniques if the desired activity is not observed, however protein G is immunogenic and therefore it may provide other complexities.

1.4.1.2 *Antibody fragments and nanobodies*

While antibodies present such high affinity towards receptors, their size inhibits their penetration into tumours. This has led to the investigation of antibody fragments as targeting moieties. The reduction of the disulphide bonds between the heavy chains of an antibody yields two functional antibody fragments. Notable for AuNPs, these antibody fragments possess free thiols which can bind to the gold core. This conjugation strategy also ensures the active site of the antibody is pointing away from the gold core and thus, is accessible. The conjugation of EGFR antibody fragments to AuNPs for PTT displayed cytotoxicity upon irradiation that varied with EGFR expression.⁶³ While the use of antibody fragments reduces the size of the targeting moiety attached to the AuNPs, these half-antibodies still display an immunogenic effect upon the body due to the presence of the Fc region. Antibody fragments known as Fab fragments have been developed to remove the Fc region, simultaneously reducing the size of the antibody and forming a non-immunogenic targeting moiety. Interestingly, there are no examples of the use of Fab fragments to target therapeutic AuNPs for drug delivery, and research into this area may provide promising results.

While antibody fragments have been investigated to account for the sheer size of antibodies, nanobodies are even smaller than antibody fragments and have recently gained extensive attention as targeting moieties. Camelids possess IgG antibodies that consist of only heavy chains and are 2/3rd of the size of human IgGs (**Figure 1.11**).⁸⁶ These camelid heavy-chain antibodies possess a variable domain that can be cloned and expressed in bacteria to give a monomeric, single-domain antigen-binding antibody fragment, named a nanobody for its small size (**Figure 1.11**).⁸⁷ Nanobodies are *ca.* 15 kDa, 1/10th of the size of an antibody, and therefore display higher tumour penetration. Alongside this, they are non-immunogenic and display higher stability than antibodies.⁸⁸

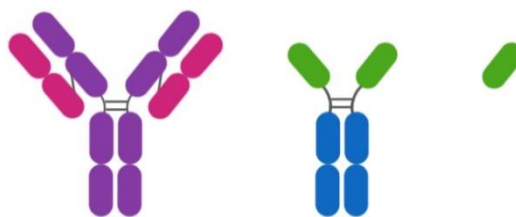


Figure 1.11: (L-R) human IgG consisting of two heavy chains (purple) and two light chains (pink), camelid IgG heavy-chain Ab with variable recognition domains (green), single-domain nanobody derived from the variable domain of a camelid IgG

An anti-HER2 nanobody has been shown to selectively target gold nanostars (AuNSs) towards HER2 positive ovarian cancer. The nanobody is shown to selectively internalise into HER2 overexpressing SKOV3 cells, with targeted PTT observed.⁸⁹ This nanobody was modified in production to express a cysteine residue on the C-terminus to allow for site-specific attachment onto AuNSs through a maleimide. Both antibody fragments and nanobodies provide solutions to the issues of antibody penetration into solid tumours. Further work is needed, however, to confirm the benefit of these targeting moieties, with studies to compare the uptake, selectivity and tumour penetration of these fragments to that of whole antibodies.

1.4.2 Protein directed gold nanoparticles

The use of other proteins as targeting agents is relatively unexplored compared to the wealth of research into antibody targeted therapies. Proteins selected as targeting moieties are either natural ligands for a receptor or lectins – carbohydrate binding proteins often isolated from fruit or vegetables. It is perhaps understandable that native protein ligands towards receptors have not been excessively explored as targeting moieties as, by nature of their abundance in the human body, there will be a large number of competing ligands that are not carrying AuNPs. These proteins will display the same affinity towards the desired receptor and possibly lead to a reduced targeting efficiency. That said, the use of human proteins and growth factors removes any immunogenic response towards these AuNPs and may be worth exploring. One growth factor that has been exploited for targeted AuNP therapy is the epidermal growth factor (EGF) which has been used to target AuNPs towards epidermal growth factor receptor overexpressing breast cancer. A disulphide bond in EGF was reduced to allow for its attachment onto AuNPs, then the EGF itself was radiolabelled with ¹¹¹In (**Figure 1.12**). These nanoconjugates showed high

uptake into EGFR overexpressing breast cancer cells and minimal uptake into cells with low EGFR expression. A competition assay with non-conjugated EGF showed that this uptake was due to EGF recognition by the cells and EGFR selective cytotoxicity was observed.⁹⁰

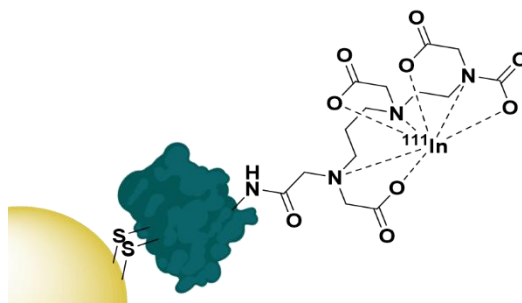


Figure 1.12: The functionalisation of AuNPs with ¹¹¹In radiolabelled EGF through disulphide reduction

The protein transferrin has been shown to target gold nanorods (AuNRs) towards transferrin receptor expressing lung cancers. While transferrin directed AuNRs carrying doxorubicin displayed lower cytotoxicity than doxorubicin alone, the cytotoxicity of these transferrin targeted AuNRs was selective towards transferrin receptor expressing cells, and toxicity was shown to vary with the concentration of transferrin receptor expressed by cell lines.⁹¹

While these examples use the receptors' native proteins, the use of recombinant proteins has been explored. Employing mutations and variations to wild type proteins for a ligand can advantageously alter their characteristics and lead to enhanced properties for these recombinant proteins over the body's native proteins. For example, a recombinant fibroblast growth factor 1 (FGF1) was engineered with four point mutations to protect FGF1 against proteolysis and therefore increase its circulatory half-life over that of native FGF1. FGF1 targets all four variations of the fibroblast growth factor receptor that are overexpressed in many cancers including lung cancer.⁹² FGF1 was also altered to attach a short peptide chain to the N-terminus containing a cysteine for conjugation onto AuNPs, and the native cysteine in the protein was removed to allow for site specific conjugation onto the AuNPs. FGFR negative cells were transfected with FGFR and the uptake of these nanocarriers confirmed to be due to endocytosis by FGFR. These AuNPs were used for PTT, with photothermal cytotoxicity only observed in FGFR expressing cell lines.⁹³ The benefits of this recombinant protein over native FGF1, however, have

not been explored in this research as no comparison has been made to the native ligand to determine the advantage of this increased circulatory half-life.

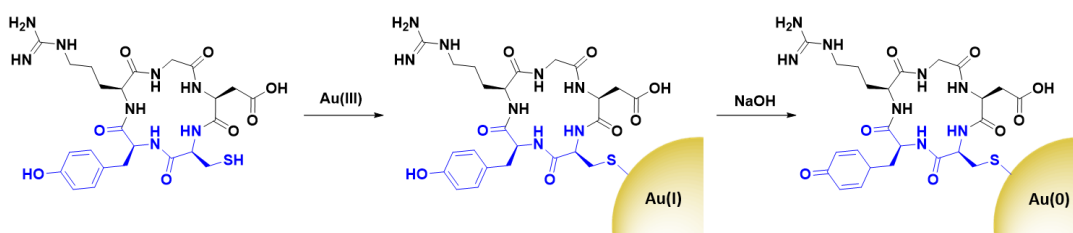
Lectins are more commonly used for biosensors than for targeted cancer therapies, however the lectin Jacalin has been employed to target a zinc phthalocyanine towards Thomsen-Friedenreich antigen (T-antigen) expressing cells for photodynamic therapy. The T-antigen is expressed in *ca.* 90% of cancers and is usually cryptic on healthy cells. Jacalin was conjugated onto a PEG shell through random amide-bond formation and cytotoxicity was observed in T-antigen expressing cells, whereas non-conjugated AuNPs displayed negligible cytotoxicity. To determine the selectivity of these nanoconjugates, the AuNPs were incubated with methyl- α -D-galactopyranoside, a glycoprotein that expresses the T-antigen. Pre-incubation with this glycoprotein decreases the photodynamic activity of the conjugate and suggests the activity is due to uptake of these nanocarriers through the Jacalin.^{74,94} Jacalin is non-immunogenic, and its affinity towards the ubiquitously oncologically expressed T-antigen makes it a very attractive targeting moiety. Jacalin has, however, been shown to bind to carbohydrate moieties on IgA antibodies, which may explain the lack of investigation into its use as a targeting ligand.^{95,96}

1.4.3 Peptide directed gold nanoparticles

Peptides are relatively short polymers of amino acids that can be fully characterised and chemically synthesised to a designed specification. While they generally display lower affinity towards receptors than antibodies and other proteins, peptides are gaining attention as targeting moieties due to their simplicity and rapid uptake kinetics. Many examples of using peptides to target AuNPs towards various cancers for imaging have been reported in the literature,⁹⁷⁻¹⁰² while surprisingly few examples exist of peptide-directed AuNP-based cancer therapeutics.

Peptides have been used to direct AuNPs carrying cytotoxic payloads to their targets. Pancreatic ductal adenocarcinoma (PDAC) has been targeted using a plectin-1 targeting peptide (KTLTP). Plectin-1 is expressed on the surface of PDAC but only within the cytoplasm of healthy cells. The modification of this peptide with a tyrosine and a cysteine residue (KTLTPYC) allows for the use of this peptide to simultaneously reduce gold(III) chloride under basic conditions to initiate the nucleation of AuNPs (Tyr), and to cap the resulting nanoparticles with the thiol side chain of cysteine. This addition of a dipeptide that simultaneously nucleates and caps AuNPs is a unique modality for peptides

over all other targeting agents. These AuNPs were further functionalised with the chemotherapeutic drug gemcitabine (Gem), which adsorbs to the AuNP core through hydrophobic interactions, as well as forming a reversible Au-N bond. These AuNPs show higher cytotoxicity towards PDAC cell lines than Gem alone and display excellent selectivity for PDAC cells over healthy tissue in mouse models.¹⁰³ This use of the YC dipeptide to simultaneously nucleate and cap AuNPs has also been used to form AuNPs for use as radiosensitisers. These AuNPs are targeted towards $\alpha_v\beta_3$ integrin expressing cells through the cyclic peptide c(RGD) (Scheme 1.1).¹⁰⁴

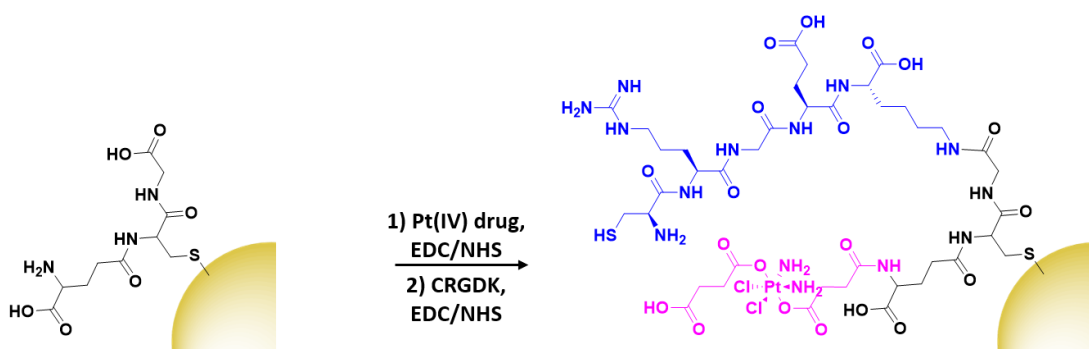


Scheme 1.1: the synthesis of cRGD directed AuNPs using a YC dipeptide (blue) to nucleate and cap the AuNPs [adapted from ref. 104]

RGD, and its cyclic derivative c(RGD), can be used to direct AuNPs to a wide variety of cancers as $\alpha_v\beta_3$ integrin is expressed by proliferating endothelial cells involved in angiogenesis.¹⁰⁵ The enhanced rate of angiogenesis in cancerous tissues means there is a high expression of $\alpha_v\beta_3$ integrin in most endothelial cancers. RGD is possibly the most well-known targeting peptide and this tripeptide highlights the ability to produce very small targeting peptides towards receptors while maintaining selectivity. Both RGD and cRGD have been shown to selectively direct AuNPs towards a variety of cancers, where these AuNPs can act as radiosensitisers.^{106,107} c(RGD) has been used to deliver siRNA to cervical cancer models to silence E6, an oncoprotein that inactivates p53. The cRGD peptide is conjugated to a PEG-poly-lysine block copolymer, which is utilised to bind the siRNA through steric repulsion and ionic pairings. Here, the ligand itself acts as the drug carrier and increased siRNA is observed intracellularly for cells treated with cRGD functionalised siRNA-AuNPs over cRAD functionalised siRNA-AuNPs; a substituted peptide sequence used as a control. The targeting ability of cRGD was further confirmed by pre-incubating cells with cRGD before the addition of cRGD-siRNA-AuNPs, with a much lower siRNA uptake observed.¹⁰⁸

The peptide CRGDK is specific towards neuropilin-1 (Nrp-1), a transmembrane glycoprotein that acts as a co-receptor for many ligands and regulates the internalisation

of membrane receptors. CRGDK has been used to direct AuNPs carrying the therapeutic peptide p12 (TSFAEYWNLSP) towards Nrp-1 expressing breast cancers,¹⁰⁹ and CRGDK-AuNPs carrying a platinum(IV) (Pt(IV)) agent have been directed towards prostate cancers (**Scheme 1.2**).¹¹⁰ p12 inhibits the binding of MDM2/MDMX to p53, a tumour suppressor, but it cannot penetrate the cell membrane, while Pt(IV) acts as a chemotherapeutic. Increased cytotoxicity was observed with increased Nrp-1 expression, and pre-treatment of cells with an Nrp-1 antibody resulted in reduced uptake of these nanoparticles, confirming the CRGDK peptide is targeting these AuNPs towards Nrp-1 overexpressing cells,^{109,110} highlighting the ability of short peptide sequences to selectively target an oncogenic receptor.



Scheme 1.2: Synthesis of CRGDK (blue) directed AuNPs carrying a Pt(IV) payload (pink). Ligands are conjugated to glutathione capping agent through EDC/NHS

The EGFR targeting peptide GE11 (YHWYGYTPQNVI) has been used to deliver AuNPs carrying the photosensitiser Pc4 to EGFR overexpressing glioblastoma cells. PEG-AuNPs were synthesised and conjugated with GE11 before Pc4 was adsorbed onto the surface of the AuNP. These nanoconjugates displayed minimal dark toxicity and significant phototoxicity in glioblastoma cells. Interestingly, it was found that few nanoparticles were accumulating within the cells, however the concentration of Pc4 internalised by these cells was seen to be dependent on the binding of GE11. Pre-incubation of the cells with GE11 reduced uptake of Pc4 into these glioblastoma cells, and therefore it was hypothesised that while the AuNPs themselves were not being internalised. It is thought that the increased interaction of these directed AuNPs with the surface of glioblastoma cells allows for the Pc4 to desorb from the nanoparticle and accumulate within glioblastoma cells.^{111,112} As these nanoparticles are designed to pass through the blood brain barrier (BBB), it is vital that their size is maintained as small as possible. The relatively small size of peptides over antibodies and other proteins is

beneficial here, and GE11 shows an affinity for the EGFR receptor only 10-fold lower than that of its natural ligand EGF, highlighting the applicability of peptides as targeting agents.

The small size and fully characterised structure of peptides provides a benefit over antibodies and other proteins. The relative stability of peptides over antibodies and other proteins means they can either be conjugated to linkers after their attachment to AuNPs or before their use for ligand exchange. Again, as with antibodies and other proteins, the use of EDC/NHS and their derivatives is very popular for peptide conjugation. As peptides are synthetically produced, their structures can be easily modified for attachment of reactive moieties. This allows for the attachment of thiols through cysteine residues that have been used to conjugate peptides directly to the gold core or to conjugate a peptide onto a linker. A summary of reported peptide conjugation techniques is listed in **Table 1.2**. Most notably, the use of peptides allows site specific conjugation of the targeting moiety to AuNPs. This ensures that the peptides are attached to the AuNPs in a way that maintains their binding capability towards their target.

Table 1.2: Reported methodologies for peptide conjugation to AuNPs

Coupling agent(s)	Linker	Notes
EDC/(sulfo)-NHS	Tiopronin ¹⁰⁹	AuNPs capped with linkers then peptides conjugated onto AuNP system
	Glutathione ¹¹⁰	
	HS-PEG-COOH ^{111,112}	
EDC	HS-PEG-COOH ¹⁰⁶	
None	HS-PEG-NHS ^{113,114}	Peptide conjugated to PEG, then used in AuNP synthesis mixture as capping agent
SPDP	Chitosan ¹¹⁵	Peptide conjugated to Chitosan, then added to AuNPs through ligand exchange
Maleimide	Adamantane (Ad)-PEG-maleimide ¹⁰⁷	Peptide added to linker before ligand exchange onto AuNPs
Cysteine	None ¹⁰⁶	AuNPs synthesised then peptide added through Au-S bond by ligand exchange

1.4.4 Aptamer directed gold nanoparticles

Aptamers are short, single stranded DNA or RNA sequences selected from a random pool of oligonucleotides. They form secondary structures through complementary base pairings that allow for selective binding towards specific receptors, proteins and small molecules (**Figure 1.13**), with an affinity for their target close to that of an antibody.^{116,117}

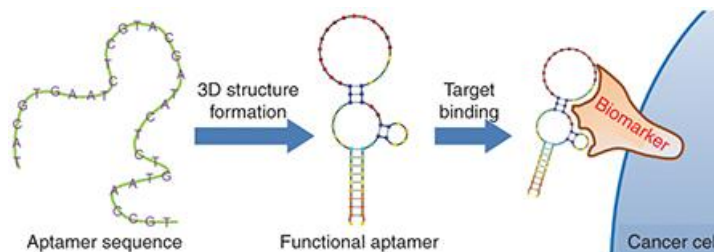


Figure 1.13: Aptamers as targeting moieties: the folding of aptamers through complementary base pairings results in secondary structures that are highly specific towards target receptors [reproduced from ref. 118]

Aptamers can be chemically synthesised and easily modified to improve their pharmacokinetics and stability, and therefore, since their development in the 1990s, have been viewed as an attractive alternative to antibodies.¹¹⁹ The synthetic production of aptamers means that most reports of aptamer-functionalised AuNPs use thiolated aptamers for direct attachment to the gold core (**Figure 1.14**), however one example does exist of amide bond formation to a PEG shell.¹²⁰

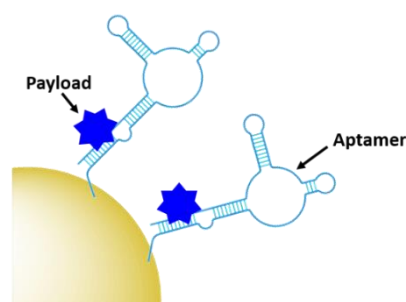


Figure 1.14: Generic structure of aptamer-directed AuNPs. Aptamers are generally attached directly to the gold core, with the payload loaded onto the aptamer

A plethora of aptamers have been designed for various targets, however only a select few of these have been applied to the delivery of AuNPs. The most widely explored aptamer for AuNP targeting is AS1411 – a 26-base guanine rich aptamer that targets nucleolin, a phosphoprotein overexpressed by cancerous cells. Nucleolin is expressed on the nucleus of healthy cells, but malignant mutation often leads to the translocation of this receptor

onto the surface of cancerous cells. The guanine rich sequence of AS1411 leads to the formation of a G-quadruplex structure that is selective towards nucleolin. AS1411 induces an anti-proliferative effect within cells itself, and this in combination with its targeting ability increases the efficacy of a therapy. AS1411 has been used for the delivery of AuNPs for PTT,¹²⁰ radiotherapy¹²¹ and to deliver AuNPs carrying Dox with nucleolin selective cell death observed.¹²² As AS1411 forms a G-quadruplex in the presence of potassium, the aptamer can be used to bind the photosensitiser N-methylmesoporphyrin IX (NMM), a G-quadruplex DNA binding ligand. The thiolation of this aptamer allows for its direct addition to the surface of AuNPs and these nanoconjugates were seen to be selectively internalised by cancer cells overexpressing nucleolin, with no uptake observed in nucleolin negative normal cell lines.¹²³ This example is particularly interesting as it utilises the aptamer sequence not only as a targeting moiety but also as a drug carrier. A second example of this involves the conjugation of the photosensitiser chlorin *e*₆ (Ce6) to the aptamer sgc8c, a protein tyrosine kinase 7 (PTK7) selective aptamer, to selectively target it towards leukaemia cell lines. Ce6 is conjugated to the 3'-end of the sgc8c aptamer, which is conjugated to a poly-T chain at the 5'-end, which, in turn, is conjugated to a sgc8c complementary DNA (cDNA) sequence. The sgc8c cDNA is further conjugated to a gold nanorod (AuNR). This means that in the absence of PTK7, the sgc8c is hybridised with the cDNA sequence, holding Ce6 close to the AuNR and quenching its fluorescence. Upon binding to PTK7, the sgc8c forms a hairpin, losing affinity for its complementary sequence and moving the Ce6 away from the AuNR, 'switching on' its fluorescence and therefore its photodynamic activity, as shown in **Figure 1.15**. Significant targeted photodynamic activity was observed in PTK7 expressing cells, with increased cytotoxicity observed in combination with PTT.¹²⁴

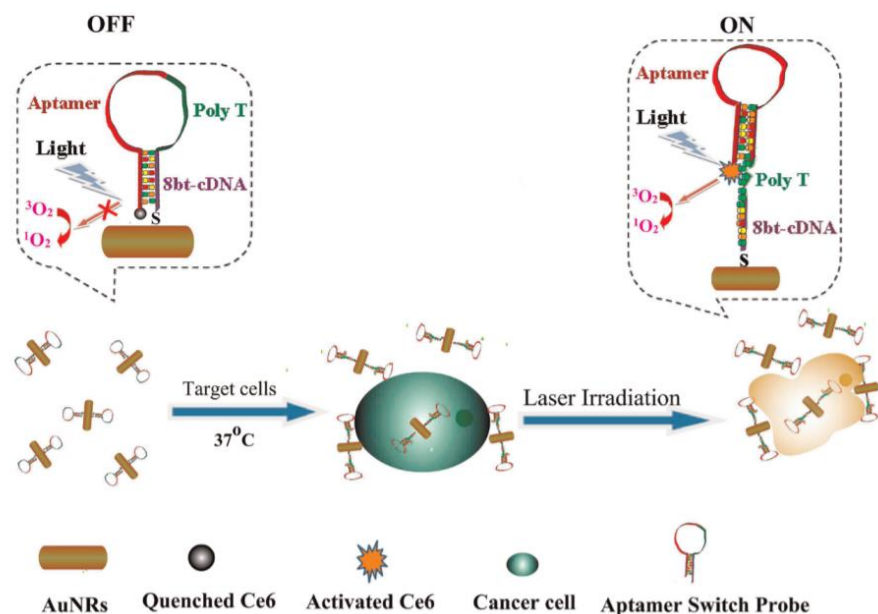


Figure 1.15: Activatable Ce6 AuNR targeted towards leukaemia cells through sgc8c aptamer [reproduced from ref. 124]

As aptamers are oligonucleotides, chemotherapeutic drugs that act by intercalating DNA can also intercalate these aptamers. Dox is a reversible DNA intercalator and therefore can be delivered to its target by binding to aptamers, notably by sgc8c and A9, a prostate specific membrane antigen (PSMA) specific aptamer.^{125,126} Here, AuNPs act as delivery systems to increase the concentration of payload delivered – multiple drug-aptamer complexes can be delivered at once, increasing the potency of one ligand finding its target. This effect has also been observed with the HER2 aptamer HApt; a trimeric aptamer that displays cytotoxicity towards HER2 overexpressing breast cancers by cross-linking HER2 receptors and sorting them for degradation. The attachment of this aptamer onto gold nanostars (AuNSs) has been shown to increase its uptake and therefore the therapeutic value of HApt.¹²⁷

Aptamers, while successful targeting moieties when used individually, have also been used in combination to target multiple receptors on a specific cancer and therefore increase the selectivity towards these cells. AS1411 has been utilised for targeting AuNPs in conjunction with sgc8c, highlighting one of the advantages of aptamers as targeting moieties. As aptamers can be synthetically designed and built to a desired specification, a polyvalent aptamer system can be designed containing both AS1411 and sgc8c.¹²⁸ The formation of a polyvalent aptamer for dual targeting displays remarkable benefits over the attachment of two individual targeting moieties as the ratio of these targeting ligands

can be completely controlled with no concerns that one aptamer may have a higher affinity for AuNPs than another. It could be possible that ligands bearing multiple aptamers, or an uneven ratio of two aptamers could be synthesised to further increase the number of receptors targeted or alter the ratio of the targeting ligands in a very controlled manner. This polyvalent aptamer was attached to AuNPs through electrostatic interactions, followed by the addition of daunorubicin (Dau), a DNA intercalating chemotherapeutic. A small amount of Dau binds to the aptamer due to its DNA intercalating ability; however, the majority is bound to the AuNP surface through electrostatic interactions. These AuNPs displayed selective cytotoxicity towards cancer cell lines expressing both nucleolin and PKT7. A synergistic effect was observed for the use of this polyvalent aptamer over AuNPs targeted with just the sgc8c aptamer,¹²⁸ highlighting a benefit of these chemically synthesised targeting moieties.

1.4.5 Carbohydrate directed gold nanoparticles

Cancer cells have been found to differentially express lectins on their surface compared to healthy cells,¹²⁹ and the affinity of carbohydrates towards these lectins can be exploited to target these cells.¹³⁰ The use of carbohydrates as targeting moieties for AuNP-based therapeutics is a new concept, with literature exploring this possibility only disclosed within the last five years. As this is such a new field, very few carbohydrate ligands have been explored.

Hyaluronic acid (HA, **Figure 1.16a**) is a naturally occurring polysaccharide consisting of a repeating unit of D-glucuronic acid and *N*-acetyl-D-glucosamine. HA selectively targets the CD44 receptor which is overexpressed by various cancers with a $K_D \approx 0.3$ nM.¹³¹ The polymeric structure of HA means that there are multiple free carboxylic acids that can be used for drug functionalisation and this has been exploited for the delivery of chemotherapeutic drugs and photosensitisers to their targets. A porphyrin photosensitiser has been conjugated onto HA alongside the fluorescent imaging agent cresyl violet and cystamine, which adds a thiol functional group for conjugation of this linker onto AuNPs (**Figure 1.16b**). Here, HA acts as both the linker and targeting moiety. When attached to AuNPs, the fluorescence of both the porphyrin and cresyl violet are quenched. Upon uptake by CD44 overexpressing cell lines, hyaluronidase enzymes can degrade the HA, releasing the attached fluorophores and allowing for both the imaging of CD44 overexpressing cancers and their targeted PDT. The uptake and cytotoxicity of these

nanoconjugates was observed to be selective towards CD44 overexpressing cancer cell lines.¹³² The highly repeated sequence of the HA polysaccharide allows HA to act as both a linker and targeting moiety, as well as allowing for functionalisation with a variety of drugs without the loss of targeting ability, a unique property of these polysaccharide targeting moieties. The photosensitiser Pheophorbide-A and the chemotherapeutic drug metformin have both been conjugated onto HA with selective uptake observed in CD44 overexpressing lung and liver cancers, respectively.^{133,134}

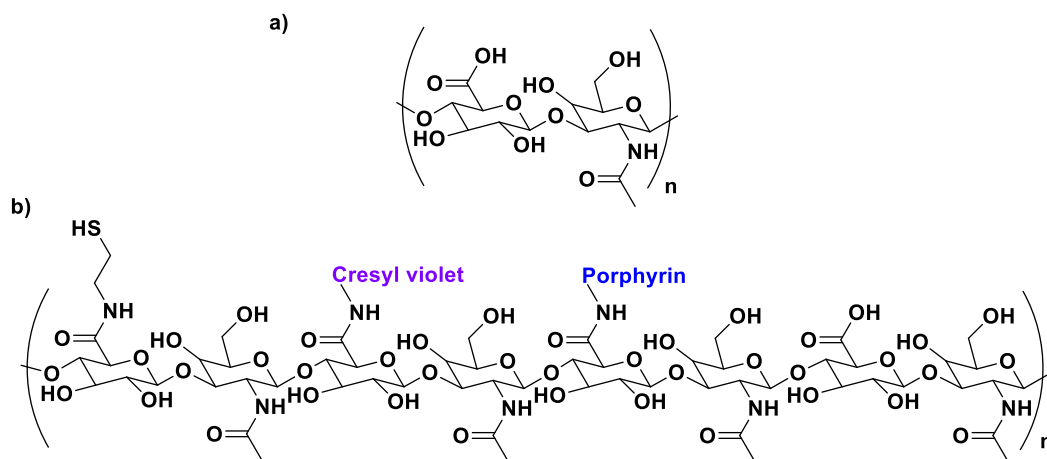


Figure 1.16: a) the repeating D-glucuronic acid & N-acetyl-D-glucosamine unit of hyaluronic acid (HA) and b) substituted HA ligand for AuNPs for the dual imaging and PDT of CD44 overexpressing cancer cells [adapted from ref. 132]

While HA is sparsely described in the literature as a targeting agent for therapeutic AuNPs, it is by far the most investigated carbohydrate ligand. One of the few examples of alternative carbohydrate ligands is that of glucose, a monosaccharide that has been shown to bind to glucose transporter-1 (GLUT1) which is overexpressed by several cancer cells. Glucose functionalised AuNPs have been used to target siRNA carrying AuNPs towards GLUT1 overexpressing breast cancers. As glucose (**Figure 1.17a**) is a monosaccharide, the technique of conjugating drugs directly to the carbohydrate as used for HA cannot be utilised. Instead, this work builds a glucose-capped ligand containing a PEG chain, followed by a 40-unit poly-lysine (PLL) chain, and terminated in lipoic acid (**Figure 1.17b**). The PEG chain acts as a spacer, while the lipoic acid provides thiols for binding to the AuNP surface. The PLL chain acts to bind siRNA through electrostatic interactions as the PLK1 siRNA used in this study contains 40 negative charges. PLK1 plays a vital role in the cell cycle of cancer cells and its knockdown leads to antitumour activity. This system was observed to specifically target GLUT1 overexpressing breast

cancer cells, with its specificity confirmed through a competition assay with the GLUT1 inhibitor phloretin.¹³⁵

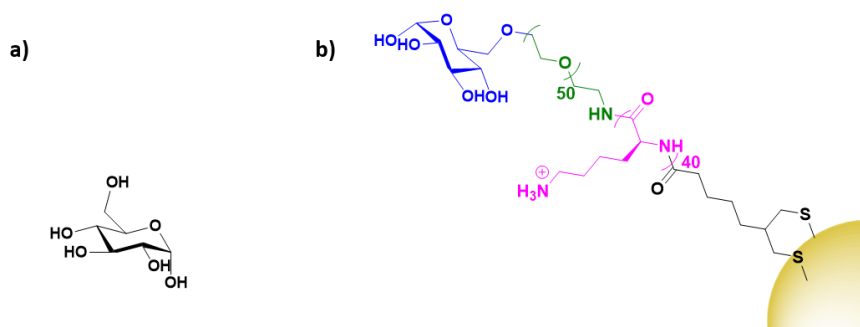


Figure 1.17: a) the structure of glucose and b) the attachment of glucose (blue) onto AuNPs through a PEG (green), PLL (pink) and lipoic acid (black) chain

Lactose (**Figure 1.18a**), a disaccharide that is recognised by the lectin galectin-1, has also been investigated as a targeting moiety for AuNP-based cancer therapeutics. It has been used to target AuNPs carrying a phthalocyanine photosensitiser towards breast cancer cells for PDT. Lactose was conjugated onto a short, thiolated PEG linker (**Figure 1.18b**) and functionalised onto the gold core in a mixed monolayer with the photosensitiser. While uptake and phototoxicity is specific towards malignant breast cells, the uptake is not determined by the presence of galectin-1.¹³⁶ This work, while demonstrating the possibility of the use of other carbohydrate based ligands as targeting moieties, requires further work to determine how this ligand is selectively targeting malignant cells.

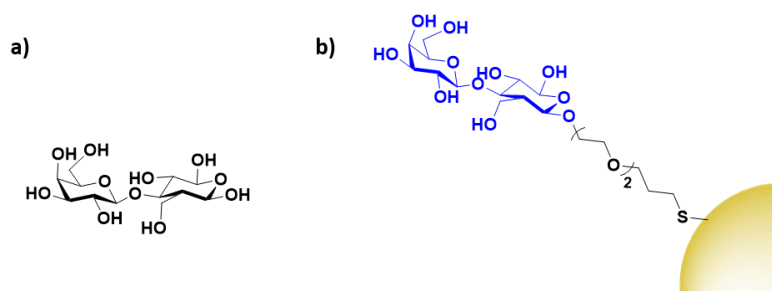


Figure 1.18: a) the structure of lactose and b) the attachment of lactose to an AuNP through a thiolated PEG linker

1.4.6 Small molecule directed gold nanoparticles

The final class of targeting moieties explored for AuNPs is small molecules, low molecular weight organic compounds that display affinity towards cell surface receptors. Benefits of small molecules include the fact that they are relatively cheap to synthesise

and generally display higher stability than the other targeting moieties discussed above. Due to their size, small molecules easily penetrate through tumours to deliver payloads to their target.

Folic acid, also known as folate, is the most commonly utilised small molecule for targeted AuNPs. It is a natural ligand towards the folate receptors, which are only accessible to the blood stream on cancerous cells and therefore useful oncogenic targets. The structure of folic acid contains two carboxylic acids (**Figure 1.19a**) which can be used for conjugation onto AuNPs. Due to the small size of folic acid, it is not possible to use this ligand to carry the payload and to conjugate it onto the AuNP itself. Folate is most commonly conjugated onto a linker such as PEG or polyethylenimine (PEI, **Figure 1.19b**) through amide bonds for attachment onto AuNPs; however, examples of using electrostatic interactions to bind folate to AuNPs do exist.¹³⁷

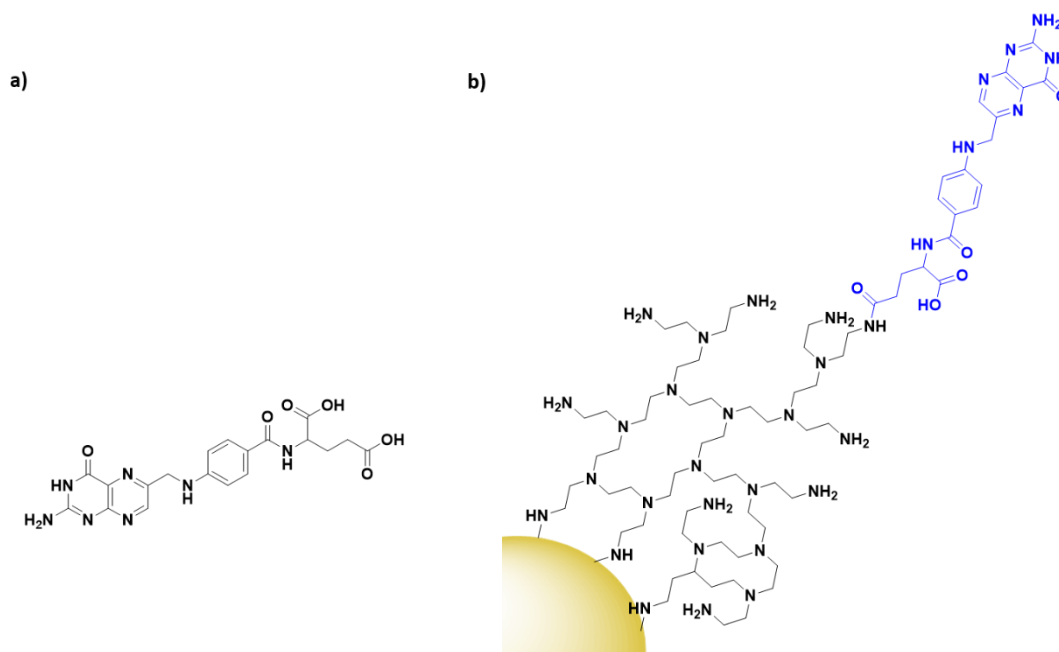


Figure 1.19: a) The structure of folic acid and b) the conjugation of folic acid (blue) onto PEI (black) functionalised AuNPs

Covalently bound folic acid has been used to deliver AuNPs carrying siRNA, photosensitisers and chemotherapeutic drugs to various cancers.^{138–140} The use of folic acid-AuNPs to deliver chemotherapeutics often relies on electrostatic interactions between the drug, such as Dox, and the surrounding ligands, such as pectin. The release of Dox from these AuNPs has been shown to increase at lower pH due to the protonation of the negatively charged pectin shell and therefore a loss of the electrostatic interaction.

The pH of tumour cells is pH 5.4, compared to 7.4 of the blood-stream, so this is a favourable characteristic for drug release in the tumour site. While in this case the AuNPs act solely as a delivery system, an increased cytotoxicity is observed for AuNP bound Dox compared to that of free Dox.¹⁴¹ As well as increasing the potency of chemotherapeutic effects, AuNPs allow for combination therapies between chemotherapeutics and PTT, with the synergistic effect resulting in increased cytotoxicity, and the folate ligand providing selectivity towards folate receptor positive tumours.^{140,142} Interestingly, for the development of folate-targeted AuNP therapies, there are many examples that display increased cytotoxicity upon the addition of folic acid,^{139,141} however no control folate receptor negative cell line or competition assay is run to prove that this increase in cytotoxicity is indeed receptor mediated and selective towards folate receptor overexpressing cancers. To assess the true benefits of folate-targeting AuNPs it is vital that the selectivity of these nanoconjugates is fully assessed, as this increase in cytotoxicity may be due to increased passive penetration and therefore these approaches may not provide any gain over non-targeted AuNPs.

While most examples of small molecule targeted AuNP therapies use folate as their targeting moiety, examples exist using other small molecules. Anisamide is known to bind to the sigma receptor which is overexpressed in prostate cancer and has been used to deliver AuNPs carrying siRNA to their target. Anisamide (**Figure 1.20a**) is a synthetically produced small molecule derived from anisole, a naturally occurring molecule found in aniseed oil.¹⁴³ The use of anisamide highlights another advantage of small molecules – they can be easily modified through structure-activity relationship studies to optimise their binding towards a target and remove unnecessary complexities from molecules that are not involved in the binding to a receptor. As with folic acid, anisamide lacks conjugation sites, meaning the siRNA is attached through electrostatic interactions with a PEI coating on the gold core (**Figure 1.20b**). The anisamide itself is synthesised by conjugating anisic acid to PEI ligands on these nanoparticles. For siRNA delivery, non-covalent attachment appears to be the most efficient delivery system as the siRNA can diffuse away upon internalisation by cancerous cells where the pH is decreased, and the PEI becomes deprotonated. Anisamide-AuNPs-siRNA are shown to trigger apoptosis due to mRNA knockdown, with this cytotoxicity observed to be receptor mediated.^{144,145}

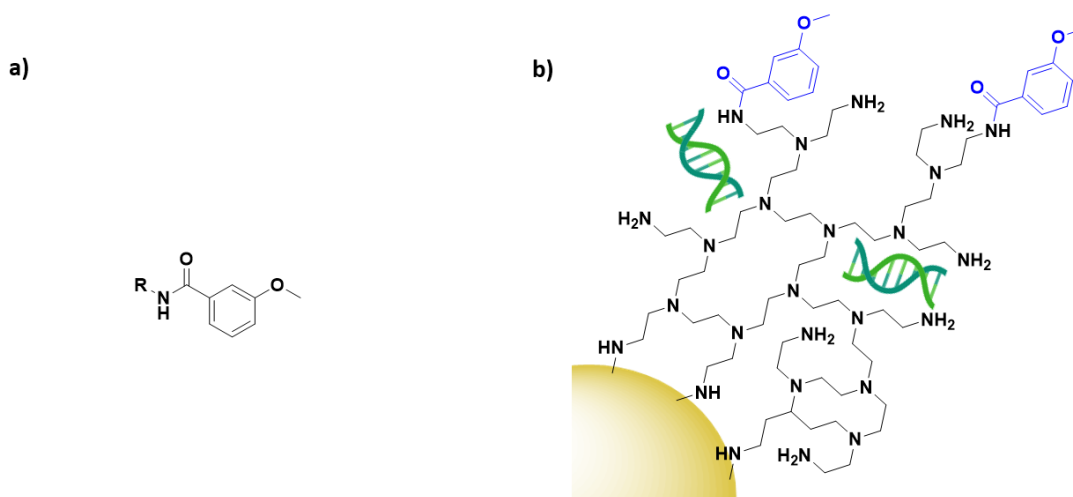


Figure 1.20: The structures of **a)** anisamide and **b)** anisamide (blue) conjugated onto AuNPs through PEI (black), with the siRNA payload (green) electrostatically coordinated to the PEI coating

α - and β -bicalutamide (**Figure 1.21**) are antiandrogens, small molecules known to bind the androgen-sensing G protein coupled receptor GPRC6A and the membrane androgen receptor (MAR), both expressed by prostate cancers. These antiandrogens are currently clinically used for chemotherapy of prostate cancer; however, their attachment onto PEGylated AuNPs has shown selective cytotoxicity in MAR/GPRC6A positive chemoresistant prostate cells.¹⁴⁶ In the work reported, the use of a selective chemotherapeutic drug as the targeting moiety for AuNP delivery displays the benefits of AuNPs as delivery vehicles. This ability of AuNP conjugation to increase the uptake of already selective chemotherapeutic drugs through multivalent binding is a very attractive prospect.

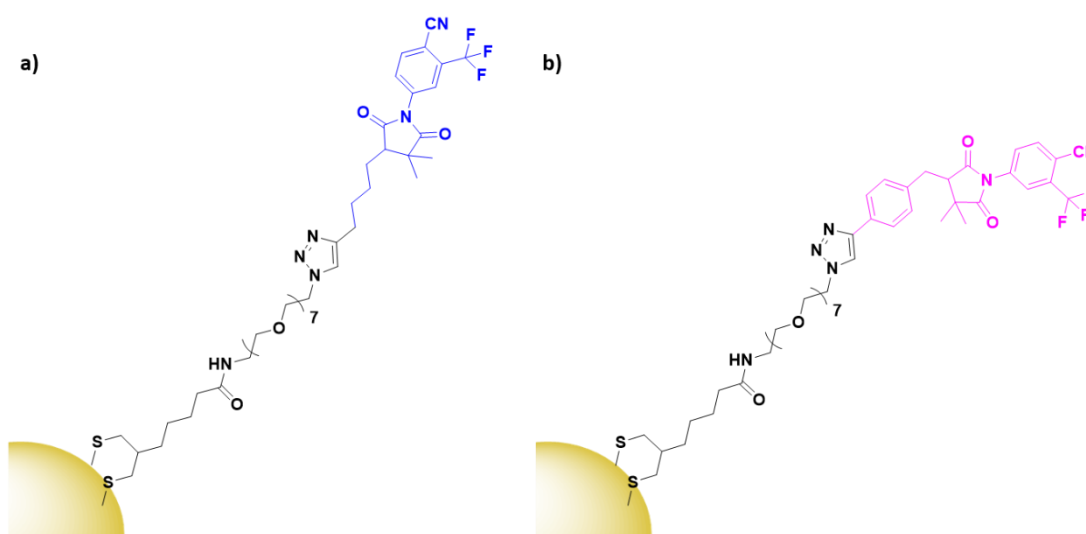


Figure 1.21: Structures of **a)** α -bicalutamide (blue) and **b)** β -bicalutamide (pink) AuNPs, conjugated through a PEG linker (black)

1.4.7 Gold nanoparticles with multiple targeting modalities

The multivalency of AuNPs provides the opportunity to functionalise them with multiple directing moieties to target multiple receptors, and these targeting moieties do not have to be of the same class. Gold nanostars (AuNSs) have been functionalised with a mixed monolayer of the aptamer A10 and the peptide DUP-1 (**Figure 1.22**). A10 is PSMA specific and DUP-1 binds to an unknown sight on prostate carcinomas. It was found that the combination of these targeting modalities allowed for selective targeted PTT of prostate cancers, regardless of their PSMA expression.¹⁴⁷

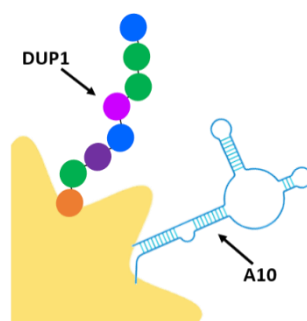


Figure 1.22: Gold nanostars functionalised with a DUP-1 peptide and the aptamer A10 for the photothermal therapy of prostate cancers

AuNPs carrying the ribosome inactivating protein curcin have been targeted towards glioblastoma using a combination of folic acid and an anti-transferrin antibody. Glioblastomas overexpress both the FR α and the transferrin receptors. Increased uptake was observed for the dual targeted AuNPs compared to AuNPs functionalised with just folic acid, highlighting the benefit of dually targeting these nanocarriers. Selective cytotoxicity was observed in glioblastoma cells, and the use of curcin was seen to display a synergistic cytotoxicity when delivered by AuNPs that were subsequently used for PTT.¹⁴⁸ These examples highlight the benefits of targeting multiple receptors to either widen the therapeutic value of an AuNP system to a higher percentage of a certain cancer type, or to use the synergistic targeting abilities of two moieties to increase specificity towards a target. Most importantly here, these results show that these targeting modalities can be mixed and matched to enhance the targeting ability of AuNPs without interfering with each other, allowing for a large variety in targeting combinations to establish the best possible treatment for specific cancers.

1.5 Conclusion and future outlook

Non-small cell lung cancer (NSCLC) is the leading cause of cancer related deaths worldwide. Current treatment options involve surgery, chemotherapy or radiotherapy, all of which cause significant damage to the lungs and have devastating side effects. Photodynamic therapy is a cancer treatment that is relatively non-invasive with minimal side effects, and for these reasons it could improve the quality of life for NSCLC patients. The photosensitiser Photofrin[®] has been used to treat NSCLC to good effect, with a complete response rate of *ca.* 78% observed. While this is a positive result, the lack of selectivity of Photofrin[®] has been connected to side effects such as erythema, fibrosis and cicatricial stenosis. Photofrin[®] is a first-generation photosensitiser and is known to show increased retention in the body. The development of second-generation photosensitisers has led to a reduction in retention in the body and improved singlet oxygen quantum yields. These photosensitisers may provide favourable characteristics for the PDT of NSCLC. Second-generation photosensitisers, however, are notoriously hydrophobic and difficult to deliver intravenously. While many delivery systems have been explored for the delivery of hydrophobic photosensitisers, perhaps the most exciting of these is the use of gold nanoparticles (AuNPs).

AuNPs present themselves as ideal drug carriers due to their biocompatibility, easy functionalisation with various ligands, their easily tuned size and shape and their enhanced absorption characteristics due to their SPR. While AuNPs display passive targeting towards tumours through the EPR effect, with the current trend in developing personalised medicines, the active targeting of AuNPs towards tumours is growing in popularity. Oncogenes expressed on the surface of cancer cells can be directly targeted by antibodies, proteins, peptides, aptamers, carbohydrates and small molecules, and their attachment onto AuNPs leads to selective uptake through receptor mediated endocytosis. The benefits and disadvantages of these targeting moieties is summarised in **Table 1.3**.

Table 1.3: A summary of the advantages and disadvantages of different targeting moieties for targeted AuNP-therapeutics

Targeting moiety	Advantages	Disadvantages
Antibodies	Extremely high selectivity and affinity towards receptors, relatively long circulatory half-life	Low tumour penetration, can elicit immune response, sensitive to pH and temperature, expensive to produce, not well chemically defined, random conjugation unless specifically engineered, crosslinking can occur
Proteins	High affinity towards receptors	High competition from native proteins, sensitive to pH and temperature, random conjugation unless specifically engineered, crosslinking can occur
Peptides	Rapid uptake kinetics, high penetration, synthetic hence easy to modify, easy and well-defined conjugation sites	Lower affinity towards receptors, can be rapidly degraded by peptidases
Aptamers	Extremely high affinity towards receptors and selectivity, synthetic hence easy to modify, payloads can be conjugated to the ligand, can be therapeutic	Low stability in circulation, lower penetration than peptides, carbohydrates and small molecules, hard to target hydrophobic or negatively charged receptors
Carbohydrates	High affinity, synthetic so can be modified, payloads can be conjugated to the ligand	Recognised by multiple receptors so some specificity lost, synthesis much more taxing than peptides and small molecules
Small molecules	High circulatory half-life, high penetration, synthetic so easy to modify, can be therapeutic	Lower affinity towards receptors

Antibodies are most commonly conjugated onto AuNPs through water soluble ligands, with the payload conjugated to the core instead of the antibody itself (**Figure 1.23a**). Antibodies are perhaps the most widely investigated targeting moiety to functionalise AuNPs due to their extremely high selectivity and affinity towards their target receptors. The use of antibodies is, however, expensive compared to most other targeting moieties and they display low tumour penetration due to their large size. Antibody fragments and nanobodies are now widely investigated to combat this low penetration, however this decrease in size reduces the circulatory lifetime.

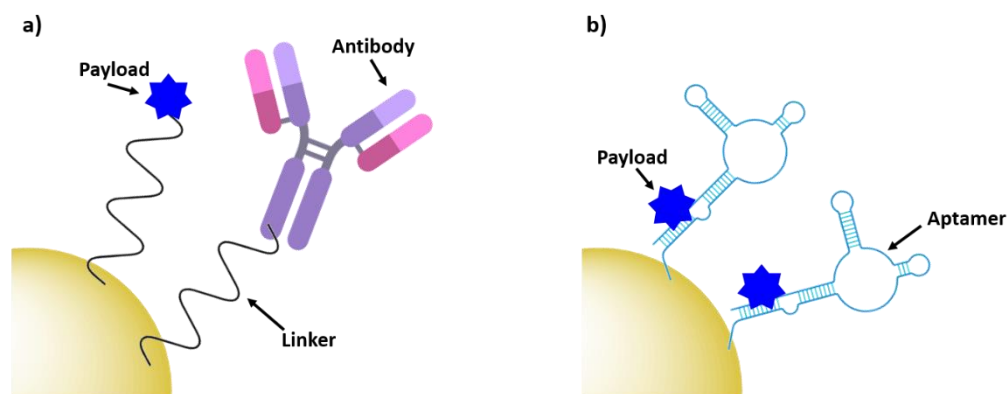


Figure 1.23: Generic structures of **a)** antibody and **b)** aptamer directed AuNPs

Aptamers display receptor affinity close to that of an antibody and due to this they highlight themselves as a very good alternative to antibodies. Aptamers display higher stability than antibodies towards organic solvents and pH which is ideal for the synthesis of nanocarriers. They are also chemically synthesised which allows for easier modification and characterisation than antibodies, and payloads can be directly attached to these targeting moieties (**Figure 1.23b**). These synthetic targeting moieties allow for the synthesis of ligands bearing multiple targeting moieties, which could allow for the targeting of multiple receptors with one nanocarrier. Aptamers can themselves elicit anti-tumour effects, and therefore can act as both a targeting moiety and a drug. Payloads can also be directly attached to aptamers without effecting their affinity to a receptor, providing an alternative method for payload delivery on AuNPs as they do not have to be directly bound to the gold core. While these benefits highlight aptamers as a highly beneficial targeting moiety, they display low stability in circulation due to nucleases in blood plasma.¹⁴⁹ Due to the inherent negative charge of aptamers, they cannot be developed to target receptors that display negatively charged surfaces, providing severe limitations to these targeting moieties.

Protein ligands are also investigated as targeting moieties, displaying a high affinity towards their target. The synthesis of therapeutic protein-AuNPs usually involves the protein and payload separately conjugated to the core through linkers (**Figure 1.24a**). Their affinity towards receptors is generally lower than that of antibodies and aptamers and their relative abundance in the body perhaps reduces their efficacy as there is a lot of natural competition for a binding site.

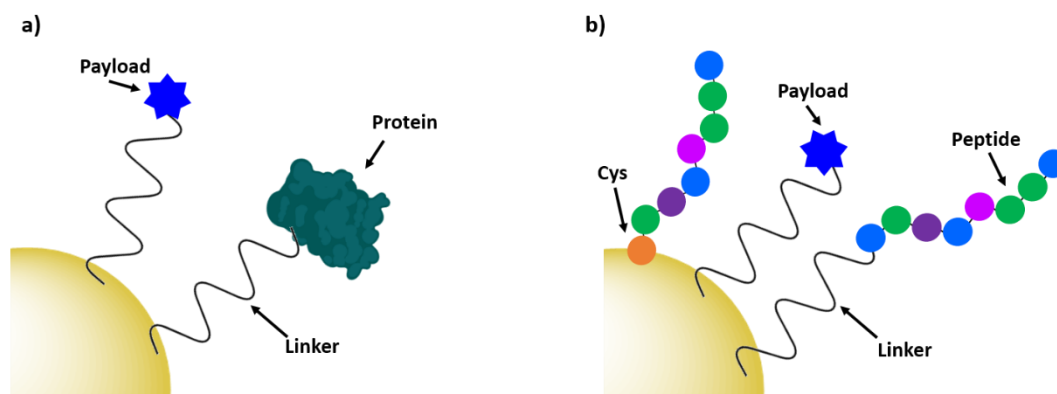


Figure 1.24: Generic structures of **a)** protein and **b)** peptide directed AuNPs

The low penetration of antibodies and other proteins into tumours has led to the investigation of peptides as targeting moieties. While peptides generally show a lower affinity towards the target receptor, the small size of peptides means they display rapid uptake into targeted cells and high penetration into tumours, and this uptake is also higher than that of aptamers. The small size of peptides means they can be synthesised, which allows for ease of modification and control over the binding of these peptides onto nanocarriers (**Figure 1.24b**). This allows for site-specific conjugation of peptides onto AuNPs and ensures that the amino acids vital for receptor binding remain exposed, a benefit over antibodies and proteins where the conjugation onto AuNPs is completely random and these binding sites could be blocked. Peptides are also more stable towards pH and organic solvents than antibodies, which increases the ease of synthesis of peptide targeted nanocarriers. While their uptake and versatility is high, peptides display a low circulatory half-life due to peptidases in blood plasma,¹⁵⁰ and their half-life is similar to that of aptamers.

The expression of lectins on the surface of cancerous tissue has recently led to the investigation of carbohydrates as targeting moieties for AuNPs. Carbohydrate ligands are either attached directly to the gold core or conjugated through linkers (**Figure 1.25a**). Carbohydrates display high affinities towards their targets and, while their synthesis is taxing, they can be modified to fit the desired purpose prior to attachment onto a nanocarrier system. Highly polymeric carbohydrates such as hyaluronic acid allow for the attachment of payloads onto the targeting ligand itself and, as with aptamers, this provides an interesting alternative to directly binding a payload to the gold core, which may display significant advantages for some payloads. The relative lack of investigation into these

targeting moieties means that it is hard to conclude on the impact these ligands may have, however some carbohydrates display affinity towards multiple receptors, and this can decrease the efficacy of carbohydrate directed therapeutics and lead to off-target effects.

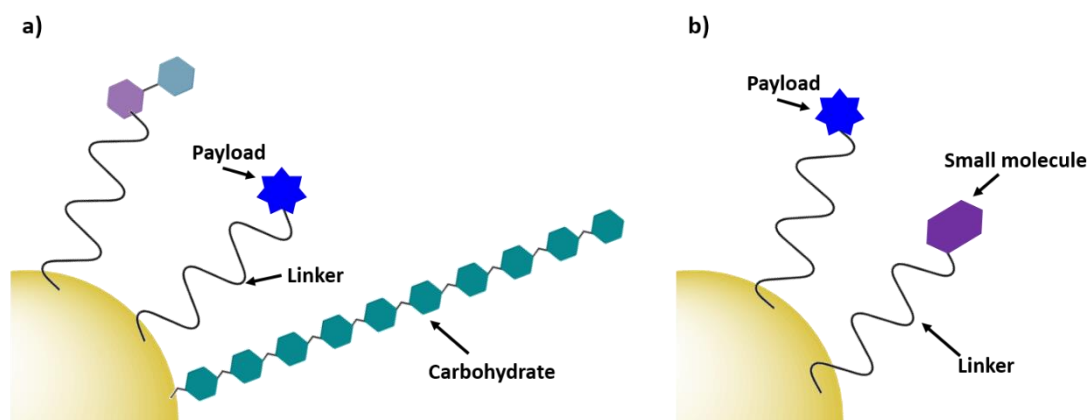


Figure 1.25: Generic structures of **a)** carbohydrate and **b)** small molecule directed AuNPs

Small molecules are low molecular weight organic compounds that display increased circulatory stability over other targeting moieties as they are not degraded by peptidases or nucleases found in the blood stream. Due to the size of small molecules, they have limited conjugation sites, so both the small molecules and payloads tend to be conjugated onto AuNPs through linkers (**Figure 1.25b**). The size of small molecules means that they generally display high tumour penetration, and small molecules can themselves illicit a therapeutic effect upon internalisation. Small molecules, however, generally display a lower affinity and selectivity towards their target than antibodies, proteins and aptamers.

While each of these targeting modalities presents their own unique characteristics and advantages (**Table 1.3**) there is very little work comparing the ability of these modalities to deliver AuNPs. This lack of comparison makes it difficult to conclude whether the benefits of one targeting moiety outweigh the disadvantages of another, and to continue to push this field forward, comparisons between different targeting modalities for the same receptor are needed to determine the most effective approach.

1.6 Thesis outline

The research in this thesis investigates targeting moieties for the delivery of phthalocyanine-gold nanocarriers to non-small cell lung cancer. Firstly, in **chapter 2**, peptides were investigated for the delivery of AuNPs to EGFR overexpressing NSCLC

cell lines. Two EGFR targeting peptides were investigated and modified for efficient conjugation onto AuNPs. This work led to the investigation of optimum synthetic conditions for the synthesis of peptide-phthalocyanine AuNPs, followed by comparison of the singlet oxygen production and phototoxicity of the produced nanoconjugates. The selectivity of the successful nanoconjugates towards EGFR overexpressing NSCLC cell lines was determined.

Chapter 3 describes an investigation into conjugation strategies for the addition of antibodies onto phthalocyanine-gold nanocarriers. The chemical conjugation strategies of EDC/NHS and maleimide-thiol were investigated, before the use of adaptor proteins and their peptide mimics for Fc-selective antibody conjugation was explored.

The use of folic acid as a targeting agent is explored in **chapter 4**. An investigation into coupling chemistries and synthetic manipulations of folic acid was carried out to ensure folate was conjugated onto phthalocyanine-gold nanocarriers in its active form. Folic acid was shown to quench the singlet oxygen production of these phthalocyanine-AuNPs, so steps towards a protease cleavable linker were taken to produce a folate-directed system in which the photodynamic activity would be ‘switched on’ intracellularly. Finally, **chapter 5** gives a detailed description of the materials, instruments and experimental procedures used throughout this research.

1.7 References

- (1) Brown, S. B.; Brown, E. A.; Walker, I. The Present and Future Role of Photodynamic Therapy in Cancer Treatment. *Lancet Oncol.* **2004**, *5* (8), 497–508.
- (2) Ethirajan, M.; Chen, Y.; Joshi, P.; Pandey, R. K. The Role of Porphyrin Chemistry in Tumor Imaging and Photodynamic Therapy. *Chem. Soc. Rev.* **2011**, *40* (1), 340–362.
- (3) Josefsen, L. B.; Boyle, R. W. Unique Diagnostic and Therapeutic Roles of Porphyrins and Phthalocyanines in Photodynamic Therapy, Imaging and Theranostics. *Theranostics* **2012**, *2* (9), 916–966.
- (4) Wang, S.; Gao, R.; Zhou, F.; Selke, M. Nanomaterials and Singlet Oxygen Photosensitizers: Potential Applications in Photodynamic Therapy. *J. Mater. Chem.* **2004**, *14* (4), 487–493.
- (5) Juarranz, Á.; Jaén, P.; Sanz-Rodríguez, F.; Cuevas, J.; González, S. Photodynamic Therapy of Cancer. Basic Principles and Applications. *Clin. Transl. Oncol.* **2008**, *10* (3), 148–154.
- (6) Robertson, C. A.; Evans, D. H.; Abrahamse, H. Photodynamic Therapy (PDT): A Short Review on Cellular Mechanisms and Cancer Research Applications for

- PDT. *J. Photochem. Photobiol. B Biol.* **2009**, *96* (1), 1–8.
- (7) Korbek, M.; Kros, G. Cellular Levels of Photosensitizers in Tumours: The Role of Proximity to the Blood Supply. *Br. J. Cancer* **1994**, *70* (4), 604–610.
- (8) Moan, J.; Berg, K. The Photodegradation of Porphyrins in Cells Can Be Used to Estimate the Lifetime of Singlet Oxygen. *Photochem. Photobiol.* **1991**, *53* (4), 549–553.
- (9) Chatterjee, D. K.; Fong, L. S.; Zhang, Y. Nanoparticles in Photodynamic Therapy: An Emerging Paradigm. *Adv. Drug Deliv. Rev.* **2008**, *60*, 1627–1637.
- (10) Camerin, M.; Moreno, M.; Marín, M. J.; Schofield, C. L.; Chambrier, I.; Cook, M. J.; Coppellotti, O.; Jori, G.; Russell, D. A. Delivery of a Hydrophobic Phthalocyanine Photosensitizer Using PEGylated Gold Nanoparticle Conjugates for the in Vivo Photodynamic Therapy of Amelanotic Melanoma. *Photochem. Photobiol. Sci.* **2016**, *15* (5), 618–625.
- (11) Plaetzer, K.; Krammer, B.; Berlanda, J.; Berr, F.; Kiesslich, T. Photophysics and Photochemistry of Photodynamic Therapy: Fundamental Aspects. *Lasers Med. Sci.* **2009**, *24* (2), 259–268.
- (12) Lucky, S. S.; Soo, K. C.; Zhang, Y. Nanoparticles in Photodynamic Therapy. *Chem. Rev.* **2015**, *115* (4), 1990–2042.
- (13) Bonnett, R. Photosensitizers of the Porphyrin and Phthalocyanine Series for Photodynamic Therapy. *Chem. Soc. Rev.* **1995**, *24*, 19–33.
- (14) Byrne, C. J.; Marshallsay, L. V.; Ward, A. D. The Composition of Photofrin II. *J. Photochem. Photobiol. B Biol.* **1990**, *6*, 13–27.
- (15) Agostinis, P.; Berg, K.; Cengel, K. A.; Foster, T. H.; Girotti, A. W.; Gollnick, S. O.; Hahn, S. M.; Hamblin, M. R.; Juzeniene, A.; Kessel, D.; et al. Photodynamic Therapy of Cancer: An Update. *CA. Cancer J. Clin.* **2011**, *61* (4), 250–281.
- (16) Macdonald, I. J.; Dougherty, T. J. Basic Principles of Photodynamic Therapy. *J. Porphyr. Phthalocyanines* **2001**, *5*, 105–129.
- (17) Peng, Q.; Warloe, T.; Berg, K.; Moan, J.; Kongshaug, M.; Giercksky, K.-E.; Nesland, J. M. 5-Aminolevulinic Acid-Based Photodynamic Therapy. *Cancer* **1997**, *79* (12), 2282–2308.
- (18) Allison, R. R.; Downie, G. H.; Cuenca, R.; Hu, X.-H.; Childs, C. J.; Sibata, C. H. Photosensitizers in Clinical PDT. *Photodiagnosis Photodyn. Ther.* **2004**, *1*, 27–42.
- (19) Mitra, S.; Foster, T. H. Photophysical Parameters, Photosensitizer Retention and Tissue Optical Properties Completely Account for the Higher Photodynamic Efficacy of Meso-Tetra-Hydroxyphenyl-Chlorin vs Photofrin. *Photochem. Photobiol.* **2005**, *81*, 849–859.
- (20) Allison, R.; Moghissi, K.; Downie, G.; Dixon, B., K. Photodynamic Therapy (PDT) for Lung Cancer. *Photodiagnosis Photodyn. Ther.* **2011**, *8*, 231–239.
- (21) Hopper, C. Photodynamic Therapy: A Clinical Reality in the Treatment of Cancer. *Lancet Oncol.* **2000**, *1* (4), 212–219.
- (22) Nyman, E. S.; Hynninen, P. H. Research Advances in the Use of Tetrapyrrolic Photosensitizers for Photodynamic Therapy. *J. Photochem. Photobiol. B Biol.* **2004**,

- 73 (1), 1–28.
- (23) Isakau, H. A.; Parkhats, M. V.; Knyukshto, V. N.; Dzhagarov, B. M.; Petrov, E. P.; Petrov, P. T. Toward Understanding the High PDT Efficacy of Chlorin E6–polyvinylpyrrolidone Formulations: Photophysical and Molecular Aspects of Photosensitizer–polymer Interaction in Vitro. *J. Photochem. Photobiol. B Biol.* **2008**, *92* (3), 165–174.
- (24) Allen, C. M.; Sharman, W. M.; Van Lier, J. E. Current Status of Phthalocyanines in the Photodynamic Therapy of Cancer. *J. Porphyr. Phthalocyanines* **2001**, *05* (02), 161–169.
- (25) Choi, C.-F.; Huang, J.-D.; Lo, P.-C.; Fong, W.-P.; Ng, D. K. P. Glycosylated Zinc(II) Phthalocyanines as Efficient Photosensitizers for Photodynamic Therapy. Synthesis, Photophysical Properties and in Vitro Photodynamic Activity. *Org. Biomol. Chem.* **2008**, *6* (12), 2173.
- (26) Conte, C.; Ungaro, F.; Mazzaglia, A.; Quaglia, F. Photodynamic Therapy for Cancer: Principles, Clinical Applications, and Nanotechnological Approaches. In *Nano-Oncologicals: New Targeting and Delivery Approaches*; Alonso, M. J., Garcia-Fuentes, M., Eds.; Springer, 2014; pp 123–162.
- (27) Rück, A.; Steiner, R. Basic Reaction Mechanisms of Hydrophilic and Lipophilic Photosensitizers in Photodynamic Tumour Treatment. *Minim. Invasive Ther. Allied Technol.* **1998**, *7* (6), 503–509.
- (28) Bray, F.; Ferlay, J.; Soerjomataram, I.; Siegel, R. L.; Torre, L. A.; Jemal, A. Global Cancer Statistics 2018: GLOBOCAN Estimates of Incidence and Mortality Worldwide for 36 Cancers in 185 Countries. *CA. Cancer J. Clin.* **2018**, *68* (6), 394–424.
- (29) Cancer Research UK. Lung cancer statistics | Cancer Research UK <https://www.cancerresearchuk.org/health-professional/cancer-statistics/statistics-by-cancer-type/lung-cancer> (accessed Nov 14, 2019).
- (30) Zappa, C.; Mousa, S. A. Non-Small Cell Lung Cancer: Current Treatment and Future Advances. *Transl. Lung Cancer Res.* **2016**, *5* (3), 288.
- (31) Nur, U.; Quaresma, M.; De Stavola, B.; Peake, M.; Rachet, B. Inequalities in Non-Small Cell Lung Cancer Treatment and Mortality. *J. Epidemiol. Community Health* **2015**, *69* (10), 985–992.
- (32) Moghissi, K.; Dixon, K. Is Bronchoscopic Photodynamic Therapy a Therapeutic Option in Lung Cancer? *Eur Respir J* **2003**, *22*, 535–541.
- (33) Hayata, Y.; Kato, H.; Konaka, C.; Ono, J.; Takizawa, N. Hematoporphyrin Derivative and Laser Photoradiation in the Treatment of Lung Cancer. *Chest* **1982**, *81* (3), 269–277.
- (34) Sutedja, T.; Lam, S.; LeRichie, J. C.; Postmus, P. Response and Pattern of Failure after Photodynamic Therapy for Intraluminal Stage I Lung Cancer. *J. Bronchology Interv. Pulmonol.* **1994**, *1*, 295–298.
- (35) Kato, H.; Usuda, J.; Okunaka, T.; Furukawa, K.; Honda, H.; Sakaniwa, N.; Suga, Y.; Hirata, T.; Ohtani, K.; Inoue, T.; et al. Basic and Clinical Research on Photodynamic Therapy at Tokyo Medical University Hospital. *Lasers Surg. Med.*

- 2006, *38* (5), 371–375.
- (36) Corti, L.; Toniolo, L.; Boso, C.; Colaut, F.; Fiore, D.; Muzzio, P.-C.; Koukourakis, M. I.; Mazzarotto, R.; Pignataro, M.; Loreggian, L.; et al. Long-Term Survival of Patients Treated with Photodynamic Therapy for Carcinoma in Situ and Early Non-Small-Cell Lung Carcinoma. *Lasers Surg. Med.* **2007**, *39* (5), 394–402.
- (37) Strebhardt, K.; Ullrich, A. Paul Ehrlich's Magic Bullet Concept: 100 Years of Progress. *Nat. Rev. Cancer* **2008**, *8* (6), 473–480.
- (38) Matsumura, Y.; Maeda, H. A New Concept for Macromolecular Therapeutics in Cancer Chemotherapy: Mechanism of Tumoritropic Accumulation of Proteins and the Antitumor Agent Smancs1. *Cancer Res.* **1986**, *46*, 6387–6392.
- (39) Liong, M.; Lu, J.; Kovichich, M.; Xia, T.; Ruehm, S. G.; Nel, A. E.; Tamanoi, F.; Zink, J. I. Multifunctional Inorganic Nanoparticles for Imaging, Targeting, and Drug Delivery. *ACS Nano* **2008**, *2* (5), 889–896.
- (40) Guo, R.; Zhang, L.; Qian, H.; Li, R.; Jiang, X.; Liu, B. Multifunctional Nanocarriers for Cell Imaging, Drug Delivery, and Near-IR Photothermal Therapy. *Langmuir* **2010**, *26* (8), 5428–5434.
- (41) Karve, S.; Werner, M. E.; Sukumar, R.; Cummings, N. D.; Copp, J. A.; Wang, E. C.; Li, C.; Sethi, M.; Chen, R. C.; Pacold, M. E.; et al. Revival of the Abandoned Therapeutic Wortmannin by Nanoparticle Drug Delivery. *Proc. Natl. Acad. Sci. U. S. A.* **2012**, *109* (21), 8230–8235.
- (42) Wicki, A.; Witzigmann, D.; Balasubramanian, V.; Huwyler, J. Nanomedicine in Cancer Therapy: Challenges, Opportunities, and Clinical Applications. *J. Control. Release* **2015**, *200*, 138–157.
- (43) Jain, R. K.; Stylianopoulos, T. Delivering Nanomedicine to Solid Tumors. *Nat. Rev. Clin. Oncol.* **2010**, *7* (11), 653–664.
- (44) Lee, K. Y. J.; Wang, Y.; Nie, S. In Vitro Study of a PH-Sensitive Multifunctional Doxorubicin–gold Nanoparticle System: Therapeutic Effect and Surface Enhanced Raman Scattering. *RSC Adv.* **2015**, *5* (81), 65651–65659.
- (45) Wang, X.; Cai, X.; Hu, J.; Shao, N.; Wang, F.; Zhang, Q.; Xiao, J.; Cheng, Y. Glutathione-Triggered “Off–On” Release of Anticancer Drugs from Dendrimer-Encapsulated Gold Nanoparticles. *J. Am. Chem. Soc.* **2013**, *135* (26), 9805–9810.
- (46) Bhattacharya, R.; Mukherjee, P. Biological Properties of “Naked” Metal Nanoparticles. *Adv. Drug Deliv. Rev.* **2008**, *60*, 1289–1306.
- (47) Connor, E. E.; Mwamuka, J.; Gole, A.; Murphy, C. J.; Wyatt, M. D. Gold Nanoparticles Are Taken Up by Human Cells but Do Not Cause Acute Cytotoxicity. *Small* **2005**, *1* (3), 325–327.
- (48) Gao, J.; Huang, X.; Liu, H.; Zan, F.; Ren, J. Colloidal Stability of Gold Nanoparticles Modified with Thiol Compounds: Bioconjugation and Application in Cancer Cell Imaging. *Langmuir* **2012**, *28* (9), 4464–4471.
- (49) Grzelczak, M.; Pérez-Juste, J.; Mulvaney, P.; Liz-Marzán, L. M. Shape Control in Gold Nanoparticle Synthesis. *Chem. Soc. Rev.* **2008**, *37* (9), 1783.

-
- (50) Chen, H.; Kou, X.; Yang, Z.; Ni, W.; Wang, J. Shape- and Size-Dependent Refractive Index Sensitivity of Gold Nanoparticles. *Langmuir* **2008**, *24* (10), 5233–5237.
- (51) Liz-Marzán, L. M. Gold Nanoparticle Research before and after the Brust-Schiffrin Method. *Chem. Comm.* **2013**, *49* (1), 16–18.
- (52) Herizchi, R.; Abbasi, E.; Milani, M.; Akbarzadeh, A. Current Methods for Synthesis of Gold Nanoparticles. *Artif. Cells, Nanomedicine, Biotechnol.* **2016**, *44* (2), 596–602.
- (53) Freitas De Freitas, L.; Henrique Costa Varca, G.; Gabriel, J.; Batista, S.; Lugão, A. B. An Overview of the Synthesis of Gold Nanoparticles Using Radiation Technologies. *Nanomaterials* **2018**, *8* (11), 939.
- (54) Hostetler, M. J.; Wingate, J. E.; Zhong, C.-J.; Harris, J. E.; Vachet, R. W.; Clark, M. R.; Londono, J. D.; Green, S. J.; Stokes, J. J.; Wignall, G. D.; et al. Alkanethiolate Gold Cluster Molecules with Core Diameters from 1.5 to 5.2 Nm: Core and Monolayer Properties as a Function of Core Size. *Langmuir* **1998**, *14* (1), 17–30.
- (55) Eustis, S.; El-Sayed, M. A. Why Gold Nanoparticles Are More Precious than Pretty Gold: Noble Metal Surface Plasmon Resonance and Its Enhancement of the Radiative and Nonradiative Properties of Nanocrystals of Different Shapes. *Chem. Soc. Rev.* **2006**, *35* (3), 209–217.
- (56) Huang, X.; Jain, P. K.; El-Sayed, I. H.; El-Sayed, M. A. Plasmonic Photothermal Therapy (PPTT) Using Gold Nanoparticles. *Lasers in Medical Science*. July 2008, pp 217–228.
- (57) Mckeage, K.; Perry, C. M. Trastuzumab A Review of Its Use in the Treatment of Metastatic Breast Cancer Overexpressing HER2. *Drugs* **2001**, *1*, 209–243.
- (58) Jonker, D. J.; O’Callaghan, C. J.; Karapetis, C. S.; Zalcborg, J. R.; Tu, D.; Au, H.-J.; Berry, S. R.; Krahn, M.; Price, T.; Simes, R. J.; et al. Cetuximab for the Treatment of Colorectal Cancer. *N. Engl. J. Med.* **2007**, *357*, 2040–2048.
- (59) Chattopadhyay, N.; Cai, Z.; Kwon, Y. L.; Lechtman, E.; Pignol, J.-P.; Reilly, R. M. Molecularly Targeted Gold Nanoparticles Enhance the Radiation Response of Breast Cancer Cells and Tumor Xenografts to X-Radiation. *Breast Cancer Res. Treat.* **2013**, *137* (1), 81–91.
- (60) Chattopadhyay, N.; Cai, Z.; Pignol, J. P.; Keller, B.; Lechtman, E.; Bendayan, R.; Reilly, R. M. Design and Characterization of HER-2-Targeted Gold Nanoparticles for Enhanced X-Radiation Treatment of Locally Advanced Breast Cancer. *Mol. Pharm.* **2010**, *7* (6), 2194–2206.
- (61) Popovtzer, A.; Mizrachi, A.; Motiei, M.; Bragilovski, D.; Lubimov, L.; Levi, M.; Hilly, O.; Ben-Aharon, I.; Popovtzer, R. Actively Targeted Gold Nanoparticles as Novel Radiosensitizer Agents: An in Vivo Head and Neck Cancer Model. *Nanoscale* **2016**, *8* (5), 2678–2685.
- (62) Mesbahi, A. A Review on Gold Nanoparticles Radiosensitization Effect in Radiation Therapy of Cancer. *Reports Pract. Oncol. Radiother.* **2010**, *15* (6), 176–180.
- (63) Chen, C. H.; Wu, Y.-J.; Chen, J.-J. Photo-Thermal Therapy of Bladder Cancer

- with Anti-EGFR Antibody Conjugated Gold Nanoparticles. *Front. Biosci., Landmark Ed.* **2016**, *21* (6), 1211–1221.
- (64) Qu, X.; Yao, C.; Wang, J.; Li, Z.; Zhang, Z. Anti-CD30-Targeted Gold Nanoparticles for Photothermal Therapy of L-428 Hodgkin's Cell. *Int. J. Nanomed.* **2012**, *7*, 6095–6103.
- (65) Zelasko-Leon, D. C.; Fuentes, C. M.; Messersmith, P. B. MUC1-Targeted Cancer Cell Photothermal Ablation Using Bioinspired Gold Nanorods. *PLoS One* **2015**, *10* (7), e0128756/1-20.
- (66) Patra, C. R.; Bhattacharya, R.; Wang, E.; Katarya, A.; Lau, J. S.; Dutta, S.; Muders, M.; Wang, S.; Buhrow, S. A.; Safgren, S. L.; et al. Targeted Delivery of Gemcitabine to Pancreatic Adenocarcinoma Using Cetuximab as a Targeting Agent. *Cancer Res.* **2008**, *68* (6), 1970–1978.
- (67) Spadavecchia, J.; Movia, D.; Moore, C.; Maguire, C. M.; Moustou, H.; Casale, S.; Volkov, Y.; Prina-Mello, A. Targeted Polyethylene Glycol Gold Nanoparticles for the Treatment of Pancreatic Cancer: From Synthesis to Proof-of-Concept in Vitro Studies. *Int. J. Nanomedicine* **2016**, *11*, 791–822.
- (68) Das, A.; Soehnen, E.; Woods, S.; Hegde, R.; Henry, A.; Gericke, A.; Basu, S. VEGFR-2 Targeted Cellular Delivery of Doxorubicin by Gold Nanoparticles for Potential Antiangiogenic Therapy. *J. Nanoparticle Res.* **2011**, *13* (12), 6283–6290.
- (69) Tummala, S.; Kumar, M. N. S.; Pindiprolu, S. K. Improved Anti-Tumor Activity of Oxaliplatin by Encapsulating in Anti-DR5 Targeted Gold Nanoparticles. *Drug Deliv.* **2016**, *23* (9), 3505–3519.
- (70) Kao, H. W.; Lin, Y. Y.; Chen, C. C.; Chi, K. H.; Tien, D. C.; Hsia, C. C.; Lin, M. H.; Wang, H. E. Evaluation of EGFR-Targeted Radioimmuno-Gold-Nanoparticles as a Theranostic Agent in a Tumor Animal Model. *Bioorganic Med. Chem. Lett.* **2013**, *23* (11), 3180–3185.
- (71) Liang, S.; Li, C.; Zhang, C.; Chen, Y.; Xu, L.; Bao, C.; Wang, X.; Liu, G.; Zhang, F.; Cui, D. CD44v6 Monoclonal Antibody-Conjugated Gold Nanostars for Targeted Photoacoustic Imaging and Plasmonic Photothermal Therapy of Gastric Cancer Stem-like Cells. *Theranostics* **2015**, *5* (9), 970–984.
- (72) Penon, O.; Marín, M. J.; Russell, D. A.; Pérez-García, L. Water Soluble, Multifunctional Antibody-Porphyrin Gold Nanoparticles for Targeted Photodynamic Therapy. *J. Colloid Interface Sci.* **2017**, *496*, 100–110.
- (73) Liu, T.; Tian, J.; Chen, Z.; Liang, Y.; Liu, J.; Liu, S.; Li, H.; Zhan, J.; Yang, X. Anti-TROP2 Conjugated Hollow Gold Nanospheres as a Novel Nanostructure for Targeted Photothermal Destruction of Cervical Cancer Cells. *Nanotechnology* **2014**, *25* (34), 345103.
- (74) Obaid, G.; Chambrier, I.; Cook, M. J.; Russell, D. A. Cancer Targeting with Biomolecules: A Comparative Study of Photodynamic Therapy Efficacy Using Antibody or Lectin Conjugated Phthalocyanine-PEG Gold Nanoparticles. *Photochem. Photobiol. Sci.* **2015**, *14* (4), 737–747.
- (75) García Calavia, P.; Marín, M. J.; Chambrier, I.; Cook, M. J.; Russell, D. A. Towards Optimisation of Surface Enhanced Photodynamic Therapy of Breast Cancer Cells Using Gold Nanoparticle–photosensitiser Conjugates. *Photochem.*

- Photobiol. Sci.* **2018**, *17*, 281–289.
- (76) Stuchinskaya, T.; Moreno, M.; Cook, M. J.; Edwards, D. R.; Russell, D. A. Targeted Photodynamic Therapy of Breast Cancer Cells Using Antibody–phthalocyanine–gold Nanoparticle Conjugates. *Photochem. Photobiol. Sci.* **2011**, *10* (5), 822–831.
- (77) Kim, G. J.; Park, S. R.; Kim, G. C.; Lee, J. K. Targeted Cancer Treatment Using Anti-EGFR and -TFR Antibody-Conjugated Gold Nanoparticles Stimulated by Nonthermal Air Plasma. *Plasma Med.* **2011**, *1* (1), 45–54.
- (78) Cai, Z.; Yook, S.; Lu, Y.; Bergstrom, D.; Winnik, M. A.; Pignol, J. P.; Reilly, R. M. Local Radiation Treatment of HER2-Positive Breast Cancer Using Trastuzumab-Modified Gold Nanoparticles Labeled With ¹⁷⁷Lu. *Pharm. Res.* **2017**, *34* (3), 579–590.
- (79) Zhang, M.; Kim, H. S.; Jin, T.; Moon, W. K. Near-Infrared Photothermal Therapy Using EGFR-Targeted Gold Nanoparticles Increases Autophagic Cell Death in Breast Cancer. *J. Photochem. Photobiol. B Biol.* **2017**, *170*, 58–64.
- (80) Kubota, T.; Kuroda, S.; Kanaya, N.; Morihira, T.; Aoyama, K.; Kakiuchi, Y.; Kikuchi, S.; Nishizaki, M.; Kagawa, S.; Tazawa, H.; et al. HER2-Targeted Gold Nanoparticles Potentially Overcome Resistance to Trastuzumab in Gastric Cancer. *Nanomedicine Nanotechnology, Biol. Med.* **2018**, *14* (6), 1919–1929.
- (81) Bassett, E. W.; Tanenbaum, S. W.; Pryzwansky, K.; Beiser, S. M.; Kabat, E. A. Studies on Human Antibodies III. Amino Acid Composition of Four Antibodies from One Individual. *J. Exp. Med.* **1965**, *122*, 251–261.
- (82) Bhattacharyya, S.; Bhattacharya, R.; Curley, S.; McNiven, M. A.; Mukherjee, P. Nanoconjugation Modulates the Trafficking and Mechanism of Antibody Induced Receptor Endocytosis. *Proc. Natl. Acad. Sci. U. S. A.* **2010**, *107* (33), 14541–14546.
- (83) Austin, C. D.; De Mazière, A. M.; Pisacane, P. I.; van Dijk, S. M.; Eigenbrot, C.; Sliwkowski, M. X.; Klumperman, J.; Scheller, R. H. Endocytosis and Sorting of ErbB2 and the Site of Action of Cancer Therapeutics Trastuzumab and Geldanamycin. *Mol. Biol. Cell* **2004**, *15* (12), 5268–5282.
- (84) Hommelgaard, A. M.; Lerdrup, M.; van Deurs, B. Association with Membrane Protrusions Makes ErbB2 an Internalization-Resistant Receptor. *Mol. Biol. Cell* **2004**, *15* (4), 1557–1567.
- (85) Sun, X.; Zhang, G.; Keynton, R. S.; O’Toole, M. G.; Patel, D.; Gobin, A. M. Enhanced Drug Delivery via Hyperthermal Membrane Disruption Using Targeted Gold Nanoparticles with PEGylated Protein-G as a Cofactor. *Nanomedicine Nanotechnology, Biol. Med.* **2013**, *9* (8), 1214–1222.
- (86) Muyldermans, S. Nanobodies: Natural Single-Domain Antibodies. *Annu. Rev. Biochem.* **2013**, *82*, 775–797.
- (87) Muyldermans, S.; Baral, T. N.; Retamozzo, V. C.; De Baetselier, P.; De Genst, E.; Kinne, J.; Leonhardt, H.; Magez, S.; Nguyen, V. K.; Revets, H.; et al. Camelid Immunoglobulins and Nanobody Technology. *Vet. Immunol. Immunopathol.* **2009**, *128* (1–3), 178–183.

-
- (88) Cortez-Retamozo, V.; Lauwereys, M.; Hassanzadeh Gh., G.; Gobert, M.; Conrath, K.; Muyltermans, S.; De Baetselier, P.; Revets, H. Efficient Tumor Targeting by Single-Domain Antibody Fragments of Camels. *Int. J. Cancer* **2002**, *98* (3), 456–462.
- (89) Van de Broek, B.; Devoogdt, N.; D’Hollander, A.; Gijs, H.-L.; Jans, K.; Lagae, L.; Muyltermans, S.; Maes, G.; Borghs, G. Specific Cell Targeting with Nanobody Conjugated Branched Gold Nanoparticles for Photothermal Therapy. *ACS Nano* **2011**, *5* (6), 4319–4328.
- (90) Song, L.; Falzone, N.; Vallis, K. A. EGF-Coated Gold Nanoparticles Provide an Efficient Nano-Scale Delivery System for the Molecular Radiotherapy of EGFR-Positive Cancer. *Int. J. Radiat. Biol.* **2016**, *92* (11), 716–723.
- (91) Amreddy, N.; Muralidharan, R.; Babu, A.; Mehta, M.; Johnson, E. V.; Zhao, Y. D.; Munshi, A.; Ramesh, R. Tumor-Targeted and PH-Controlled Delivery of Doxorubicin Using Gold Nanorods for Lung Cancer Therapy. *Int. J. Nanomedicine* **2015**, *10*, 6773–6788.
- (92) Theelen, W. S. M. E.; Mittempergher, L.; Willems, S. M.; Bosma, A. J.; Peters, D. D. G. C.; van der Noort, V.; Japenga, E. J.; Peeters, T.; Koole, K.; Šuštić, T.; et al. FGFR1, 2 and 3 Protein Overexpression and Molecular Aberrations of FGFR3 in Early Stage Non-Small Cell Lung Cancer. *J. Pathol. Clin. Res.* **2016**, *2* (4), 223–233.
- (93) Szlachcic, A.; Pala, K.; Zakrzewska, M.; Jakimowicz, P.; Wiedlocha, A.; Otlewski, J. FGF1-Gold Nanoparticle Conjugates Targeting FGFR Efficiently Decrease Cell Viability upon NIR Irradiation. *Int. J. Nanomedicine* **2012**, *7*, 5915–5927.
- (94) Obaid, G.; Chambrier, I.; Cook, M. J.; Russell, D. A. Targeting the Oncofetal Thomsen-Friedenreich Disaccharide Using Jacalin-PEG Phthalocyanine Gold Nanoparticles for Photodynamic Cancer Therapy. *Angew. Chemie Int. Ed.* **2012**, *51* (25), 6158–6162.
- (95) Hozumi, K.; Kunihiro, K.; Keiji, H. A Simple Procedure for the Isolation of Human Secretory IgA of IgA1 and IgA2 Subclass by a Jackfruit Lectin, Jacalin, Affinity Chromatography. *Mol. Immunol.* **1987**, *24*, 1219–1222.
- (96) Fassina, G.; Ruvo, M.; Palombo, G.; Verdoliva, A.; Marino, M. Novel Ligands for the Affinity-Chromatographic Purification of Antibodies. *Journal of Biochemical and Biophysical Methods*. October 30, 2001, pp 481–490.
- (97) Biscaglia, F.; Rajendran, S.; Conflitti, P.; Benna, C.; Sommaggio, R.; Litti, L.; Mocellin, S.; Bocchinfuso, G.; Rosato, A.; Palleschi, A.; et al. Enhanced EGFR Targeting Activity of Plasmonic Nanostructures with Engineered GE11 Peptide. *Adv. Healthc. Mater.* **2017**, *6* (23), 1700596.
- (98) Simpson, E. J.; Gobbo, P.; Bononi, F. C.; Murrell, E.; Workentin, M. S.; Luyt, L. G. Bombesin-Functionalized Water-Soluble Gold Nanoparticles for Targeting Prostate Cancer. *J. Interdiscip. Nanomed.* **2017**, *2* (4), 174–187.
- (99) Xu, X.; Zhao, L.; Li, X.; Wang, P.; Zhao, J.; Shi, X.; Shen, M. Targeted Tumor SPECT/CT Dual Mode Imaging Using Multifunctional RGD-Modified Low Generation Dendrimer-Entrapped Gold Nanoparticles. *Biomater. Sci.* **2017**, *5* (12), 2393–2397.

-
- (100) Jha, S.; Ramadori, F.; Quarta, S.; Biasiolo, A.; Fabris, E.; Baldan, P.; Guarino, G.; Ruvoletto, M.; Villano, G.; Turato, C.; et al. Binding and Uptake into Human Hepatocellular Carcinoma Cells of Peptide-Functionalized Gold Nanoparticles. *Bioconjug. Chem.* **2017**, *28* (1), 222–229.
- (101) Yin, H.-Q.; Mai, D.-S.; Gan, F.; Chen, X.-J. One-Step Synthesis of Linear and Cyclic RGD Conjugated Gold Nanoparticles for Tumour Targeting and Imaging. *RSC Adv.* **2014**, *4* (18), 9078–9085.
- (102) Avvakumova, S.; Galbiati, E.; Pandolfi, L.; Mazzucchelli, S.; Cassani, M.; Gori, A.; Longhi, R.; Prosperi, D. Development of U11-Functionalized Gold Nanoparticles for Selective Targeting of Urokinase Plasminogen Activator Receptor-Positive Breast Cancer Cells. *Bioconjug. Chem.* **2014**, *25* (8), 1381–1386.
- (103) Pal, K.; Al-Suraih, F.; Gonzalez-Rodriguez, R.; Dutta, S. K.; Wang, E.; Kwak, H. S.; Caulfield, T. R.; Coffey, J. L.; Bhattacharya, S. Multifaceted Peptide Assisted One-Pot Synthesis of Gold Nanoparticles for Plectin-1 Targeted Gemcitabine Delivery in Pancreatic Cancer. *Nanoscale* **2017**, *9* (40), 15622–15634.
- (104) Liang, G.; Jin, X.; Zhang, S.; Xing, D. RGD Peptide-Modified Fluorescent Gold Nanoclusters as Highly Efficient Tumor-Targeted Radiotherapy Sensitizers. *Biomaterials* **2017**, *144*, 95–104.
- (105) Desgrosellier, J. S.; Chesh, D. A. Integrins in Cancer: Biological Implications and Therapeutic Opportunities. *Nat. Rev. Cancer* **2010**, *10* (1), 9–22.
- (106) Wu, P.-H.; Hashimoto, T.; Shirato, H.; Nam, J.-M.; Onodera, Y.; Ichikawa, Y.; Watanabe, Y.; Ichikawa, Y.; Qian, W.; Rankin, E. B.; et al. Targeting Integrins with RGD-Conjugated Gold Nanoparticles in Radiotherapy Decreases the Invasive Activity of Breast Cancer Cells. *Int. J. Nanomedicine* **2017**, *12*, 5069–5085.
- (107) Wang, S.; Chen, K. J.; Wu, T. H.; Wang, H.; Lin, W. Y.; Ohashi, M.; Chiou, P. Y.; Tseng, H. R. Photothermal Effects of Supramolecularly Assembled Gold Nanoparticles for the Targeted Treatment of Cancer Cells. *Angew. Chemie - Int. Ed.* **2010**, *49* (22), 3777–3781.
- (108) Yi, Y.; Kim, H. J.; Mi, P.; Zheng, M.; Takemoto, H.; Toh, K.; Kim, B. S.; Hayashi, K.; Naito, M.; Matsumoto, Y.; et al. Targeted Systemic Delivery of siRNA to Cervical Cancer Model Using Cyclic RGD-Installed Unimer Polyion Complex-Assembled Gold Nanoparticles. *J. Control. Release* **2016**, *244*, 247–256.
- (109) Kumar, A.; Ma, H.; Zhang, X.; Huang, K.; Jin, S.; Liu, J.; Wei, T.; Cao, W.; Zou, G.; Liang, X. J. Gold Nanoparticles Functionalized with Therapeutic and Targeted Peptides for Cancer Treatment. *Biomaterials* **2012**, *33* (4), 1180–1189.
- (110) Kumar, A.; Huo, S.; Zhang, X.; Liu, J.; Tan, A.; Li, S.; Jin, S.; Xue, X.; Zhao, Y.; Ji, T.; et al. Neuropilin-1-Targeted Gold Nanoparticles Enhance Therapeutic Efficacy of Platinum(IV) Drug for Prostate Cancer Treatment. *ACS Nano* **2014**, *8* (5), 4205–4220.
- (111) Cheng, Y.; Meyers, J. D.; Agnes, R. S.; Doane, T. L.; Kenney, M. E.; Broome, A.-M. M.; Burda, C.; Bacion, J. P. Addressing Brain Tumors with Targeted Gold Nanoparticles: A New Gold Standard for Hydrophobic Drug Delivery? *Small* **2011**, *7* (16), 2301–2306.
- (112) Meyers, J. D.; Cheng, Y.; Broome, A. M. M.; Agnes, R. S.; Schlachter, M. D.;

- Margevicius, S.; Wang, X.; Kenney, M. E.; Burda, C.; Bacion, J. P. Peptide-Targeted Gold Nanoparticles for Photodynamic Therapy of Brain Cancer. *Part. Part. Syst. Charact.* **2015**, *32* (4), 448–457.
- (113) Mangadlao, J. D.; Wang, X.; McCleese, C.; Escamilla, M.; Ramamurthy, G.; Wang, Z.; Govande, M.; Bacion, J. P.; Burda, C. Prostate-Specific Membrane Antigen Targeted Gold Nanoparticles for Theranostics of Prostate Cancer. *ACS Nano* **2018**, *12* (4), 3714–3725.
- (114) Luo, D.; Wang, X.; Zeng, S.; Ramamurthy, G.; Burda, C.; Bacion, J. P. Prostate-Specific Membrane Antigen Targeted Gold Nanoparticles for Prostate Cancer Radiotherapy: Does Size Matter for Targeted Particles? *Chem. Sci.* **2019**, *10* (35), 8119–8128.
- (115) Saber, M. M.; Bahrainian, S.; Dinarvand, R.; Atyabi, F. Targeted Drug Delivery of Sunitinib Malate to Tumor Blood Vessels by CRGD-Chitosan-Gold Nanoparticles. *Int. J. Pharm.* **2017**, *517*, 269–278.
- (116) Jayasena, S. D. Aptamers: An Emerging Class of Molecules That Rival Antibodies in Diagnostics. *Clin. Chem.* **1999**, *45* (9), 1628–1650.
- (117) Bouchard, P. R.; Hutabarat, R. M.; Thompson, K. M. Discovery and Development of Therapeutic Aptamers. *Annu. Rev. Pharmacol. Toxicol.* **2010**, *50*, 237–257.
- (118) Sun, H.; Zhu, X.; Lu, P. Y.; Rosato, R. R.; Tan, W.; Zu, Y. Oligonucleotide Aptamers: New Tools for Targeted Cancer Therapy. *Mol. Ther. - Nucleic acids* **2014**, *3* (8), 1–14.
- (119) Han, K.; Liang, Z.; Zhou, N. Design Strategies for Aptamer-Based Biosensors. *Sensors* **2010**, *10* (5), 4541–4557.
- (120) Hong, E. J.; Kim, Y.-S.; Choi, D. G.; Shim, M. S. Cancer-Targeted Photothermal Therapy Using Aptamer-Conjugated Gold Nanoparticles. *J. Ind. Eng. Chem.* **2018**, *67*, 429–436.
- (121) Ghahremani, F.; Shahbazi-Gahrouei, D.; Kefayat, A.; Motaghi, H.; Mehrgardi, M. A.; Javanmard, S. H. AS1411 Aptamer Conjugated Gold Nanoclusters as a Targeted Radiosensitizer for Megavoltage Radiation Therapy of 4T1 Breast Cancer Cells. *RSC Adv.* **2018**, No. 8, 4249–4258.
- (122) Latorre, A.; Posch, C.; Garcimartín, Y.; Celli, A.; Sanlorenzo, M.; Vujic, I.; Ma, J.; Zekhtser, M.; Rappersberger, K.; Ortiz-Urda, S.; et al. DNA and Aptamer Stabilized Gold Nanoparticles for Targeted Delivery of Anticancer Therapeutics. *Nanoscale* **2014**, *6* (13), 7436–7442.
- (123) Ai, J.; Xu, Y.; Lou, B.; Li, D.; Wang, E. Multifunctional AS1411-Functionalized Fluorescent Gold Nanoparticles for Targeted Cancer Cell Imaging and Efficient Photodynamic Therapy. *Talanta* **2014**, *118*, 54–60.
- (124) Wang, J.; Zhu, G.; You, M.; Song, E.; Shukoor, M. I.; Zhang, K.; Altman, M. B.; Chen, Y.; Zhu, Z.; Huang, C. Z.; et al. Assembly of Aptamer Switch Probes and Photosensitizer on Gold Nanorods for Targeted Photothermal and Photodynamic Cancer Therapy. *ACS Nano* **2012**, *6* (6), 5070–5077.
- (125) Luo, Y.-L.; Shiao, Y.-S.; Huang, Y.-F. Release of Photoactivatable Drugs from

- Plasmonic Nanoparticles for Targeted Cancer Therapy. *ACS Nano* **2011**, *5* (10), 7796–7804.
- (126) Kim, D.; Jeong, Y. Y.; Jon, S. A Drug-Loaded Aptamer-Gold Nanoparticle Bioconjugate for Combined CT Imaging and Therapy of Prostate Cancer. *ACS Nano* **2010**, *4* (7), 3689–3696.
- (127) Lee, H.; Dam, D. H. M.; Ha, J. W.; Yue, J.; Odom, T. W. Enhanced Human Epidermal Growth Factor Receptor 2 Degradation in Breast Cancer Cells by Lysosome-Targeting Gold Nanoconstructs. *ACS Nano* **2015**, *9* (10), 9859–9867.
- (128) Taghdisi, S. M.; Danesh, N. M.; Lavaee, P.; Emrani, A. S.; Hassanabad, K. Y.; Ramezani, M.; Abnous, K. Double Targeting, Controlled Release and Reversible Delivery of Daunorubicin to Cancer Cells by Polyvalent Aptamers-Modified Gold Nanoparticles. *Mater. Sci. Eng. C* **2016**, *61*, 753–761.
- (129) Lotan, R.; Raz, A. Lectins in Cancer Cells. *Ann. N. Y. Acad. Sci.* **1988**, *551* (1), 385–398.
- (130) Yamazaki, N.; Kojima, S.; Bovin, N. V.; André, S.; Gabius, S.; Gabius, H. J. Endogenous Lectins as Targets for Drug Delivery. *Adv. Drug Deliv. Rev.* **2000**, *43* (2–3), 225–244.
- (131) Bourguignon, L. Y.; Lokeshwar, V. B.; Chen, X.; Kerrick, W. G. Hyaluronic Acid-Induced Lymphocyte Signal Transduction and HA Receptor (GP85/CD44)-Cytoskeleton Interaction. *J. Immunol.* **1993**, *151* (12), 6634–6644.
- (132) Song, Y.; Wang, Z.; Li, L.; Shi, W.; Li, X.; Ma, H. Gold Nanoparticles Functionalized with Cresyl Violet and Porphyrin via Hyaluronic Acid for Targeted Cell Imaging and Phototherapy. *Chem. Commun.* **2014**, *50* (99), 15696–15698.
- (133) Kang, S. H.; Nafiujjaman, M.; Nurunnabi, M.; Li, L.; Khan, H. A.; Cho, K. J.; Huh, K. M.; Lee, Y. K. Hybrid Photoactive Nanomaterial Composed of Gold Nanoparticles, Pheophorbide-A and Hyaluronic Acid as a Targeted Bimodal Phototherapy. *Macromol. Res.* **2015**, *23* (5), 474–484.
- (134) Kumar, C. S.; Raja, M. D.; Sundar, D. S.; Gover Antoniraj, M.; Ruckmani, K. Hyaluronic Acid Co-Functionalized Gold Nanoparticle Complex for the Targeted Delivery of Metformin in the Treatment of Liver Cancer (HepG2 Cells). *Carbohydr. Polym.* **2015**, *128*, 63–74.
- (135) Yi, Y.; Kim, H. J.; Zheng, M.; Mi, P.; Naito, M.; Kim, B. S.; Min, H. S.; Hayashi, K.; Perche, F.; Toh, K.; et al. Glucose-Linked Sub-50-Nm Unimer Polyion Complex-Assembled Gold Nanoparticles for Targeted siRNA Delivery to Glucose Transporter 1-Overexpressing Breast Cancer Stem-like Cells. *J. Control. Release* **2019**, *295*, 268–277.
- (136) García Calavia, P.; Chambrier, I.; Cook, M. J.; Haines, A. H.; Field, R. A.; Russell, D. A. Targeted Photodynamic Therapy of Breast Cancer Cells Using Lactose-Phthalocyanine Functionalized Gold Nanoparticles. *J. Colloid Interface Sci.* **2018**, *512*, 249–259.
- (137) Ngernyuang, N.; Seubwai, W.; Daduang, S.; Boonsiri, P.; Limpai boon, T.; Daduang, J. Targeted Delivery of 5-Fluorouracil to Cholangiocarcinoma Cells Using Folic Acid as a Targeting Agent. *Mater. Sci. Eng., C* **2016**, *60*, 411–415.

- (138) Guo, J.; O'Driscoll, C. M.; Holmes, J. D.; Rahme, K. Bioconjugated Gold Nanoparticles Enhance Cellular Uptake: A Proof of Concept Study for siRNA Delivery in Prostate Cancer Cells. *Int. J. Pharm.* **2016**, *509* (1–2), 16–27.
- (139) Zhao, L.; Kim, T. H.; Kim, H. W.; Ahn, J. C.; Kim, S. Y. Enhanced Cellular Uptake and Phototoxicity of Verteporfin-Conjugated Gold Nanoparticles as Theranostic Nanocarriers for Targeted Photodynamic Therapy and Imaging of Cancers. *Mater. Sci. Eng. C* **2016**, *67*, 611–622.
- (140) Feng, B.; Xu, Z.; Zhou, F.; Yu, H.; Sun, Q.; Wang, D.; Tang, Z.; Yu, H.; Yin, Q.; Zhang, Z.; et al. Near Infrared Light-Actuated Gold Nanorods with Cisplatin-Polypeptide Wrapping for Targeted Therapy of Triple Negative Breast Cancer. *Nanoscale* **2015**, *7* (36), 14854–14864.
- (141) Devendiran, R. M.; Chinnaiyan, S. K.; Yadav, N. K.; Moorthy, G. K.; Ramanathan, G.; Singaravelu, S.; Sivagnanam, U. T.; Perumal, P. T. Green Synthesis of Folic Acid-Conjugated Gold Nanoparticles with Pectin as Reducing/Stabilizing Agent for Cancer Theranostics. *RSC Adv.* **2016**, *6* (35), 29757–29768.
- (142) Banu, H.; Sethi, D. K.; Edgar, A.; Sheriff, A.; Rayees, N.; Renuka, N.; Faheem, S. M.; Premkumar, K.; Vasanthakumar, G. Doxorubicin Loaded Polymeric Gold Nanoparticles Targeted to Human Folate Receptor upon Laser Photothermal Therapy Potentiates Chemotherapy in Breast Cancer Cell Lines. *J. Photochem. Photobiol. B Biol.* **2015**, *149*, 116–128.
- (143) Dasargyri, A.; Kümin, C. D.; Leroux, J.-C. Targeting Nanocarriers with Anisamide: Fact or Artifact? *Adv. Mater.* **2017**, *29* (7), 1603451.
- (144) Fitzgerald, K. A.; Rahme, K.; Guo, J.; Holmes, J. D.; O'Driscoll, C. M. Anisamide-Targeted Gold Nanoparticles for siRNA Delivery in Prostate Cancer - Synthesis, Physicochemical Characterisation and in Vitro Evaluation. *J. Mater. Chem. B* **2016**, *4* (13), 2242–2252.
- (145) Luan, X.; Rahme, K.; Cong, Z.; Wang, L.; Zou, Y.; He, Y.; Yang, H.; Holmes, J. D.; O'Driscoll, C. M.; Guo, J. Anisamide-Targeted PEGylated Gold Nanoparticles Designed to Target Prostate Cancer Mediate: Enhanced Systemic Exposure of siRNA, Tumour Growth Suppression and a Synergistic Therapeutic Response in Combination with Paclitaxel in Mice. *Eur. J. Pharm. Biopharm.* **2019**, *137*, 56–67.
- (146) Dreaden, E. C.; Gryder, B. E.; Austin, L. A.; Tene Defo, B. A.; Hayden, S. C.; Pi, M.; Quarles, L. D.; Oyelere, A. K.; El-Sayed, M. A. Antiandrogen Gold Nanoparticles Dual-Target and Overcome Treatment Resistance in Hormone-Insensitive Prostate Cancer Cells. *Bioconjug. Chem.* **2012**, *23* (8), 1507–1512.
- (147) Jo, H.; Youn, H.; Lee, S.; Ban, C. Ultra-Effective Photothermal Therapy for Prostate Cancer Cells Using Dual Aptamer-Modified Gold Nanostars. *J. Mater. Chem. B* **2014**, *2* (30), 4862–4867.
- (148) Mohamed, M. S.; Veerananarayanan, S.; Poulouse, A. C.; Nagaoka, Y.; Minegishi, H.; Yoshida, Y.; Maekawa, T.; Kumar, D. S. Type 1 Ribotoxin-Curcun Conjugated Biogenic Gold Nanoparticles for a Multimodal Therapeutic Approach towards Brain Cancer. *Biochim. Biophys. Acta, Gen. Subj.* **2014**, *1840* (6), 1657–1669.
- (149) Keefe, A. D.; Pai, S.; Ellington, A. Aptamers as Therapeutics. *Nat. Rev. Drug*

Discov. **2010**, *9* (7), 537–550.

- (150) Lau, J. L.; Dunn, M. K. Therapeutic Peptides: Historical Perspectives, Current Development Trends, and Future Directions. *Bioorg. Med. Chem.* **2018**, *26* (10), 2700–2707.

Chapter Two
Design, Synthesis and
Biological Evaluation of
Peptide Directed
Phthalocyanine-Gold
Nanocarriers

2.1 Introduction

2.1.1 The overexpression of receptors in cancer

The transformation of cells from normal to malignant often involves the mutation of genes for receptors that encourage proliferation, survival, angiogenesis and migration. The upregulation of genes encoding for these receptors leads to the overexpression of receptors on the surface of cancer cells.¹ While these receptors encourage the rapid and uncontrolled growth of tumours, the overexpression of receptors differentiates cancerous cells from normal cells. Targeted therapies often take advantage of the high density of surface receptors on malignant cells to encourage uptake of cancer treatments specifically into these cells. Surface receptors overexpressed on non-small cell lung cancers (NSCLCs) include the epidermal growth factor receptor (EGFR), fibroblast growth factor receptor 1 (FGFR1), discoidin domain receptor 2 (DDR2) and neurotrophic tyrosine kinase receptor (NTKR). EGFR and NTKR are overexpressed on *ca.* 60%² and *ca.* 3%³ of NSCLCs respectively, while FGFR1 and DDR2 are limited to squamous cell carcinomas, where they are expressed by *ca.* 20%⁴ and *ca.* 4%⁵ of carcinomas respectively.⁶ Due to the ubiquity of EGFR overexpression in NSCLCs, this receptor presents itself as a desirable target for delivering photosensitisers directly to non-small cell lung cancers.

2.1.2 The epidermal growth factor receptor

The EGFR is a receptor tyrosine kinase found to be overexpressed in many human epithelial cancers, such as lung, prostate, ovarian, colorectal, bladder and head and neck carcinomas.^{2,7} It is a member of the ErbB family, which consists of four proteins: EGFR (ErbB-1), HER2 (ErbB-2), HER3 (ErbB-3) and HER4 (ErbB-4). These proteins are similar in their basic structure but differ in their tyrosine kinase activity.⁸ EGFR itself is a 170 kDa plasma membrane glycoprotein mainly found on cells of epithelial origin, consisting of a cysteine-rich extracellular region, an uninterrupted kinase domain and multiple autophosphorylation sites clustered at a C-terminal tail.^{9,10} In healthy tissue, it moderates cell growth, survival, adhesion, migration and differentiation. The extracellular region binds to ligands such as epidermal growth factor (EGF) and transforming growth factor α (TGF α) to form a 2:2 receptor:ligand complex.¹¹ Homodimers and heterodimers can form between EGFR and other members of the ErbB family. The formation of these dimers (**Figure 2.1**), leads to cross-phosphorylation between tyrosine residues within the EGFR, forming docking sites for signalling complexes such as effector and adaptor

proteins. These signalling complexes dissociate and stimulate a cascade of cellular pathways.

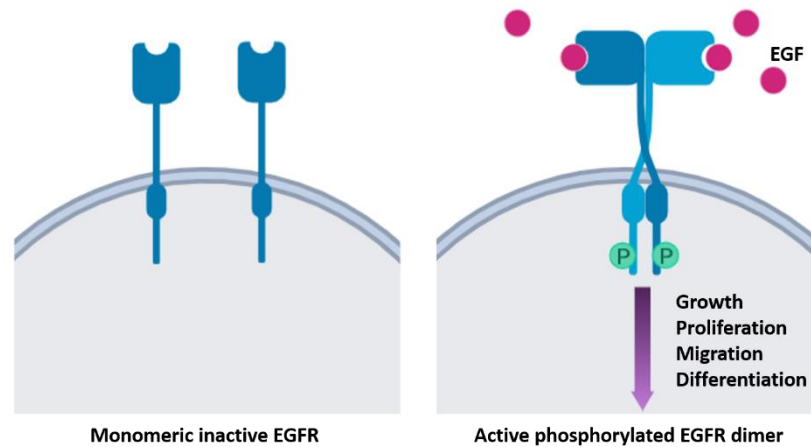


Figure 2.1: Activation of EGFR by ligands such as EGF leads to the formation of an active dimer and the activation of downstream processes controlling cell survival, proliferation, migration and differentiation

To terminate the signal, endocytosis occurs, absorbing the EGFR dimer into the cell. Within the cell, the EGFR, and any other members of the ErbB family used to form a heterodimer, are either recycled back to the surface or degraded. One of the many pathways modulated by the EGFR is that of cell proliferation and cell maintenance by the inhibition of apoptosis.¹² By overexpressing EGFR on the cell surface, carcinomas can maintain uncontrolled cell growth, and therefore the overexpression of EGFR is seen as a poor prognostic marker for survival and an essential driving force for aggressive cell growth. The high frequency of EGFR overexpression in NSCLC has led to the receptor being extensively investigated as a target for cancer treatments.^{13–15}

2.1.3 Targeting the EGFR

As the EGFR presents itself as such a lucrative target, many therapies have been designed to directly target this receptor. Much of the research into targeting the EGFR revolves around the use of monoclonal antibodies or tyrosine kinase inhibitors (TKIs). Both of these treatment methods have been successful, leading to clinically approved drugs.^{16,17}

TKIs for targeting the EGFR include gefitinib and erlotinib which are both approved for the treatment of NSCLC.^{18,19} These TKIs inhibit the ATP-binding pocket on the C-terminus of EGFR, blocking the downstream signalling^{20,21} and induce cell death by triggering apoptosis.²² While these drugs have been seen to efficiently treat NSCLC,

resistance towards TKIs rapidly develops, and both gefitinib and erlotinib are only seen to be effective in patients for one year of treatment.²³ These mutations have led to the development of second generation TKIs, including afatinib in 2013,²⁴ however mutations towards second generation therapies were quickly developed, leading to the design and approval for the third generation TKI osimertinib in 2018.²⁵ This rapid development of resistance to TKIs is not ideal for development of a drug as new mutations seem to arise as quickly as TKIs are developed. These TKIs act upon a pocket of the EGFR found intracellularly, so TKIs are not ideal for the development of targeting moieties to direct treatments to EGFR overexpressing NSCLC.

Antibodies towards the EGFR are directed towards the external section of the receptor and therefore are a more relevant drug type for this work. EGFR targeted antibodies such as cetuximab and panitumumab have been approved for treatment of metastatic colorectal cancer,^{26,27} and cetuximab is also approved for head and neck squamous cell carcinoma,²⁸ either as stand-alone treatments or in combination with chemotherapeutic drugs. These antibodies display a higher affinity towards EGFR than its natural ligands and prevent the activation of tyrosine kinases, inhibiting the activation of downstream signalling that promotes cell proliferation. They also promote the internalisation of the EGFR by receptor mediated endocytosis and the degradation of the receptor. While panitumumab is a human monoclonal antibody, cetuximab is a chimeric human-mouse antibody, and as such can promote antibody-dependent cell mediated cytotoxicity.²⁹ These antibodies display good activity towards the EGFR, however these current approved therapies rely on the antibody itself for activity towards EGFR expressing cancers. The conjugation of drugs onto antibodies is not a trivial task and antibody drug conjugates towards EGFR are yet to gain clinical approval.

Antibody drug conjugates (ADCs) combine the specificity of antibodies towards a target receptor with the cytotoxicity of an attached drug to selectively deliver a payload. The overexpression of EGFR in many epithelial cancers has meant that EGFR has been widely investigated as a target for ADCs³⁰⁻³³ and the development of EGFR ADCs has led to several clinical trials.^{34,35} ADCs carrying photosensitisers as their payload are collectively known as photoimmunotherapeutics. Photoimmunotherapy has been reported using a number of photosensitisers conjugated onto cetuximab, panitumumab and other EGFR antibodies.³⁶⁻³⁸ It has been found that the hydrophobic nature of most photosensitisers leads to aggregation of antibodies upon conjugation. To counter this, water soluble linkers such as PEG chains have been used to increase the solubility of the

system.³⁹ Hydrophilic photosensitisers such as IR700, while poor photosensitisers in their own right, have been conjugated onto EGFR antibodies (**Figure 2.2, 2.1**). Their hydrophilicity prevents aggregation of the antibody, and the targeting ability of the antibody internalises the photosensitiser, increasing its efficiency.⁴⁰

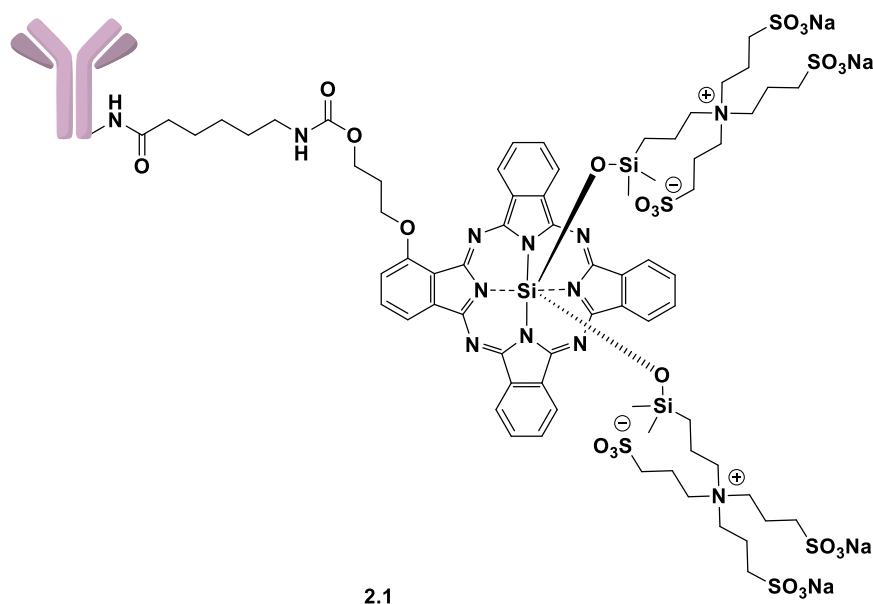


Figure 2.2: Structure of an IR700 photoimmunoconjugate

EGFR antibodies have also been used to deliver nanoparticles carrying photosensitisers for photodynamic therapy. EGFR antibodies have been used to deliver a wide range of nanoparticles, including gold nanoparticles, quantum dots, liposomes and polymeric nanoparticles, with excellent selectivity observed.^{41–45} Nanoparticles have the ability to carry large quantities of a photosensitiser and this photosensitiser does not have to be conjugated directly to the antibody. Nanoparticles such as liposomes or polymeric nanoparticles can encapsulate a hydrophobic photosensitiser, meaning the attached targeting antibody is only subjected to the hydrophilic surface of the nanocarrier. Inorganic nanoparticles such as gold, iron oxide and copper sulphate use solubilising ligands such as PEG or amphiphilic polymers to increase their water solubility and the antibodies are attached directly to these water soluble moieties.^{46–48} This increased hydrophilicity is favourable for the stability of antibodies and presents a benefit over photoimmunotherapeutics.

While antibodies have been widely investigated as targeting agents for photodynamic therapy, their complex and often unknown structure makes their conjugation to

photosensitisers or delivery vehicles difficult to control and the characterisation of the resulting conjugate challenging. The most common conjugation strategy relies on the presence of surface amines in lysine residues to couple antibodies to their target. A typical IgG antibody has *ca.* 10 lysines on its surface⁴⁹ and it is very difficult to control which, if any, of these lysines will react, or whether any lysine residues in the active site of an antibody will be involved in this conjugation. The conjugation of a drug to an antibody is also never uniform, with some antibodies in a batch carrying more drugs than others,⁵⁰ as demonstrated in **Figure 2.3**. In fact, variation between zero and eight drugs per antibody has been observed in the clinically approved ADC Trastuzumab Emtansine, which is reported to have a drug to antibody ratio of 3.5.⁵¹ This variability in conjugation means it is questionable whether the same dosage of payload is delivered in each treatment, and different levels of conjugation can slightly alter the pharmacokinetics and tissue distribution of an antibody.⁵²



Figure 2.3: Example of the heterogeneity of ADCs. Here, this mixture of ADCs has an average drug (red) to antibody (blue) ratio of 2

Antibodies are also very sensitive to pH, organic solvents and temperature and they show low penetration into solid tumours due to their large size. These problems have led to the investigation of simpler, smaller targeting moieties that show specificity towards their target, such as peptides.

2.1.4 Peptides as targeting agents

Peptides are short chains of amino acids that can be manually synthesised with a known sequence. They are relatively cheap and simple to synthesise, can be fully characterised, are non-immunogenic and are relatively robust compared to antibodies, thus provide an attractive alternative to antibodies. Cell-targeting peptides can be specifically designed for a receptor based on its natural ligand (such as EGF for EGFR) or from the crystal structure of a receptor. Less specific techniques such as combinatorial libraries and phage display can be used to design and screen a large number of peptides against a target

receptor. EGF itself has been isolated and used to deliver phthalocyanines to tumours,⁵³ however this relatively complex growth factor (6 kDa) still results in many of the same conjugation issues as antibodies. The use of peptides as targeting agents is a relatively new field of research and their fast diffusion rates and ease of modification has led to a growing interest in their applicability. Peptide drug conjugates (PDCs) are an emerging field of therapeutics, carrying cytotoxic payloads to their target through the specificity of a peptide. PDCs have been designed for a range of targets, displaying excellent uptake into cells alongside high drug loading and good biocompatibility.^{54–57} PDCs also have the advantage of defined conjugation sites and simple analysis, meaning a homogeneous, fully characterised drug is produced, usually with peptide and payload in a 1:1 ratio.

While peptides have been designed for a wide variety of targets, interestingly there are few diverse examples of peptides as targeting agents for the delivery of photosensitisers. The conjugation of a photosensitiser to a peptide can increase its hydrophilicity, and often a soluble linker such as PEG is inserted between the photosensitiser and the targeting peptide to further increase the hydrophilicity of the conjugate^{58,59} increasing their applicability for delivery. The cyclic peptide cRGD, a ligand for $\alpha_v\beta_3$ integrin, has been used to deliver porphyrins and chlorins and is the most explored peptide for photosensitiser delivery.^{59–63} Peptide-photosensitiser conjugates directed towards neuropilin-1,⁶⁴ gastrin releasing peptide receptors⁶⁵ and EGFR^{66–68} have also been described. The peptide RGD and its cyclic derivative cRGD were first reported over 20 years ago^{69,70} and have been staple examples of targeting peptides in the literature ever since. $\alpha_v\beta_3$ integrin is overexpressed by proliferating endothelial cells involved in angiogenesis but has limited expression in normal cells⁷¹ so it can be used as a target for a wide variety of cancers. cRGD displays high selectivity towards $\alpha_v\beta_3$ integrin, and this wealth of understanding of the binding and selectivity of cRGD, alongside the ubiquity of $\alpha_v\beta_3$ integrin expression in tumours, may have led to preference towards cRGD for targeting photosensitisers.

Peptides have also been investigated as targeting agents for nanoparticles. Again, cRGD has been extensively investigated for the successful targeted delivery of a wide variety of nanoparticles.^{72,73} A wide range of peptides have been used to target nanoparticles towards tumours, including a range of EGFR targeting peptides. Interestingly, while there are many reports of EGFR peptide targeted nanoparticles, there are only two examples of using EGFR-targeted peptides for the delivery of nanoparticles for PDT.^{74–76}

2.1.5 Peptides for targeting the EGFR

To date, four peptides have been reported for EGFR targeting: GE11, D4, QRHKPRE and AEYLR. The most investigated of these peptides, GE11 (YHWYGYTPQNVI), was discovered using a phage display library and has subsequently been used by many groups to target the EGFR,^{74,75,77–79} including the delivery of phthalocyanine-based peptide drug conjugates (**Figure 2.4a, 2.2**).⁶⁶ GE11 has been shown to bind specifically to EGFR and displays a dissociation constant (k_d) of *ca.* 22 nM, which is only 10-fold lower than that of EGFR's natural ligand EGF. It shows no mitogenic activity while being easily internalised by cells overexpressing EGFR.⁷⁷ GE11 has been employed for delivering micelles and gold nanoparticles carrying the photosensitiser Pc4 to EGFR overexpressing cells with enhanced uptake and phototoxicity observed for these targeted nanocarriers.^{74,76}

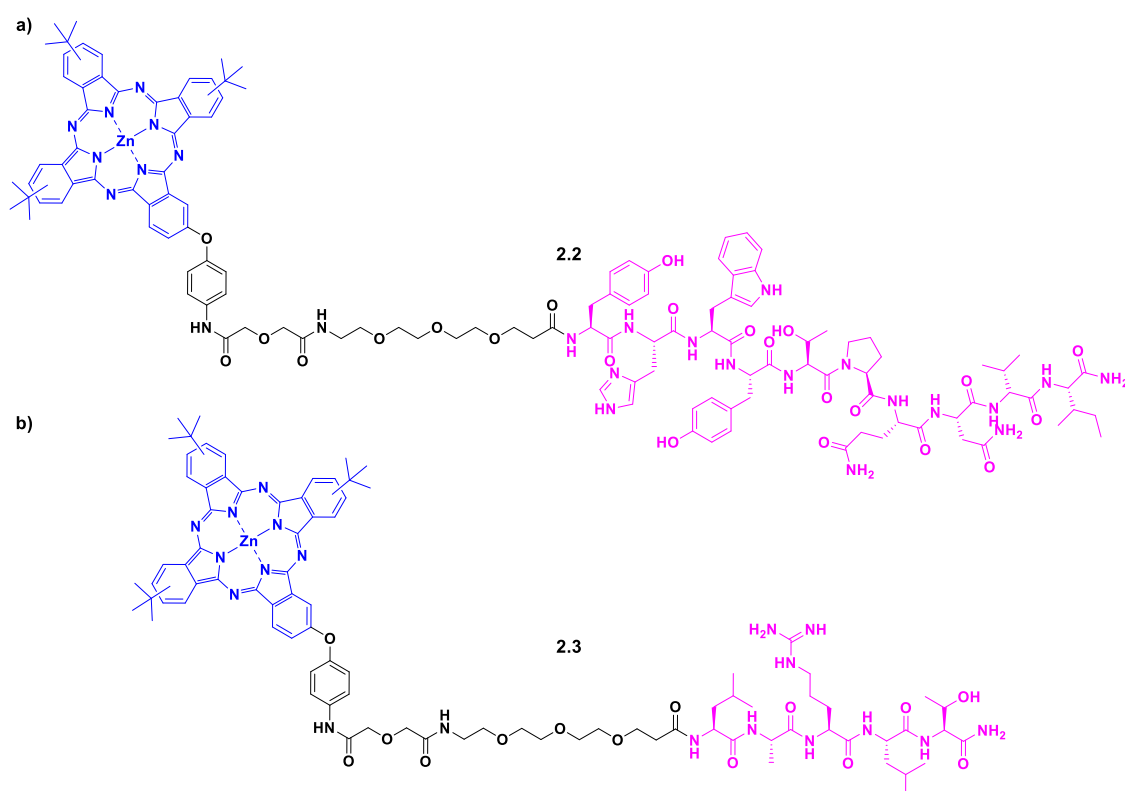


Figure 2.4: Structures of **a**) the phthalocyanine-GE11 PDC, consisting of a phthalocyanine (blue), linker (black) and GE11 (pink) and **b**) the phthalocyanine-D4 PDC consisting of a phthalocyanine (blue), linker (black) and D4 (pink)

Peptide D4 (LARLLT) was identified using computer assisted design from a virtual peptide library, using the crystal structure of EGFR to dock the peptide into a surface pocket⁸⁰ and has also been used to deliver phthalocyanine-PDCs (**Figure 2.4b, 2.3**). GE11 and D4 have been compared as targeting agents to deliver a phthalocyanine or

BODIPY (**Figure 2.5a**) for fluorescent imaging of EGFR positive tumours, and for the delivery of the photosensitiser mesoporphyrin IX (**Figure 2.5b**).^{66,67,81} The peptides were linked to the photosensitisers through PEG chains to increase solubility. The shorter peptide D4 was found to be internalised much more readily by human cell lines than GE11 due to its higher hydrophilicity, with the GE11-BODIPY complex observed to aggregate at concentrations above 10 μM .⁸¹ A difference in uptake of these conjugates was observed depending on the cellular expression of EGFR, highlighting that both peptides are selectively targeting the EGFR.⁶⁷

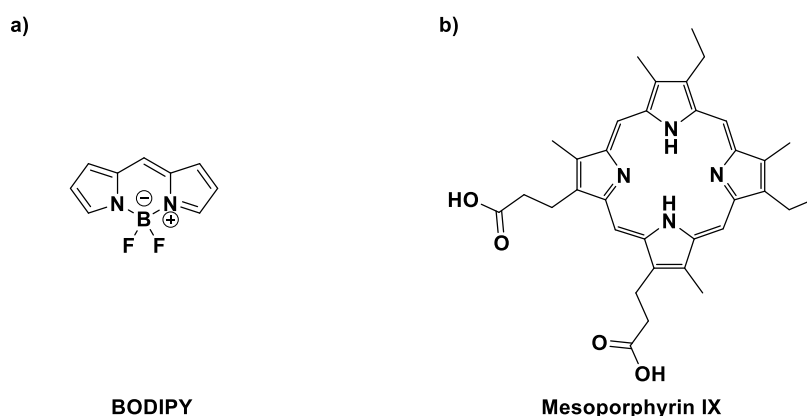
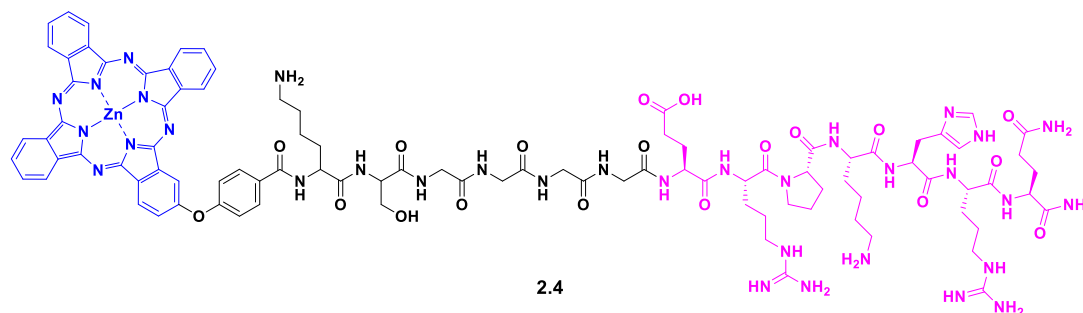


Figure 2.5: Structures of **a)** BODIPY and **b)** mesoporphyrin IX

Both QRHKPRE and AEYLR are relatively newly discovered EGFR targeting peptides. QRHKPRE was identified from a phage display library and was found to bind to the extracellular domain of EGFR with a k_d of 50 nM,⁸² approximately twice that of GE11. This peptide has been used for fluorescent imaging⁸³ and has been conjugated onto iron oxide nanoparticles for targeted magnetic resonance imaging (MRI).⁸⁴ QRHKPRE has been used to target a zinc phthalocyanine towards colorectal cancer with high selectivity towards EGFR overexpressing cancers observed (**Figure 2.6a, 2.4**).⁸³ AEYLR was derived from the major autophosphorylation site Y1173⁸⁵ on the EGFR and was initially designed as a tyrosine kinase inhibitor before its targeting ability was determined. It has been shown to co-localise with EGFR in human non-small cell lung cancer⁸⁶ and has been used to target liposomes and the fluorophore cyanine 7 (Cy7, **Figure 2.6b, 2.5**) towards EGFR expressing tumours in a mouse model.⁸⁷ AEYLR was shown to have a higher binding affinity towards EGFR than D4 and the binding of AEYLR was shown to be specific towards EGFR expressing cell lines.⁸⁶ Minimal work has been done using

this new EGFR peptide, but the stronger binding of AEYLR to the EGFR over D4 makes it an attractive targeting agent.

a)



b)

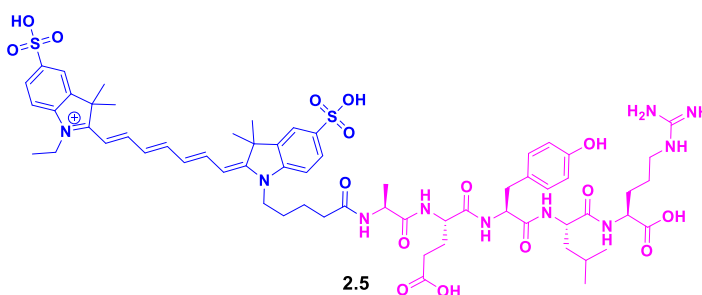


Figure 2.6: Structures of **a)** phthalocyanine-QRHKPRE PDC, consisting of a phthalocyanine (blue), linker (black) and QRHKPRE (pink) and **b)** Cy7-AEYLR conjugate for imaging, consisting of Cy7 (blue) and AEYLR (pink)

All four of these EGFR directing peptides show potential for the development of EGFR-directed gold nanocarriers for PDT. As only GE11 has previously been explored for the targeted delivery of gold nanoparticles, D4, QRHKPRE and AEYLR present an opportunity to develop novel nanocarriers for photodynamic therapy. D4 and AEYLR are of particular interest due to their short length, increasing ease of synthesis, and their high uptake into EGFR overexpressing cells.

2.2 Summary and chapter aims

The EGFR has been validated as a receptor for targeted treatments on NSCLC through current clinically relevant therapies. Its overexpression in *ca.* 60% of NSCLC cases has made it an extensively investigated receptor. Antibodies have been comprehensively investigated as targeting moieties with a lot of success, however the sensitivity of antibodies towards pH, temperature and solvents, along with the relative difficulty of controlling their conjugation limits their use as targeting agents.

Peptides display selective binding towards their target receptor and are more stable, cheaper to synthesise and more easily characterised than antibodies. Recently, possibly due to the difficulties of forming ADCs, a greater focus has been applied to PDCs as drug delivery systems. Four peptides that show selective binding to EGFR (GE11, D4, AEYLR and QRHKPRE) have been described in the literature. While no comparison has been made between QRHKPRE and the other EGFR targeting peptides, it has been reported that AEYLR shows a higher binding affinity towards EGFR than D4, which in turn shows higher uptake into cells than GE11. AEYLR, D4, QRHKPRE and GE11 have all been used to deliver payloads to EGFR overexpressing cell lines, with selective uptake observed. While PDCs and nanoparticle conjugates have been formed with these peptides, only GE11 and D4 have been explored for targeted photodynamic therapy. Furthermore, only GE11 has been investigated for delivery of nanoparticles carrying a photosensitiser. Since GE11 has been seen to be less efficient for uptake than D4 and AEYLR, investigating these peptides as targeting moieties for the delivery of nanoparticles is an exciting prospect.

In this chapter the peptides D4 and AEYLR were investigated as targeting moieties for phthalocyanine gold nanoparticles. Firstly, these peptides were modified to obtain the functionalities necessary for conjugation onto nanoparticles, then their ability to bind to EGFR overexpressing cells assessed. These peptides were then conjugated onto thiolated PEG (HS-PEG-COOH), before forming peptide-C11Pc-PEG-AuNPs. The synthesis of these nanoparticles was optimised before they were assessed for their ability to produce singlet oxygen, and the phototoxicity of these peptide-directed phthalocyanine-gold nanoparticles was assessed.

2.3 Results and discussion

2.3.1 Peptide selection and synthesis

As described in **section 2.1.5**, four peptides targeting EGFR have been reported. Of these, it is reported that AEYLR has the highest affinity for EGFR, followed by D4, GE11, and then QRHKPRE. AEYLR and D4 are also more attractive than GE11 due to their much shorter length, and therefore more accessible synthesis. All the reported data highlights AEYLR as the most attractive targeting peptide, however, there is only

one report of AEYLR as a targeting ligand for EGFR so both AEYLR and D4 were investigated in this study.

To synthesise these targeting peptides, fluorenylmethyloxycarbonyl (Fmoc) solid phase peptide synthesis (SPPS) was utilised. SPPS involves the growth of a peptide chain on a solid support or resin. The use of a solid resin means that many equivalents of reagents can be used in the synthesis of these peptides to drive couplings to completion, and then remaining reagents are simply washed away. This process allows for the quick, efficient and clean synthesis of peptides. Most resins are polystyrene beads and are functionalised with a linker to allow the growth of the peptide. A plethora of different resins with different linkers exist to allow for the desired functionality upon cleavage. For the peptide synthesis described throughout this thesis, rink amide MBHA resin was used. This resin has an acid labile linker, which forms a terminal amide on the C-terminus upon cleavage. This provides a neutral, non-reactive terminus to the synthesised peptides. Rink amide MBHA resin is purchased with an Fmoc protecting group on the linker. Fmoc is a base labile protecting group that can be removed by treatment of the resin with the base piperidine, leaving a free amine upon cleavage. Fmoc SPPS involves the use of Fmoc protected amino acids, preventing the formation of polymers of the same amino acid. Any amino acids with reactive functionalities in their side chains are protected with acid labile protecting groups, such as tert-butyl (*t*Bu) for acids and 2,2,4,6,7-pentamethyldihydrobenzofuran-5-sulfonyl (pbf) for amines, so these will remain protected throughout the peptide synthesis and prevent any unwanted reactions on amino acid side chains. Once Fmoc deprotection has been completed, five equivalents of the next Fmoc-protected amino acid is added to the resin, alongside five equivalents of the coupling agent and ten equivalents of *N,N*-diisopropylethylamine (DIPEA). DIPEA is a non-nucleophilic base that acts as a proton scavenger and activates the carboxylic acid. As it is non-nucleophilic, it does not compete with the amine nucleophile. Throughout this thesis two coupling agents were utilised. Peptides synthesised by hand used the coupling agent *N*-[(Dimethylamino)-1*H*-1,2,3-triazolo-[4,5-*b*]pyridin-1-ylmethylene]-*N*-methylmethanaminium hexafluorophosphate *N*-oxide (HATU) and peptides synthesised on the automatic peptide synthesiser used a mixture of *N,N,N',N'*-Tetramethyl-*O*-(1*H*-benzotriazol-1-yl)uronium hexafluorophosphate (HBTU) and 1-hydroxybenzotriazole hydrate (HOBt). The structures of HATU, HBTU and HOBt are given in **Figure 2.7**.

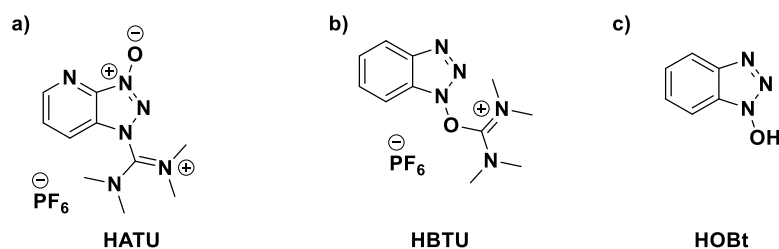
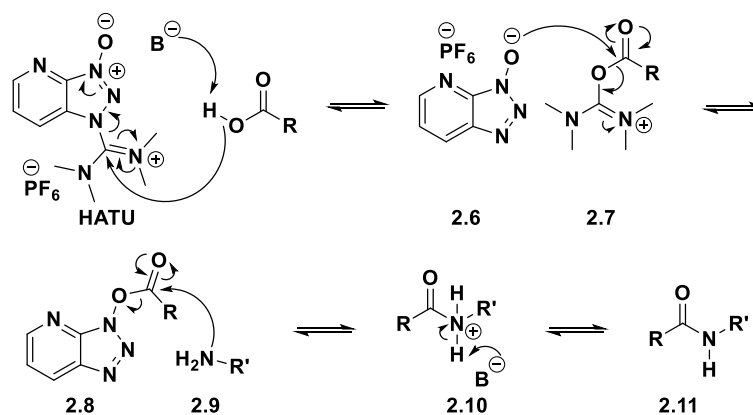


Figure 2.7: The structures of **a) HATU**, **b) HBTU** and **c) HOBT**

HATU is a more efficient coupling agent and is favoured for difficult couplings, but HBTU has a higher stability in DMF so is selected as a coupling agent for automatic peptide synthesis where large volumes of coupling agents are prepared for use over long periods of time. HATU and HBTU are similar in structure, however HATU is an azabenzotriazole derivative whereas HBTU is a benzotriazole derivative, as shown in **Scheme 2.1**, and HBTU contains a urea whereas HATU contains a guanidine. While these differences exist, their chemistry for amide bond formation is much the same. The general mechanism of both coupling agents is demonstrated in **Scheme 2.1** using HATU. The carboxylic acid of an amino acid is deprotonated by DIPEA, allowing for a nucleophilic attack on the carbocation on the coupling agent. This leads to an elimination of the azabenzotriazole, **2.6**. This in turn can attack the electrophilic carbonyl centre of **2.7** and eliminate tetramethylurea. The resulting activated ester, **2.8**, is attacked by the nucleophilic amine on the terminal amino acid of the growing peptide chain, **2.9**, releasing the azabenzotriazole and forming an amide bond. This additional basic nitrogen in HATU is thought to increase the efficiency of the amidation compared to that of HBTU, resulting in a lower level of racemisation. HBTU is used in conjunction with HOBT to prevent racemisation of amino acids. HBTU is more basic than HATU and can deprotonate the α -position of amino acids,⁸⁸ so HOBT is used to form an equilibrium with HBTU to limit the concentration of free active HBTU present in the reaction.

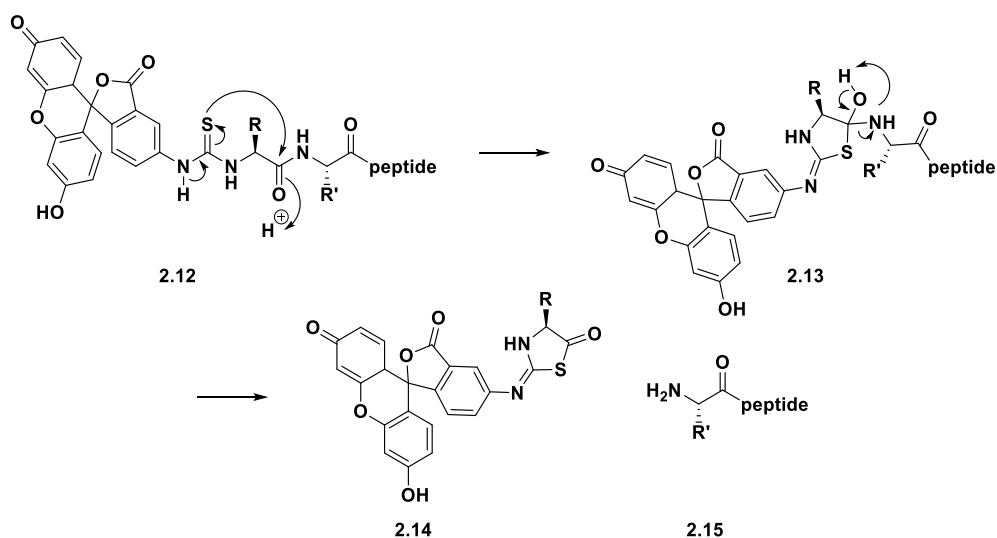


Scheme 2.1: The mechanism for amide bond formation using HATU

Once peptide synthesis is complete, the peptide can be removed from the resin by the addition of acid. In the case of rink amide MBHA, a cleavage cocktail of 95% trifluoroacetic acid (TFA), 2.5% triisopropylsilane (TIPS) and 2.5% water is used. Rink amide MBHA requires a relatively high concentration of acid to cleave, and this acid also cleaves any acid labile protecting groups on the side chains of amino acids. The TIPS and water in the cleavage cocktail act as a free radical scavengers to prevent any unwanted side reactions with cleaved protecting groups.

In this work, both AEYLR and D4 were modified slightly to make them fit for purpose as a directing ligand on gold nanoparticles. Both peptides were modified with a lysine residue on the N-terminus. As neither peptide contains a free amine in the side chains of their sequences, the addition of a primary amine through the lysine side chain provided an opportunity for site-specific conjugation using commonly used amide bond formation chemistry. These peptides were also modified with a fluorescent tag, fluorescein isothiocyanate (FITC), to allow for the determination of their binding to EGFR and their functionalisation onto gold nanoparticles.

FITC can undergo self-elimination from a peptide, **2.12**, under acidic conditions through a cyclisation with the neighbouring amino acid to give fluorescein thiazolinone, **2.14**, and a truncated peptide, **2.15**, as shown in **Scheme 2.2**. This elimination is driven by the formation of the thiazolinone, which can only be formed if the adjacent amino acid is an α -amino acid.



Scheme 2.2: elimination of FITC under acidic peptide cleavage conditions to give fluorescein thiazolinone and a truncated peptide

To overcome this elimination, a β -alanine spacer was inserted into the sequence before the addition of FITC.⁸⁹ Following these modifications, the two peptides built on the solid phase were FITC- β AAEYLRK (**2.16**) and FITC- β ALARLLTK (**2.17**). The structures of these peptides are shown in **Figure 2.8**.

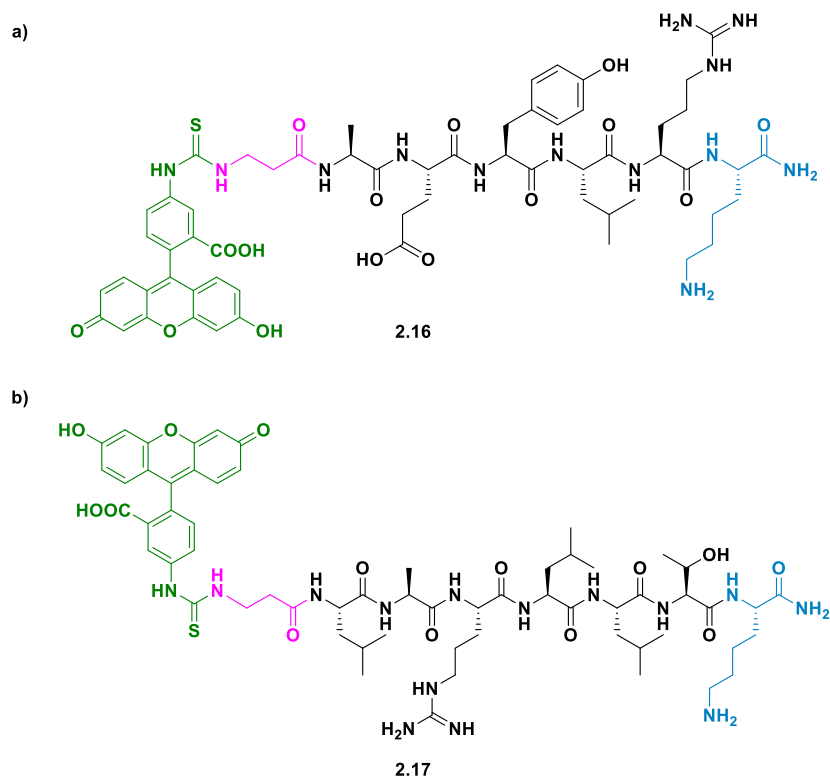


Figure 2.8: The structures of **a)** FITC- β AAEYLRK (**2.16**) and **b)** FITC- β ALARLLTK (**2.17**). The added lysine is highlighted in blue, the β -alanine spacer in pink and the FITC in green

2.16 and **2.17** were synthesised using SPPS as described above. Post cleavage, both peptides were purified by reverse-phase preparative HPLC, then their purity assessed by reverse-phase analytical HPLC. In some HPLC traces, two overlapping peaks are observed upon the cleavage of these peptides. Upon separation, these peaks show the same mass, both corresponding to the mass of the desired peptide. FITC, and its core structure fluorescein, are commonly depicted as a quinoid structure (**2.21**) with a carboxylic acid group. However, fluorescein and its derivatives possess seven prototropic forms (**Figure 2.9**) and under neutral conditions they can exist as three different structures; the quinoid structure (**2.21**), a lactone (**2.22**) or as a zwitterion (**2.23**).⁹⁰ It is then possible that due to the presence of TFA in the HPLC solvents, cationic FITC (**2.24**) could also exist. The difference between the lactone structure and the open ring quinoid (and charged species thereof) is significant enough that it could lead to marginally different retention times on the HPLC, giving rise to this double peak. These peaks were separated, then run again through the HPLC and the second peak then reappeared, further confirming the likelihood of these being two prototropic forms of FITC. Due to this effect, these peaks were both collected and used as the pure peptide. The successful synthesis of **2.16** and **2.17** was confirmed using MALDI mass spectrometry and high resolution LCMS. **2.16** was found to have the desired m/z of 1236.4804, which corresponded to $[M-H]^-$ with a mass of 1236.5226. **2.17** was calculated to have a $[M+2H]^{2+}$ mass calculated as 673.3235, and a m/z of 637.3260 was found.

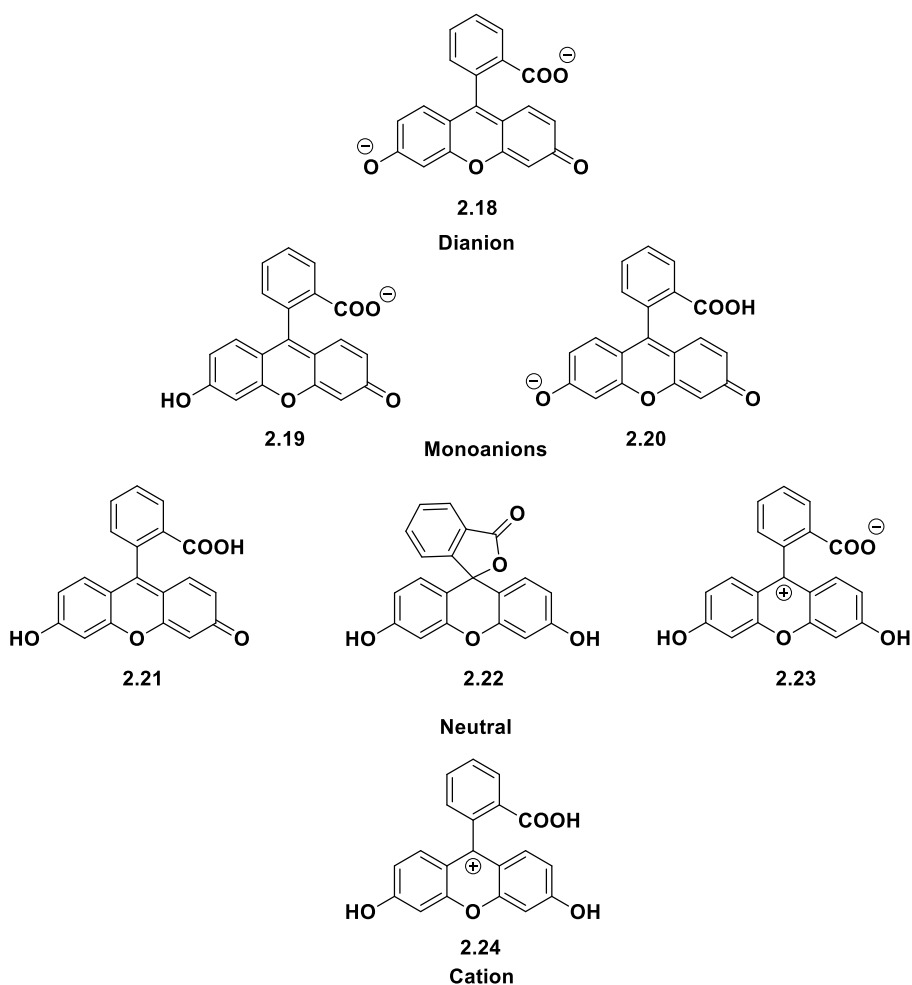


Figure 2.9: Prototropic forms of fluorescein

2.3.2 Determination of receptor presence on cell lines

To explore the targeting ability of these peptides towards EGFR present in non-small cell lung cancer, the EGFR overexpressing NSCLC cell line A549⁹¹ was investigated. To determine whether this cell line does indeed overexpress EGFR, flow cytometry was utilised. Flow cytometry involves the incubation of cells with a primary antibody specific to the receptor, in this case an anti-EGFR antibody. The cells are incubated alongside this antibody on ice to prevent internalisation of the receptors. Bovine serum albumin (BSA) is added to the PBS for all incubations to block any non-specific interactions between the antibody and the cell surface. Once incubated for one hour, the primary antibody is washed off and a fluorescently tagged secondary antibody is added and incubated on ice for one hour. This secondary antibody has affinity for the heavy chain of the primary antibody and is specific to the animal host that the primary antibody was cultured in. In this case a FITC-goat anti-mouse antibody was used as the primary antibody was cultured

in mice. The specificity of this secondary antibody towards the primary antibody, and not any part of the cell, means that only cells which the primary antibody has bound to will be fluorescently tagged, and in turn, only cells that possess the EGFR receptor will be tagged. The flow cytometer counts individual cells and measures the fluorescence intensity of each cell. This means that the fluorescence intensity of a sample can be used to compare the relative quantities of EGFR on the cell surface, as each secondary antibody binds 1:1 with a primary antibody. This means a higher fluorescence correlates to a higher density of EGFR on the surface. For each sample a negative control is run, with these cells incubated with BSA/PBS without the primary antibody, then the secondary antibody, to account for any background fluorescence. **Figure 2.10a** shows a large increase in the FITC fluorescence intensity of A549 cells when incubated with anti-EGFR antibody and the FITC-tagged secondary antibody when compared to the negative control (31-fold increase in fluorescence, **Table 2.1**), showing a high amount of EGFR is present on this cell line. Due to the ubiquity of EGFR throughout epithelial cells, it is very difficult to find a cell line with no EGFR to use as a control cell line. The epithelial embryonic kidney cell line HEK293⁹² was found to show a 6.7-fold increase in fluorescence upon incubation with an anti-EGFR antibody compared to that of the control (**Table 2.1**), suggesting HEK293 cells (**Figure 2.10b**) have a much lower level of EGFR compared to A549 cells. This suggests that HEK293 cells should have a reduced uptake of EGFR targeted nanoparticles and can be used as a control.

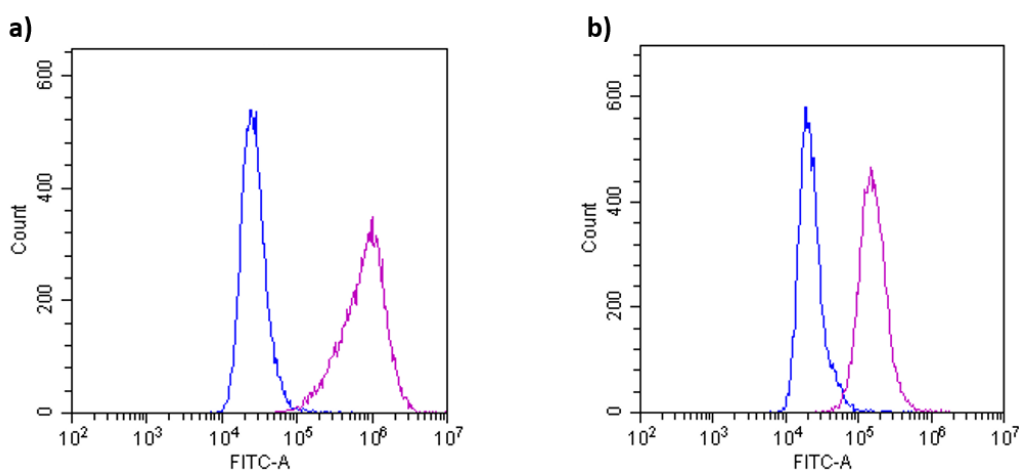


Figure 2.10: Flow cytometry histograms of **a)** A549 and **b)** HEK293 cells incubated with an anti-EGFR Ab then FITC-goat antimouse secondary Ab (purple) or just with the secondary Ab (blue)

Table 2.1: Mean fluorescence of A549 and HEK293 cells incubated with anti-EGFR antibody, then FITC-goat anti-mouse secondary Ab, or with the secondary Ab alone, and the fold increase in fluorescence upon addition of anti-EGFR antibody

Cell line	Average fluorescence, anti-EGFR treated	Average fluorescence, control	Fold increase in fluorescence
A549	924348.2	29837.9	31.0
HEK293	176635.9	26198.8	6.7

2.3.3 Confirmation of peptide binding

The binding of **2.16** and **2.17** was confirmed using fluorescence microscopy. A549 cells, shown to overexpress the EGFR receptor, were grown overnight in 96 well plates and incubated with **2.16** or **2.17** for one hour, alongside a fluorescein control. After washing with PBS, the cells were imaged, as shown in **Figure 2.11**.

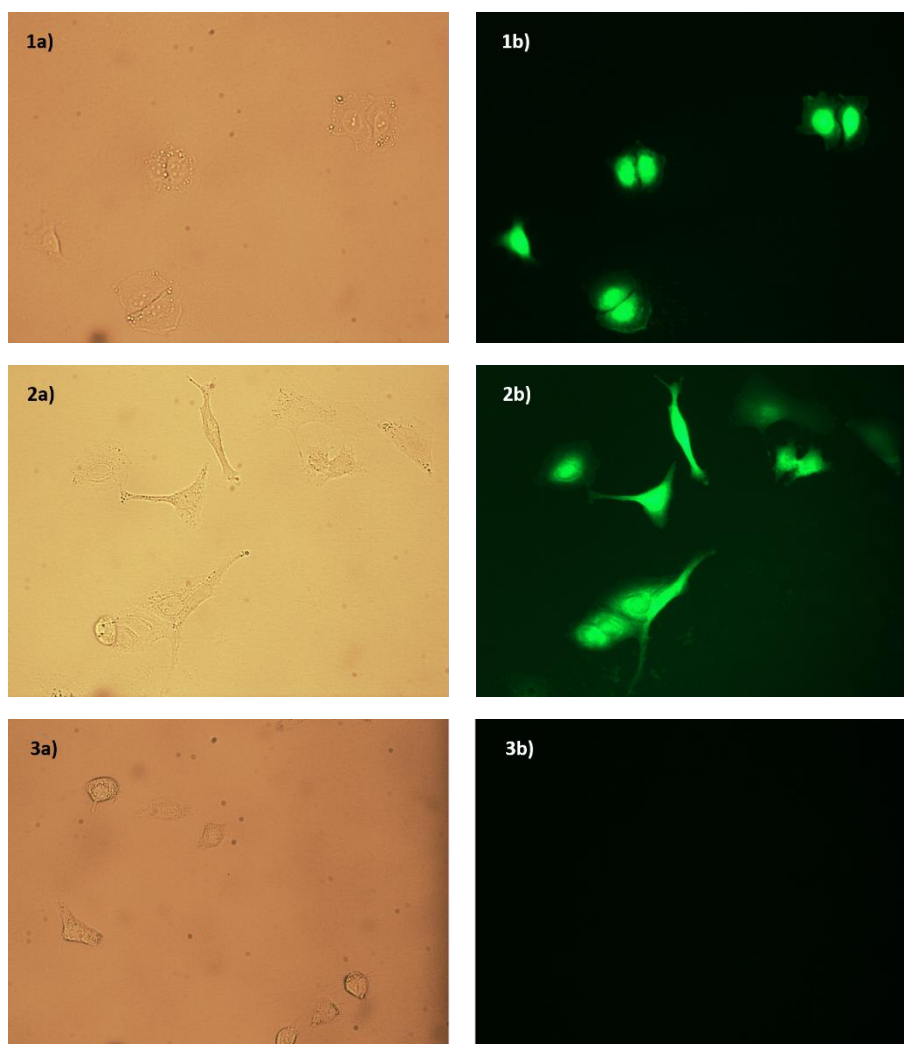


Figure 2.11: a) Bright field and b) fluorescence microscopy images of A549 cells incubated for 1 hour with 1) 100 μ M **2.16**, 2) 100 μ M **2.17** and 3) 100 μ M fluorescein

A549 cells were seen to uptake both peptides, but not fluorescein, suggesting these peptides still bind to EGFR overexpressing cells post modification and that the fluorescein tag does not influence their uptake.

2.3.4 Cell viability assays

To determine whether **2.16** or **2.17** affected cell viability, they were incubated alongside A549 and HEK293 cells for 72 hrs before the cell viability was assessed with the cell proliferation assay 3-(4,5-dimethylthiazol-2-yl)-5-(3-carboxymethoxyphenyl)-2-(4-sulfophenyl)-2H-tetrazolium (MTS). MTS is a yellow dye including a tetrazole that can be metabolised by dehydrogenases in live cells to produce a purple formazan product, **2.25**, as shown in **Figure 2.12**.

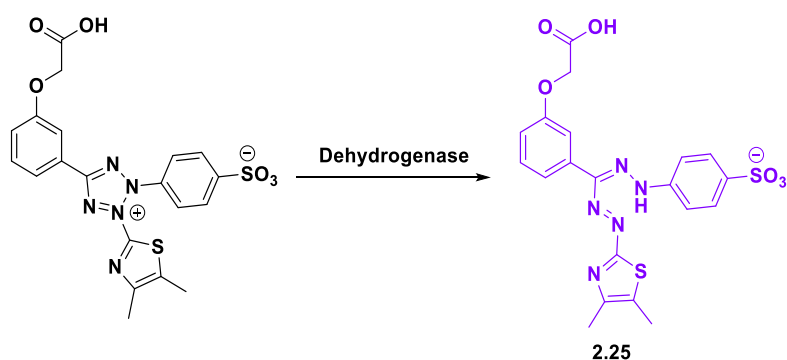


Figure 2.12: The conversion of MTS to formazan by dehydrogenases

These dehydrogenases are only reductive in metabolically active cells, so the consumption of MTS can give a snapshot of the relative number of metabolically active cells within a well. Staurosporine is an antibiotic which is known to cause apoptosis in human cell lines so can be used as a positive control for cell death. Both **2.16** and **2.17** were seen to display neither agonistic nor antagonistic activity towards either cell line, as shown in **Figure 2.13**.

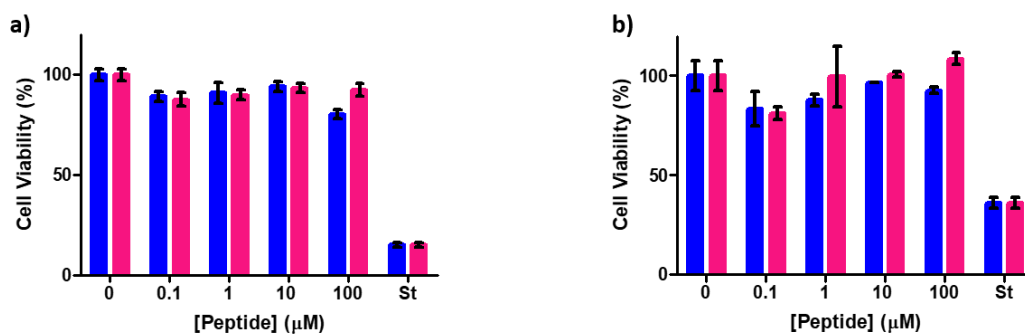


Figure 2.13: Cell viability of *a)* A594 and *b)* HEK293 cells incubated with **2.16** (blue) or **2.17** (pink). St= positive control of staurosporine

2.3.5 Synthesis of a scrambled peptide to confirm targeting effect of AEYLRLK

The scrambled and substituted peptide FITC-RALEL has been described as a negative control for **2.16**.⁸⁷ The tyrosine residue in **2.16** has been shown to be vital for binding so in this negative control it is substituted for leucine. Again, as for **2.16** and **2.17**, the structure of this peptide was modified with lysine at the N-terminus and β -alanine-FITC at the C-terminus. The resulting peptide FITC- β ARALELK (**2.26**, **Figure 2.14**) was synthesised by solid phase peptide synthesis and the synthesis confirmed by high resolution mass spectroscopy; an m/z of 396.8570 was found, corresponding to $[M+3H]^{3+}$, which was consistent with the calculated mass of 396.8551.

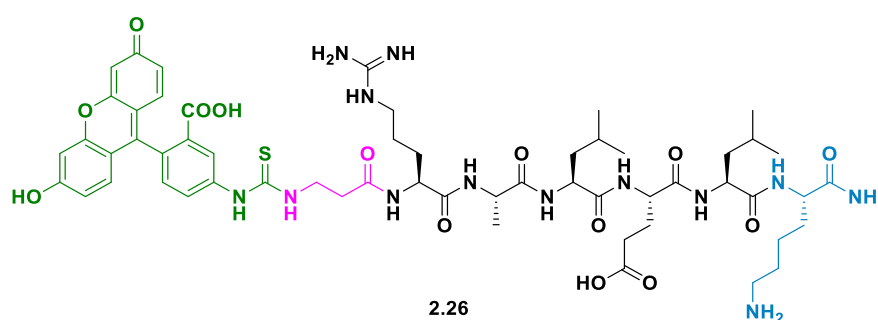


Figure 2.14: Structure of FITC- β ARALELK (**2.26**), with the added lysine residue shown in blue, the β -alanine in pink and the FITC in green

To determine that **2.26** was no longer internalised by EGFR overexpressing cells, it was incubated alongside A549 cells and imaged using a fluorescent microscope. **Figure 2.15** shows A549 cells incubated with **2.26**. No fluorescence is observed suggesting that this scrambled and substituted peptide is no longer recognised by EGFR and is not internalised by A549 cells.

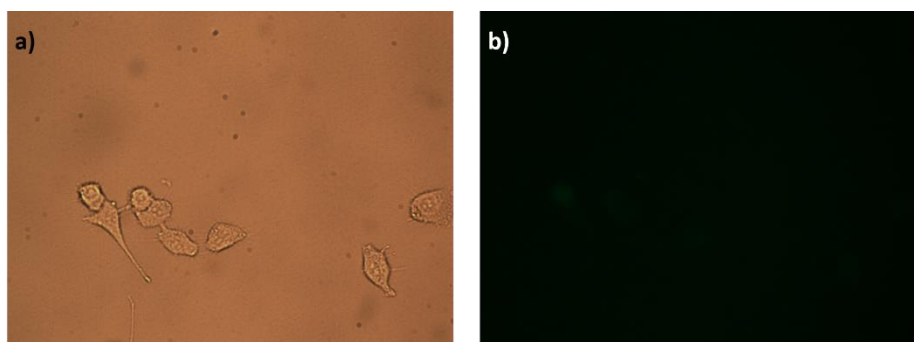


Figure 2.15: a) Bright field and b) fluorescence microscopy images of A549 cells incubated with 100 μM 2.26 for one hour

2.3.6 Nanoparticle synthesis and characterisation

2.3.6.1 Synthesis of peptide directed phthalocyanine-gold nanoparticles

Throughout this thesis, the photosensitiser (1,1',4,4',8,8',15,15',18,18',22,22'-tetradecakisdecyl-25,25'-(11,11'dithiodiundecyl) diphthalocyanine zinc (C11Pc) has been used (**Figure 2.16**). This diphthalocyanine has been investigated as a photosensitiser, with its disulphide allowing for easy attachment onto AuNPs. Russell and co-workers have established an efficient synthesis for *ca.* 4 nm AuNPs functionalised with both C11Pc and PEG,⁹³ with this mixed monolayer forming a water soluble nanocarrier, important as C11Pc itself is very hydrophobic.

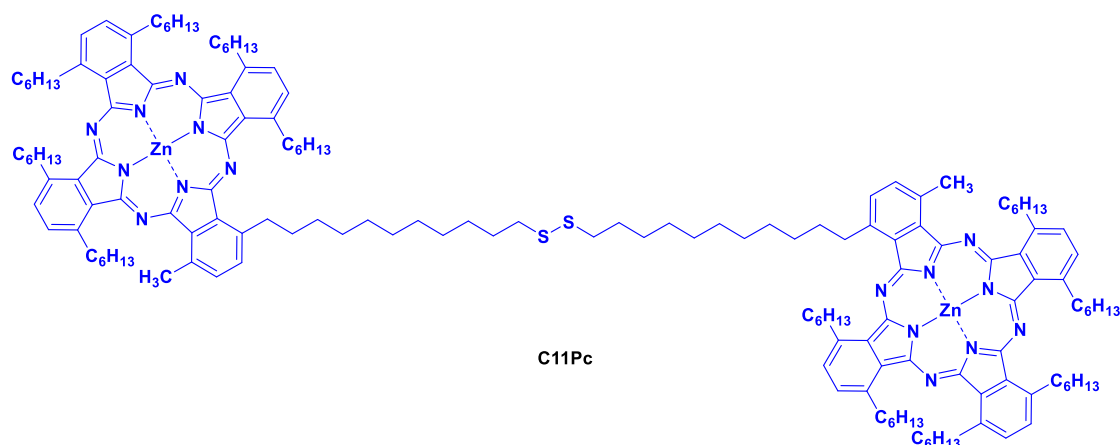


Figure 2.16: Structure of the C11Pc dimer

Russell and co-workers have also found that the use of bifunctionalised HS-PEG-COOH allows for the easy addition of this PEG to the AuNPs through gold-sulphur bonds, and the carboxylic acid allows for further functionalisation of these AuNPs with targeting agents. The group has investigated the use of the lectin Jacalin and an anti-HER2 antibody for targeted therapy of the Thomsen-Friedenreich antigen, a ubiquitous cancerous marker

found in prostate cancer, and HER2 positive breast cancers respectively.^{94–96} Due to the relatively sensitive nature of proteins and antibodies, the conjugation of these onto AuNPs must occur post-synthesis of the core as proteins have a very low tolerance for organic solvents. The hydrophobicity of C11Pc means it is not soluble in aqueous media so the synthesis of these nanoconjugates must be completed in organic solvents, with the most efficient synthesis occurring in THF. There is currently no validated method to determine the concentration of antibodies or proteins on the surface of gold nanoparticles and the complex and unknown 3D structure of these synthesised nanoparticles makes it hard to predict how much of these targeting proteins are present on the surface of these nanoconjugates.

As peptides are more robust than the previously used proteins, this provides the opportunity to have a tighter control over the directing group functionalisation of the nanoparticles. The carbodiimide mediated coupling of directing groups post nanoparticle synthesis used by Russell and co-workers is a very random event, limiting the efficiency of this reaction. As peptides can tolerate organic solvents, the peptide can be conjugated onto the PEG before the synthesis of the nanoparticles. It has been shown that the attachment of a directing group to the PEG prior to nanoparticle synthesis does not affect the nanoparticle synthesis.⁹⁷ For the conjugation of **2.16** and **2.17** to HS-PEG-COOH, HATU/DIPEA coupling was utilised, using DMF as a solvent, with the reaction left overnight, giving **2.16**-PEG (**2.27**) and **2.17**-PEG (**2.28**). This coupling is very efficient and increases the confidence that the peptide is conjugating onto the PEG. Due to the polydisperse nature of the PEG, it is difficult to track this reaction, but due to the long timeframe of the reaction and the excess peptide added to the reaction, it can be assumed that this reaction goes to completion. This pre-functionalised PEG can be used directly in the synthesis of nanoparticles. A flow diagram for the synthesis and purification of peptide-functionalised C11Pc-PEG-AuNPs is shown in **Figure 2.17**. For the initial synthesis of these nanoconjugates, it was decided that a ratio of 50:50 PEG:peptide-PEG would be used as it has been reported that overcrowding nanoparticles with targeting groups can lead to a reduction in efficiency of this targeting.⁹⁸

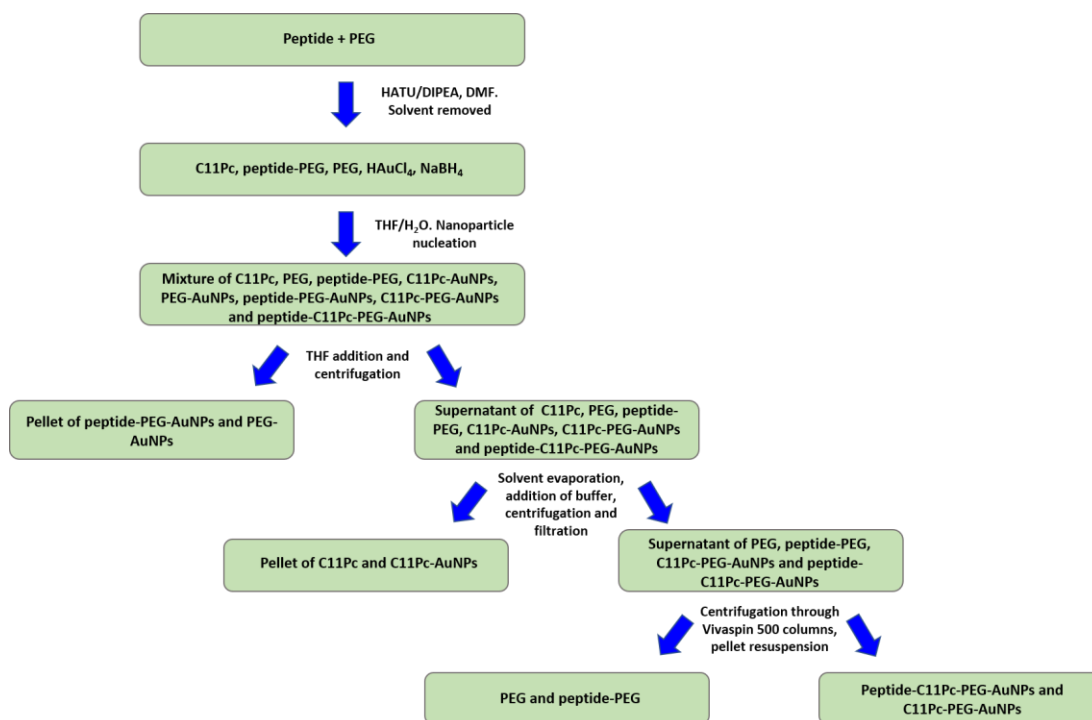


Figure 2.17: Flow diagram of the synthesis and purification of peptide-C11Pc-PEG-AuNPs

The synthesis of **2.16**-C11Pc-PEG-AuNPs (**2.29**) and **2.17**-C11Pc-PEG-AuNPs (**2.30**) involved the mixing of C11Pc, PEG, peptide-PEG and HAuCl₄ in anhydrous THF, followed by the addition of sodium borohydride in water under vigorous stirring. The sodium borohydride reduces the Au(III) to Au(0), leading to the formation of AuNPs by nucleation. The borohydride also reduces the disulphide in C11Pc, then the free thiols of C11Pc, PEG and peptide-PEG act as capping agents, forming very strong gold-sulphur bonds with the nanoparticles. This capping is completely random, so a mixture of nanoparticles is formed in the initial synthesis, including AuNPs with only C11Pc on the surface (C11Pc-AuNPs), AuNPs with only peptide-PEG on the surface (peptide-PEG-AuNPs), AuNPs with only PEG on the surface (PEG-AuNPs), C11Pc-PEG-AuNPs and the desired peptide-C11Pc-PEG-AuNPs. This mixture also contains unreacted ligands (C11Pc, PEG and peptide-PEG) as these are added in a high excess to limit the size of the nanoparticles to *ca.* 4 nm.

Once synthesised, the nanoconjugates were purified, first by addition of more THF. This led to the precipitation of any peptide-PEG-AuNPs or PEG-AuNPs that had formed in the synthesis as they have a much lower solubility in THF. These could be removed by centrifugation, giving a pellet of peptide-PEG-AuNPs and PEG-AuNPs. The

supernatant was removed, containing a mixture of C11Pc, PEG, peptide-PEG, C11Pc-AuNPs, C11Pc-PEG-AuNPs and peptide-C11Pc-PEG-AuNPs.

The supernatant containing this mixture was then dried under vacuum. PBS was added to the dry product to dissolve the desired nanocarriers with a mixture of C11Pc, peptide-PEG and PEG on the surface. A mixture of C11Pc and C11Pc-AuNPs remained undissolved in the solution and were removed by centrifugation and syringe filtration.

The resulting mixture was very yellow due to the presence of free peptide-PEG, so the nanoparticles were purified through Vivaspin 500 columns, collecting the nanoparticles and washing through any unconjugated PEG or peptide-PEG. The resulting nanoparticle pellet contained peptide-C11Pc-PEG-AuNPs (**Figure 2.18**) and was resuspended in PBS buffer.

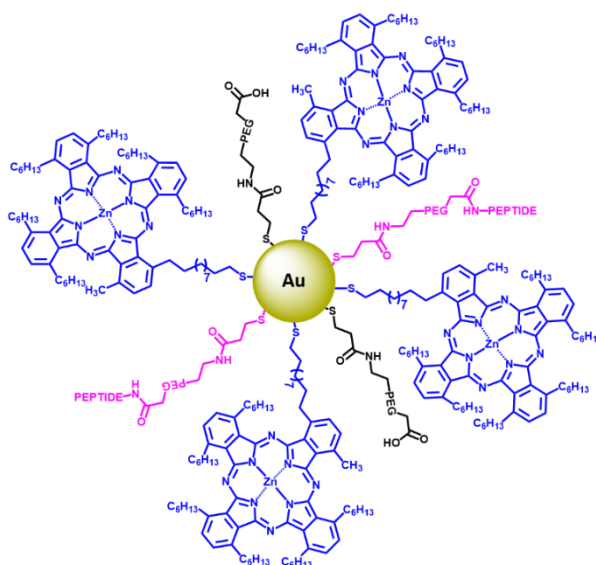


Figure 2.18: A 2D representation of peptide-C11Pc-PEG-AuNPs. A gold core is functionalised with C11Pc, PEG and peptide-PEG through stable gold-thiol bonds, forming a mixed monolayer

There is a possibility that a small number of non-functionalised C11Pc-PEG-AuNPs were also synthesised and these would also be present in this pellet. In this work, these C11Pc-PEG-AuNPs have not been separated from the peptide-C11Pc-PEG-AuNPs. In future work it may be possible to separate these conjugates by using the recognition of this peptide by EGFR to immobilise these nanoparticles on a resin or surface. The non-functionalised C11Pc-PEG-AuNPs could then be washed away before eluting the peptide-C11Pc-PEG-AuNPs with excess peptide. A second methodology could involve the synthesis of a branched PEG linker with both conjugated and non-conjugated PEG

present, yet only one thiol (**Figure 2.19, 2.31**). This would mean that the concentration of peptide could be controlled by this linker and no AuNPs could be synthesised without directing peptide on their surface.

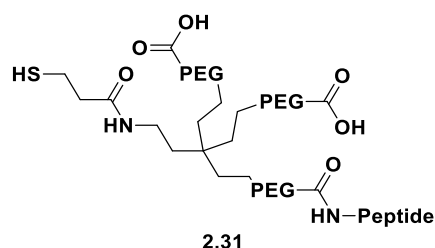


Figure 2.19: Trimeric PEG linker for controlling peptide concentration on AuNPs but ensuring all nanoparticles are functionalised with peptide

The resulting nanoparticles were characterised by UV-vis spectroscopy, as shown in **Figure 2.20**. The characteristic double peak spectrum of C11Pc was observed at 643 nm and 696 nm, and a second small peak at 495 nm showed the presence of FITC on these nanoconjugates, and therefore that the peptides were successfully conjugated to the nanocarriers. The UV-vis spectrum of AuNPs can also be used to determine their size due to a size-dependent surface plasmon resonance (SPR) band. It has been seen that very small AuNPs (*ca.* 3-4 nm) have a very weak SPR band, with AuNPs above 5 nm showing an intense SPR at *ca.* 520 nm.^{99,100} The lack of significant SPR band in the UV spectra of **2.29** and **2.30** suggests the synthesised nanoparticles are below 5 nm in size.

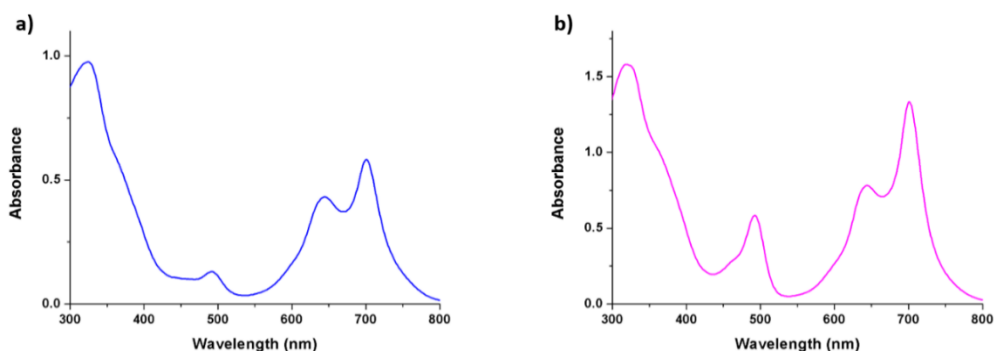


Figure 2.20: UV-vis spectra of **a) 2.29** and **b) 2.30** in PBS

2.3.6.2 Synthesis of control nanoparticles

In order to assess the photodynamic activity of **2.29** and **2.30**, a set of control nanoparticles were synthesised, as summarised in **Table 2.2**. Firstly, PEG-AuNPs were synthesised to act as a control for singlet oxygen production. As these nanoparticles are

not functionalised with a photosensitiser, they should not be able to convert triplet oxygen to singlet oxygen and therefore should not display any photodynamic activity. To synthesise PEG-AuNPs, a solution of PEG and gold chloride was reduced with sodium borohydride, forming a solution of brown nanoparticles. The resulting PEG-AuNPs were purified in Vivaspin 500 columns and resuspended in phenol-red free RPMI 1640 cell media for cell testing. The resulting nanoconjugates were characterised by UV-vis spectroscopy, as shown in **Figure 2.21**, and the resulting UV spectrum was characteristic of *ca.* 4 nm PEG-AuNPs.⁹⁹

Table 2.2: Summary of the synthesised control AuNPs

Control AuNPs	Reason for control
PEG-AuNPs	No photosensitiser or targeting moiety. Control for singlet oxygen production of photosensitiser
FITC-PEG-AuNPs (2.31)	Only FITC attached. Control to determine if there is any photodynamic activity from the FITC tag
2.16-PEG-AuNPs (2.32)	FITC and targeting ligand attached. Targeted control to determine if there is any photodynamic activity from the FITC tag
C11Pc-PEG-AuNPs	Non-targeted phthalocyanine AuNPs. Control for effect of targeting peptide on singlet oxygen production and phototoxicity
FITC-C11Pc-PEG-AuNPs (2.33)	Both potential photosensitisers but no targeting ligand. Control for whether peptide or FITC is encouraging internalisation

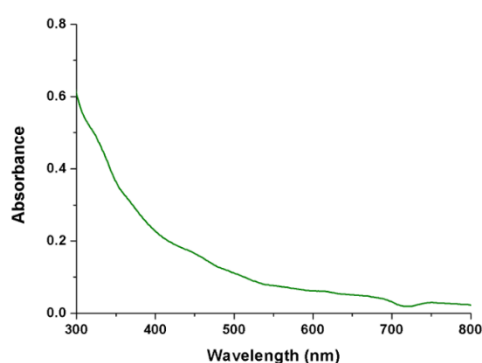


Figure 2.21: UV-vis spectra of PEG-AuNPs in phenol red free RPMI

As fluorescein has been shown to act as a photosensitiser,¹⁰¹ and other fluorescein derivatives such as Rose Bengal are commonly used photosensitisers,^{102,103} control FITC-PEG-AuNPs (2.31) were synthesised to determine whether any activity of 2.29 or 2.30

was due to photosensitisation by FITC instead of due to the C11Pc photosensitiser itself. These nanoparticles were synthesised by functionalising PEG with 5-(3-(3-aminopropyl)thioureido)-2-(6-hydroxy-3-oxo-3H-xanthen-9-yl) benzoic acid (**Figure 2.22, 2.34**), before a solution of gold chloride was reduced with sodium borohydride in the presence of a 50:50 mix of FITC-PEG:PEG. **2.31** were purified in Vivaspin 500 columns and characterised by UV-vis spectrometry (**Figure 2.23a**). The characteristic UV spectrum of *ca.* 4 nm PEG-AuNPs was again observed, with a large peak at 495 nm, showing the presence of FITC on these nanoparticles.

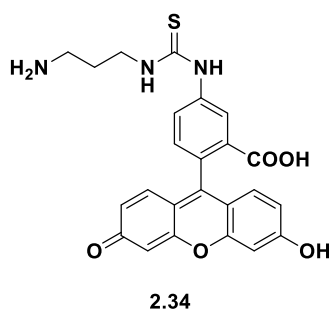


Figure 2.22: The structure of 5-(3-(3-aminopropyl)thioureido)-2-(6-hydroxy-3-oxo-3H-xanthen-9-yl) benzoic acid

To further confirm that the FITC tag itself was not responsible for any photodynamic activity, **2.16**-PEG-AuNPs (**2.32**) were synthesised. These nanocarriers were functionalised with the targeting peptide but no C11Pc photosensitiser. These conjugates would therefore show the same targeted uptake into EGFR overexpressing cell lines as **2.29**, and therefore can be used to assess if all the photodynamic activity observed *in vivo* is due to the phthalocyanine itself. **2.32** were synthesised by functionalising PEG with **2.16**, before a solution of gold chloride was reduced with sodium borohydride in the presence of a 50:50 mix of **2.16**-PEG:PEG. These nanocarriers were purified by centrifugation in Vivaspin 500 columns, then the nanocarriers resuspended in phenol red free RPMI and the UV-vis spectrum recorded (**Figure 2.23b**). As with **2.31**, a characteristic peak at 495 nm shows the presence of FITC on these nanocarriers, and the lack of an SPR band confirms these AuNPs to be below 5 nm in size.

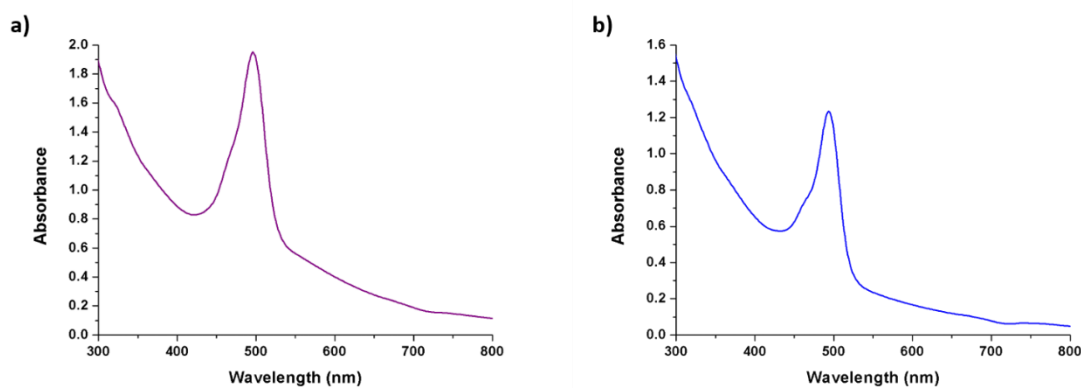


Figure 2.23: UV-vis spectra of a) 2.31 and b) 2.32 in phenol red free RPMI

Control C11Pc-PEG-AuNPs were synthesised following the method of Garcia-Calavia *et al.*⁹⁶ to allow the comparison of the singlet oxygen production of 2.29 and 2.30 with previously reported AuNPs. These C11Pc-PEG-AuNPs also provided a non-directed control for phototoxicity assays to determine whether there was any increased phototoxicity upon peptide conjugation due to selective uptake of the nanocarriers. The UV-vis spectrum of the C11Pc-PEG-AuNPs is shown in Figure 2.24a, showing the characteristic double peak of C11Pc.

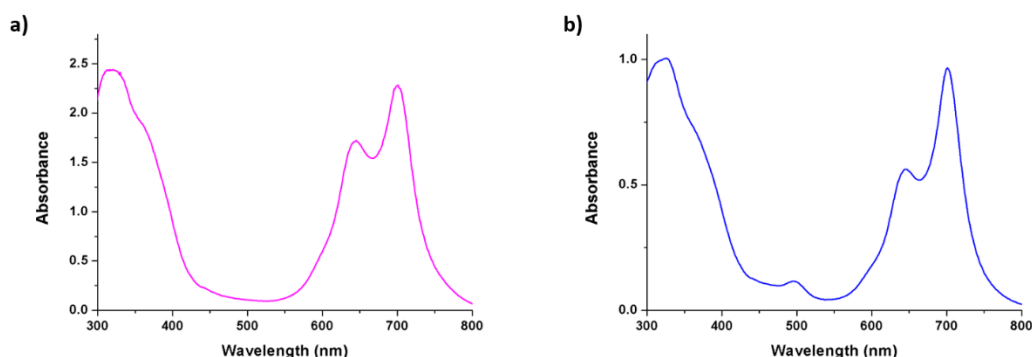


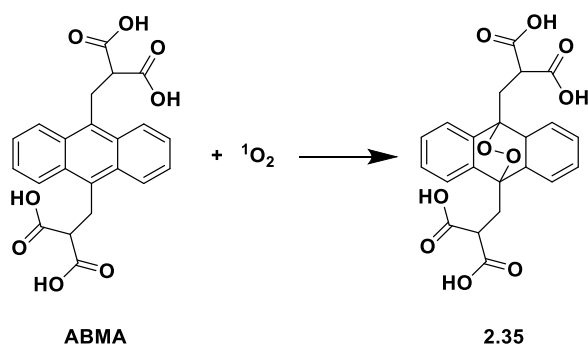
Figure 2.24: UV-vis spectra of a) C11PC-PEG-AuNPs and b) 2.33 in phenol red free RPMI

The final control AuNPs synthesised in this thesis were FITC-C11Pc-PEG-AuNPs (2.33). These AuNPs contained both the photosensitiser and the fluorescent tag which is conjugated on to the directing peptide in 2.29 and 2.30. While again providing a control for whether FITC induces a photodynamic effect, these nanocarriers also provided a control to determine that the targeted activity of 2.29 and 2.30 was due to the peptide sequences themselves, and not due to an increased uptake due to the presence of a large, hydrophobic tag. 2.33 were synthesised following the method described for the synthesis

of peptide-AuNPs (section 2.3.6.1) but FITC-PEG was used in the place of peptide-PEG. The resulting UV-vis spectrum (Figure 2.24b) showed the characteristic peaks of both C11Pc and FITC, confirming their synthesis.

2.3.6.3 Singlet oxygen production

To determine whether the synthesised nanocarriers produce singlet oxygen as desired, the singlet oxygen probe 9,10-anthracenediyl-bis(methylene) dimalononic acid (ABMA) was used. ABMA is a fluorescent anthracene derivative which undergoes a photobleaching reaction upon exposure to singlet oxygen, forming a non-fluorescent 9,10-endoperoxide, **2.35**, as shown in Scheme 2.3. This means that the production of singlet oxygen can be tracked by a decrease in fluorescence of the anthracene probe.



Scheme 2.3: Photobleaching reaction of ABMA, producing a non-fluorescent endoperoxide

A $1\ \mu\text{M}$ solution of **2.29** or **2.30** in PBS was mixed with ABMA in a cuvette and the fluorescence emission of ABMA recorded. The cuvette was then irradiated at 633 nm for 30 minutes, with the 10 mW HeNe laser placed 50 cm away from the cuvette. The fluorescence emission of ABMA was recorded every five minutes and the effect of irradiation on the emission observed. The singlet oxygen production of **2.29** and **2.30** was compared to $1\ \mu\text{M}$ non-targeted C11Pc-PEG-AuNPs, control PEG-AuNPs and PBS, with the singlet oxygen production summarised in Figure 2.25. The lifetime of singlet oxygen in aqueous solvents is very short so the production of singlet oxygen does not produce a large decrease in ABMA fluorescence. It was found that irradiation of PBS and PEG-AuNPs resulted in no photobleaching of ABMA, which is expected as no photosensitiser is present. Non-targeted C11Pc-PEG-AuNPs produced singlet oxygen, and over 30 minutes resulted in a 22% decrease in fluorescence. **2.29** also showed

significant singlet oxygen production, causing an 11% decrease. Surprisingly, **2.30** did not show production of singlet oxygen.

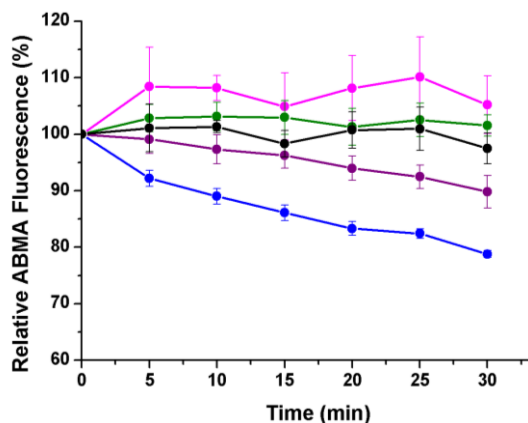


Figure 2.25: Singlet oxygen production PBS (pink), **2.30** (green), PEG-AuNPs (black), **2.29** (purple) and C11Pc-PEG-AuNPs (blue). All AuNPs were tested at 1 μ M C11Pc with 1 μ M ABMA

The amino acids methionine, histidine, tryptophan and tyrosine are known to quench singlet oxygen production.^{104–106} This may contribute to the reduction in singlet oxygen production by C11Pc upon the addition of **2.16** to these nanoconjugates, however **2.17** does not contain any of these amino acids.

The emission spectrum of C11Pc does not overlap with the excitation spectrum of FITC, as shown in **Figure 2.26**, so there is no possibility of energy transfer between these two molecules accounting for the lack of singlet oxygen production. Photosensitisers can self-quench when placed close together,^{107,108} so one explanation for the observed quenching of **2.30** is that the distribution of C11Pc on the surface of **2.30** may lead to the self-quenching. As **2.30** were found to not produce singlet oxygen, these nanoconjugates were not investigated any further.

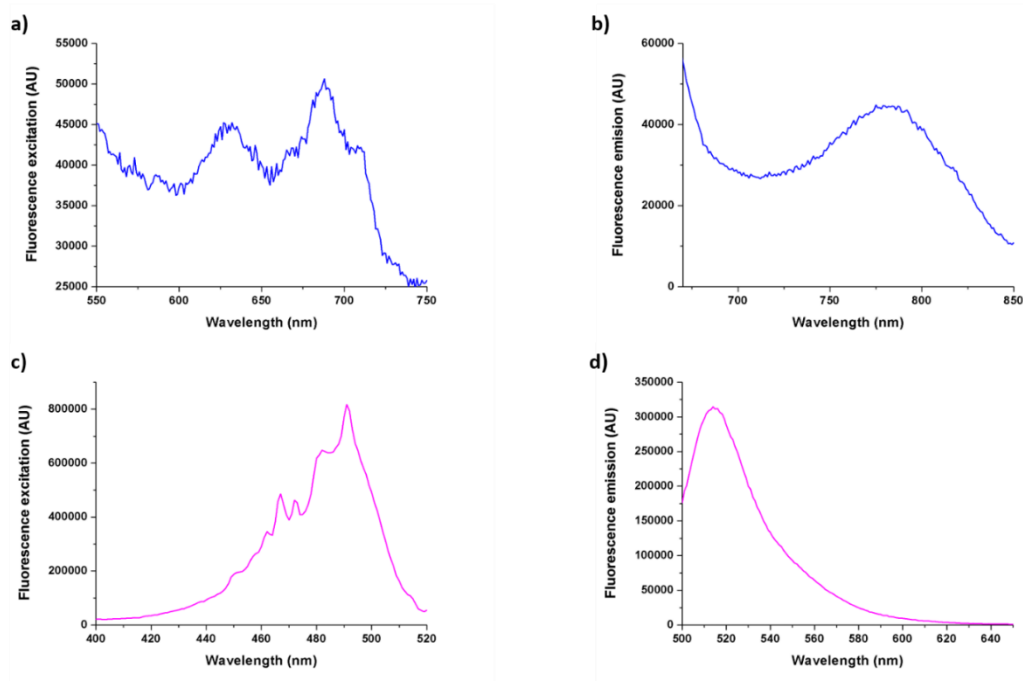


Figure 2.26: Fluorescence excitation spectra of **a)** C11Pc and **c)** FITC and fluorescence emission spectra of **b)** C11Pc and **d)** FITC ligands on **2.29** in PBS.

2.3.6.4 Solvent variation

While the synthetic procedure described in **section 2.3.6** was initially successful, the formation of nanoparticles was found to be very temperamental, and with no obvious pattern to whether this reaction would proceed or not. Due to this, different conditions were attempted to try to optimise the synthesis of **2.29** and gain a more reliable method. Initially, the solvent system was investigated as the functionalised **2.16**-PEG (**2.27**) did not appear to fully dissolve in THF. Due to this, both methanol and DMF were trialled as solvents, varying from just for the PEG, to the solvent for all but the C11Pc, as detailed in **Table 2.3**.

The synthesis of **2.29** in methanol (**method 4**) resulted in nanoparticle formation, but the resulting solution was miscoloured. The solution appeared to be a mixture of nanoparticles and any purification attempts did not purify this solution, so this solvent system was discounted. The syntheses of nanocarriers in solely DMF (**method 5**) and using DMF to solubilise the **2.27** while keeping all other conditions the same (**method 8**) were successful, but only method 8 showed singlet oxygen production. The synthesis using DMF (**method 5**) resulted in a much higher concentration of phthalocyanine than either of the syntheses using THF (**method 1 & 8**).

Table 2.3: Synthesis conditions trialled for **2.29**. All organic solvents were anhydrous

Method	2.27 coupling conditions	AuNPs synthesis conditions	Successful synthesis?	Singlet oxygen production?
1	1.5 eq HATU, 12 hrs, DMF	C11Pc, 2.16 -PEG, PEG and HAuCl ₄ in THF, NaBH ₄ in H ₂ O	Sporadically	Yes
2	1.5 eq HATU, 12 hrs, DMF	C11Pc and HAuCl ₄ in THF, PEG and 2.16 -PEG in DMF, NaBH ₄ in H ₂ O	No	-
3	1.5 eq HATU, 12 hrs, DMF	C11Pc in THF, PEG, 2.16 -PEG and HAuCl ₄ in DMF, NaBH ₄ in H ₂ O	No	-
4	PEG-NHS, 12 hrs, DMF	C11Pc, PEG and HAuCl ₄ in THF, 2.16 -PEG, PEG in MeOH, NaBH ₄ in H ₂ O	Yes, but hard to purify	-
5	1.5 eq HATU, 12 hrs, DMF	C11Pc in THF, PEG, 2.16 -PEG, HAuCl ₄ and NaBH ₄ in DMF	Yes	No
6	PEG-NHS, 12 hrs, DMF	C11Pc, 2.16 -PEG, PEG and HAuCl ₄ in THF, NaBH ₄ in H ₂ O	No	-
7	1.5 eq HATU, 1 hr, DMF	C11Pc, 2.16 -PEG, PEG and HAuCl ₄ in THF, NaBH ₄ in H ₂ O	No	-
8	1.5 eq HATU, 15 mins, DMF	C11Pc, PEG and HAuCl ₄ in THF, 2.16 -PEG in DMF, NaBH ₄ in H ₂ O	Yes	Yes

To understand the impact of this, the concentration of C11Pc was compared to the estimated concentration of gold nanoparticles to determine how many photosensitisers were attached to a nanoparticle. The extinction coefficient for bare 4 nm nanoparticles has been determined at 450 nm.¹⁰⁹ As FITC has absorbance at 450 nm, this value was used to estimate the extinction coefficient of AuNPs at 400 nm ($4.78 \times 10^6 \text{ M}^{-1} \text{ cm}^{-1}$), and this value was used to estimate the concentration of gold nanoparticles in solution. These calculated values are summarised in **Table 2.4**. The concentration of C11Pc on **2.29** synthesised using **method 5** was higher than that of **method 1** and **method 8**. It is possible that this higher concentration leads to self-quenching of the photosensitiser, preventing the production of singlet oxygen.

Table 2.4: Estimation of the number of photosensitisers per AuNP in each of the successful synthetic conditions

2.29 synthesis method	C11Pc (μM)	AuNPs (nM)	Estimated number of C11Pc ligands per AuNP
1	8.64	167.61	51
5	10.04	173.39	58
8	11.35	266.01	50

Of all the conditions trialled, the only repeatable and successful conditions were those which involved shortening the peptide-PEG coupling time to 15 minutes and using anhydrous DMF instead of anhydrous THF for the addition of the peptide-PEG for the nanoparticle synthesis, keeping all other conditions the same (**method 8**). HATU is known to cause side reactions if left too long, so it is possible that allowing this reaction to proceed for longer than 15 minutes leads to too many unwanted side reactions, reducing the availability of the desired product. The addition of the conjugated PEG to the nanoparticle synthesis in anhydrous DMF overcomes the shortfall of the solubility of the **2.27**. While the initial synthesis involving the addition of peptide-PEG in THF appeared successful, often the peptide-PEG would appear undissolved in THF, greatly due to the lack of solubility of the peptide itself in THF. The addition of just the conjugated PEG in DMF allowed for the complete dissolution of the peptide-PEG but maintained a solvent mix desirable for the nanoparticle synthesis – it was observed that the addition of both the conjugated and unconjugated PEG in DMF was unfavourable for the successful synthesis of these nanoconjugates. **Table 2.5** compares the ratio of FITC to C11Pc attached to the nanoparticles in each solvent system (**method 1** and **method 8**), and both reactions resulted in very similar ratios, suggesting the synthesis is producing nanoparticles with a comparable quantity of both C11Pc and directing peptide.

Table 2.5: Ratio of FITC to C11Pc in examples of **2.29** synthesised using **method 1** or **method 8**

	C11Pc (μM)	FITC (μM)	Ratio FITC:C11Pc
Method 1	2.62	1.83	1:1.4
Method 8	2.33	1.94	1:1.2

Upon dispersing **2.29** in PBS, the solution was very yellow, and upon centrifugation of these nanoparticles in Vivaspin 500 columns, it was found that much of this was due to unbound **2.27**. To make sure all the free **2.27** was removed from the nanoparticles, three

different purification methods were trialled, with the resulting UV-vis spectra shown in **Figure 2.27**. Firstly, the nanocarriers were purified through Vivaspin 500 columns. With one wash, a significant quantity of unbound **2.27** was still present in the sample. The resulting pellets after one wash through Vivaspin 500 columns were purified through Zebaspin desalting columns with a MWCO of 7,000. This should retain all the free peptide and PEG in the resin and allow the nanoparticles to pass through. As expected, a strong yellow band could be seen in the resin of the desalting column and the collected nanoparticles still showed the presence of FITC, confirming the peptide had been conjugated onto the surface of the nanoparticles. It was found that washing the nanoparticles with PBS and purifying them through Vivaspin 500 columns a second time had also a similar effect, as seen in **Figure 2.27**, and for ease of purification this technique was used throughout this work.

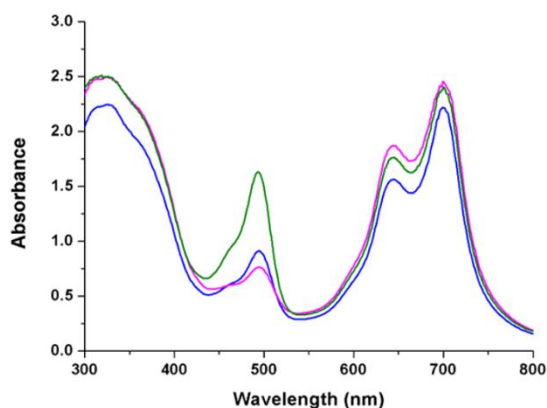


Figure 2.27: UV-vis spectra of **2.29** (**method 8**) after purification with Vivaspin columns x1 (green), Vivaspin columns x1 then Zebaspin desalting columns (pink) or Vivaspin columns x2 (blue)

Once **2.29** (**method 8**) were purified, singlet oxygen studies were repeated on these nanoparticles to determine if there was any variability between the nanoparticles produced in these differing solvent systems. **Figure 2.28** shows the singlet oxygen production of **2.29** synthesised using **method 1** or **method 8**. There was no significant difference in singlet oxygen production observed between these synthetic conditions, suggesting this alternate solvent system did not affect the constituent parts of the produced nanocarriers, but allowed for more reliable synthesis.

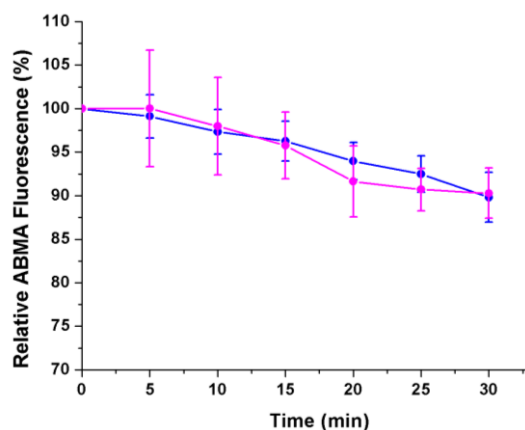


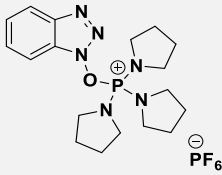
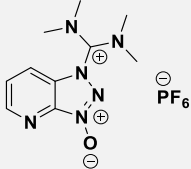
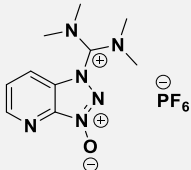
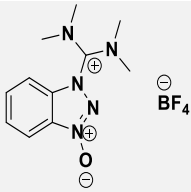
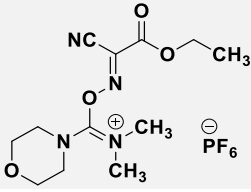
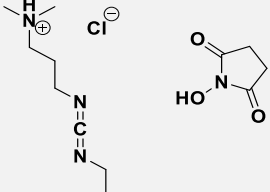
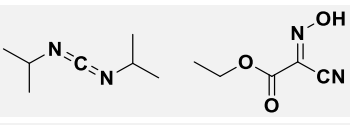
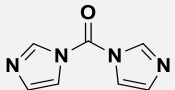
Figure 2.28: Singlet oxygen of **2.29** synthesised using *method 1* (blue) or *method 8* (pink). Spectra were recorded with $1\ \mu\text{M}$ C11Pc in PBS with $1\ \mu\text{M}$ ABMA

2.3.6.5 Coupling agent investigation

Up until this point, HATU has been used as the coupling agent for conjugating PEG with **2.16**. HATU is a bicyclic uronium salt known as the ‘gold-standard’ of coupling agents, yet many other coupling agents exist with slightly different characteristics. These may be more favourable for this amide bond formation and result in a more efficient synthesis of the nanocarriers, so a series of coupling agents were trialled. The investigated coupling agents are summarised in **Table 2.6**. Initially, the equivalents of HATU to PEG were reduced to one, alongside one equivalent of DIPEA and one equivalent of peptide to minimise the chances of any polymerisation through the activation of the glutamic acid residue of the peptide by any free coupling agent. For every coupling agent trialled, all reagents were used in one equivalent.

Firstly, the effect of the counterion was assessed using 2-(1H-benzotriazole-1-yl)-1,1,3,3-tetramethylaminium tetrafluoroborate (TBTU). This benzotriazole derivative undergoes a similar mechanism for amide bond formation as HATU but has a borate counterion as opposed to the phosphonium counterion of HATU. (Benzotriazol-1-yloxy) tripyrrolidinophosphonium hexafluorophosphate (PyBOP), a second benzotriazole, was also trialled to determine the effect of steric bulk on the coupling.

Table 2.6: Summary of coupling agents trialled for conjugation of **2.16** to PEG and their ability to produce singlet oxygen. All coupling agents were used in 1 eq unless otherwise stated

Coupling agent	Structure	Singlet oxygen produced?
PyBOP		A small amount
HATU 1.5 eq		Yes
HATU		Yes
TBTU		No
COMU		No
EDC/NHS		No
DIC/Oxyma		Yes
CDI		Yes

Carbodiimides, a second class of coupling agents, were trialled to assess whether the benzotriazoles released through couplings with HATU or TBTU were influencing the synthesis of the nanocarriers. The positively charged carbodiimide *N*-(3-dimethylaminopropyl)-*N'*-ethylcarbodiimide hydrochloride (EDC) is a very commonly

used coupling agent and activates carboxylic acids through the reactivity of the strained central carbon of the carbodiimide. EDC is commonly used in conjunction with *N*-hydroxysuccinimide (NHS) which releases the urea product of EDC and forms an activated NHS-ester. Neutral carbodiimides were also considered to see if the positive charge of EDC influences its coupling. *N,N'*-diisopropylcarbodiimide (DIC) is a neutral carbodiimide which produces a urea byproduct with a much higher solubility than similar coupling agents such as *N,N'*-dicyclohexylcarbodiimide (DCC), meaning it was selected over DCC for ease of synthesis. Carbodiimides are often used in conjunction with Oxyma, an oxime that forms an active ester with the PEG carbonyl after activation with DIC. It prevents racemisation and has been seen to provide more efficient coupling than other additives such as HOBt.¹¹⁰ Due to its increase in the efficiency of the coupling, DIC was trialled in conjunction with Oxyma.

The coupling agent COMU is an example of an immonium based coupling agent and was trialled to determine the effect of this moiety over uronium salts or carbodiimides. It is the equivalent of a morpholonium based immonium salt activated by Oxyma with a phosphonium counterion.¹¹¹

Carbonyldiimidazole (CDI) was the final coupling agent trialled and falls into a class of its own. CDI reacts with carboxylic acids under basic conditions to form an imidazole ester, a very good leaving group with reactivity comparable to an acyl chloride.¹¹² This reaction is driven by the release of carbon dioxide and a second imidazole. An amine can displace the imidazole to yield an amide with minimal racemisation.

Nanoparticles were successfully synthesised using peptide-PEG formed with each coupling agent following the optimised synthesis described in **section 2.3.6.4**, further confirming the effectiveness of this optimised synthetic procedure. Each conjugate was then screened for singlet oxygen production, comparing each reaction to the original coupling conditions with 1.5 equivalents of HATU. A solution of each conjugate was mixed with ABMA and irradiated for 20 minutes, with spectra recorded before and after, as shown in **Figure 2.29**. In this quick screen, DIC/Oxyma and CDI were the only coupling agents that showed promise for higher singlet oxygen production than that of the nanoconjugates synthesised with HATU.

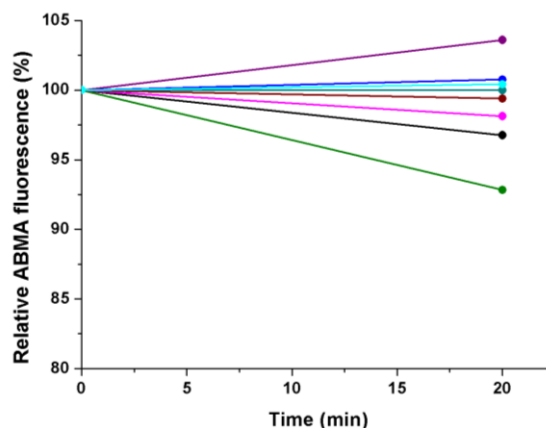


Figure 2.29: Singlet oxygen screen of **2.29** synthesised using EDC/NHS (purple), COMU (dark blue), TBTU (light blue), 1 eq HATU (turquoise), PyBOP (red), 1.2 eq HATU (pink), CDI (black) or DIC/Oxyma (green) as the coupling agent. All nanoparticles were screened at 0.1 μ M C11Pc, 1 μ M ABMA

Larger batches of **2.29** were synthesised using DIC/Oxyma and CDI to couple **2.16** to the PEG, then a more in-depth analysis of their singlet oxygen production was completed. Nanoparticles from each synthesis were irradiated for 30 minutes in methanol alongside ABMA and the fluorescence of ABMA recorded every five minutes. The lifetime of singlet oxygen is longer in methanol than PBS so a larger decrease in ABMA is observed in methanol as there is an increased chance of the singlet oxygen reacting with ABMA. **Figure 2.30** shows the singlet oxygen production of **2.29** (**method 8**), with a 43% decrease in ABMA fluorescence observed compared to a 10% decrease in PBS (**Figure 2.28**), confirming the increased lifetime of singlet oxygen in methanol. **2.29** synthesised using DIC/Oxyma showed much lower singlet oxygen production than those synthesised with HATU, with the singlet oxygen production of these nanoconjugates unobservable in PBS, and AuNPs synthesised with CDI showed no significant singlet oxygen production. As neither of these conjugates displayed improved characteristics over those synthesised with HATU, these coupling conditions were not investigated any further. While these results show that the coupling agent used for the conjugation of **2.16** to PEG had no obvious effect on the synthesis of the nanoparticles, the coupling agent was seen to influence the ability of these nanoconjugates to produce singlet oxygen, with HATU seen to be the best coupling agent trialled in this screen.

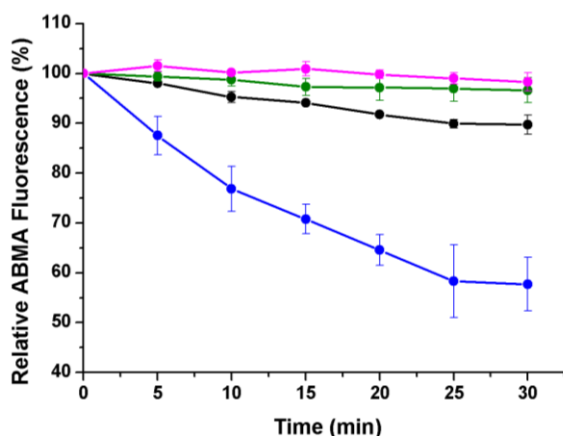


Figure 2.30: Singlet oxygen production of MeOH (pink), **2.29** synthesised using HATU (blue), DIC/Oxyma (black) or CDI (green) to conjugate **2.16** to PEG in MeOH irradiated with 1 μ M ABMA. All AuNPs were tested at 1 μ M C11Pc

2.3.7 Phototoxicity of AuNPs

2.3.7.1 Phototoxicity of peptide-conjugated C11Pc-PEG-AuNPs

The phototoxicity of the **2.29** synthesised in THF/water (**method 1**) or THF/DMF/water (**method 8**) was tested in A549 EGFR overexpressing NSCLC cells. A549 cells were grown overnight in 96 well plates. **2.29** were then incubated alongside A549s for three hours, in foetal calf serum (FCS) free RPMI. The lack of FCS in the wells induces starvation and encourages the uptake of the nanoparticles into the cells. Cells were also treated with just FCS free RPMI and with staurosporine in FCS free RPMI to act as negative and positive controls for cell death respectively. After incubation, the cells were washed three times with PBS to remove any nanocarriers that had not been internalised, then complete RPMI (with FCS) was added to each well. The wells were then irradiated with a 10 mW 633 nm HeNe laser for six minutes per well, with the laser placed 50 cm above each well. After irradiation, the cells were incubated for 48 hours at 37 °C, 5% CO₂ before treatment with MTS to assess the cell viability. A second plate was treated in the same way, but not irradiated to act as a control for dark toxicity for the nanocarriers. **2.29** synthesised using both **method 1** (**Figure 2.31a**) and **method 8** were seen to have minimal dark toxicity in A549 cells below 250 nM. Interestingly, while **2.29** synthesised using **method 1** were seen to show significant cell death upon irradiation in a dose dependent manner, as shown in **Figure 2.31a**, those synthesised using **method 8** displayed no phototoxicity in A549 cells. This suggests that the solvent has a strong

influence on the composition of these nanoparticles, and that THF is the most favourable solvent for the formation of these peptide-targeted nanocarriers.

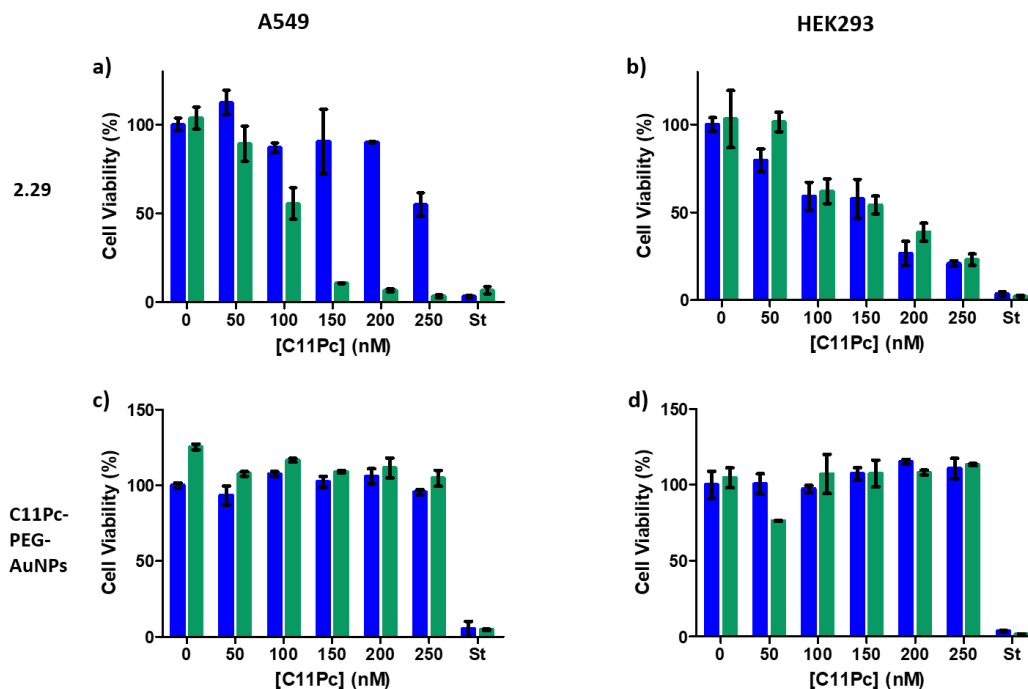


Figure 2.31: MTS cell viability assays of **a**) & **c**) A549 and **b**) & **d**) HEK293 cells after 3 hr treatment with either **2.29** (method 1) (**a**, **b**) or C11Pc-PEG-AuNPs (**c**, **d**). The cells were either kept in the dark (blue) or irradiated (green) at 633 nm for 6 minutes. St = positive control of staurosporine

To determine the selectivity of **2.29**, these nanocarriers were incubated with HEK293 cells as these cells were seen to have a lower level of EGFR expression. HEK293 cells were treated with **2.29** under starvation conditions for three hours, then irradiated at 633 nm for 6 minutes per well, or incubated in the dark, then the cell viability tested with MTS. Strangely, the nanocarriers appeared to have an anti-proliferative effect, so while there was no visual cell death, the MTS assay showed a decrease in cell metabolism due to a decrease in proliferation with increasing concentration of **2.29**, as shown in **Figure 2.31b**. Notably, no difference in cell viability was observed between irradiated and non-irradiated cells, showing no cell death was observed due to the photodynamic activity of these nanocarriers, suggesting some targeting towards EGFR overexpressing cells may be occurring. To test this theory, HEK293 cells were incubated alongside **2.16**, and fluorescence microscopy images showed negligible uptake of the peptide (**Figure 2.32**). This is in stark contrast to A549 cells which showed strong fluorescence after incubation with **2.16** (**Figure 2.32** and **Figure 2.11**). Due to the low level of EGFR expression on

the surface of HEK293 cells, this suggests the uptake of **2.16** may be encouraged in EGFR overexpressing cells.

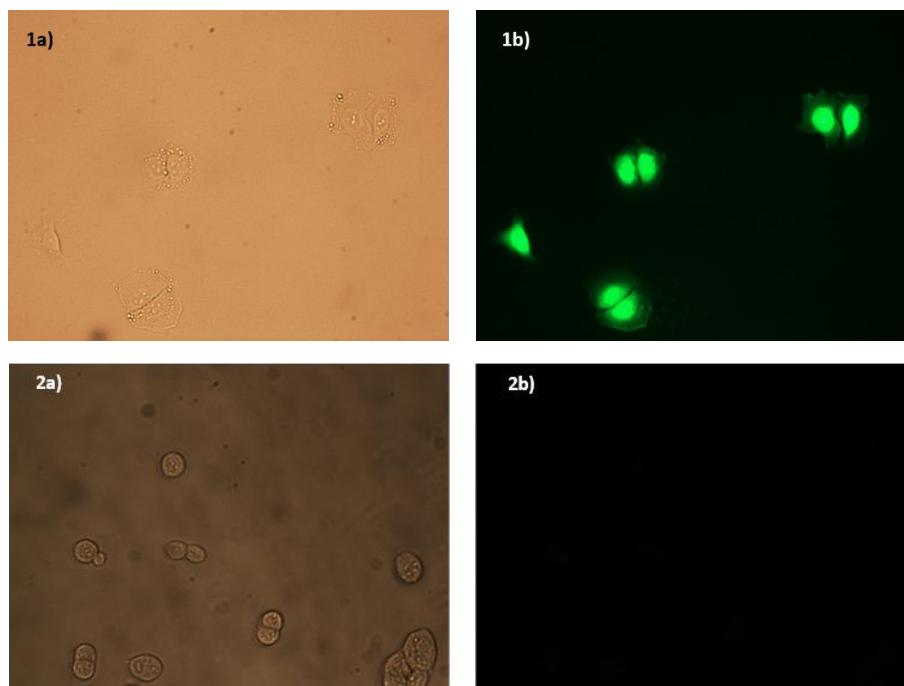


Figure 2.32: a) bright field and b) fluorescence microscopy images of 1) A549 and 2) HEK293 cells incubated with 100 μ M **2.16** for one hour. **1a** and **1b** are reproduced from **Figure 2.11**

To further assess the targeting ability of these nanoconjugates, non-targeted C11Pc-PEG-AuNPs were incubated with both A549 and HEK293 cells for three hours under starvation conditions, then the cells irradiated for six minutes per well. After 48 hours, an MTS cell proliferation assay displayed no photodynamic activity or dark toxicity for these non-targeted conjugated in either cell line, as shown in **Figure 2.31c&d**. This suggests that the selective phototoxicity observed is therefore due to increased uptake of **2.29** due to the recognition of **2.16** by EGFR.

2.3.7.2 Phototoxicity of control AuNPs

It is very unlikely that the FITC is being activated to produce singlet oxygen as the excitation of FITC is very sharp at 495 nm and would not be excited by a 633 nm laser. However, to determine that the phototoxicity is due to the activation of C11Pc as expected, each part of the nanocarrier system was sequentially screened intracellularly. A set of three different nanoconjugates without C11Pc were tested: PEG-AuNPs, FITC-PEG-AuNPs (**2.31**) and **2.16**-PEG-AuNPs (**2.32**). These represented nanoparticles with

no photosensitiser of any type, nanoparticles with just the FITC to determine whether there is any activity from the FITC, and nanoparticles with the targeting moiety and FITC. If FITC itself is acting as a photosensitiser and the peptide is targeting A549s, **2.32** should show some photodynamic activity. Nanoconjugates with C11Pc, but without **2.16** were also screened to determine if the peptide is having a targeting effect were also tested. These nanoconjugates were C11Pc-PEG-AuNPs and FITC-C11Pc-PEG-AuNPs (**2.33**). Each of these nanocarrier systems were incubated with A549s before irradiation as described in **section 2.3.4**. As **2.29** showed a strong photodynamic activity at 200 nM C11Pc with minimal dark toxicity in A549s, all AuNP C11Pc containing systems were tested at this concentration. Systems containing FITC were tested at 200 nM FITC to add a comparative concentration of this FITC photosensitiser. **2.16** itself was also tested as this carries a photosensitiser and the targeting moiety so could induce photodynamic killing itself. 48 hrs after incubation and irradiation, the cells were analysed for cell viability using an MTS assay. No cell death was observed for any of these nanoconjugates or **2.16** itself, as shown in **Figure 2.33**, highlighting that C11Pc is indeed the photosensitiser causing the photodynamic activity, and suggesting that **2.16** is inducing cellular uptake.

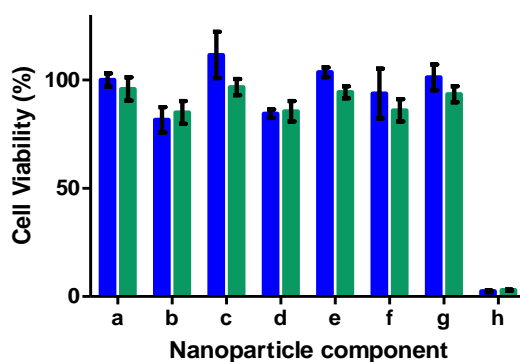


Figure 2.33: Cell viability of non-irradiated (blue) and irradiated (green) A549 cells treated with **a**) media, **b**) **2.16** **c**) PEG-AuNPs, **d**) **2.31**, **e**) **2.32**, **f**) C11Pc-PEG-AuNPs, **g**) **2.33** and **h**) staurosporine. All nanocarriers were tested at 200 nM C11Pc or FITC.

2.3.8 Nanoparticle binding by fluorescent microscopy

As **2.29** synthesised using **method 8** showed singlet oxygen production but surprisingly no cytotoxicity, fluorescent microscopy was used to determine whether these nanoparticles were being internalised by cells. **2.29** were incubated with A549 cells using the same conditions as in **section 2.3.7.1** for the photodynamic cell viability assays. Again, serum free RPMI was used to encourage the uptake of the nanocarriers into the cells.

After three hours the cells were washed with PBS and imaged using a fluorescence microscope. **Figure 2.34** shows the resulting images for A549 cells incubated with 5 μ M **2.29** (C11Pc), a concentration much higher than that needed to induce phototoxicity for **2.29** synthesised using **method 1**. For **method 8** there was no obvious uptake by A549s which may explain their lack of phototoxicity.

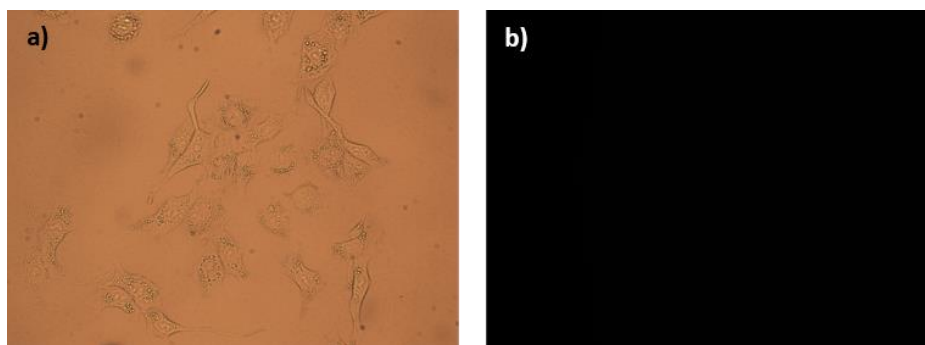


Figure 2.34: a) bright field and b) fluorescent microscopy images of A549 cells incubated with 5 μ M **2.29** (method 8) for three hours in serum free RPMI

2.4 Conclusion and future work

In this chapter, two peptides, AEYLR and LARLLT, were selected as EGFR targeting ligands. Both peptides were modified with the addition of a terminal lysine residue to provide an amine for site-selective conjugation to gold nanocarriers and a fluorescent FITC tag to allow quantification of the peptide on the nanocarriers and to view the uptake of the resulting nanocarriers into cells. Post-modification, both peptides still displayed uptake into EGFR overexpressing A549 lung adenocarcinoma cells. These peptides were conjugated onto bifunctionalised HS-PEG-COOH through amide bonds and then the resulting conjugated PEG used to synthesise *ca.* 4 nm AuNPs functionalised with the photosensitiser C11Pc, peptide-PEG and non-conjugated PEG. Interestingly, the nanoparticles synthesised with **2.17**, **2.30**, showed no singlet oxygen production. This may be due to self-quenching of the photosensitiser, but further investigation is required to explain this phenomenon. To determine if the structure of the peptide has any effect on the singlet oxygen production, an alanine screen could be used to see if a change in the sequence of structure of the peptide reinstates the singlet oxygen production of these nanocarriers.

2.29 (**2.16**-C11Pc-PEG-AuNPs) were synthesised in a THF/water mixture (**method 1**) and showed significant singlet oxygen production. While these results were encouraging,

these nanoconjugates synthesised in a THF/water mix were very temperamental and the synthesis hard to reliably repeat. Due to this, steps were taken towards the optimisation of the synthesis of these nanocarriers. Firstly, the solvent system was varied, and it was found that dissolving the peptide-PEG in DMF instead of THF (**method 8**), keeping all other solvents unchanged, resulted in a reliable and repeatable synthesis. A range of coupling agents were also investigated to determine whether HATU was the most efficient reagent for coupling the peptide onto PEG. Nanoparticles were successfully synthesised with a range of coupling agents, however nanocarriers synthesised with DIC/Oxyma or CDI to couple **2.16** to PEG showed a decrease in singlet oxygen production from that of nanoconjugates synthesised with HATU as the coupling agent, suggesting HATU is the best coupling agent for this synthesis.

On incubation of **2.29** with EGFR overexpressing A549 cells, phototoxicity was observed in a dose dependent manner, with a cell viability of *ca.* 7% observed for cells treated with 200 nM **2.29** synthesised in THF/water (**method 1**). Minimal dark toxicity was observed for these nanoconjugates, and no photodynamic activity was observed in HEK293 cells which do not overexpress EGFR, suggesting **2.29** are targeted towards EGFR overexpressing cell lines. Interestingly **2.29** synthesised in THF/DMF/water (**method 8**) showed identical singlet oxygen production to those synthesised in THF/water (**method 1**), however no phototoxicity was observed upon incubation in A549 cells.

As the 3D structure of these nanocarriers is not fully known, it is possible that the peptide, while confirmed to be conjugated to the nanocarriers, is buried in the nanoparticle corona and not in fact available on the surface of the nanocarriers for binding to the EGFR. To determine whether this is the case, shorter chain PEGs could be used to encourage the accessibility of the peptide. It has been shown that *ca.* 4 nm AuNPs functionalised with C11Pc and a PEG(3) chain are stable in aqueous environments⁹⁷ and that shorter PEG chains encourage the PEG to remain brush-like on a nanoparticle surface,¹¹³ leaving the attached ligand accessible to the surrounding environment. For example, an NHS-PEG(8)-disulphide dimer is commercially available and could be trialled to determine whether a shorter PEG will help with peptide availability. This PEG has the second advantage of being pre-activated for amide bond formation, meaning no coupling agent is needed, removing any influence these may have on the formation of these nanocarriers.

Once the synthesis of these nanocarriers has been optimised, it is important that the concentration of peptide on the surface is varied to determine the optimum

concentration. It has been shown that the overcrowding of nanoparticle surfaces with directing ligands can in fact reduce the efficiency of their uptake⁹⁸ so determining the optimum peptide concentration for these nanocarriers could further increase their potency for photodynamic therapy.

There are very few examples of the use of peptides to actively target nanoparticles towards tumours for photodynamic therapy. The work presented in this chapter has highlighted the applicability of peptides as targeting moieties for the delivery of photosensitiser-nanoconjugates and has demonstrated the potential of the peptide AEYLR for the selective delivery of nanocarriers to EGFR overexpressing non-small cell lung cancers.

2.5 References

- (1) Albertson, D. G. Gene Amplification in Cancer. *Trends Genet.* **2006**, *22* (8), 447–455.
- (2) Grandis, J. R.; Sok, J. C. Signaling through the Epidermal Growth Factor Receptor during the Development of Malignancy. *Pharmacol. Ther.* **2004**, *102*, 37–46.
- (3) Farago, A. F.; Le, L. P.; Zheng, Z.; Muzikansky, A.; Drilon, A.; Patel, M.; Bauer, T. M.; Liu, S. V.; Ou, S. H. I.; Jackman, D.; et al. Durable Clinical Response to Entrectinib in NTRK1-Rearranged Non-Small Cell Lung Cancer. *J. Thorac. Oncol.* **2015**, *10* (12), 1670–1674.
- (4) Cihoric, N.; Savic, S.; Schneider, S.; Ackermann, I.; Bichsel-Naef, M.; Schmid, R. A.; Lardinois, D.; Gugger, M.; Bubendorf, L.; Zlobec, I.; et al. Prognostic Role of FGFR1 Amplification in Early-Stage Non-Small Cell Lung Cancer. *Br. J. Cancer* **2014**, *110* (12), 2914–2922.
- (5) Hammerman, P. S.; Sos, M. L.; Ramos, A. H.; Xu, C.; Dutt, A.; Zhou, W.; Brace, L. E.; Woods, B. A.; Lin, W.; Zhang, J. Mutations in the DDR2 Kinase Gene Identify a Novel Therapeutic Target in Squamous Cell Lung Cancer. *Cancer Discov.* **2011**, *1*, 78–89.
- (6) Barr Kumarakulasinghe, N.; Zanwijk, N. Van; Soo, R. A. Molecular Targeted Therapy in the Treatment of Advanced Stage Non-Small Cell Lung Cancer (NSCLC). *Respirology*. Blackwell Publishing April 1, 2015, pp 370–378.
- (7) Nicholson, R. I.; Gee, J. M. W.; Harper, M. E. EGFR and Cancer Prognosis. *Eur. J. Cancer* **2001**, *37*, 9–15.
- (8) Yarden, Y. The EGFR Family and Its Ligands in Human Cancer: Signalling Mechanisms and Therapeutic Opportunities. *Eur. J. Cancer* **2001**, *37*, 3–8.
- (9) Fruehauf, J. EGFR Function and Detection in Cancer Therapy. *J. Exp. Ther. Oncol.* **2006**, *5*, 231–246.
- (10) Bishayee, S. Role of Conformational Alteration in the Epidermal Growth Factor

- Receptor (EGFR) Function. *Biochem. Pharmacol.* **2000**, *60* (8), 1217–1223.
- (11) Kawamoto, T.; Sato, J. D.; Le, A.; Polikoff, J.; Sato, G. H.; Mendelsohn, J. Growth Stimulation of A431 Cells by Epidermal Growth Factor: Identification of High-Affinity Receptors for Epidermal Growth Factor by an Anti-Receptor Monoclonal Antibody. *Proc. Natl. Acad. Sci. USA* **1983**, *80*, 1337–1341.
- (12) Bethune, G.; Bethune, D.; Ridgway, N.; Xu, Z. Epidermal Growth Factor Receptor (EGFR) in Lung Cancer: An Overview and Update. *J. Thorac. Dis.* **2010**, *2* (1), 48–51.
- (13) Lynch, T. J.; Bell, D. W.; Sordella, R.; Gurubhagavatula, S.; Okimoto, R. A.; Brannigan, B. W.; Harris, P. L.; Haserlat, S. M.; Supko, J. G.; Haluska, F. G.; et al. Activating Mutations in the Epidermal Growth Factor Receptor Underlying Responsiveness of Non-Small-Cell Lung Cancer to Gefitinib. *N. Engl. J. Med.* **2004**, *350* (21), 2129–2139.
- (14) Hirsch, F.; Varella-Garcia, M.; Cappuzzo, F. Predictive Value of EGFR and HER2 Overexpression in Advanced Non-Small-Cell Lung Cancer. *Oncogene* **2009**, *28*, 32–37.
- (15) Mukohara, T.; Kudoh, S.; Yamauchi, S.; Kimura, T.; Yoshimura, N.; Kanazawa, H.; Hirata, K.; Wanibuchi, H.; Fukushima, S.; Inoue, K.; et al. Expression of Epidermal Growth Factor Receptor (EGFR) and Downstream-Activated Peptides in Surgically Excised Non-Small-Cell Lung Cancer (NSCLC). *Lung Cancer* **2003**, *41* (2), 123–130.
- (16) Melosky, B. Review of EGFR TKIs in Metastatic NSCLC, Including Ongoing Trials. *Front. Oncol.* **2014**, *4*, 244.
- (17) Martinelli, E.; De Palma, R.; Orditura, M.; De Vita, F.; Ciardiello, F. Anti-Epidermal Growth Factor Receptor Monoclonal Antibodies in Cancer Therapy. *Clin. Exp. Immunol.* **2009**, *158* (1), 1–9.
- (18) Muhsin, M.; Graham, J.; Kirkpatrick, P. Gefitinib. *Nat. Rev. Drug Discov.* **2003**, *2* (7), 515–516.
- (19) Dowell, J.; Minna, J. D.; Kirkpatrick, P. Erlotinib Hydrochloride. *Nat. Rev. Drug Discov.* **2005**, *4* (1), 13–14.
- (20) Brehmer, D.; Greff, Z.; Godl, K.; Blencke, S.; Kurtenbach, A.; Weber, M.; Müller, S.; Klebl, B.; Cotten, M.; Kéri, G.; et al. Cellular Targets of Gefitinib. *Cancer Res.* **2005**, *65* (2), 379–382.
- (21) Pérez-Soler, R.; Chachoua, A.; Hammond, L. A.; Rowinsky, E. K.; Huberman, M.; Karp, D.; Rigas, J.; Clark, G. M.; Santabárbara, P.; Bonomi, P. Determinants of Tumor Response and Survival with Erlotinib in Patients with Non-Small-Cell Lung Cancer. *J. Clin. Oncol.* **2004**, *22* (16), 3238–3247.
- (22) Cragg, M. S.; Kuroda, J.; Puthalakath, H.; Huang, D. C. S.; Strasser, A. Gefitinib-Induced Killing of NSCLC Cell Lines Expressing Mutant EGFR Requires BIM and Can Be Enhanced by BH3 Mimetics. *PLoS Med.* **2007**, *4* (10), e316.
- (23) Huang, L.; Fu, L. Mechanisms of Resistance to EGFR Tyrosine Kinase Inhibitors. *Acta Pharm. Sin. B* **2015**, *5* (5), 390–401.
- (24) Nelson, V.; Ziehr, J.; Agulnik, M.; Johnson, M. Afatinib: Emerging next-

- Generation Tyrosine Kinase Inhibitor for NSCLC. *Onco. Targets. Ther.* **2013**, *6*, 135–143.
- (25) Takeda, M.; Nakagawa, K. First- and Second-Generation EGFR-TKIs Are All Replaced to Osimertinib in Chemo-Naive EGFR Mutation-Positive Non-Small Cell Lung Cancer? *Int. J. Mol. Sci.* **2019**, *20*, 146.
- (26) Saltz, L.; Easley, C.; Kirkpatrick, P. Panitumumab. *Nat. Rev. Drug Discov.* **2006**, *5* (12), 987–988.
- (27) Wong, S.-F. Cetuximab: An Epidermal Growth Factor Receptor Monoclonal Antibody for the Treatment of Colorectal Cancer. *Clin. Ther.* **2005**, *27* (6), 684–694.
- (28) Vincenzi, B.; Schiavon, G.; Silletta, M.; Santini, D.; Tonini, G. The Biological Properties of Cetuximab. *Crit. Rev. Oncol. Hematol.* **2008**, *68* (2), 93–106.
- (29) Kurai, J.; Chikumi, H.; Hashimoto, K.; Yamaguchi, K.; Yamasaki, A.; Sako, T.; Touge, H.; Makino, H.; Takata, M.; Miyata, M.; et al. Antibody-Dependent Cellular Cytotoxicity Mediated by Cetuximab against Lung Cancer Cell Lines. *Clin. Cancer Res.* **2007**, *13* (5), 1552–1561.
- (30) Hamblett, K. J.; Kozlosky, C. J.; Siu, S.; Chang, W. S.; Liu, H.; Foltz, I. N.; Trueblood, E. S.; Meininger, D.; Arora, T.; Twomey, B.; et al. Large Molecule Therapeutics AMG 595, an Anti-EGFRvIII Antibody-Drug Conjugate, Induces Potent Antitumor Activity against EGFRvIII-Expressing Glioblastoma. *Mol. Cancer Ther.* **2015**, *14* (7).
- (31) Yip, W. L.; Weyergang, A.; Berg, K.; Tønnesen, H. H.; Selbo, P. K. Targeted Delivery and Enhanced Cytotoxicity of Cetuximab–Saporin by Photochemical Internalization in EGFR-Positive Cancer Cells. *Mol. Pharm.* **2007**, *4* (2), 241–251.
- (32) Glatt, D. M.; Beckford Vera, D. R.; Prabhu, S. S.; Mumper, R. J.; Luft, J. C.; Benhabbour, S. R.; Parrott, M. C. Synthesis and Characterization of Cetuximab–Docetaxel and Panitumumab–Docetaxel Antibody–Drug Conjugates for EGFR-Overexpressing Cancer Therapy. *Mol. Pharm.* **2018**, *15* (11), 5089–5102.
- (33) Ojima, I.; Geng, X.; Wu, X.; Qu, C.; Borella, C. P.; Xie, H.; Wilhelm, S. D.; Leece, B. A.; Bartle, L. M.; Victor S. Goldmacher; et al. Tumor-Specific Novel Taxoid–Monoclonal Antibody Conjugates. *J. Med. Chem.* **2002**, *45* (26), 5620–5623.
- (34) van den Bent, M.; Gan, H. K.; Lassman, A. B.; Kumthekar, P.; Merrell, R.; Butowski, N.; Lwin, Z.; Mikkelsen, T.; Nabors, L. B.; Papadopoulos, K. P.; et al. Efficacy of Depatuxizumab Mafodotin (ABT-414) Monotherapy in Patients with EGFR-Amplified, Recurrent Glioblastoma: Results from a Multi-Center, International Study. *Cancer Chemother. Pharmacol.* **2017**, *80* (6), 1209–1217.
- (35) Tolcher, A.; Papadopoulos, K.; Cole, Y.; Rivas, K.; Chandana, S.; Sinclair, S.; Wood, D.; Nadler, P. I.; Lakhani, N. 460A Phase 1a/2a Trial of AVID100, an Anti-EGFR Antibody-Drug Conjugate. *Ann. Oncol.* **2018**, *29* (3), 8.
- (36) Abu-Yousif, A. O.; Moor, A. C. E.; Zheng, X.; Savellano, M. D.; Yu, W.; Selbo, P. K.; Hasan, T. Epidermal Growth Factor Receptor-Targeted Photosensitizer Selectively Inhibits EGFR Signaling and Induces Targeted Phototoxicity in Ovarian Cancer Cells. *Cancer Lett.* **2012**, *321* (2), 120–127.

-
- (37) Nakajima, T.; Sano, K.; Choyke, P. L.; Kobayashi, H. Improving the Efficacy of Photoimmunotherapy (PIT) Using a Cocktail of Antibody Conjugates in a Multiple Antigen Tumor Model. *Theranostics* **2013**, *3* (6), 357–365.
- (38) Savellano, M. D.; Hasan, T. Photochemical Targeting of Epidermal Growth Factor Receptor: A Mechanistic Study. *Clin. Cancer Res.* **2005**, *11*, 1658–1668.
- (39) Savellano, M. D.; Hasan, T. Targeting Cells That Overexpress the Epidermal Growth Factor Receptor with Polyethylene Glycolated BPD Verteporfin Photosensitizer Immunoconjugates. *Photochem. Photobiol.* **2007**, *77* (4), 431–439.
- (40) Railkar, R.; Krane, L. S.; Li, Q. Q.; Sanford, T.; Siddiqui, M. R.; Haines, D.; Vourganti, S.; Brancato, S. J.; Choyke, P. L.; Kobayashi, H.; et al. Epidermal Growth Factor Receptor (EGFR)-Targeted Photoimmunotherapy (PIT) for the Treatment of EGFR-Expressing Bladder Cancer. *Mol. Cancer Ther.* **2017**, *16*, 2201–2214.
- (41) Curley, S. A.; Cherukuri, P.; Briggs, K.; Patra, C. R.; Upton, M.; Dolson, E.; Mukherjee, P. Noninvasive Radiofrequency Field-Induced Hyperthermic Cytotoxicity in Human Cancer Cells Using Cetuximab-Targeted Gold Nanoparticles. *J. Exp. Ther. Oncol.* **2008**, *7* (4), 313–326.
- (42) Lee, J.; Choi, Y.; Kim, K.; Hong, S.; Park, H.-Y.; Lee, T.; Cheon, G. J.; Song, R. Characterization and Cancer Cell Specific Binding Properties of Anti-EGFR Antibody Conjugated Quantum Dots. *Bioconjug. Chem.* **2010**, *21* (5), 940–946.
- (43) Lee, J. S.; Groothuis, T.; Cusan, C.; Mink, D.; Feijen, J. Lysosomally Cleavable Peptide-Containing Polymersomes Modified with Anti-EGFR Antibody for Systemic Cancer Chemotherapy. *Biomaterials* **2011**, *32* (34), 9144–9153.
- (44) Low, K. P.; Bhuvaneswari, R.; Thong, P. S.; Bunte, R. M.; Soo, K. C. Novel Delivery of Chlorin E6 Using Anti-EGFR Antibody Tagged Virosomes for Fluorescence Diagnosis of Oral Cancer in a Hamster Cheek Pouch Model. *Eur. J. Pharm. Sci.* **2016**, *83*, 143–154.
- (45) Mir, Y.; Elrington, S. A.; Hasan, T. A New Nanoconstruct for Epidermal Growth Factor Receptor-Targeted Photo-Immunotherapy of Ovarian Cancer. *Nanomedicine Nanotechnology, Biol. Med.* **2013**, *9* (7), 1114–1122.
- (46) He, Y.; Hsiao, J.-H.; Yu, J.-H.; Tseng, P.-H.; Hua, W.-H.; Low, M.-C.; Tsai, Y.-H.; Cai, C.-J.; Hsieh, C.-C.; Kiang, Y.-W.; et al. Cancer Cell Death Pathways Caused by Photothermal and Photodynamic Effects through Gold Nanoring Induced Surface Plasmon Resonance. *Nanotechnology* **2017**, *28* (27), 1–13.
- (47) Li, B.; Jiang, Z.; Xie, D.; Wang, Y.; Lao, X. Cetuximab-Modified CuS Nanoparticles Integrating near-Infrared-II-Responsive Photothermal Therapy and Anti-Vessel Treatment. *Int. J. Nanomedicine* **2018**, *13*, 7289–7302.
- (48) Hadjipanais, C. G.; Machaidze, R.; Kaluzova, M.; Wang, L.; Schuette, A. J.; Chen, H.; Wu, X.; Mao, H. EGFRvIII Antibody-Conjugated Iron Oxide Nanoparticles for Magnetic Resonance Imaging-Guided Convection-Enhanced Delivery and Targeted Therapy of Glioblastoma. *Ther. Targets Chem. Biol.* **2010**, *70* (15), 6303–6312.
- (49) Chari, R. V. J. Targeted Cancer Therapy: Conferring Specificity to Cytotoxic Drugs. *Acc. Chem. Res.* **2007**, *41* (1), 98–107.

- (50) Debaene, F.; Bœuf, A.; Wagner-Rousset, E.; Colas, O.; Ayoub, D.; Corvaia, N.; Van Dorsselaer, A.; Beck, A.; Cianfèrani, S. Innovative Native MS Methodologies for Antibody Drug Conjugate Characterization: High Resolution Native MS and IM-MS for Average DAR and DAR Distribution Assessment. *Anal. Chem.* **2014**, *86* (21), 10674–10683.
- (51) Kim, M. T.; Chen, Y.; Marhoul, J.; Jacobson, F. Statistical Modeling of the Drug Load Distribution on Trastuzumab Emtansine (Kadcyla), a Lysine-Linked Antibody Drug Conjugate. *Bioconjug. Chem.* **2014**, *25* (7), 1223–1232.
- (52) Boylan, N. J.; Zhou, W.; Proos, R. J.; Tolbert, T. J.; Wolfe, J. L.; Laurence, J. S. Conjugation Site Heterogeneity Causes Variable Electrostatic Properties in Fc Conjugates. *Bioconjug. Chem.* **2013**, *24* (6), 1008–1016.
- (53) Lutsenko, S. V.; Feldman, N. B.; Finakova, G. V.; Posypanova, G. A.; Severin, S. E.; Skryabin, K. G.; Kirpichnikov, M. P.; Lukyanets, E. A.; Vorozhtsov, G. N. Targeting Phthalocyanines to Tumor Cells Using Epidermal Growth Factor Conjugates. *Tumor Biol.* **1999**, *20* (4), 218–224.
- (54) Tai, W.; Shukla, R. S.; Qin, B.; Li, B.; Cheng, K. Development of a Peptide–Drug Conjugate for Prostate Cancer Therapy. *Mol. Pharm.* **2011**, *8* (3), 901–912.
- (55) Wang, Y.; Cheetham, A. G.; Angacian, G.; Su, H.; Xie, L.; Cui, H. Peptide–Drug Conjugates as Effective Prodrug Strategies for Targeted Delivery. *Adv. Drug Deliv. Rev.* **2017**, *110*, 112–126.
- (56) Cox, N.; Kintzing, J. R.; Smith, M.; Grant, G. A.; Cochran, J. R. Integrin-Targeting Knottin Peptide-Drug Conjugates Are Potent Inhibitors of Tumor Cell Proliferation. *Angew. Chemie Int. Ed.* **2016**, *55* (34), 9894–9897.
- (57) Chen, X.; Plasencia, C.; Hou, Y.; Neamati, N. Synthesis and Biological Evaluation of Dimeric RGD Peptide–Paclitaxel Conjugate as a Model for Integrin-Targeted Drug Delivery. *J. Med. Chem.* **2005**, *48* (4), 1098–1106.
- (58) Boisbrun, M.; Vanderesse, R.; Engrand, P.; Oliè, A.; Hupont, S.; Regnouf-de-Vains, J.-B.; Frochot, C. Design and Photophysical Properties of New RGD Targeted Tetraphenylchlorins and Porphyrins. *Tetrahedron* **2008**, *64* (16), 3494–3504.
- (59) Li, W.; Tan, S.; Xing, Y.; Liu, Q.; Li, S.; Chen, Q.; Yu, M.; Wang, F.; Hong, Z. CRGD Peptide-Conjugated Pyropheophorbide-a Photosensitizers for Tumor Targeting in Photodynamic Therapy. *Mol. Pharm.* **2018**, *15* (4), 1505–1514.
- (60) Srivatsan, A.; Ethirajan, M.; Pandey, S. K.; Dubey, S.; Zheng, X.; Liu, T.-H.; Shibata, M.; Missert, J.; Morgan, J.; Pandey, R. K. Conjugation of CRGD Peptide to Chlorophyll *a* Based Photosensitizer (HPPH) Alters Its Pharmacokinetics with Enhanced Tumor-Imaging and Photosensitizing (PDT) Efficacy. *Mol. Pharm.* **2011**, *8* (4), 1186–1197.
- (61) Chaleix, V.; Sol, V.; Guilloton, M.; Granet, R.; Krausz, P. Efficient Synthesis of RGD-Containing Cyclic Peptide–Porphyrin Conjugates by Ring-Closing Metathesis on Solid Support. *Tetrahedron Lett.* **2004**, *45* (27), 5295–5299.
- (62) Frochot, C.; Stasio, B. Di; Vanderesse, R.; Belgy, M. J.; Dodeller, M.; Guillemin, F.; Viriot, M.-L.; Barberi-Heyob, M. Interest of RGD-Containing Linear or Cyclic Peptide Targeted Tetraphenylchlorin as Novel Photosensitizers for

- Selective Photodynamic Activity. *Bioorg. Chem.* **2007**, *35* (3), 205–220.
- (63) Conway, C. L.; Walker, I.; Bell, A.; Roberts, D. J. H.; Brown, S. B.; Vernon, D. I. In Vivo and in Vitro Characterisation of a Protoporphyrin IX–Cyclic RGD Peptide Conjugate for Use in Photodynamic Therapy. *Photochem. Photobiol. Sci.* **2008**, *7* (3), 290–298.
- (64) Tirand, L.; Frochot, C.; Vanderesse, R.; Thomas, N.; Trinquet, E.; Pinel, S.; Viriot, M.-L.; Guillemin, F.; Barberi-Heyob, M. A Peptide Competing with VEGF165 Binding on Neuropilin-1 Mediates Targeting of a Chlorin-Type Photosensitizer and Potentiates Its Photodynamic Activity in Human Endothelial Cells. *J. Control. Release* **2006**, *111*, 153–164.
- (65) Ranyuk, E.; Cauchon, N.; Klarskov, K.; Guérin, B.; van Lier, J. E. Phthalocyanine–Peptide Conjugates: Receptor-Targeting Bifunctional Agents for Imaging and Photodynamic Therapy. *J. Med. Chem.* **2013**, *56* (4), 1520–1534.
- (66) Fontenot, K. R.; Ongarora, B. G.; LeBlanc, L. E.; Zhou, Z.; Jois, S. D.; Vicente, M. G. H. Targeting of the Epidermal Growth Factor Receptor with Mesoporphyrin IX-Peptide Conjugates. *J. Porphyr. Phthalocyanines* **2016**, *20*, 352–366.
- (67) Ongarora, B. G.; Fontenot, K. R.; Hu, X.; Sehgal, I.; Satyanarayana-Jois, S. D.; Vicente, M. G. H. Phthalocyanine–Peptide Conjugates for Epidermal Growth Factor Receptor Targeting. *J. Med. Chem.* **2012**, *55* (8), 3725–3738.
- (68) Li, F.; Liu, Q.; Liang, Z.; Wang, J.; Pang, M.; Huang, W.; Wu, W.; Hong, Z. Synthesis and Biological Evaluation of Peptide-Conjugated Phthalocyanine Photosensitizers with Highly Hydrophilic Modifications. *Org. Biomol. Chem.* **2016**, *14* (13), 3409–3422.
- (69) Pierschbacher, M. D.; Ruoslahti, E. Cell Attachment Activity of Fibronectin Can Be Duplicated by Small Synthetic Fragments of the Molecule. *Nature* **1984**, *309* (5963), 30–33.
- (70) Kumagai, H.; Tajima, M.; Ueno, Y.; Giga-Hama, Y.; Ohba, M. Effect of Cyclic RGD Peptide on Cell Adhesion and Tumor Metastasis. *Biochem. Biophys. Res. Commun.* **1991**, *177* (1), 74–82.
- (71) Desgrosellier, J. S.; Cheresch, D. A. Integrins in Cancer: Biological Implications and Therapeutic Opportunities. *Nat. Rev. Cancer* **2010**, *10* (1), 9–22.
- (72) Kopelman, R.; Lee Koo, Y. E.; Philbert, M.; Moffat, B. A.; Ramachandra Reddy, G.; McConville, P.; Hall, D. E.; Chenevert, T. L.; Bhojani, M. S.; Buck, S. M.; et al. Multifunctional Nanoparticle Platforms for in Vivo MRI Enhancement and Photodynamic Therapy of a Rat Brain Cancer. *J. Magn. Magn. Mater.* **2005**, *293* (1), 404–410.
- (73) Zhou, A.; Wei, Y.; Wu, B.; Chen, Q.; Xing, D. Pyropheophorbide A and c(RGDyK) Comodified Chitosan-Wrapped Upconversion Nanoparticle for Targeted Near-Infrared Photodynamic Therapy. *Mol. Pharm.* **2012**, *9* (6), 1580–1589.
- (74) Meyers, J. D.; Cheng, Y.; Broome, A. M. M.; Agnes, R. S.; Schluchter, M. D.; Margevicius, S.; Wang, X.; Kenney, M. E.; Burda, C.; Basilion, J. P. Peptide-Targeted Gold Nanoparticles for Photodynamic Therapy of Brain Cancer. *Part.*

- Part. Syst. Charact.* **2015**, *32* (4), 448–457.
- (75) Cheng, Y.; Meyers, J. D.; Agnes, R. S.; Doane, T. L.; Kenney, M. E.; Broome, A.-M. M.; Burda, C.; Bacion, J. P. Addressing Brain Tumors with Targeted Gold Nanoparticles: A New Gold Standard for Hydrophobic Drug Delivery? *Small* **2011**, *7* (16), 2301–2306.
- (76) Master, A. M.; Qi, Y.; Oleinick, N. L.; Gupta, A. Sen. EGFR-Mediated Intracellular Delivery of Pc 4 Nanoformulation for Targeted Photodynamic Therapy of Cancer: In Vitro Studies. *Nanomedicine Nanotechnology, Biol. Med.* **2012**, *8* (5), 655–664.
- (77) Li, Z.; Zhao, R.; Wu, X.; Sun, Y.; Yao, M.; Li, J.; Xu, Y.; Gu, J. Identification and Characterization of a Novel Peptide Ligand of Epidermal Growth Factor Receptor for Targeted Delivery of Therapeutics. *FASEB J.* **2005**, *19* (14), 1978–1985.
- (78) Pi, J.; Jiang, J.; Cai, H.; Yang, F.; Jin, H.; Yang, P.; Cai, J.; Chen, Z. W. GE11 Peptide Conjugated Selenium Nanoparticles for EGFR Targeted Oridonin Delivery to Achieve Enhanced Anticancer Efficacy by Inhibiting EGFR-Mediated PI3K/AKT and Ras/Raf/MEK/ERK Pathways. *Drug Deliv.* **2017**, *24* (1), 1549–1564.
- (79) Jin, H.; Pi, J.; Zhao, Y.; Jiang, J.; Li, T.; Zeng, X.; Yang, P.; Evans, C. E.; Cai, J. EGFR-Targeting PLGA-PEG Nanoparticles as a Curcumin Delivery System for Breast Cancer Therapy. *Nanoscale* **2017**, *9*, 16365–16374.
- (80) Song, S.; Liu, D.; Peng, J.; Deng, H.; Guo, Y.; Xu, L. X.; Miller, A. D.; Xu, Y. Novel Peptide Ligand Directs Liposomes toward EGF-R High-Expressing Cancer Cells *in Vitro* and *in Vivo*. *FASEB J.* **2009**, *23* (5), 1396–1404.
- (81) Zhao, N.; Williams, T. M.; Zhou, Z.; Fronczek, F. R.; Sibrian-Vazquez, M.; Jois, S. D.; Vicente, M. G. H. Synthesis of BODIPY-Peptide Conjugates for Fluorescence Labeling of EGFR Overexpressing Cells. *Bioconjug. Chem.* **2017**, *28* (5), 1566–1579.
- (82) Zhou, J.; Joshi, B. P.; Duan, X.; Pant, A.; Qiu, Z.; Kuick, R.; Owens, S. R.; Wang, T. D. EGFR Overexpressed in Colonic Neoplasia Can Be Detected on Wide-Field Endoscopic Imaging. *Clin. Transl. Gastroenterol.* **2015**, *6* (7), e101.
- (83) Xue, E. Y.; Wong, R. C. H.; Wong, C. T. T.; Fong, W.-P.; Ng, D. K. P. Synthesis and Biological Evaluation of an Epidermal Growth Factor Receptor-Targeted Peptide-Conjugated Phthalocyanine-Based Photosensitizer. *RSC Adv.* **2019**, *9* (36), 20652–20662.
- (84) Chen, Y.; Zhou, Q.; Li, X.; Wang, F.; Heist, K.; Kuick, R.; Owens, S. R.; Wang, T. D. Ultrasmall Paramagnetic Iron Oxide Nanoprobe Targeting Epidermal Growth Factor Receptor for In Vivo Magnetic Resonance Imaging of Hepatocellular Carcinoma. *Bioconjug. Chem.* **2017**, *28* (11), 2794–2803.
- (85) Abe, M.; Kuroda, Y.; Hirose, M.; Watanabe, Y.; Nakano, M.; Handa, T. Inhibition of Autophosphorylation of Epidermal Growth Factor Receptor by Small Peptides *in Vitro*. *Br. J. Pharmacol.* **2006**, *147* (4), 402–411.
- (86) Han, C. Y.; Yue, L. L.; Tai, L. Y.; Zhou, L.; Li, X. Y.; Xing, G. H.; Yang, X. G.; Sun, M. S.; Pan, W. S. A Novel Small Peptide as an Epidermal Growth Factor

- Receptor Targeting Ligand for Nanodelivery in Vitro. *Int. J. Nanomedicine* **2013**, *8*, 1541–1549.
- (87) Han, C. Y.; Li, Y.; Sun, M.; Liu, C.; Ma, X.; Yang, X.; Yuan, Y.; Pan, W. Small Peptide-Modified Nanostructured Lipid Carriers Distribution and Targeting to EGFR-Overexpressing Tumor in Vivo Small Peptide-Modified Nanostructured Lipid Carriers Distribution and Targeting to EGFR-Overexpressing Tumor in Vivo. *Artif. Cells, Nanomedicine, Biotechnol.* **2014**, *42*, 161–166.
- (88) Chan, W. C.; White, P. D. Fmoc Solid Phase Peptide Synthesis. In *Fmoc Solid Phase Peptide Synthesis A Practical Approach*; Chan, W. C., White, P. D., Eds.; Oxford University Press: Oxford, 2000; pp 41–74.
- (89) Jullian, M.; Hernandez, A.; Maurras, A.; Puget, K.; Amblard, M.; Martinez, J.; Subra, G. N-Terminus FITC Labeling of Peptides on Solid Support: The Truth behind the Spacer. *Tetrahedron Lett.* **2009**, *50* (3), 260–263.
- (90) Klonis, N.; Sawyer, W. H. Spectral Properties of the Prototropic Forms of Fluorescein in Aqueous Solution. *J. Fluoresc.* **1996**, *6* (3), 147–157.
- (91) Lieber, M.; Todaro, G.; Smith, B.; Szakal, A.; Nelson-Rees, W. A Continuous Tumor-Cell Line from a Human Lung Carcinoma with Properties of Type II Alveolar Epithelial Cells. *Int. J. Cancer* **1976**, *17* (1), 62–70.
- (92) Russell, W. C.; Graham, F. L.; Smiley, J.; Nairn, R. Characteristics of a Human Cell Line Transformed by DNA from Human Adenovirus Type 5. *J. Gen. Virol.* **1977**, *36* (1), 59–72.
- (93) Stuchinskaya, T.; Moreno, M.; Cook, M. J.; Edwards, D. R.; Russell, D. A. Targeted Photodynamic Therapy of Breast Cancer Cells Using Antibody–Phthalocyanine–Gold Nanoparticle Conjugates. *Photochem. Photobiol. Sci.* **2011**, *10* (5), 822–831.
- (94) Obaid, G.; Chambrier, I.; Cook, M. J.; Russell, D. A. Targeting the Oncofetal Thomsen-Friedenreich Disaccharide Using Jacalin-PEG Phthalocyanine Gold Nanoparticles for Photodynamic Cancer Therapy. *Angew. Chemie Int. Ed.* **2012**, *51* (25), 6158–6162.
- (95) Obaid, G.; Chambrier, I.; Cook, M. J.; Russell, D. A. Cancer Targeting with Biomolecules: A Comparative Study of Photodynamic Therapy Efficacy Using Antibody or Lectin Conjugated Phthalocyanine-PEG Gold Nanoparticles. *Photochem. Photobiol. Sci.* **2015**, *14* (4), 737–747.
- (96) García Calavia, P.; Marín, M. J.; Chambrier, I.; Cook, M. J.; Russell, D. A. Towards Optimisation of Surface Enhanced Photodynamic Therapy of Breast Cancer Cells Using Gold Nanoparticle–Photosensitiser Conjugates. *Photochem. Photobiol. Sci.* **2018**, *17*, 281–289.
- (97) García Calavia, P.; Chambrier, I.; Cook, M. J.; Haines, A. H.; Field, R. A.; Russell, D. A. Targeted Photodynamic Therapy of Breast Cancer Cells Using Lactose-Phthalocyanine Functionalized Gold Nanoparticles. *J. Colloid Interface Sci.* **2018**, *512*, 249–259.
- (98) Byzova, N. A.; Safenkova, I. V.; Slutskaia, E. S.; Zherdev, A. V.; Dzantiev, B. B. Less Is More: A Comparison of Antibody–Gold Nanoparticle Conjugates of Different Ratios. *Bioconjug. Chem.* **2017**, *28* (11), 2737–2746.

-
- (99) Tian, L.; Lee, P.; Singhana, B.; Chen, A.; Qiao, Y.; Lu, L.; Martinez, J. O.; Tasciotti, E.; Melancon, A.; Huang, S.; et al. Radiopaque Resorbable Inferior Vena Cava Filter Infused with Gold Nanoparticles. *Sci. Rep.* **2017**, *7* (1), 2147.
- (100) Hussain, I.; Graham, S.; Wang, Z.; Tan, B.; Sherrington, D. C.; Rannard, S.; Cooper, A. I.; Brust, M. Size-Controlled Synthesis of Near-Monodisperse Gold Nanoparticles in the 1–4 Nm Range Using Polymeric Stabilizers. *J. Am. Chem. Soc.* **2005**, *127*, 16398–16399.
- (101) Balny, C.; Douzou, P. Production of Superoxide Ions by Photosensitization of Dyes. *Biochem. Biophys. Res. Commun.* **1974**, *56* (2), 386–391.
- (102) Wang, B.; Wang, J. H.; Liu, Q.; Huang, H.; Chen, M.; Li, K.; Li, C.; Yu, X. F.; Chu, P. K. Rose-Bengal-Conjugated Gold Nanorods for in Vivo Photodynamic and Photothermal Oral Cancer Therapies. *Biomaterials* **2014**, *35*, 1954–1966.
- (103) Uppal, A.; Jain, B.; Gupta, P. K.; Das, K. Photodynamic Action of Rose Bengal Silica Nanoparticle Complex on Breast and Oral Cancer Cell Lines. *Photochem. Photobiol.* **2011**, *87*, 1146–1151.
- (104) Matheson, I. B. C.; Etheridge, R. D.; Kratowich, N. R.; Lee, J. The Quenching of Singlet Oxygen by Amino Acids and Proteins. *Photochem. Photobiol.* **1975**, *21*, 165–171.
- (105) Matheson, I. B. C.; Lee, J. Chemical Reaction Rates of Amino Acids with Singlet Oxygen. *Photochem. Photobiol.* **1979**, *29*, 879–881.
- (106) Michaeli, A.; Feitelson, J. Reactivity of Singlet Oxygen toward Amino Acids and Peptides. *Photochem. Photobiol.* **1994**, *59*, 284–289.
- (107) Choi, Y.; Weissleder, R.; Tung, C.-H. Selective Antitumor Effect of Novel Protease-Mediated Photodynamic Agent. *Cancer Res.* **2006**, *66* (14), 7225–7229.
- (108) Ke, M. R.; Ng, D. K. P.; Lo, P. C. A PH-Responsive Fluorescent Probe and Photosensitizer Based on a Self-Quenched Phthalocyanine Dimer. *Chem. Commun.* **2012**, *48* (72), 9065–9067.
- (109) Haiss, W.; Thanh, N. T. K.; Aveyard, J.; Fernig, D. G. Determination of Size and Concentration of Gold Nanoparticles from UV-Vis Spectra. *Anal. Chem.* **2007**, *79*, 4215–4221.
- (110) Subiros-Funosas, R.; Prohens, R.; Barbas, R.; El-Faham, A.; Albericio, F. Oxyma: An Efficient Additive for Peptide Synthesis to Replace the Benzotriazole-Based HOBt and HOAt with a Lower Risk of Explosion. *Chem. Eur. J.* **2009**, *15* (37), 9394–9403.
- (111) El-Faham, A.; Albericio, F. COMU: A Third Generation of Uronium-Type Coupling Reagents. *J. Pept. Sci.* **2010**, *16*, 6–9.
- (112) Rajappa Vaidyanathan; Vikram G. Kalthod; Duc P. Ngo; Jerad M. Manley, A.; Lapekas, S. P. Amidations Using N,N'-Carbonyldiimidazole: Remarkable Rate Enhancement by Carbon Dioxide. *J. Org. Chem.* **2004**, *69* (7), 2565–2568.
- (113) Rahme, K.; Chen, L.; Hobbs, R. G.; Morris, M. A.; O'Driscoll, C.; Holmes, J. D. PEGylated Gold Nanoparticles: Polymer Quantification as a Function of PEG Lengths and Nanoparticle Dimensions. *RSC Adv.* **2013**, *3*, 6085–6094.

Chapter Three
Investigations into Antibody
Conjugation for the
Development of Antibody
Directed Phthalocyanine-Gold
Nanocarriers

3.1 Introduction

3.1.1 Antibodies

Antibodies are Y shaped glycoproteins secreted by B lymphocytes that are produced to selectively bind to a specific antigen. They consist of four polypeptide chains that form a constant region (Fc), a hinge region and a variable region (Fab), and this variable region contains antigen binding sites, as shown in **Figure 3.1**. Due to the Y shape of antibodies, each antibody contains two antigen binding sites, one at the top of each arm.

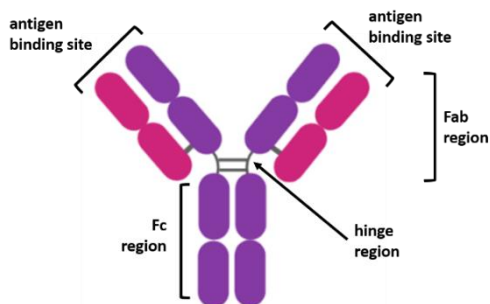


Figure 3.1: The structure of an IgG antibody showing the antigen binding sites, the Fab region, the Fc region and the hinge region

Antibodies are also known as immunoglobulins (Ig), and five classes of Ig are found in mammals: IgA, IgD, IgE, IgG and IgM (**Figure 3.2**), differing in the composition of their heavy chains. IgG antibodies are the most common of these isotypes and can be subdivided into subclasses due to polymorphisms in the Fc region of these proteins.¹ IgG antibodies are *ca.* 150 kDa proteins, consisting of two light chains (*ca.* 25 kDa) and two heavy chains (*ca.* 50 kDa) held together by disulphide bonds and non-covalent interactions.² As IgG antibodies are the most common class of antibody, they are the most extensively investigated class for targeted delivery, both of antibody-drug conjugates and nanoparticle systems.

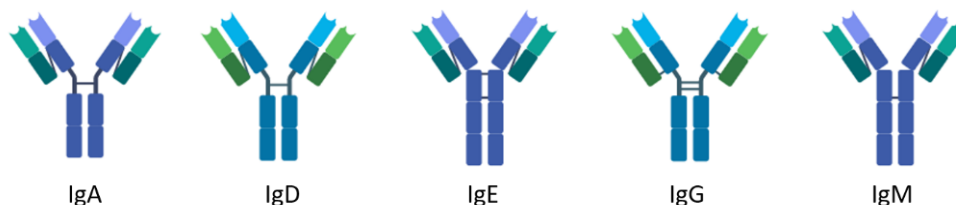


Figure 3.2: The structure of IgA, IgD, IgE, IgG and IgM antibodies

The use of antibodies to deliver gold nanoparticle (AuNP)-based therapeutics has been discussed in **section 1.4.1**. Interestingly, very few antibody conjugation methodologies have been investigated for the addition of antibodies onto AuNPs for therapeutics, while a wide range of conjugation techniques exist and their application to nanoparticles has recently been extensively reviewed.³ Current methodologies for conjugation of antibodies onto nanoparticles can be broadly split into non-covalent adsorption, covalent conjugation and protein-based conjugation. These different conjugation techniques each have their benefits and may be worth investigating to determine the most efficient conjugation technique for the synthesis of the desired nanoconstruct, and therefore the synthesis of nanocarriers with high therapeutic activity.

3.1.2 Non-covalent antibody conjugation

Antibodies can be adsorbed directly onto the surface of AuNPs, using a combination of hydrophobic and electrostatic interactions.⁴ AuNPs are commonly synthesised through a citrate reduction of HAuCl₄, which results in a negatively charged gold core.⁵ Generally, antibody conjugation through adsorption will be performed at a pH above the isoelectric point of the antibody. This increases the number of positively charged residues on the antibody that can form electrostatic interactions with the gold core, as shown in **Figure 3.3a**. Once the antibody is held close enough to the core, hydrophobic residues can interact with the core, and further strengthen the complex.^{4,6}

Non-covalent interactions have been used by a number of groups to functionalise nanoparticles with antibodies. These nanocarriers have been used for a range of applications including molecular probes, imaging and therapies, with successful targeting observed,^{6,7} but there can be issues with the specificity of these conjugates. For example, there is a possibility that other antibodies and proteins in the body could displace the chosen antibody (**Figure 3.3b**), resulting in non-targeted delivery. This concern has led to the community developing nanocarriers covalently bound to antibodies, removing the possibility of displacement.

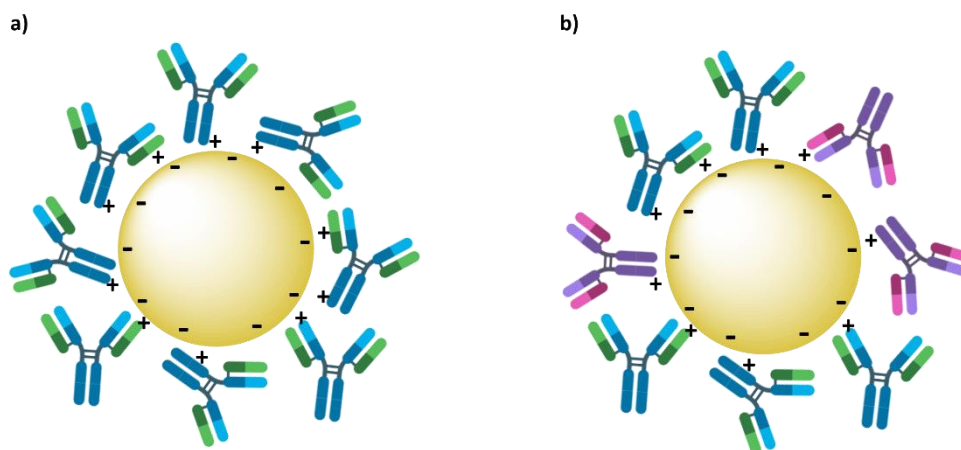


Figure 3.3: **a)** The non-covalent binding of an antibody to a gold core relies on electrostatic and hydrophobic interactions between the negatively charged nanoparticle and positively charged residues on the antibody. **b)** Non-covalent antibody conjugation allows for antibody exchange *in vivo*, leading to off-target effects

3.1.3 Covalent antibody conjugation

A plethora of covalent antibody conjugation techniques have been reported in the literature including, but not limited to, those summarised in **Table 3.1**. These techniques involve the reaction between a target functionality found on native antibodies and a reactive group attached to the molecule to be conjugated. For the bioconjugation of nanoparticles, this involves the functionalisation of a ligand with an antibody either before or after the attachment of the ligand onto the gold core. While carbonyls, hydroxyls and reactive carbons have been explored as conjugation targets, most commonly free amines or thiols on antibodies are utilised for bioconjugation and the popular use of these chemistries for the synthesis of antibody-conjugated nanoparticles highlights these moieties as good targets. The most commonly utilised methodologies for the conjugation of free amines and thiols are shown in bold in **Table 3.1** and their applicability to nanoparticle bioconjugation is discussed further.

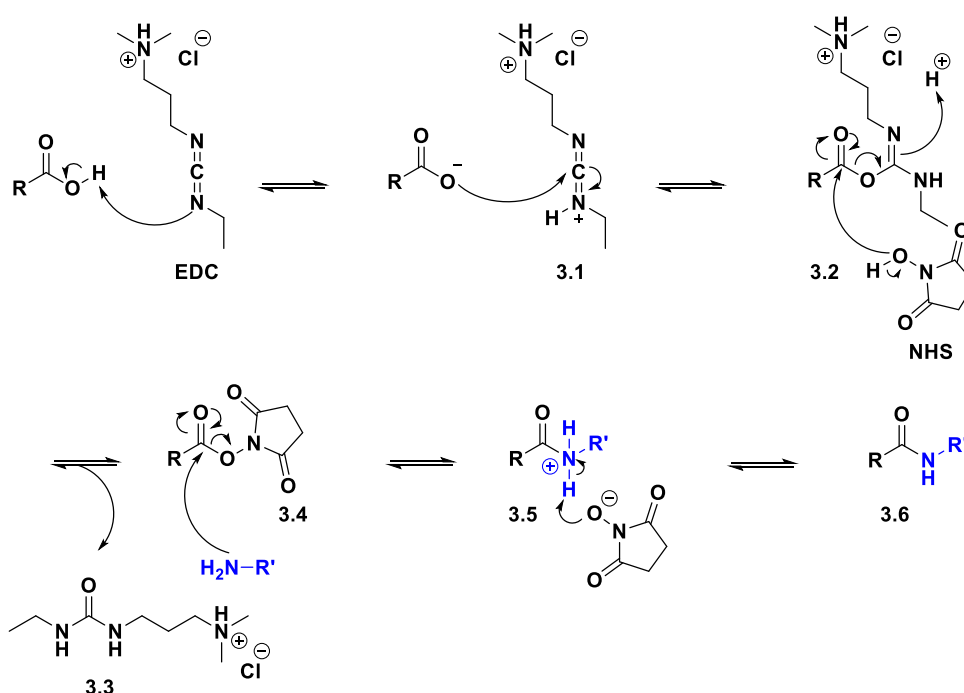
Table 3.1: Functional groups and chemistries used in the literature for antibody conjugation. Those commonly investigated for antibody conjugation to nanoparticles are shown in bold [adapted from ref. 8]

Target in antibody	Reactive group	Product
Carboxylate	Carbodiimides, carbonyldiimidazole	Amides
	Diazoalkanes, diazoacetyl	Esters
Free amine	N-hydroxysuccinimide , acyl azide, carbodiimides , anhydrides	Amides
	Isocyanates, isothiocyanates	(thio)urea
	Sulfonyl chlorides	Sulfonamide
	Aldehydes	Imine
	Epoxides	Secondary amine
	Carbonates	Carbamate
	Arylating agents	Arylamine
	Imidoesters	Amidine
Free thiol	Maleimide , halacetyl halide, alkyl halide, arylating agents, aziridine, acryloyl derivatives	Thioether
	Pyridyl disulphides , 5-thio-2-nitrobenzoic acid	Mixed disulphides
Aldehyde/ketone	Hydrazine	Hydrazone
	Amines	Imine
Hydroxyl	Epoxide, alkyl halide	Ether
	Periodate	Aldehyde
	Isocyanates, carbonyldiimidazole, <i>N,N'</i> -disuccinimidyl carbonate	Carbamate or urethane
Reactive carbon on a phenol	Diazonium	Diazo bond

3.1.3.1 Conjugation through amines

Conjugation of antibodies to nanoparticles through free amines is the most common coupling reaction utilised, and carbodiimides, with formula $RN=C=NR$, are almost always used for this conjugation, yielding the formation of an amide bond.⁹ This family contains a plethora of molecules, with perhaps the most well-known being dicyclohexylcarbodiimide (DCC) and 1-ethyl-3-(3-dimethylaminopropyl)carbodiimide hydrochloride (EDC). DCC is not soluble in aqueous media, so EDC, which is water soluble, is the most commonly utilised coupling agent for antibody conjugation. The mechanism for EDC amide bond formation is shown in **Scheme 3.1**. This amide bond

formation is a dehydration reaction that involves the activation of a carboxylic acid through the carbodiimide nitrogen lone pair accepting a proton. Once activated, **3.1**, the carboxylic acid can react with the central carbon of the carbodiimide, forming an activated o-acylisourea ester, **3.2**. This activated carbonyl can then be attacked by nucleophiles, releasing an isourea, **3.3**. Amines themselves can be used to attack this activated carbonyl, but more commonly *N*-hydroxysuccinimide (NHS), or its sulfonated derivative *N*-hydroxysulfosuccinimide (s-NHS), is used to attack, forming an activated succinimidyl-ester, **3.4**. This molecule is more stable than the o-acylisourea ester and allows for purification before addition of the amine. Generally, the nanoparticle ligands will be activated with EDC/NHS, then excess coupling agents removed before the addition of the antibody to prevent the activation of carboxylic acids on the antibody which would lead to crosslinking and polymerisation.¹⁰ Once the succinimidyl ester has been formed and excess reagents removed, the target amine can be added, substituting for the succinimide and forming an amide bond.



Scheme 3.1: The mechanism of EDC/NHS amide bond formation

While the use of EDC/NHS is the most commonly investigated antibody conjugation chemistry for the formation of antibody-AuNP-based therapeutics, the synthesised NHS-esters can be hydrolysed in the aqueous solutions necessary for antibody conjugation, limiting the efficiency to only 20%, meaning a high excess of antibody is often needed.¹¹

IgG antibodies also contain *ca.* 80 lysine residues¹² and EDC/NHS chemistry is not regiospecific, meaning conjugation may occur in the Fab region of the antibody, blocking its activity, as shown in **Figure 3.4**.¹³

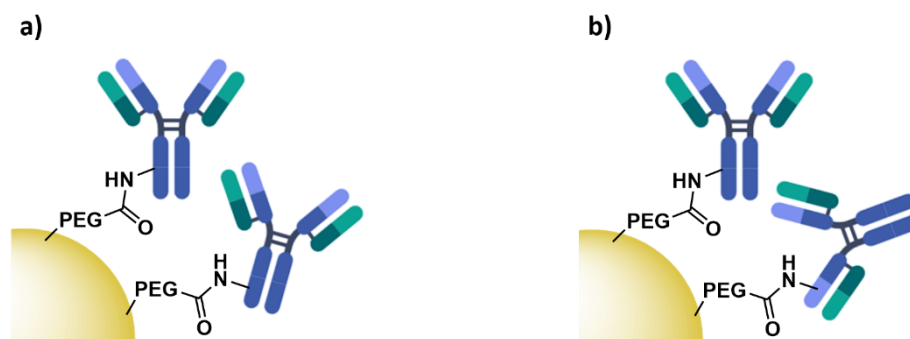


Figure 3.4: *a) ideal EDC/NHS conjugation and b) the reality of EDC/NHS conjugation – the chemistry is not regiospecific so some antibodies may be linked through the Fab region and therefore lose specificity for the receptor*

3.1.3.2 Conjugation through thiols

One method to try to increase selectivity of the conjugation is to use the thiols present on an antibody in the form of cysteine residues. On average, on a typical IgG antibody there are 32 cysteine residues,¹⁴ with only eight of these accessible under native conditions.¹⁵ These accessible cysteine residues are found as interchain disulphide bonds at physiological pH (**Figure 3.5a**).¹⁶ This reduction in the number of accessible reactive moieties compared to lysine residues presents thiol conjugation as a more regiospecific functionalisation methodology. Free cysteine residues can occasionally be present on an antibody and show reactivity, but often selective reduction of disulphides provides the free thiols for conjugation. Reagents such as tris(2-carboxyethyl)phosphine (TCEP) or 2-mercaptoethylamine (2-MEA) can be used to reduce these disulphides to release thiols for conjugation.¹⁷ This reduction allows for further control over the conjugation, as the number of equivalents of reducing agent added to the antibody will determine how many disulphides are reduced.¹⁶ While it has been shown that interchain disulphides between the two heavy chains are more easily reduced than light chain-heavy chain disulphides,¹⁵ this chemistry is not regiospecific, meaning random disulphides will be reduced, leading to a mixture of products, as shown in **Figure 3.5b**. Notably, these disulphides are not involved in antigen binding so the conjugation does not interrupt their recognition ability, however, if light chain-heavy chain disulphides are reduced, the Fab region of the antibody will be destroyed, leading to loss of receptor recognition.

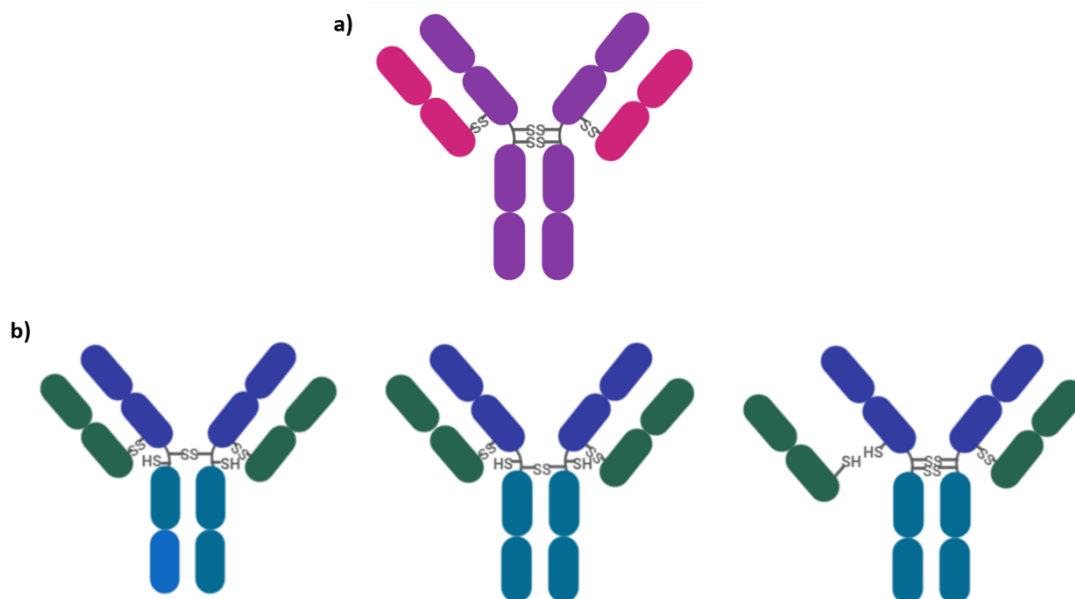


Figure 3.5: a) The location of the interchain disulphides on an IgG antibody accessible for thiol conjugation and b) the antibody fragments formed upon reduction of one disulphide

To conjugate these free thiols on an antibody to AuNPs, maleimides can be used as linkers. Maleimides selectively react with thiols between pH 6.5-7.5, undergoing a Michael addition to form a thioether bond, as shown in **Figure 3.6a**. While the reduction of disulphides allows for site-specific antibody conjugation, the reduction can destabilise the structure of an antibody. To counter this, re-bridging agents such as dibromomaleimides are commonly used for antibody conjugation to reinstate the stability of the disulphide bond into the conjugated antibody (**Figure 3.6b**).^{18,19} While thioethers are generally considered to be irreversible bonds, some reports have been shown these bonds to be reversible in environments containing high thiol content, leading to thiol exchange. Off target drug release has been observed for antibody-drug conjugates (ADCs) formed through maleimides,²⁰ but ring opening reactions have been shown to stabilise this thioether bond.^{21,22}

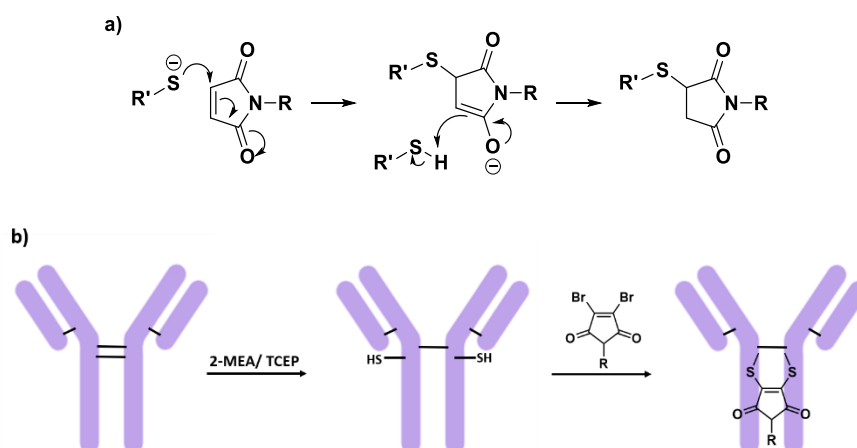


Figure 3.6: a) Michael addition of a thiol to a maleimide to form a thioether and b) dibromomaleimide bridges two thiols to reinstate stability of the reduced disulphide

3.1.3.3 Conjugation through cross-linkers

Other chemistries for thiol conjugation involve pyridyl disulphide cross-linkers such as succinimidyl 3-(2-pyridyldithio)propionate) (SPDP, **Figure 3.7a**) and pyridine dithioethylamine hydrochloride (PDEA, **Figure 3.7b**). These linkers contain a disulphide moiety that reacts with thiols in the antibody, forming a new disulphide and releasing pyridine-2-thione. The latter compound has a characteristic absorbance at 343 nm,²³ meaning the reaction can be monitored using UV-vis spectroscopy. Each cross-linker also possesses a reactive group on the opposite terminus of the molecule, with SPDP possessing an amine reactive succinimide and PDEA an amine terminus for crosslinking to carbonyls. Pyridyl disulphides show efficient conjugation to thiols and can be used to conjugate antibodies onto nanoparticles (**Figure 3.7c**).²³ The formation of a disulphide is, however, less favourable for antibody conjugation than thioethers as this is a reversible bond. This opens up similar issues to non-covalent attachment as other proteins or antibodies could displace the desired antibody and lead to non-specific targeting. To counter this, SPDP is often used in conjunction with the maleimide containing cross-linker succinimidyl 4-(*N*-maleimidomethyl) cyclohexane-1-carboxylate (SMCC). Here, the dithiol is reduced before addition of the maleimide containing linker, leading to the formation of the thioether, which is much more stable than the mixed disulphides otherwise formed.^{24,25}

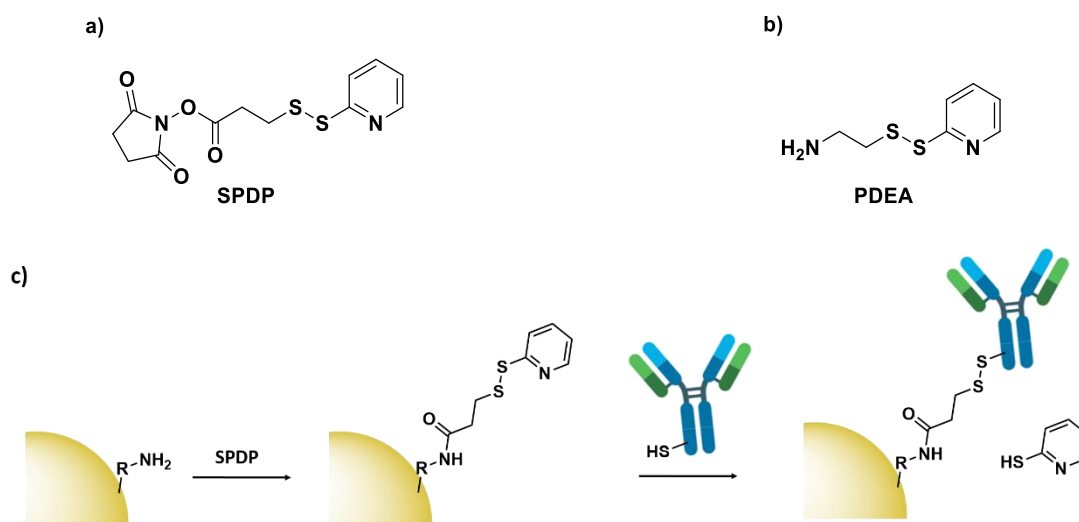


Figure 3.7: Structures of **a)** SPDP and **b)** PDEA. **c)** The addition of antibodies to nanoparticles through SPDP, releasing pyridine-2-thione

SMCC (**Figure 3.8a**) is a heterofunctional crosslinker that contains a thiol reactive maleimide on one end of the molecule and an amine reactive succinimidyl-ester on the other and has been used to conjugate antibodies onto a variety of nanoparticles. Interestingly, most reports use the succinimidyl-ester to conjugate onto the antibody through amide bond formation and the maleimide to form a thioether bond to the nanoparticle surface.^{26,27} This surprisingly uses a less specific conjugation method for addition to the antibody, however perhaps this is favoured as no manipulation of the antibody is required. While SMCC is more commonly used in this manner, there are some examples of using the maleimide to conjugate the antibody.^{28,29} Generally, the succinimidyl-ester of SMCC is reacted with an amine, before purification, followed by the addition of the thiol. While the heterofunctionality of this linker is appealing, both succinimidyl-esters and maleimides are hydrolysed in aqueous media, so the two step cross-linking necessary for antibody conjugation using SMCC may be less efficient than other coupling agents.³⁰

Bis(sulfosuccinimidyl)suberate (BS3, **Figure 3.8b**) is a popular homofunctional cross-linker consisting of a hexyl chain bifunctionalised with sulfosuccinimidyl esters, allowing for the cross-linking of two amine-functionalised molecules. The homofunctionality of BS3 means that a high excess of cross-linker must be added to a reaction to prevent aggregation of the nanoparticles instead of cross-linking between nanoparticles and an antibody. It has been observed, however, that aggregation of nanoparticles occurs upon

treatment of nanoparticles with a 10-fold excess of BS3³¹ so this homofunctional cross-linker may not be appropriate for the formation of antibody-functionalised nanoparticles.

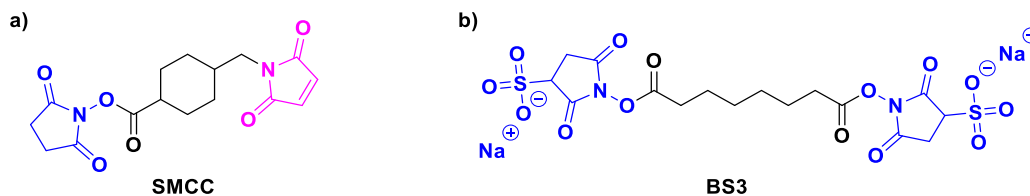
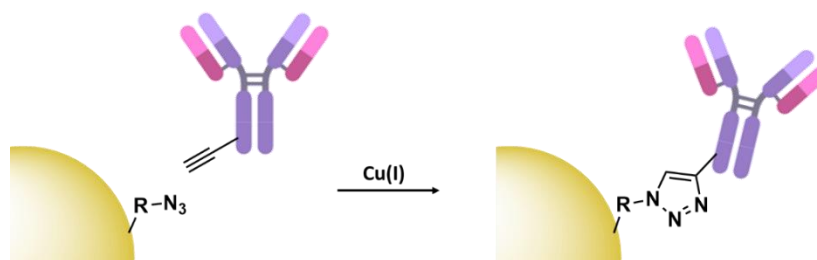


Figure 3.8: The structures of **a)** SMCC and **b)** BS3 showing amine reactive succinimides (blue) and thiol reactive maleimide (pink)

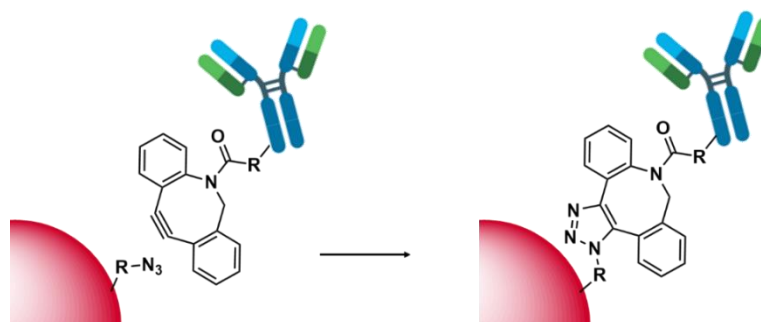
3.1.3.4 Conjugation through click chemistry

While the above examples of antibody conjugation utilise native functionalities in antibodies to bind to AuNPs, these chemistries can be used for the addition of further reactive moieties to increase the efficiency of antibody conjugation reactions. One example of this is the addition of alkyne moieties to antibodies through EDC/NHS chemistry for bioconjugation through click chemistry.¹¹ Click chemistry describes a group of reactions that are high yielding, producing few, easily removable byproducts while using readily available reagents.³² The most common click reaction is that between an azide and an alkyne, catalysed by copper, forming a 1,4-triazole, as shown in **Scheme 3.2**. The copper catalysed click reaction involves the association of the Cu(I) catalyst with the alkyne, which subsequently replaces the alkyne proton and can coordinate to the positively charged nitrogen of the azide. This coordination leads to the formation of solely the 1,4-triazole. The azide and alkyne react to form a six membered ring, then rearrange to release the strain of the allene, giving the triazole with the copper complex still associated. The copper is replaced with a proton to yield the final triazole and regenerate the catalyst. Chemical modification of antibodies with alkynes through an NHS-PEG-alkyne linker has been shown to be highly efficient and lead to higher antibody conjugation onto nanoparticles compared to conventional EDC/NHS chemistry.¹¹



Scheme 3.2: Copper catalyzed click reaction involving nanoparticle-immobilised azide and an alkyne functionalised antibody. These residues can be swapped and a click reaction would still occur

While copper catalyzed click chemistry is commonly employed, copper is toxic within cells so meticulous purification of the nanoparticles functionalised using this metal is necessary before any conjugates can be used in biological systems.³³ One alternative to this toxic catalyst is the use of strain-promoted azide-alkyne cycloaddition (SPAAC). SPAAC commonly uses cyclooctyne derivatives which allow click chemistry to occur without the copper catalyst or extreme temperatures. Cyclooctyne consists of a strained eight membered ring with an alkyne moiety which makes it very reactive towards azides. Derivatives such as dibenzocyclooctyne (DBCO) have been designed to allow the use of this functionality for conjugation. DBCO has been used to conjugate antibodies onto quantum dots, as shown in **Scheme 3.3**. The DBCO moiety is conjugated onto the antibody through random amide bond formation before SPAAC allows for efficient conjugation of this antibody onto the quantum dot.³⁰



Scheme 3.3: SPAAC addition of a DBCO-conjugated antibody to a quantum dot-immobilised azide

While random amide bond formation is again used to attach the linker onto the antibody, SPAAC has been seen to be a more efficient conjugation strategy than EDC/NHS. For example, the alternative SPAAC reagent bicyclononyne (**Figure 3.9**) has been used to conjugate an antibody onto PGLA nanoparticles. Bicyclononyne has been shown to

display an antibody conjugation efficiency of 18%, compared to just 6% for EDC/NHS chemistry. The bicyclononyne moiety in this work was attached to the antibody through disulphide reduction and bridging, combining the selectivity of disulphide conjugation with the efficiency of SPAAC.³⁴

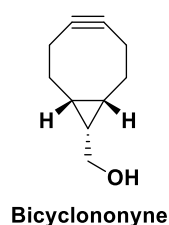


Figure 3.9: The structure of the SPAAC reagent bicyclononyne

While in the above examples SPAAC exhibited increased efficiency in antibody conjugation compared to EDC/NHS, the reactivity of cyclooctyne derivatives has been shown to greatly decrease with steric hindrance.³⁵ Both antibodies and nanoparticles are large, complex structures so it is hard to predict how efficient SPAAC conjugation may be upon these systems. For example, it has been shown that SPAAC between antibody-bound DBCO and a polymeric nanoparticle bound azide no longer proceeds under physiological conditions.³⁶ Furthermore, SPAAC relies on the addition of these reactive moieties through non-regiospecific conjugation techniques, meaning there is a possibility of these antibodies being conjugated in a non-functional manner.

3.1.4 Protein-based antibody conjugation

While chemical conjugation methods are widely used and have been shown to be successful, frustrations with the non-specificity of many of these conjugation techniques has led the community to investigate more specific antibody conjugation strategies. The mutation of antibodies to site-specifically install reactive moieties or unnatural amino acids has been widely investigated, but this is very expensive, time consuming and requires specialist knowledge. A second methodology investigated to increase the regiospecificity of antibody conjugation is the use of adaptor proteins. Adaptor proteins contain protein binding motifs that can be used to regiospecifically couple antibodies to nanoparticles. Commonly investigated adaptor proteins include avidin, streptavidin and Fc binding proteins.

3.1.4.1 Biotin-(strept)avidin for bioconjugation

The proteins avidin and streptavidin bind the small molecule ligand biotin through one of the strongest non-covalent biological interactions currently known.³⁷ This strong interaction has been exploited for the conjugation of antibodies onto nanoparticles,^{38,39} as shown in **Figure 3.10a**. Generally, the nanoparticle surface is modified with avidin or streptavidin through covalent binding, using chemistries such as EDC/NHS. Here the non-specificity of this chemistry has less impact as avidin and streptavidin contain four biotin binding sites,⁴⁰ meaning total loss of biotin binding activity upon covalent binding is very unlikely.

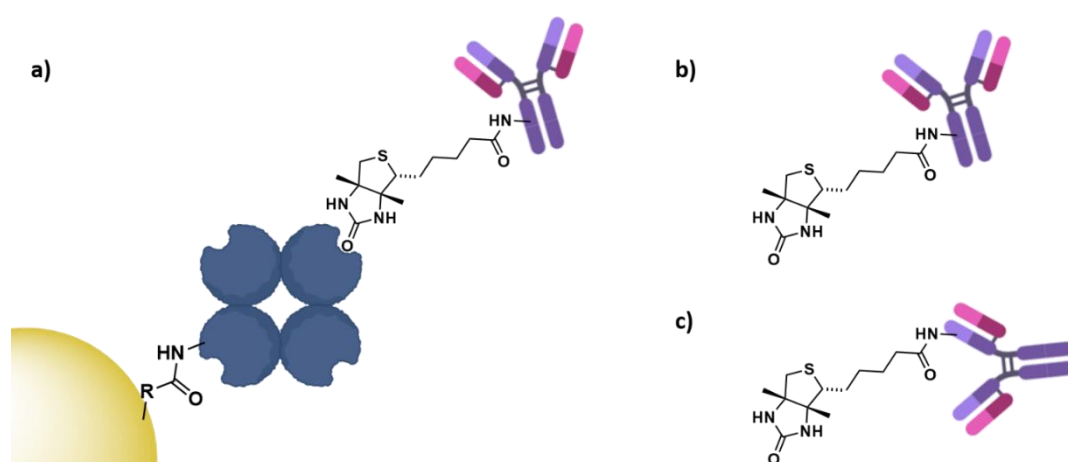


Figure 3.10: *a) The use of (strept)avidin-biotin to conjugate antibodies onto nanoparticles, b) the desired conjugation of biotin to an antibody and c) the conjugation of biotin through non-regiospecific bond formation can lead to the inhibition of antibody binding*

While the biotin binding ability of (strept)avidin is not lost by its covalent conjugation to nanoparticles, the complications with this technique arise from the tagging of an antibody with biotin. The biotinylation of antibodies relies on the chemical conjugation of biotin to residues on the antibodies surface, such as amines, carboxylic acids or thiols.⁴¹ As previously discussed, these methods are not regiospecific and can lead to loss of antibody activity, as shown in **Figure 3.10b&c**. Steps have been taken towards the specific conjugation of biotin to antibodies through hinge region disulphide reduction,⁴² but as discussed in **section 3.1.3.2**, this chemistry also leads to a mixture of products and some loss of active antibody. The use of (strept)avidin is remarkably more expensive than chemical conjugation, and its lack of significant advantage over chemical methods means that this technique is currently not a favourable methodology for antibody conjugation to nanoparticles.

3.1.4.2 Fc binding proteins for bioconjugation

As described in **section 3.1.1**, antibodies consist of a variable (Fab) and constant (Fc) region. The Fc region is not involved in the binding of the antibody to its target, and therefore presents itself as the ideal binding site. Two proteins isolated from *staphylococcus aureus* and *streptococcal G*, protein A and protein G respectively, have been shown to specifically bind to the Fc region of IgG antibodies.^{43,44} These proteins have been used to regiospecifically bind antibodies to nanoparticles, resulting in nanoconjugates with antibodies all orientated with their active sites free for binding,⁴⁵ as shown in **Figure 3.11**. An attractive feature of protein A or G based bioconjugation is the fact that the Fc region of IgG antibodies is conserved, meaning antibodies can be interchanged to deliver nanocarriers to any desired target, presenting a way to produce a universal system for delivery of a therapeutic to any desired location.

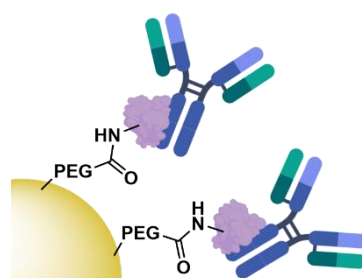
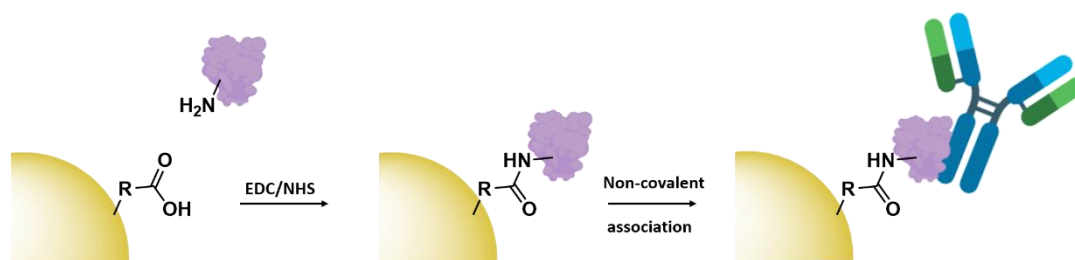


Figure 3.11: Proteins A and G control the orientation of antibodies on nanoparticles by regiospecifically binding to the Fc region

Protein A^{46,47} and protein G^{48,49} have both been successfully used to conjugate antibodies to nanoparticles, with selective uptake observed. While this controlled orientation conjugation ensures that all the attached antibodies have their antigen binding sites accessible, this conjugation is entirely non-covalent so antibody exchange may occur *in vivo*. Interestingly, it has been observed that the dissociation kinetics of an IgG antibody from protein A are slow enough that no antibody exchange occurs within an hour,⁵⁰ but this time frame is not long enough to assess whether antibody exchange would occur if these nanocarriers were used as therapeutics. It is possible that an antibody could be cross-linked to protein A or G to prevent this dissociation *in vivo*, but there are no reports of this technique being utilised. A second consideration for the use of these Fc binding proteins is the addition of protein A or G onto the nanoparticle itself. This addition tends to involve the use of EDC/NHS (**Scheme 3.4**) or cross-linkers such as BS3, again raising questions about whether these conjugations could block the binding sites of the adaptor proteins, reducing the efficiency of this technique.



Scheme 3.4: The use of adaptor proteins A and G for antibody conjugation. Adaptor proteins are covalently conjugated onto nanoparticles, before mixing with antibodies where they form non-covalent interactions with the Fc region

3.2 Summary and chapter aims

Antibody conjugation to gold nanoparticles for therapeutics has thus far mainly focussed on the use of carbodiimides to form random amide bonds between lysine residues on an antibody and carboxylic acids on a linker. While this use of EDC/NHS chemistry has been seen to be very successful for antibody conjugation, its lack of regiospecificity means that antibodies may be conjugated onto nanoparticles in a way which prevents their ability to bind to the desired receptor, and therefore reducing the targeting ability of these nanoconjugates. Many other chemical conjugation strategies such as thiol conjugation, cross-linkers and click chemistry have been explored for antibody conjugation and each technique presents its own virtues. These alternate conjugation techniques are worth exploring since they may lead to increased conjugation efficiencies, leading to increased potency of the designed nano-therapeutic.

Conjugation of antibodies to nanoparticles through thiols often involves the reduction of interchain disulphides within the hinge region of antibodies, with these free thiols able to react with maleimides or pyridyl disulphides on the nanoparticle surface. This chemistry is more specific than carbodiimide amide bond formation, but the reduction of these disulphides is hard to control. The reduction of interchain disulphides between light and heavy chains will destroy the antigen binding site of an antibody, leaving the conjugated antibody fragment inactive towards its target.

Cross-linkers such as SMCC and BS3 have also been investigated for antibody conjugation. BS3 contains two amide reactive termini, but this cross-linker has been seen to cause aggregation of nanoparticles and is therefore unlikely to be a good option. SMCC possesses a thiol reactive terminus and an amine reactive terminus. This heterofunctional linker prevents the aggregation of nanoparticles upon addition, but as both maleimides

and succinimides are easily hydrolysed, the two-step conjugation necessary for this antibody addition leads to low conjugation.

Click chemistry involves the reaction of an azide and an alkyne to form a 1,4-triazole. This chemistry can either be mediated by copper or use strained alkynes to promote copper-free SPAAC. SPAAC is a more popular methodology as copper is highly toxic. The efficiency of SPAAC, however, is greatly reduced by steric bulk, and the addition of reactive moieties to an antibody tends to involve non-regiospecific techniques such as EDC/NHS.

Due to the lack of specificity of chemical-based conjugations, adaptor proteins have been investigated for site-specific antibody conjugation. Avidin and streptavidin display essentially non-reversible non-covalent binding towards biotin and this interaction has been exploited. The biotinylation of antibodies, however, involves chemical methodologies such as EDC/NHS so this expensive technique may not improve on current chemical conjugation methods. The Fc binding proteins protein A and protein G are known to specifically bind to the constant region of antibodies and can be used to bind antibodies in a set orientation with their antigen binding sites away from the nanoparticle surface. This ability to determine the orientation of an antibody on the surface of a nanoparticle is very appealing, but this interaction is non-covalent so antibody exchange may occur *in vivo*.

This chapter aims to explore antibody conjugation techniques to produce antibody-functionalised nanoparticles with the highest activity towards EGFR overexpressing non-small cell lung cancer. The non-targeted nanocarriers discussed throughout this thesis, C11Pc-PEG-AuNPs, have previously been directed towards HER2 overexpressing breast cancer by attaching an anti-HER2 antibody onto the surface of these nanocarriers through EDC/NHS chemistry.⁵¹ Here, we expanded on this work by exploring the binding of an anti-EGFR antibody to these nanoparticles through EDC/NHS chemistry and thiol-maleimide couplings to determine the most efficient antibody conjugation technique. These conjugation techniques were chosen as the majority of the chemical conjugation strategies discussed in this chapter rely on one of these methods for the addition of reactive moieties.

Along with this comparison of chemical conjugation strategies, the possibility to produce a nanoparticle system where the antibody could be easily interchanged to target any desired receptor led to the exploration of the use of Fc binding proteins. Here, the

use of protein G to site-specifically bind antibodies was investigated. While a current issue with the use of Fc binding proteins is their non-covalent binding, here we explored whether cross-linking of an antibody to protein G could form a stable conjugate with higher activity than current favoured chemical conjugation techniques. The use of random chemical conjugation strategies to conjugate protein G onto AuNPs led to the investigation of Fc binding peptides to eliminate the non-specificity of the addition of protein G, leading to the possibility of highly specific antibody conjugation to AuNPs.

3.3 Results and discussion

3.3.1 Functionalisation of C11Pc-PEG-AuNPs with anti-EGFR antibodies

As antibodies are sensitive to organic solvents, and as the synthesis of the *ca.* 4 nm C11Pc-PEG-AuNPs relies on tetrahydrofuran (THF), the functionalisation of C11Pc-PEG-AuNPs with antibodies must be completed after the formation of the nanoparticles. The synthesis of C11Pc-PEG-AuNPs was completed as described in **section 2.3.2**, with the purified nanocarriers resuspended in MES buffer, pH 5.5. These nanocarriers were characterised by UV-vis and fluorescence spectrometry, with the resulting spectra shown in **Figure 3.12**. As described in **section 2.3.2.2**, this UV-vis spectrum confirmed the core of the resulting nanocarriers was below 5 nm due to the lack of an SPR band in the spectrum.

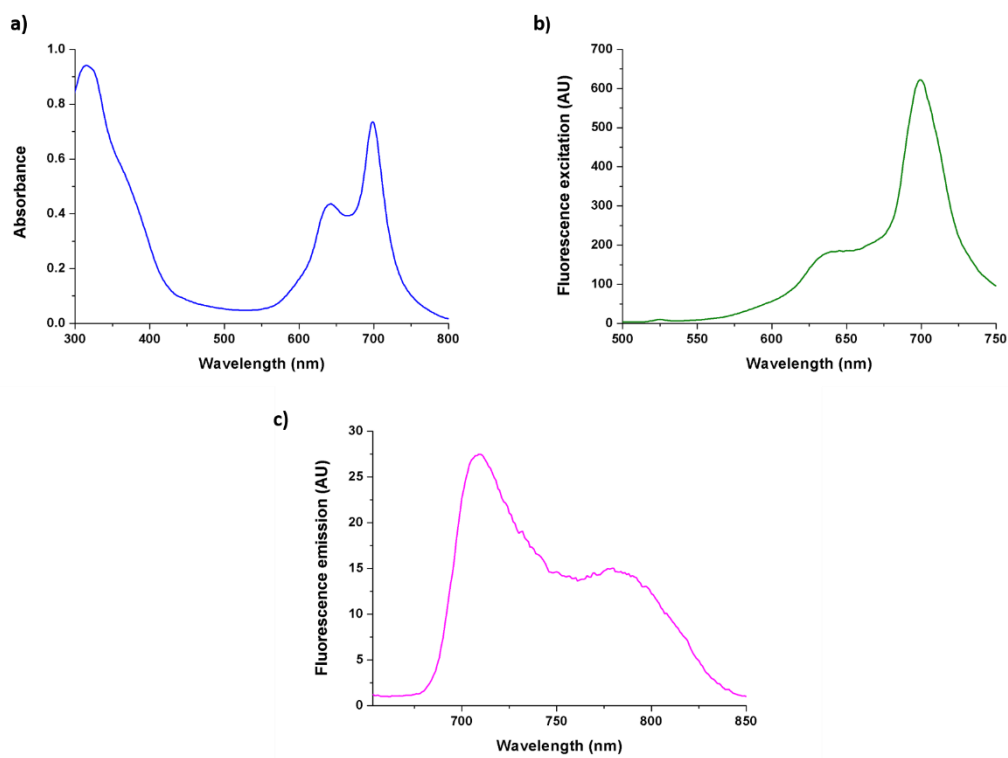


Figure 3.12: a) UV-vis, b) fluorescence excitation and c) fluorescence emission spectra of C11Pc-PEG-AuNPs in MES buffer

3.3.1.1 Antibody functionalisation through EDC/NHS chemistry

The bi-functionalised HS-PEG-COOH used for the synthesis of C11Pc-PEG-AuNPs provides a free carboxylic acid at the terminus of the PEG for functionalisation with an antibody. The most common, and previously used,^{51–53} method for functionalisation of these nanocarriers is EDC/NHS chemistry, and therefore this was chosen as a starting point for the conjugation of anti-EGFR antibodies onto C11Pc-PEG-AuNPs. Currently, there are no validated methods for determining the antibody concentration on AuNPs. Gold has been shown to interfere with common colorimetric techniques such as bicinchoninic acid (BCA) assays⁵⁴ and gold nanoparticles are known to quench the fluorescence of attached fluorophores,⁵⁵ meaning fluorescent tagging cannot be confidently used for quantification. Due to these downfalls, proof of concept studies for EDC/NHS conjugation were completed using fluorescent tags to ensure that antibody conjugation to C11Pc-PEG-AuNPs would proceed using EDC/NHS. Here, these fluorescent tags were solely used for proof of principle, not for the quantification of antibody concentration. For this study, an anti-EGFR antibody was purchased from Abcam. Firstly, as the structure of this anti-EGFR antibody is unknown, it was tested for the presence of free lysine residues on its surface. Fluorescein isothiocyanate (FITC,

Figure 3.13a), is a fluorescent molecule known to spontaneously react with amines. FITC was mixed with the antibodies, allowing for conjugation of FITC to any accessible lysines, then the antibodies were purified through Zeba spin desalting columns (MWCO 7,000 Da) to remove any unreacted FITC from the sample. The fluorescence of the collected FITC-antibodies, **3.7**, was compared to the fluorescence of non-tagged antibodies, and a significant increase in fluorescence intensity was observed (**Figure 3.13b**), showing the binding of FITC to the antibodies and therefore the presence of lysine on their surface.

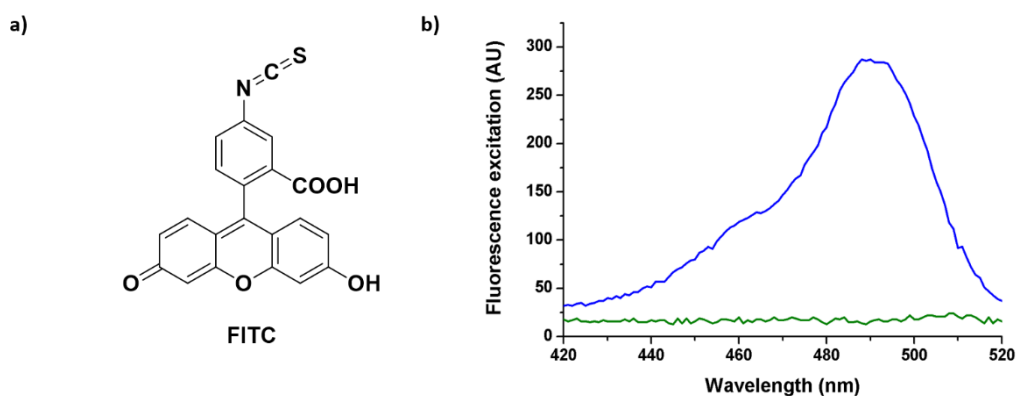


Figure 3.13: **a)** The structure of FITC and **b)** the fluorescence excitation of 1 mg/mL FITC-EGFR-Ab (**3.7**, blue) and non-conjugated EGFR Ab (green) in PBS

The functionalisation of C11Pc-PEG-AuNPs with antibodies with EDC/NHS involves the activation of the PEG carboxylic acids in MES buffer at pH 5.5, before the excess EDC/NHS is washed away and the desired antibody is added to the activated nanoparticles in PBS at pH 7.4.⁵⁶ The activation of the PEG is carried out at pH 5.5 to minimise the rate of ester hydrolysis, a competing reaction in aqueous media that greatly reduces the efficiency of the antibody conjugation. To ensure that these reaction conditions indeed allow for the conjugation of the anti-EGFR antibodies onto C11Pc-PEG-AuNPs, they were first tested with a second fluorescent tag. 5-carboxyfluorescein (5-FAM, **Figure 3.14a**) is a fluorescein derivative containing a free carboxylic acid that can act as a fluorescent model of the PEG carboxylic acid for conjugation to the anti-EGFR antibodies. 5-FAM was activated using EDC/NHS in MES buffer at pH 5.5, then combined with anti-EGFR antibody in PBS at pH 7.4 and incubated for 6 hours at room temperature with occasional shaking. Excess 5-FAM was removed from the solution using Zeba spin desalting columns (MWCO 7,000 Da). The fluorescence of the 5-FAM-antibody, **3.8**, was compared to that of non-modified antibody, as shown in **Figure 3.14b**,

and a strong fluorescence was observed in the presence of 5-FAM, suggesting the EDC/NHS chemistry will allow functionalisation of the C11Pc-PEG-AuNPs with antibody using these buffer systems.

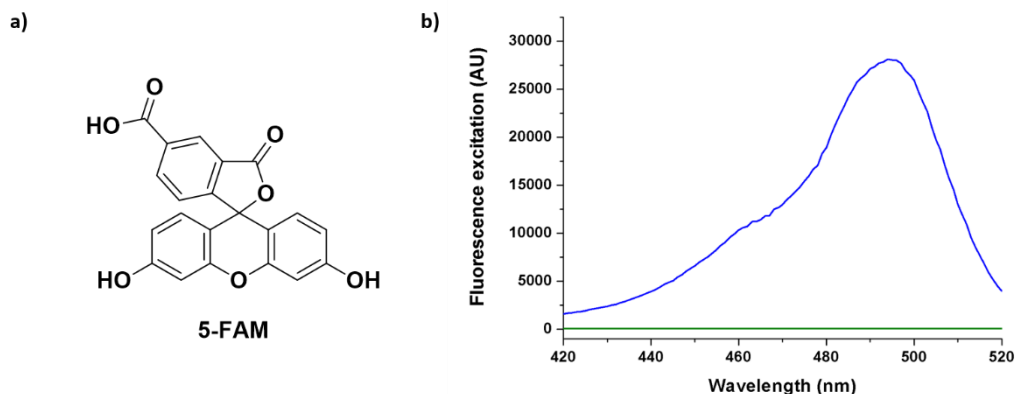


Figure 3.14: a) The structure of 5-FAM and b) the fluorescence excitation of 1 mg/mL 5-FAM-EGFR-Ab (3.8, blue) and non-conjugated EGFR Ab (green) in PBS

While the conjugation of 5-FAM to the antibody is a promising result, the complexity of a nanoparticle shell is not taken into account. The C11Pc-PEG-AuNPs used throughout this thesis have a completely unknown 3D structure and therefore it is not known how many of the terminal carboxylic acids on the PEG ligands functionalising the nanoparticle are accessible for conjugation. To explore this problem, a third fluorescein derivative, 5-(3-(3-aminopropyl)thioureido)-2-(6-hydroxy-3-oxo-3H-xanthen-9-yl) benzoic acid (**2.34**, **Figure 3.15a**), was synthesised to form a fluorescein derivative with a terminal reactive amine group. **2.34** was used as a fluorescent mimic of the antibody to ensure that conjugation to C11Pc-PEG-AuNPs under the desired reaction conditions was possible. C11Pc-PEG-AuNPs were activated with EDC/NHS in MES buffer at pH 5.5 then, after centrifugation in Vivaspin 500 columns, mixed with 0.15 mg/mL **2.34** overnight in PBS. After conjugation, the resulting FITC-C11Pc-PEG-AuNPs (**3.9**) were purified through Vivaspin 500 columns to remove any unconjugated **2.34**, then analysed by UV-vis spectroscopy. Here, a peak was observed at 495 nm corresponding to FITC, as shown in **Figure 3.15b**. This demonstrates that molecules can be conjugated onto the C11Pc-PEG-AuNPs through EDC/NHS couplings, and therefore suggests that antibody conjugation under these conditions should be successful.

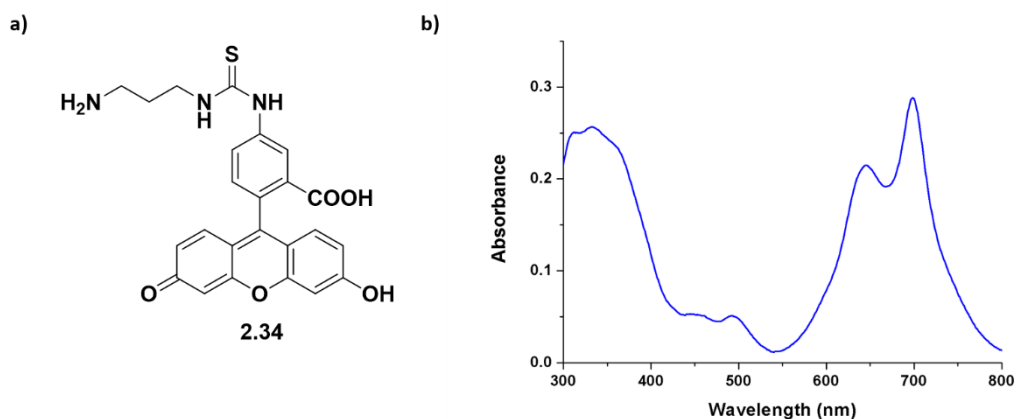


Figure 3.15: a) The structure of **2.34** and b) UV-vis of **3.9** in PBS showing a peak at 495 nm due to the presence of **2.34**

These proof of concept studies strongly suggested that the method planned for the attachment of antibody to C11Pc-PEG-AuNPs with EDC/NHS had a great potential. Therefore, post synthesis, C11Pc-PEG-AuNPs were treated with EDC/NHS and mixed with anti-EGFR antibody to give anti-EGFR-C11Pc-PEG-AuNPs (**3.10**). After conjugation, **3.10** were purified in Vivaspin 500 columns. UV-vis spectra of the washings (**Figure 4.19a**) showed the decrease in antibody in successive washes, with the third wash being almost free of antibody and therefore that non-conjugated antibody had been removed from the nanoparticle solution. Once the unbound antibody was removed, the nanoparticles were resuspended in PBS buffer and a UV-vis spectrum was recorded, as shown in **Figure 3.16b**. Unfortunately, due to the presence of an absorbance peak from the gold core at 254 nm, the absorbance maxima for antibodies, this UV-vis spectrum cannot be used to determine the presence of antibody on these nanocarriers. Further studies to confirm whether this conjugation was successful will be discussed in **section 3.3.2**.

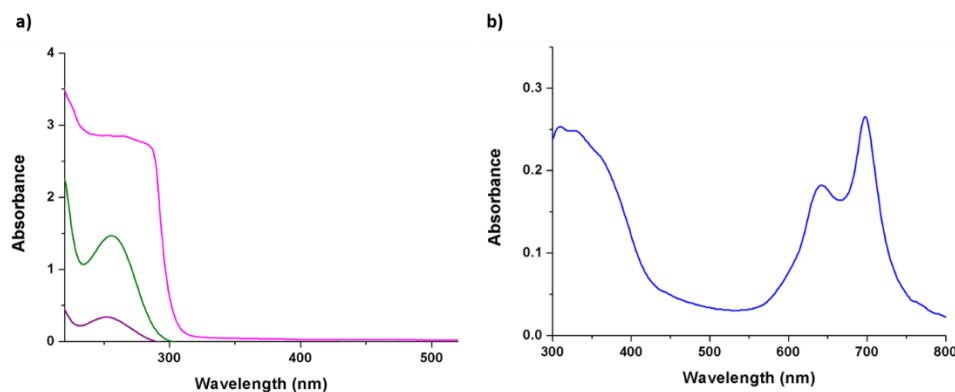


Figure 3.16: **a)** UV-vis spectra of sequential washings collected from the EDC/NHS functionalisation of C11Pc-PEG-AuNPs with anti-EGFR Ab and **b)** the UV-vis spectrum of **3.10** in PBS buffer

3.3.1.2 Antibody functionalisation through maleimide chemistry

To explore the possibility of using thiols present on antibodies for conjugation, first the crosslinking agent pyridine dithioethylamine hydrochloride (PDEA) was explored. The amine terminus of PDEA was conjugated to C11Pc-PEG-AuNPs through EDC/NHS, then the washings collected and analysed by UV-vis spectrometry. Unfortunately, PDEA was found to be unsuitable for conjugation to these nanoparticle systems as the disulphide constituent immediately reacted with the gold core, shown by a release of pyridine-2-thione upon addition to the nanoparticles.

Due to this, the maleimide analogue 1-(2-aminoethyl)maleimide hydrochloride (**Figure 3.17, 3.11**) was selected as a thiol reactive coupling moiety. The amine functionality of this molecule allows for the use of EDC/NHS chemistry to attach the maleimide to the nanoparticles.

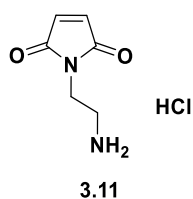


Figure 3.17: The structure of 1-(2-aminoethyl)maleimide hydrochloride

Once the maleimide was conjugated to the PEG shell of the nanoparticles through EDC/NHS, giving mal-C11Pc-PEG-AuNPs, **3.12**, anti-EGFR antibody was stirred overnight with nanoparticles, allowing for the reaction of free thiols with the maleimide present, yielding anti-EGFR-mal-C11Pc-PEG-AuNPs (**3.13**). These AuNPs were

purified through Vivapsin 500 columns and the removal of antibody was tracked using UV-vis spectroscopy. **Figure 3.18** shows the sequential washings of **3.13** and the UV-vis spectrum of the purified AuNPs. Again, this spectrum cannot be used to confirm the conjugation of the antibody, and this will be discussed in **section 3.3.2**.

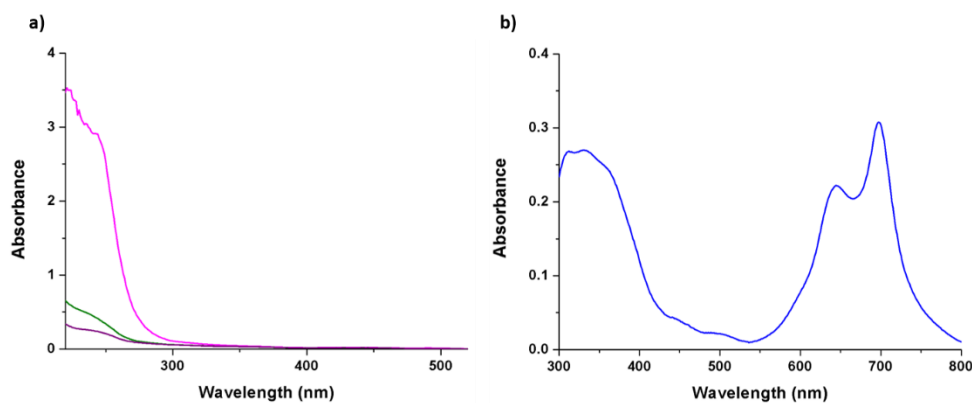


Figure 3.18: **a)** UV-vis spectra of sequential washings collected and **b)** the UV-vis spectrum of **3.13** in PBS buffer

As the presence of free thiols on the surface of antibodies is generally unlikely due to their preference at slightly basic pHs to form disulphides, the antibody was treated with TCEP prior to conjugation to partially reduce the disulphide bonds. It has been found that the addition of 2.75 equivalents of TCEP to an IgG antibody results in the reduction of two interchain disulphides,¹⁶ therefore 1.2 equivalents were used to aim to reduce one disulphide to keep the conjugation as site specific as possible. The antibody was incubated with TCEP for 30 minutes, purified using Zeba spin desalting columns and immediately added to a solution of mal-C11Pc-PEG-AuNPs (**3.12**) to prevent re-oxidation of these thiols. This reaction was left to proceed overnight, then any unconjugated antibody was removed from the solution using Vivapsin 500 columns. Again, the removal of unconjugated antibody was tracked using UV-vis spectroscopy (**Figure 3.19a**), and after three PBS washes the resulting anti-EGFR-mal-C11Pc-PEG-AuNPs synthesised with a reduced disulphide (**3.14**) were resuspended in PBS and the UV-vis spectrum recorded (**Figure 3.19b**).

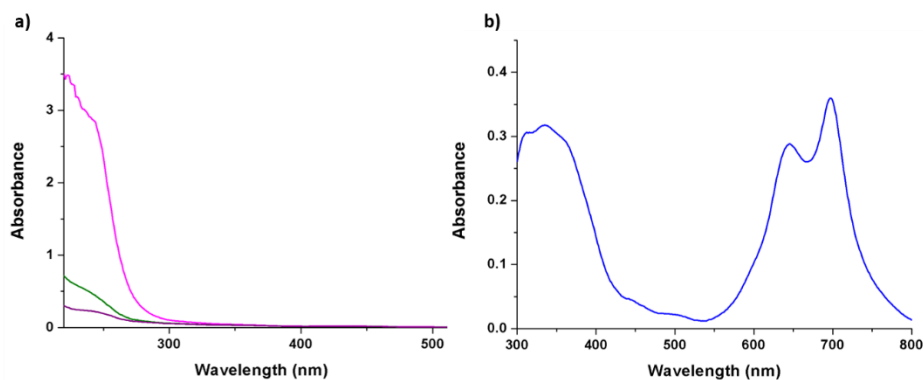


Figure 3.19: a) UV-vis spectra of sequential washings collected from the TCEP reduction-maleimide functionalisation of C11Pc-PEG-AuNPs with EGFR Ab and b) the UV-vis spectrum of **3.14**

3.3.2 Determination of antibody functionalisation

To determine whether the antibody conjugation methods described in **section 3.3.1** had worked, sodium dodecyl sulphate polyacrylamide gel electrophoresis (SDS-PAGE) was used.⁵⁷ This technique allows for the separation of proteins by their molecular weight using an electrical current through a polyacrylamide gel. Smaller proteins are able to move faster through the gel and therefore separation occurs. Samples are mixed with the denaturant sodium dodecyl sulphate (SDS) which disrupts the tertiary structure of the antibody, and a reductant such as dithiothreitol (DTT) is added to reduce the disulphides within the antibody, dissociating the heavy and light chains, allowing them to run separately. The light chain of an antibody has an average molecular weight of 25 kDa and the heavy chain and average molecular weight of 50 kDa. The addition of a reductant to the nanoparticle systems will allow the breakdown of the antibody disulphides, releasing the chains of the antibody that are not covalently bound to the nanoparticle. The antibody chain that has been covalently bound to the nanoparticle, however, will remain conjugated and therefore display a much higher molecular weight and thus show less movement down the polyacrylamide gel. It is therefore possible to use this technique to determine the selectivity of a conjugation technique towards the different chains of an antibody; if only the heavy chain is conjugated to the nanoparticles, this band should be retarded on the gel and appear at retention equivalent to a much higher molecular mass.

Throughout this work, an anti-EGFR antibody purchased from Abcam has been analysed and conjugated onto C11Pc-PEG-AuNPs to form **3.10**, **3.13** and **3.14**. Here, the conjugation of a second anti-EGFR antibody, produced by R&D systems, was also tested as this antibody has recently been reported to display selective uptake of liposomes by EGFR overexpressing lung cancer cell lines.⁵⁸ This second antibody was conjugated to

C11Pc-PEG-AuNPs through EDC/NHS (**3.15**), a maleimide (**3.16**) and a maleimide after TCEP reduction (**3.17**), as described in **section 3.3.1. 3.10** and **3.13-17** were concentrated (50-fold) in Vivapsin 500 columns, then heated to 100 °C with tris-glycine buffered SDS and DTT. Once the AuNP solutions had cooled, the samples were loaded onto a 4-12% polyacrylamide gel in 3-(*N*-morpholino)propanesulphonic acid (MOPS) SDS running buffer, alongside a molecular weight ladder. Controls of C11Pc-PEG-AuNPs and both antibodies were also treated with SDS and DTT and loaded onto the gel. The gel was run at 170 V for 75 min, then stained with Coomassie Blue which binds electrostatically to positive residues within proteins. A de-staining solution was used to remove excess dye from the gel and dark blue bands remained where protein was present. **Figure 3.20** shows the resulting gel. The control of C11Pc-PEG-AuNPs (lane 2) shows a light blue streak due to the phthalocyanine, and this streak is present in each lane containing nanoparticles. The control antibody lanes (3 and 7) show two bands, one at approximately 25 kDa corresponding to the light chain of the antibody, and one at approximately 50 kDa corresponding to the heavy chain. In the case of the Abcam antibody, for each conjugation technique a faint band could be observed between 115 and 140 kDa (lanes 4-6) which was not present for the free antibody (lane 3). This suggests that conjugation to the nanoparticles has occurred as a small amount of antibody shows a significant increase in molecular weight. Lanes 4-6 also display bands corresponding to the light and heavy chain of the control Abcam antibody. These bands are due to the fragmented antibody, but the relatively strong colour of these compared to the nanoparticle-conjugated band suggests that there may also be some unconjugated antibody remaining in these samples. Interestingly, the R&D antibody shows the expected light and heavy chains for the free antibody (lane 7), but no bands are observed for any of the conjugated samples, suggesting these conjugations were either less successful than that with Abcam antibody or unsuccessful.

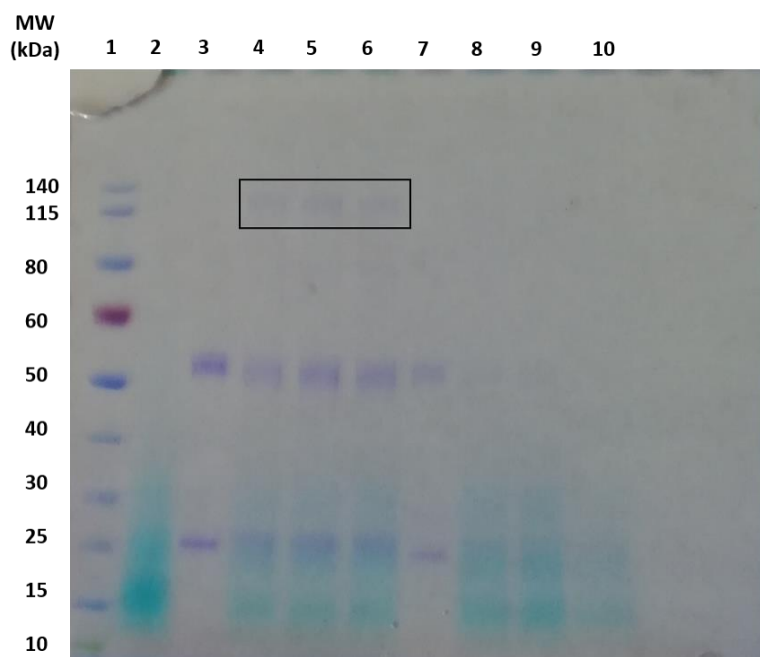


Figure 3.20: SDS-PAGE gel of antibody-functionalised AuNPs. Lane 1: MW ladder, 2: C11Pc-PEG-AuNPs, 3: Abcam antibody reference, 4: 3.10, 5: 3.13 6: 3.14, 7: R&D antibody reference, 8: 3.15, 9: 3.16 and 10: 3.17. Highlighted on lanes 4-6 is the faint band of high molecular weight corresponding to antibody conjugated to AuNPs

3.3.3 Antibody binding to EGFR receptors

The Abcam anti-EGFR antibody was used in **chapter 2** to confirm the presence of EGFR on A549 cells and therefore is known to bind to the receptor. The ability of the antibody purchased from R&D systems to bind to the EGFR was tested using flow cytometry, as described in **section 2.3.2**. A549 and H292 cells, which are known to overexpress EGFR, were incubated on ice alongside the R&D antibody and BSA for one hour, then excess antibody was washed off. A FITC-tagged secondary antibody was then incubated with these cells on ice for a further hour and then washed off. Control cells were treated with BSA then the secondary antibody to account for any non-specific interactions between the secondary antibodies and the cells. The Abcam antibody was also tested against A549 (as in **section 2.3.2**) and H292 cells in this same manner. The flow cytometry data indicated that the Abcam antibody displayed binding to EGFR on both A549 and H292 cells, whereas the R&D antibody did not bind to the receptor, as no shift in fluorescence intensity is observed for the cells incubated alongside the antibody as compared to the control, as seen in **Figure 3.21**. This, alongside the weak binding of the antibody to nanoparticles, meant the R&D Systems antibody was not used any further in this work, and all the following results were collected using the Abcam anti-EGFR antibody.

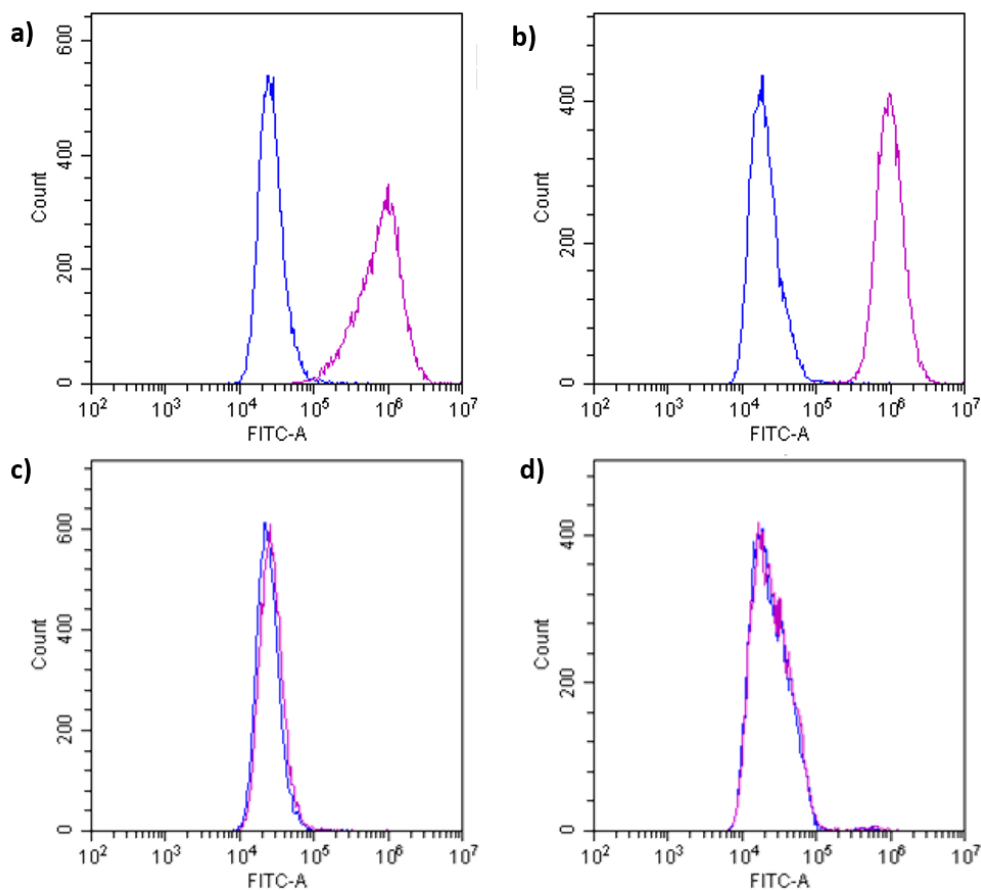


Figure 3.21: Flow cytometry histograms of *a*) A549 and *b*) H292 cells treated with goat anti-mouse FITC secondary antibody (blue) or Abcam anti-EGFR antibody & goat anti-mouse FITC secondary antibody (purple). *c*) A549 and *d*) H292 cells treated with goat anti-mouse FITC secondary antibody (blue) or R&D anti-EGFR antibody & goat anti-mouse FITC secondary antibody (purple)

3.3.4 Analysis of the singlet oxygen production of the anti-EGFR antibody conjugates

Once the conjugation of antibody to **3.10**, **3.13**, and **3.14** was confirmed, these nanoparticles were tested for their ability to produce singlet oxygen. The nanoparticles were suspended in PBS, mixed with the singlet oxygen probe ABMA and irradiated for 30 minutes at 633 nm, with fluorescence spectra recorded every five minutes. As seen in **Figure 3.22**, **3.10**, **3.13**, and **3.14** all displayed singlet oxygen production. The singlet oxygen production of these antibody functionalised AuNPs showed a slight decrease compared to that of the unconjugated C11Pc-PEG-AuNPs. This is likely because of the presence of tryptophan, methionine and histidine residues on the antibody which are known singlet oxygen quenchers.^{59–61}

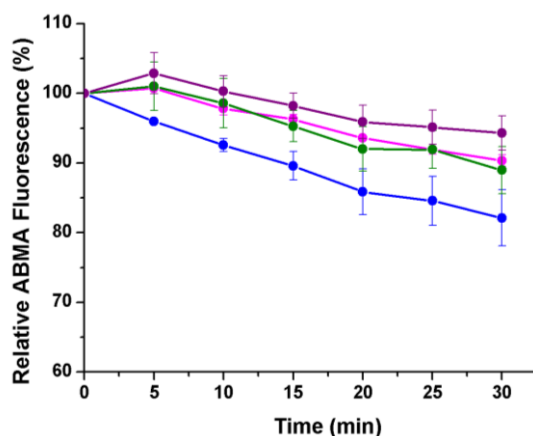


Figure 3.22: Singlet oxygen production of C11Pc-PEG-AuNPs (blue), **3.10** (pink), **3.13** (green) and **3.14** (purple) irradiated with 1 μ M ABMA. All spectra recorded in PBS at 1 μ M C11Pc

3.3.5 Phototoxicity of antibody conjugated C11Pc-PEG-AuNPs

Once the ability of these nanoconjugates to produce singlet oxygen was confirmed, they were tested for their phototoxicity in EGFR overexpressing lung cancer cells. As EDC/NHS is the most established conjugation strategy for antibody addition to AuNPs, **3.10** were tested first to provide a reference point for comparison of these conjugation methods. **3.10** were incubated with A549 cells for three hours in serum free RPMI. After incubation, the cells were washed three times with PBS, then complete RPMI was added to each well. The cells were then irradiated for 6 minutes per well with a 633 nm HeNe laser placed 50 cm above the wells. A second plate was prepared in the same way but not irradiated to account for any dark toxicity. The cells were incubated for a further 48 hours, before an MTS assay was used to determine the cell viability. Staurosporine was used as a positive control for cell death, as described in **section 2.3.3.1**. While no dark toxicity was observed for these conjugates, unfortunately no phototoxicity was observed for **3.10** at or below 200 nM, as shown in **Figure 3.23a**. **3.10** were tested at concentrations as high as 1.4 μ M without any phototoxicity observed, and an increase in irradiation time from six to eight minutes per well was not seen to have any effect on the cell viability (**Figure 3.23b**).

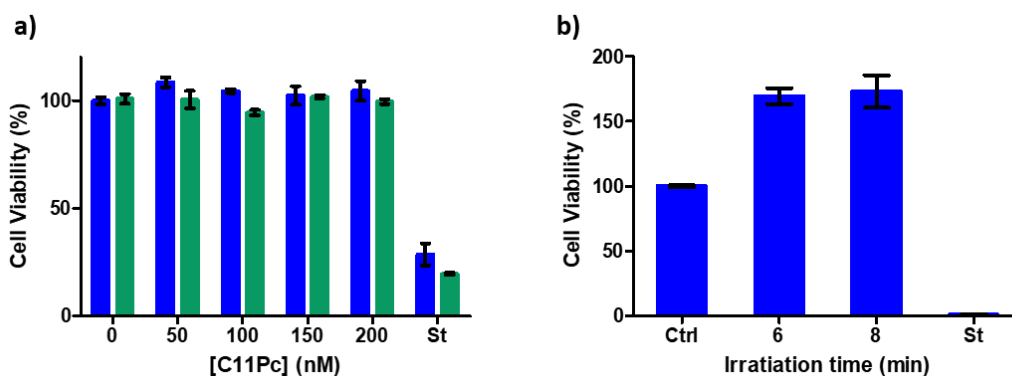


Figure 3.23: **a)** cell viability of A549 cells incubated with **3.10** for three hours then non-irradiated (blue) or irradiated at 633 nm for 6 min (green) and **b)** cell viability of A549 cells after incubation with 1.41 μM **3.10** for three hours and irradiation for either six or eight minutes with a 633 nm laser. Ctrl = non-treated A549 cells irradiated for six minutes at 633 nm

As no cell death was observed in A549 cells, **3.10** were also tested in the H292 cell line to determine whether this lack of phototoxicity was cell-line dependent. **3.10** were incubated with H292 cells for three hours in serum-free RPMI, then cells were irradiated for six minutes with the laser placed 50 cm above the well, but no phototoxicity was observed. Overnight incubation of **3.10** with H292 cells in serum-free RPMI and increased light fluence rates were tested to attempt to induce a phototoxic response but no decrease in cell viability was observed under any of these conditions. **3.13** and **3.14** were also incubated with A549 and H292 cells for three hours before irradiation for six minutes per well. Again, no phototoxicity was observed for these conjugates, suggesting that the less random conjugation of the anti-EGFR antibody through thiols has not improved the targeting ability of these conjugates.

3.3.6 Determination of antibody binding post conjugation

So far, the ability of the Abcam anti-EGFR antibody to bind to the EGFR has been confirmed and the conjugation of this antibody to C11Pc-PEG-AuNPs through various conjugation techniques has been proven successful. As each of these conjugates has been shown to produce singlet oxygen, the next step was to confirm that these conjugation techniques have not destroyed the binding ability of the antibody due to the lack of regioselectivity of the reactions. To determine if the activity of the antibodies was maintained, FITC-PEG-AuNPs (**2.31**) were synthesised with a 50:50 ratio of FITC-PEG:PEG, as described in **section 2.3.2.2**. These nanocarriers were functionalised with anti-EGFR antibody through EDC/NHS, a maleimide and through partial reduction

with TCEP before reaction with a maleimide, as described in **section 3.3.1**. A549 cells were incubated with these nanoconjugates for three hours alongside control **2.31**. After washing to remove any unbound nanoparticles, the cells were imaged using a fluorescent microscope. For each sample and the control of **2.31**, no fluorescence could be observed suggesting these nanocarriers were not binding to the EGFR on the surface of A549 cells. As evidence suggests the antibody is binding to the nanoparticles, and the antibody has activity before functionalisation, it is likely that the non-regioselective conjugation to this anti-EGFR antibody is affecting the activity of the antibody, rendering the resulting conjugates inactive towards the EGFR receptor. Antibody conjugation can affect the charge of an antibody, which in turn can affect the pharmacokinetics, stability and solubility.⁶² It is also possible that the formation of the conjugate occurs within the Fab region of the antibody, blocking the activity, or that the act of conjugation distorts the shape of the antibody, changing the shape of the recognition sites and destroying the antibody specificity. The possibility of the nanoparticle binding in the Fab region can be addressed by using site-specific conjugation which only allows conjugation to the Fc region of the antibody.

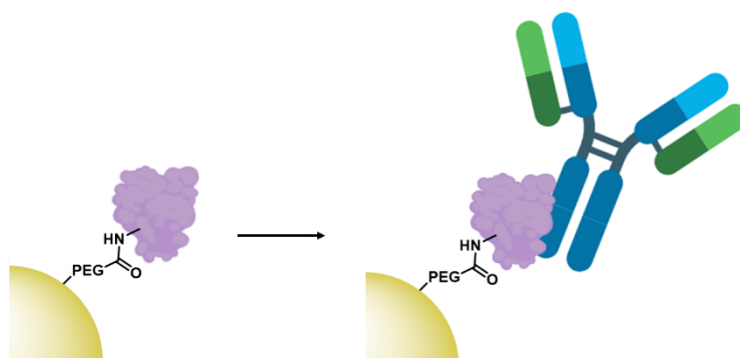
3.3.7 Site-Specific antibody conjugation – using the Fc region

While the addition of antibodies through a maleimide is more specific than the use of EDC/NHS chemistry, this chemistry is still non-regioselective and presents the same issue of lack of control over the region of the antibody that binds to the nanoparticle. The use of Fc binding proteins, as described in **section 3.1.4.2**, provides an opportunity for selective conjugation of antibodies through the constant region of antibodies, guaranteeing the antigen binding region of antibody remains free for receptor recognition.

3.3.7.1 Protein G for site specific antibody conjugation

For this work, an anti-HER2 antibody was selected as previous work by Russell and co-workers has shown selective photodynamic therapy with this antibody.^{51,56,63} While HER2 is only overexpressed in a small number of non-small cell lung cancer cases (*ca.* 15%),^{64,65} the use of this anti-HER2 antibody allows for a proof of concept study that can be applied to more disease-relevant antibodies at a later date. The HER2 antibody in this study is a rat IgG2a antibody to which protein A displays no affinity,^{66,67} and therefore protein G was investigated for antibody conjugation. Initially, protein G was conjugated onto *ca.* 4

nm PEG-AuNPs through EDC/NHS chemistry as described in **section 3.3.1.1**, giving protein G-PEG-AuNPs (**3.19**). Again, this chemistry is non-regioselective and so it is hoped that the addition of protein G to these nanoparticles does not occur in the active site, allowing for further addition of an antibody. After addition of protein G, two methods were explored for the addition of antibody. Firstly, the antibody was non-covalently bound to protein G. **3.19** were incubated with the anti-HER2 antibody in PBS (pH 7.4) for one hour, then purified by centrifugation in Vivaspin columns to remove any unconjugated antibody, giving anti-HER2-proteinG-PEG-AuNPs (**3.20**, **Scheme 3.5**).



Scheme 3.5: Non-covalent association of AuNP-bound protein G with an anti-HER2 IgG antibody, giving **3.20**

While the affinity of protein G for IgG2a antibodies should allow for the complexation of the antibody to protein G *via* the Fc region, the lack of covalent bond raises questions about the specificity of this nanoconstruct. It is possible that the anti-HER2 antibody may dissociate from protein G *in vivo*, allowing for other antibodies to conjugate to these nanocarriers and lead to targeting of unwanted receptors with these nanoparticles.

To remove the possibility of the antibody dissociating from protein G *in vivo*, covalent conjugation of the antibody to protein G was attempted. Here, the cross-linker dimethyl pimelimidate dihydrochloride (DMP, **Figure 3.24**) was utilised.

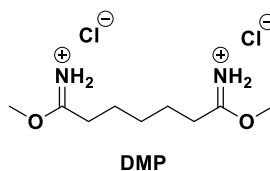
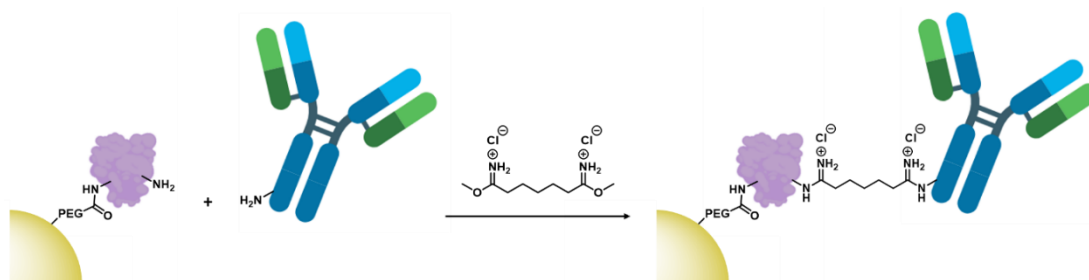


Figure 3.24: The structure of dimethyl pimelimidate dihydrochloride (DMP)

DMP has been used to cross-link antibodies to protein G immobilised on magnetic beads for the purification of antibodies,^{68,69} and therefore it is known that this cross-linker can be utilised to covalently bind protein G to an antibody. Protein G conjugated AuNPs, **3.19**, were incubated with anti-HER2 antibody in PBS (pH 7.4) for one hour to allow for the protein G to complex with the antibody. These AuNPs were then centrifuged in Vivaspin 500 columns to remove any non-bound antibody, and the AuNP pellet resuspended in triethanolamine buffer (pH 8.2) containing DMP. This approach utilises the non-covalent interactions between protein G and the antibody to hold the antibody in the desired conformation, before the cross-linking agent is added to solution, forming covalent bonds between the two molecules, as shown in **Scheme 3.6**. After 45 minutes, the nanoparticles were again centrifuged in Vivaspin 500 columns to remove any excess DMP, then resuspended in ethanolamine buffer (pH 8.2). The ethanolamine acts to cap any partially reacted DMP conjugated to either the antibody or protein G, removing this highly reactive group that could conjugate to biomolecules *in vivo*. These cross-linked nanoparticles, anti-HER2-DMP-proteinG-PEG-AuNPs (**3.21**), were again purified and resuspended in PBS.



Scheme 3.6: Cross-linking of AuNP-bound protein G and an anti-HER2 IgG antibody with DMP

SDS-PAGE was used to assess the outcome of these conjugation experiments. Samples of **3.19**, **3.20** and **3.21** were prepared for SDS-PAGE as described in **section 3.3.2**. Controls of anti-HER2 antibody, PEG-AuNPs and protein G were also prepared by heating to 100 °C with tris-glycine SDS and DTT. The SDS-PAGE was run at 170 V for 75 minutes in MOPS SDS running buffer, then stained with Coomassie blue to mark the protein bands on the gel. The resulting gel is shown in **Figure 3.25**. The control PEG-AuNPs (lane 7), as expected, shows no protein content but this lane shows a brown smudge at the top of the gel due to the high concentration of AuNPs. The protein G control (lane 8) shows a strong band between 25 and 30 kDa. **3.19** (lane 6) also displayed this band and a brown smudge due to AuNPs but shows no protein band at a significantly

higher molecular weight. The blue smear in lane 6 may be indicative of some conjugation of protein G to the AuNPs, but the strong band at *ca.* 27 kDa is likely to be due to the presence of non-conjugated protein G.

Interestingly, while the HER2 antibody (lane 4) shows the expected light and heavy chains at *ca.* 25 and 50 kDa, it also shows a third band at *ca.* 12 kDa which may indicate this antibody is contaminated. **3.20** (lane 3) shows the antibody bands but no protein G band and **3.21** (lane 2) unfortunately did not stain for any protein. It is possible that these samples were not concentrated enough to stain for protein on the gel and the bands observed in lane 3 are due to unconjugated antibody that has not been fully removed from the solution. The lack of AuNP smudge at the top of lanes 2 and 3 also support the theory that much less sample has been loaded into these lanes. To further assess whether these conjugations have been successful, these experiments need to be repeated with a much higher concentration of AuNPs loaded onto the gel.

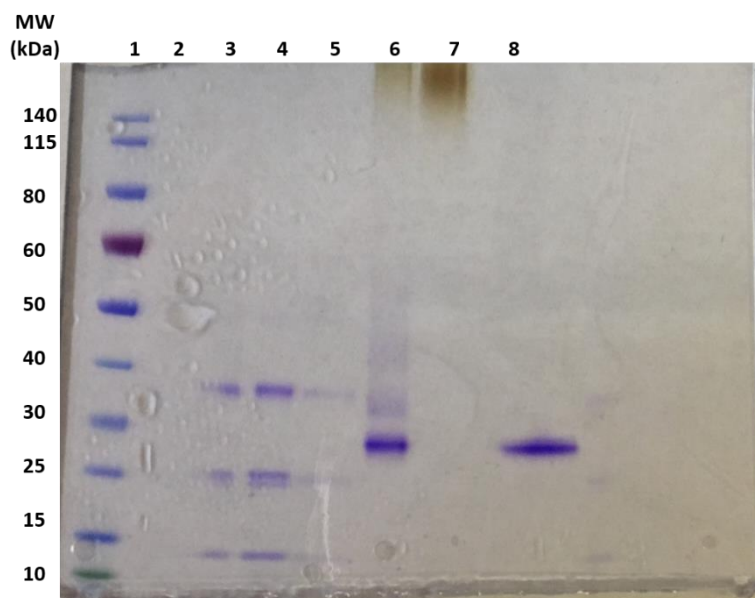


Figure 3.25: SDS-PAGE gel: lane 1: MW marker (kDa), 2: **3.21**, 3: **3.20**, 4: HER2 Ab, 5: HER2 Ab, 6: **3.19**, 7: PEG-AuNPs, 8: protein G

While protein G provides a method for specifically binding the Fc region of antibodies, this protein is still relatively complex and provides multiple conjugation sites for its addition to AuNPs. The addition of protein G still depends on random amide bond formation through EDC/NHS and therefore the Fc binding site of protein G may be affected by conjugation onto nanoparticles. It is also possible that protein G may invoke

an immune response *in vivo* as it is a foreign protein isolated from bacteria. Due to these concerns, research has led to the development of peptides that can bind to the Fc region.

3.3.7.2 Peptide mimics of protein A/G – Fc-III

The peptide Fc-III (DCAWHLGELVWC) has been described as an Fc binding cyclic peptide with high affinity towards the Fc region.⁷⁰ In fact, its binding affinity has been shown to be only two-fold lower than that of protein A or G.⁷⁰ It binds to the IgG Fc hinge region with a K_d of 185 nM.⁷¹ This peptide has benefits over protein A or G as it is likely to be non-immunogenic, it is much shorter and simpler to synthesise and it can easily be modified to fit a desired application. Different variations of the Fc-III peptide have been reported, including Fc-III-4c (CDCAWHLGELVWCTC), a double cyclic peptide which forms a tighter binding loop and therefore displays higher affinity towards the Fc region.⁷¹ Most notably, site specific modifications of the Fc-III peptide with the unnatural amino acid *p*-benzoylphenylalanine (Bpa, **Figure 3.26**) have shown that the substitution of the 10th amino acid in Fc-III (valine) to Bpa results in a peptide with high affinity towards the Fc region. The Bpa residue can react with methionine 252 in the constant region of an antibody under UV irradiation to form a covalent bond, thus covalently binding an antibody to its payload while specifically maintaining its conformation, leaving the Fab region free for binding. The diazirine based amino acids ‘photo-Leu’ and ‘photo-Phe’ have also been tested for photo cross-linking to antibodies, but Bpa has been seen to be the most efficient photocrosslinker.⁷²

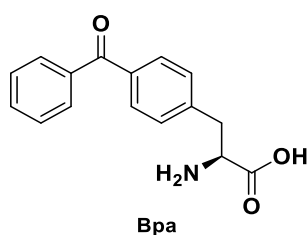


Figure 3.26: The structure of the unnatural amino acid *p*-benzoylphenylalanine (Bpa)

In this work, the peptide Fc-III-Bpa (DCAWHLGELBpaWCT) was further modified with the addition of a glycine linker, providing a spacer between the peptide and the amine terminus that will subsequently be used to conjugate this peptide onto nanoparticles *via* the PEG linker, giving the peptide Gly-Fc-III-Bpa (GDCAWHLGELBpaWCT, **3.22**, **Figure 3.27**). This peptide was synthesised by solid phase peptide synthesis, as described in **section 2.3.1**. The peptide was cleaved from the resin in 92.5:2.5:2.5:2.5

TFA:EDT:TIPS:H₂O. 1,2-ethanedithiol (EDT) was added to the cleavage cocktail to prevent intermolecular disulphide formation, yielding polymers of **3.22**. After cleavage, the peptide was stirred overnight in phosphate buffer, pH 8.0 at 35 °C to oxidise the cysteine residues and form the intramolecular disulphide. The peptide was highly diluted in phosphate buffer to prevent the formation of intermolecular disulphides. After the cyclisation of **3.22**, the peptide was purified by preparative RP-HPLC and its synthesis confirmed by MALDI-ToF.

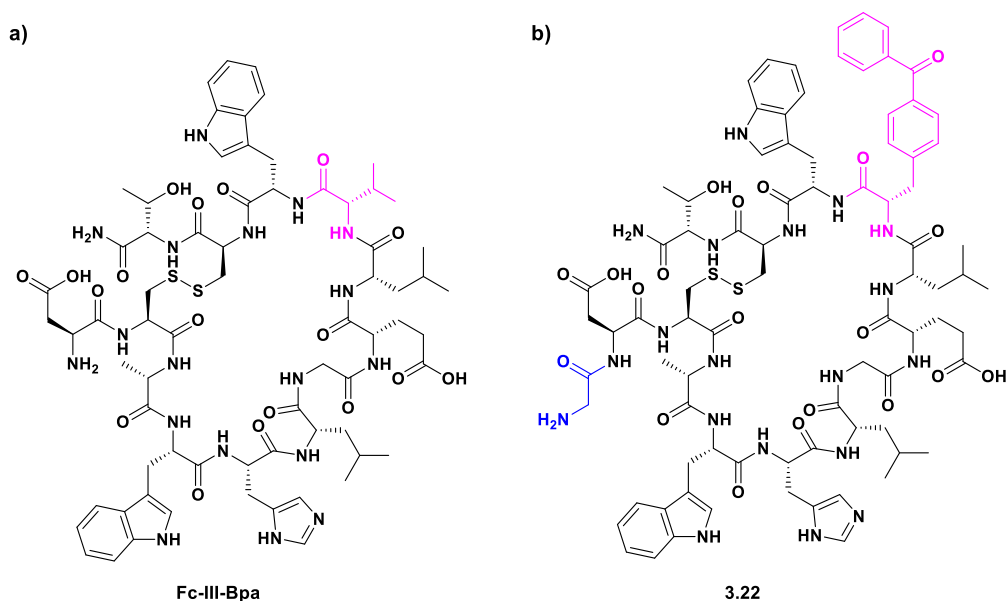


Figure 3.27: The structures of a) Fc-III-Bpa and b) **3.22** with valine substituted for Bpa in the 10th position (pink) and the addition of glycine as a linker (blue)

To attach **3.22** to the anti-EGFR IgG antibody used throughout this work, the peptide and antibody were mixed together in a 10:1 ratio in PBS buffer before irradiation for four hours using a Spot Lite SCL2-6 UV wand, then conjugation was investigated using SDS-PAGE. A sample of unconjugated antibody was run as a control and compared to that of the irradiated sample. Unfortunately, no shift in mass was observed for either the light or heavy chains of the antibody. However, it is possible that the mass of the peptide would not result in an obvious increase in mass as 1.7 kDa is not a huge difference in protein mass compared to a heavy chain of 50 kDa. To further analyse the ability of **2** to bind the anti-EGFR antibody used in this work, a FITC-tagged derivative of **3.22** (FITC- β ADCAWHLGELBpaWCT, **3.23**, **Figure 3.28**) was synthesised.

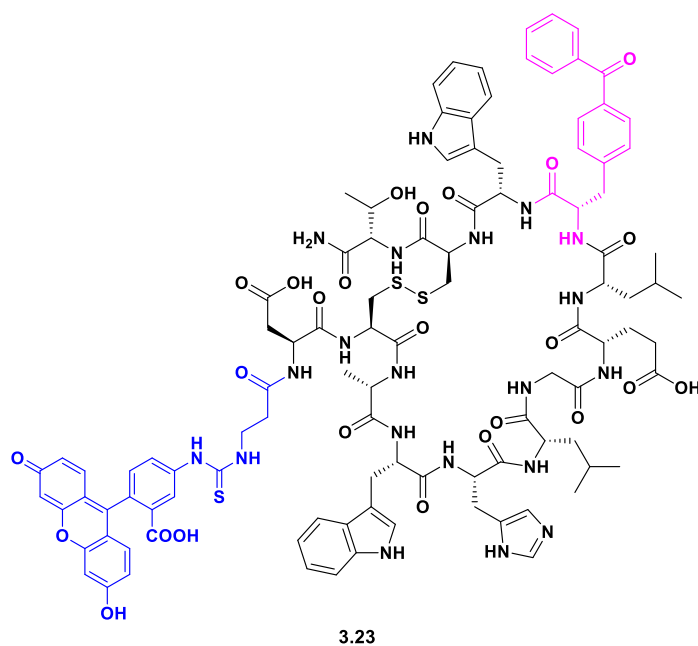


Figure 3.28: The structure of FITC- β ADCAWHLGELBpaWCT (3.23)

The fluorescence of this peptide could be used to determine whether it has been conjugated onto the antibody. **3.23** was mixed with the anti-EGFR antibody and irradiated for four hours in PBS. A second sample was irradiated for four hours in 20 mM histidine acetate buffer (pH 5.4) to determine the effect of pH on this addition. 5-hydroxyindole was added to both reaction mixtures as it is known to protect antibodies from UV damage.⁷² A sample of each of these reaction mixtures was taken after two hours to track the reaction. After four hours of irradiation, samples were collected, precipitated in cold acetone and the pellet resuspended in PBS to concentrate the samples. SDS-PAGE of the resulting antibody samples was run at 200 V for 40 minutes. Control samples of the anti-EGFR antibody and a FITC-goat anti-mouse secondary antibody were also run. The FITC-tagged secondary antibody acted as a control for fluorescence and the anti-EGFR antibody was used to compare the relative weights of the antibody chains. The resulting gel was imaged for fluorescence, as shown in **Figure 3.29a**. As expected, the control FITC-secondary antibody displayed strong fluorescence (lane 3). Lanes 4-7, those containing irradiated antibody-**3.23** mixtures, all showed a strong fluorescent band at the very bottom of the gel due to unconjugated peptide. Faint fluorescent bands could be observed in lane 7 (4 h irradiation in PBS) which, while present for both the light and heavy chains, could indicate some peptide conjugation to the antibody. The gel was then stained for protein using Coomassie blue, **Figure 3.29b**. The

fluorescent bands observed under irradiation were seen to align with the antibody bands stained with Coomassie blue. Unfortunately, the control anti-EGFR antibody (lane 2) did not stain for antibody bands and therefore this experiment would need repeating to assess whether any visible shift in heavy chain mass has occurred due to the possible conjugation of **3.23**. The fluorescence of these bands is also very weak, so a higher concentration of antibody is needed to fully determine whether these bands are artefacts or conjugated antibody. Techniques such as LCMS may allow for further analysis of whether this peptide has indeed conjugated onto the antibody and allow for a drug-to-peptide ratio to be calculated. It would also be important to analyse whether this conjugation is specific to the heavy chain as desired or if this Bpa UV cross-linking is in fact somewhat unspecific.

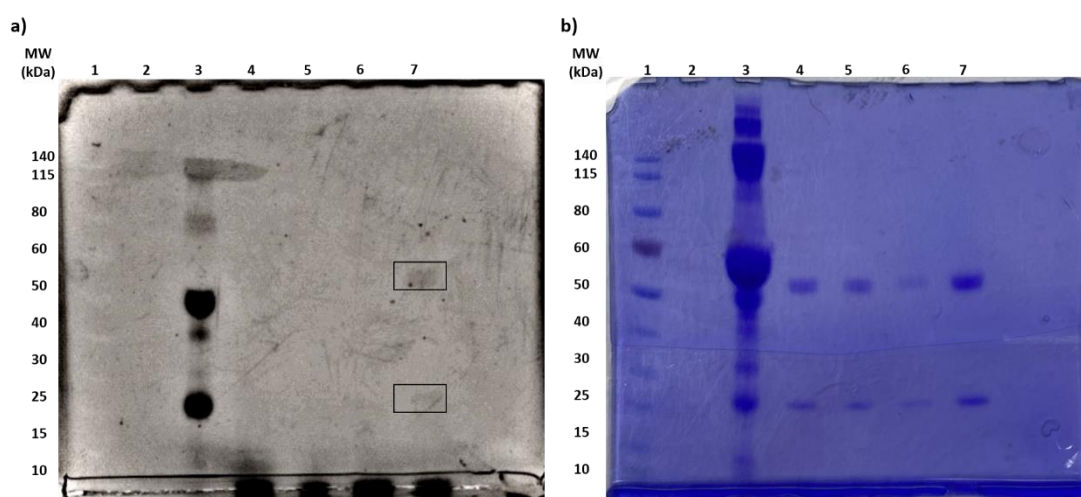


Figure 3.29: SDS-PAGE of antibody functionalisation with **3.23** **a)** under fluorescent light and **b)** after Coomassie staining. Lane 1: molecular weight marker, 2: anti-EGFR antibody, 3: FITC-goat anti-mouse secondary antibody. Lanes 4-7: antibody irradiated with **3.23** in 4: histidine acetate buffer 2 h, 5: histidine acetate buffer 4 h, 6: PBS 2 h, 7: PBS 4 h. Highlighted on **a)** is the faint fluorescent bands observed in lane 7

3.4 Conclusions and future work

In this chapter, two chemical conjugation strategies for the addition of anti-EGFR antibodies onto gold nanoparticles were explored, with the produced conjugates summarised in **Table 3.2**. As there are currently no validated techniques for assessing the concentration of antibody on the surface of AuNPs, a proof of concept study with fluorescent tags was used to ensure that the conjugation of an antibody to C11Pc-PEG-AuNPs *via* EDC/NHS chemistry would be successful. Once confirmed, two anti-EGFR antibodies were conjugated onto AuNPs using this method to give **3.10** and **3.15**. These antibodies were also conjugated onto gold nanoparticles through thiol-maleimide

chemistry. Initially, C11Pc-PEG-AuNPs were conjugated with a maleimide, then mixed with the antibodies to allow for the conjugation of any free thiols on the antibody surface, giving **3.13** and **3.16**. The reduction of disulphides for the addition of these antibodies was also trialled using TCEP. 1.2 equivalents of TCEP were used to attempt to reduce just one disulphide in these antibodies, before the resulting reduced antibodies were incubated with mal-C11Pc-PEG-AuNPs, giving **3.14** and **3.17**. The conjugation of these antibodies was assessed using SDS-PAGE, then their ability to bind to the EGFR receptor assessed using flow cytometry. **3.10**, **3.13** and **3.14** were seen to show antibody conjugated to their surface and the Abcam antibody used to synthesise these nanoconjugates was seen to bind to the EGFR receptor. **3.10**, **3.13** and **3.14** all showed significant singlet oxygen production but disappointingly no phototoxicity *in vitro*.

Table 3.2: Summary of the antibody conjugation techniques trialled and the activity of the produced nanoconjugates

Conjugation type	Coupling mechanism	Antibody	Confirmation of conjugation to AuNPs	Photodynamic activity
Random amide bond	EDC/NHS	Anti-EGFR	Yes	No
Random thio-ether	Maleimide	Anti-EGFR	Yes	No
Hinge region thio-ether	Disulphide reduction & maleimide	Anti-EGFR	Yes	No
Site-specific	Protein G non-covalent	Anti-HER2	No	-
Site-specific	Protein G covalent	Anti-HER2	No	-
Site-specific	Gly-Fc-III-Bpa (3.22)	Anti-EGFR	-	-
Site-specific	FITC-Fc-III-Bpa (3.23)	Anti-EGFR	-	-

Fluorescent microscopy images suggested that these nanoconjugates were not being internalised by cells, suggesting that the conjugation of the antibody was affecting its affinity for EGFR. Assessment of whether this antibody is being internalised by A549 cells both before and after conjugation with smaller systems such as dyes may shed some light on why these nanocarriers do not appear to be internalised. The investigation of different anti-EGFR antibodies may allow for the synthesis of anti-EGFR antibody-

conjugated C11Pc-PEG-AuNPs that display phototoxicity in non-small cell lung cancer cell lines and allow for the comparison of the conjugation techniques tested in this study.

This chapter also explored the use of protein G and its peptide mimic Fc-III-Bpa to site-specifically conjugate antibodies to nanoparticles, as summarised in **Table 3.2**. Protein G was conjugated onto *ca.* 4 nm PEG-AuNPs through EDC/NHS amide bond formation, then mixed with an anti-HER2 antibody to allow for non-covalent bonding. To attempt to form a covalent bond between protein G and the antibody, the cross-linking agent dimethyl pimelimidate dihydrochloride (DMP) was utilised. SDS-PAGE unfortunately showed no evidence of antibody conjugation in this method. As protein G is a complex molecule that may induce an immune response, the peptide mimic Fc-III-Bpa was investigated. This peptide allows for the site-specific conjugation of the peptide onto a nanoparticle, and Bpa can be used to cross-link to a methionine residue in the Fc region of IgG antibodies under UV irradiation. The addition of a FITC-tag to this sequence (**3.23**) allowed for the visualisation of a small amount of conjugation between the peptide and the antibody using SDS-PAGE, but both the light and heavy chain of the antibody showed fluorescence, raising questions about the selectivity of this technique. Further studies with mass spectroscopy would confirm whether this fluorescence observed for the light band is an artefact or indeed the addition of the Fc peptide non-specifically. Once this is confirmed and the Bpa conjugation optimised, **3.22** can be conjugated onto AuNPs through the glycine linker, conjugated to an antibody, and the phototoxicity of these conjugates analysed.

While Fc-III-Bpa has been shown to cross-link to antibodies under UV light, there has recently been two reports of site-specific antibody conjugation through the Fc region using other chemical modifications which do not require external stimulation to cross-link. The first of these site-specifically altered the B domain of protein A with the non-canonical amino acid 4-fluorophenyl carbamate lysine (FPheK, **Figure 3.30a**). They found that the substitution of Glu25 with FPheK allowed for cross-linking to Lys337 on IgG antibodies with efficiencies above 95%.⁷³ While the large size of this B domain makes it undesirable for antibody conjugation, the binding site of this B domain is characterised, so it may be possible to build a peptide based on this to bind the Fc region of an antibody through FPheK with high efficiency. The second reported chemical conjugation involves the use of a cyclic Fc binding peptide GPDCAYHRGELVWCTFH. It has been found that the side chain of the arginine in this sequence points towards Lys248 in the Fc region of IgG antibodies, and the mutation of this arginine to a lysine allows for the addition of

the cross-linking agent disuccinimidyl glutarate, giving Lys-glutarate-succinimide (**Figure 3.30b**). This cross-linker has been shown to specifically cross-link to Lys248 within 15 minutes.⁷⁴ Both of these cross-linking techniques may yield the desired conjugated IgG antibody more efficiently than the Fc-III-Bpa peptide and may be worth exploring.

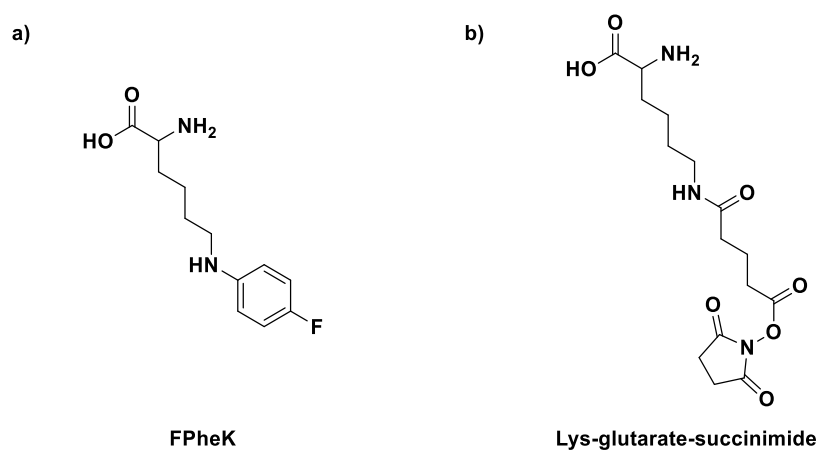


Figure 3.30: The structure of **a)** FPheK and **b)** Lys-glutarate-succinimide for cross-linking to the Fc region of IgG antibodies

The work presented in this chapter shows that antibodies can be conjugated onto AuNPs through both EDC/NHS and maleimide-thiol chemistries, and with the right antibody a comparison between these conjugation techniques can be drawn. It also demonstrates the applicability of a methodology for selectively binding antibodies to AuNPs through the Fc region, despite the need for perfecting this conjugation technique. As the Fc region is conserved in all IgG antibodies, this means that this conjugation technique can produce a universal methodology for the selective attachment of any IgG antibody to AuNPs.

3.5 References

- (1) Lipman, N. S.; Jackson, L. R.; Trudel, L. J.; Weis-Garcia, F. Monoclonal Versus Polyclonal Antibodies: Distinguishing Characteristics, Applications, and Information Resources. *ILAR J.* **2005**, *46* (3), 258–268.
- (2) Janeway, C. A.; Travers, P.; Walport, M.; Shlomchik, M. J. *Immunobiology: The Immune System in Health and Disease*, 5th ed.; Garland Science: New York, 2001.
- (3) Sivaram, A. J.; Wardiana, A.; Howard, C. B.; Mahler, S. M.; Thurecht, K. J. Recent Advances in the Generation of Antibody-Nanomaterial Conjugates. *Adv. Healthc. Mater.* **2018**, *7*, 1700607.
- (4) Jazayeri, M. H.; Amani, H.; Pourfatollah, A. A.; Pazoki-Toroudi, H.; Sedighimoghaddam, B. Various Methods of Gold Nanoparticles (GNPs)

- Conjugation to Antibodies. *Sens. Bio-Sensing Res.* **2016**, *9*, 17–22.
- (5) Turkevich, J.; Stevenson, P. C.; Hillier, J. A Study of the Nucleation and Growth Processed in the Synthesis of Colloidal Gold. *J. Discuss. Faraday Soc.* **1951**, *11*, 55–75.
- (6) Rayavarapu, R. G.; Petersen, W.; Ungureanu, C.; Post, J. N.; van Leeuwen, T. G.; Manohar, S. Synthesis and Bioconjugation of Gold Nanoparticles as Potential Molecular Probes for Light-Based Imaging Techniques. *Int. J. Biomed. Imaging* **2007**, *2007*, 29817.
- (7) El-Sayed, I. H.; Huang, X.; El-Sayed, M. A. Selective Laser Photo-Thermal Therapy of Epithelial Carcinoma Using Anti-EGFR Antibody Conjugated Gold Nanoparticles. *Cancer Lett.* **2006**, *239* (1), 129–135.
- (8) Sapsford, K. E.; Algar, W. R.; Berti, L.; Gemmill, K. B.; Casey, B. J.; Oh, E.; Stewart, M. H.; Medintz, I. L. Functionalizing Nanoparticles with Biological Molecules: Developing Chemistries That Facilitate Nanotechnology. *Chem. Rev.* **2013**, *113*, 1904–2074.
- (9) Bauminger, S.; Wilchek, M. The Use of Carbodiimides in the Preparation of Immunizing Conjugates. *Methods Enzymol.* **1980**, *70*, 151–159.
- (10) Grabarek, Z.; Gergely, J. Zero-Length Crosslinking Procedure with the Use of Active Esters. *Anal. Biochem.* **1990**, *185* (1), 131–135.
- (11) Thorek, D. L. J.; Elias, R.; Tsourkas, A. Comparative Analysis of Nanoparticle-Antibody Conjugations: Carbodiimide Versus Click Chemistry. *Mol. Imaging* **2009**, *8* (4), 221–229.
- (12) Chari, R. V. J. Targeted Cancer Therapy: Conferring Specificity to Cytotoxic Drugs. *Acc. Chem. Res.* **2007**, *41* (1), 98–107.
- (13) Kocbek, P.; Obermajer, N.; Cegnar, M.; Kos, J.; Kristl, J. Targeting Cancer Cells Using PLGA Nanoparticles Surface Modified with Monoclonal Antibody. *J. Control. Release* **2007**, *120*, 18–26.
- (14) Pu, Y.; Chen, Y.; Nguyen, T.; Xu, C. F.; Zang, L.; Susic, Z.; Carlage, T. Application of a Label-Free and Domain-Specific Free Thiol Method in Monoclonal Antibody Characterization. *J. Chromatogr. B Anal. Technol. Biomed. Life Sci.* **2019**, *1114–1115*, 93–99.
- (15) Liu, H.; Chumsae, C.; Gaza-Bulseco, G.; Hurkmans, K.; Radziejewski, C. H. Ranking the Susceptibility of Disulfide Bonds in Human IgG1 Antibodies by Reduction, Differential Alkylation, and LC–MS Analysis. *Anal. Chem.* **2010**, *82* (12), 5219–5226.
- (16) Sun, M. M. C.; Beam, K. S.; Cervený, C. G.; Hamblett, K. J.; Blackmore, R. S.; Torgov, M. Y.; Handley, F. G. M.; Ihle, N. C.; Senter, P. D.; Alley, S. C. Reduction-Alkylation Strategies for the Modification of Specific Monoclonal Antibody Disulfides. *Bioconjug. Chem.* **2005**, *16* (5), 1282–1290.
- (17) Makaraviciute, A.; Jackson, C. D.; Millner, P. A.; Ramanaviciene, A. Considerations in Producing Preferentially Reduced Half-Antibody Fragments. *J. Immunol. Methods* **2016**, *429*, 50–56.
- (18) Schumacher, F. F.; Nunes, J. P. M.; Maruani, A.; Chudasama, V.; Smith, M. E. B.;

- Chester, K. A.; Baker, J. R.; Caddick, S. Next Generation Maleimides Enable the Controlled Assembly of Antibody–drug Conjugates via Native Disulfide Bond Bridging. *Org. Biomol. Chem.* **2014**, *12*, 7261–7269.
- (19) Behrens, C. R.; Ha, E. H.; Chinn, L. L.; Bowers, S.; Probst, G.; Fitch-Bruhns, M.; Monteon, J.; Valdiosera, A.; Bermudez, A.; Liao-Chan, S.; et al. Antibody–Drug Conjugates (ADCs) Derived from Interchain Cysteine Cross-Linking Demonstrate Improved Homogeneity and Other Pharmacological Properties over Conventional Heterogeneous ADCs. *Mol. Pharm.* **2015**, *12* (11), 3986–3998.
- (20) Jackson, D.; Atkinson, J.; Guevara, C. I.; Zhang, C.; Kery, V.; Moon, S.-J.; Virata, C.; Yang, P.; Lowe, C.; Pinkstaff, J.; et al. In Vitro and In Vivo Evaluation of Cysteine and Site Specific Conjugated Herceptin Antibody-Drug Conjugates. *PLoS One* **2014**, *9* (1), e83865.
- (21) Ryan, C. P.; Smith, M. E. B.; Schumacher, F. F.; Grohmann, D.; Papaioannou, D.; Waksman, G.; Werner, F.; Baker, J. R.; Caddick, S. Tunable Reagents for Multi-Functional Bioconjugation: Reversible or Permanent Chemical Modification of Proteins and Peptides by Control of Maleimide Hydrolysis. *Chem. Commun.* **2011**, *47* (19), 5452.
- (22) Fontaine, S. D.; Reid, R.; Robinson, L.; Ashley, G. W.; Santi, D. V. Long-Term Stabilization of Maleimide–Thiol Conjugates. *Bioconjug. Chem.* **2015**, *26* (1), 145–152.
- (23) Grüttner, C.; Müller, K.; Teller, J.; Westphal, F.; Foreman, A.; Ivkov, R. Synthesis and Antibody Conjugation of Magnetic Nanoparticles with Improved Specific Power Absorption Rates for Alternating Magnetic Field Cancer Therapy. *J. Magn. Magn. Mater.* **2007**, *311*, 181–186.
- (24) Lee, J.; Choi, Y.; Kim, K.; Hong, S.; Park, H.-Y.; Lee, T.; Cheon, G. J.; Song, R. Characterization and Cancer Cell Specific Binding Properties of Anti-EGFR Antibody Conjugated Quantum Dots. *Bioconjug. Chem.* **2010**, *21* (5), 940–946.
- (25) Thomas, T. P.; Patri, A. K.; Myc, A.; Myaing, M. T.; Ye, J. Y.; Norris, T. B.; Baker, J. R. In Vitro Targeting of Synthesized Antibody-Conjugated Dendrimer Nanoparticles. *Biomacromolecules* **2004**, *5* (6), 2269–2274.
- (26) Jo, S. M.; Noh, S. H.; Jin, Z.; Lim, Y.; Cheon, J.; Kim, H. S. Simple and Efficient Capture of EGFR-Expressing Tumor Cells Using Magnetic Nanoparticles. *Sensors Actuators B Chem.* **2014**, *201*, 144–152.
- (27) Karra, N.; Nassar, T.; Ripin, A. N.; Schwob, O.; Borlak, J.; Benita, S. Antibody Conjugated PLGA Nanoparticles for Targeted Delivery of Paclitaxel Palmitate: Efficacy and Biofate in a Lung Cancer Mouse Model. *Small* **2013**, *9* (24), 4221–4236.
- (28) Cruz, L. J.; Tacke, P. J.; Fokkink, R.; Figdor, C. G. The Influence of PEG Chain Length and Targeting Moiety on Antibody-Mediated Delivery of Nanoparticle Vaccines to Human Dendritic Cells. *Biomaterials* **2011**, *32* (28), 6791–6803.
- (29) Sukhanova, A.; Even-Desrumeaux, K.; Kisserli, A.; Tabary, T.; Reveil, B.; Millot, J.-M.; Chames, P.; Baty, D.; Artemyev, M.; Oleinikov, V.; et al. Oriented Conjugates of Single-Domain Antibodies and Quantum Dots: Toward a New Generation of Ultrasmall Diagnostic Nanoprobes. *Nanomedicine Nanotechnology, Biol. Med.* **2012**, *8* (4), 516–525.

-
- (30) Kotagiri, N.; Li, Z.; Xu, X.; Mondal, S.; Nehorai, A.; Achilefu, S. Antibody Quantum Dot Conjugates Developed via Copper-Free Click Chemistry for Rapid Analysis of Biological Samples Using a Microfluidic Microsphere Array System. *Bioconjug. Chem.* **2014**, *25* (7), 1272–1281.
- (31) Kralj, S.; Rojnik, M.; Kos, J.; Makovec, D. Targeting EGFR-Overexpressed A431 Cells with EGF-Labeled Silica-Coated Magnetic Nanoparticles. *J. Nanoparticle Res.* **2013**, *15* (5), 1666.
- (32) Kolb, H. C.; Finn, M. G.; Sharpless, K. B. Click Chemistry: Diverse Chemical Function from a Few Good Reactions. *Angew. Chemie Int. Ed.* **2001**, *40* (11), 2004–2021.
- (33) Gaetke, L. M.; Chow, C. K. Copper Toxicity, Oxidative Stress, and Antioxidant Nutrients. *Toxicology* **2003**, *189* (1–2), 147–163.
- (34) Greene, M. K.; Richards, D. A.; Nogueira, J. C. F.; Campbell, K.; Smyth, P.; Fernández, M.; Scott, C. J.; Chudasama, V. Forming Next-Generation Antibody–nanoparticle Conjugates through the Oriented Installation of Non-Engineered Antibody Fragments. *Chem. Sci.* **2018**, *9* (1), 79–87.
- (35) Gordon, C. G.; Mackey, J. L.; Jewett, J. C.; Sletten, E. M.; Houk, K. N.; Bertozzi, C. R. Reactivity of Biarylazacyclooctynones in Copper-Free Click Chemistry. *J. Am. Chem. Soc.* **2012**, *134*, 9199–9208.
- (36) Beck, S.; Schultze, J.; Räder, H.-J.; Holm, R.; Schinnerer, M.; Barz, M.; Koynov, K.; Zentel, R. Site-Specific DBCO Modification of DEC205 Antibody for Polymer Conjugation. *Polymers.* **2018**, *10* (2), 141.
- (37) Green, M. N. Avidin and Streptavidin. *Methods Enzymol.* **1990**, *184*, 51–67.
- (38) Dinauer, N.; Balthasar, S.; Weber, C.; Kreuter, J.; Langer, K.; von Briesen, H. Selective Targeting of Antibody-Conjugated Nanoparticles to Leukemic Cells and Primary T-Lymphocytes. *Biomaterials* **2005**, *26* (29), 5898–5906.
- (39) Wartlick, H.; Michaelis, K.; Balthasar, S.; Strebhardt, K.; Kreuter, J.; Langer, K. Highly Specific HER2-Mediated Cellular Uptake of Antibody-Modified Nanoparticles in Tumour Cells. *J. Drug Target.* **2004**, *12* (7), 461–471.
- (40) Green, M. N. Avidin and Streptavidin. *Methods Enzymol.* **1990**, *184*, 51–67.
- (41) Wartlick, H.; Michaelis, K.; Balthasar, S.; Strebhardt, K.; Kreuter, J.; Langer, K. Highly Specific HER2-Mediated Cellular Uptake of Antibody-Modified Nanoparticles in Tumour Cells. *J. Drug Target.* **2004**, *12* (7), 461–471.
- (42) Cho, I. H.; Paek, E. H.; Lee, H.; Kang, J. Y.; Kim, T. S.; Paek, S. H. Site-Directed Biotinylation of Antibodies for Controlled Immobilization on Solid Surfaces. *Anal. Biochem.* **2007**, *365*, 14–23.
- (43) Sjodahl, J. Repetitive Sequences in Protein A from *Staphylococcus Aureus*. Arrangement of Five Regions within the Protein, Four Being Highly Homologous and Fc-Binding. *Eur. J. Biochem.* **1977**, *73*, 343–351.
- (44) Akerström, B.; Brodin, T.; Reis, K.; Björck, L. Protein G: A Powerful Tool for Binding and Detection of Monoclonal and Polyclonal Antibodies. *J. Immunol.* **1985**, *135* (4), 2589–2592.

-
- (45) Jin, T.; Tiwari, D. K.; Tanaka, S.; Inouye, Y.; Yoshizawa, K.; Watanabe, T. M. Antibody–ProteinA Conjugated Quantum Dots for Multiplexed Imaging of Surface Receptors in Living Cells. *Mol. Biosyst.* **2010**, *6*, 2325.
- (46) Zrazhevskiy, P.; Gao, X. Quantum Dot Imaging Platform for Single-Cell Molecular Profiling. *Nat. Commun.* **2013**, *4*, 1619.
- (47) Jin, T.; Tiwari, D. K.; Tanaka, S.; Inouye, Y.; Yoshizawa, K.; Watanabe, T. M. Antibody–ProteinA Conjugated Quantum Dots for Multiplexed Imaging of Surface Receptors in Living Cells. *Mol. Biosyst.* **2010**, *6*, 2325.
- (48) Sun, X.; Zhang, G.; Keynton, R. S.; O’Toole, M. G.; Patel, D.; Gobin, A. M. Enhanced Drug Delivery via Hyperthermal Membrane Disruption Using Targeted Gold Nanoparticles with PEGylated Protein-G as a Cofactor. *Nanomedicine Nanotechnology, Biol. Med.* **2013**, *9* (8), 1214–1222.
- (49) Centi, S.; Ratto, F.; Tatini, F.; Lai, S.; Pini, R. Ready-to-Use Protein G-Conjugated Gold Nanorods for Biosensing and Biomedical Applications. *J. Nanobiotechnology* **2018**, *16*, 5.
- (50) Zrazhevskiy, P.; Gao, X. Quantum Dot Imaging Platform for Single-Cell Molecular Profiling. *Nat. Commun.* **2013**, *4*, 1619.
- (51) Stuchinskaya, T.; Moreno, M.; Cook, M. J.; Edwards, D. R.; Russell, D. A. Targeted Photodynamic Therapy of Breast Cancer Cells Using Antibody–phthalocyanine–gold Nanoparticle Conjugates. *Photochem. Photobiol. Sci.* **2011**, *10* (5), 822–831.
- (52) Obaid, G.; Chambrier, I.; Cook, M. J.; Russell, D. A. Targeting the Oncofetal Thomsen-Friedenreich Disaccharide Using Jacalin-PEG Phthalocyanine Gold Nanoparticles for Photodynamic Cancer Therapy. *Angew. Chemie Int. Ed.* **2012**, *51* (25), 6158–6162.
- (53) Penon, O.; Marín, M. J.; Russell, D. A.; Pérez-García, L. Water Soluble, Multifunctional Antibody-Porphyrin Gold Nanoparticles for Targeted Photodynamic Therapy. *J. Colloid Interface Sci.* **2017**, *496*, 100–110.
- (54) Eck, W.; Craig, G.; Sigdel, A.; Ritter, G.; Old, L. J.; Tang, L.; Brennan, M. F.; Allen, P. J.; Mason, M. D. PEGylated Gold Nanoparticles Conjugated to Monoclonal F19 Antibodies as Targeted Labeling Agents for Human Pancreatic Carcinoma Tissue. *ACS Nano* **2008**, *2* (11), 2263–2272.
- (55) Dulkeith, E.; Ringler, M.; Klar, T. A.; Feldmann, J.; And, A. M. J.; Parak, W. J. Gold Nanoparticles Quench Fluorescence by Phase Induced Radiative Rate Suppression. *Nano Lett.* **2005**, *5* (4), 585–589.
- (56) García Calavia, P.; Marín, M. J.; Chambrier, I.; Cook, M. J.; Russell, D. A. Towards Optimisation of Surface Enhanced Photodynamic Therapy of Breast Cancer Cells Using Gold Nanoparticle–photosensitiser Conjugates. *Photochem. Photobiol. Sci.* **2018**, *17*, 281–289.
- (57) van der Heide, S.; Russell, D. A. Optimisation of Immuno-Gold Nanoparticle Complexes for Antigen Detection. *J. Colloid Interface Sci.* **2016**, *471*, 127–135.
- (58) Liu, C.; Shaurova, T.; Shoemaker, S.; Petkovich, M.; Hershberger, P. A.; Wu, Y. Tumor-Targeted Nanoparticles Deliver a Vitamin D-Based Drug Payload for the

- Treatment of EGFR Tyrosine Kinase Inhibitor-Resistant Lung Cancer. *Mol. Pharm.* **2018**, *15* (8), 3216–3226.
- (59) Matheson, I. B. C.; Etheridge, R. D.; Kratowich, N. R.; Lee, J. The Quenching of Singlet Oxygen by Amino Acids and Proteins. *Photochem. Photobiol.* **1975**, *21*, 165–171.
- (60) Matheson, I. B. C.; Lee, J. Chemical Reaction Rates of Amino Acids with Singlet Oxygen. *Photochem. Photobiol.* **1979**, *29*, 879–881.
- (61) Michaeli, A.; Feitelson, J. Reactivity of Singlet Oxygen toward Amino Acids and Peptides. *Photochem. Photobiol.* **1994**, *59*, 284–289.
- (62) Boylan, N. J.; Zhou, W.; Proos, R. J.; Tolbert, T. J.; Wolfe, J. L.; Laurence, J. S. Conjugation Site Heterogeneity Causes Variable Electrostatic Properties in Fc Conjugates. *Bioconjug. Chem.* **2013**, *24* (6), 1008–1016.
- (63) Obaid, G.; Chambrier, I.; Cook, M. J.; Russell, D. A. Cancer Targeting with Biomolecules: A Comparative Study of Photodynamic Therapy Efficacy Using Antibody or Lectin Conjugated Phthalocyanine-PEG Gold Nanoparticles. *Photochem. Photobiol. Sci.* **2015**, *14* (4), 737–747.
- (64) Hirsch, F. R.; Varella-Garcia, M.; Franklin, W. A.; Veve, R.; Chen, L.; Helfrich, B.; Zeng, C.; Baron, A.; Bunn, P. A. Evaluation of HER-2/Neu Gene Amplification and Protein Expression in Non-Small Cell Lung Carcinomas. *Br. J. Cancer* **2002**, *86*, 1449–1456.
- (65) Heinmüller, P.; Gross, C.; Beyser, K.; Schmidtgen, C.; Maass, G.; Pedrocchi, M.; Rü, J.; Hoffmann, J. R. J.; Lüd, L.-R. HER2 Status in Non-Small Cell Lung Cancer: Results from Patient Screening for Enrollment to a Phase II Study of Herceptin. *Clin. Cancer Res.* **2003**, *9*, 5238–5244.
- (66) Springer, T. A.; Bhattacharya, A.; Cardoza, J. T.; Sanchez-Madrid, F. Monoclonal Antibodies Specific for Rat IgG1, IgG2a, and IgG2b Subclasses, and Kappa Chain Monotypic and Allotypic Determinants: Reagents for Use with Rat Monoclonal Antibodies. *Hybridoma* **1982**, *1* (3), 257–273.
- (67) Rousseaux, J.; Picque, M. T.; Bazin, H.; Biserte, G. Rat IgG Subclasses: Differences in Affinity to Protein A-Sepharose. *Mol. Immunol.* **1981**, *18* (7), 639–645.
- (68) Sousa, M. M.; Steen, K. W.; Hagen, L.; Slupphaug, G. Antibody Cross-Linking and Target Elution Protocols Used for Immunoprecipitation Significantly Modulate Signal-to Noise Ratio in Downstream 2D-PAGE Analysis. *Proteome Sci.* **2011**, *9*, 45.
- (69) Schneider, C.; Newman, R. A.; Sutherland, D. R.; Asser, U.; Greaves, M. F. A One Step Purification of Membrane Proteins Using a High Efficiency Immunomatrix. *J. Biol. Chem.* **1982**, *257* (18), 10766–10769.
- (70) Brünger, A. T.; Ultsch, M. H.; de Vos, A. M.; Wells, J. A. Convergent Solutions to Binding at a Protein-Protein Interface. *Science* **2000**, *287*, 1279–1283.
- (71) Gong, Y.; Zhang, L.; Li, J.; Feng, S.; Deng, H. Development of the Double Cyclic Peptide Ligand for Antibody Purification and Protein Detection. *Bioconjug. Chem.* **2016**, *27*, 1569–1573.

-
- (72) Vance, N.; Zacharias, N.; Ultsch, M.; Li, G.; Fourie, A.; Liu, P.; LaFrance-Vanasse, J.; Ernst, J. A.; Sandoval, W.; Kozak, K. R.; et al. Development, Optimization, and Structural Characterization of an Efficient Peptide-Based Photoaffinity Cross-Linking Reaction for Generation of Homogeneous Conjugates from Wild-Type Antibodies. *Bioconjug. Chem.* **2019**, *30*, 148–160.
- (73) Yu, C.; Tang, J.; Loredó, A.; Chen, Y.; Jung, S. Y.; Jain, A.; Gordon, A.; Xiao, H. Proximity-Induced Site-Specific Antibody Conjugation. *Bioconjug. Chem.* **2018**, *29* (11), 3522–3526.
- (74) Kishimoto, S.; Nakashimada, Y.; Yokota, R.; Hatanaka, T.; Adachi, M.; Ito, Y. Site-Specific Chemical Conjugation of Antibodies by Using Affinity Peptide for the Development of Therapeutic Antibody Format. *Bioconjug. Chem.* **2019**, *30* (3), 698–702.

Chapter Four
Towards Protease Cleavable
Sequences to ‘Turn on’ the
Photodynamic Activity of Folate
Directed Phthalocyanine-Gold
Nanocarriers

4.1 Introduction

4.1.1 Small molecules as targeting agents

Small molecules tend not to be favoured as targeting moieties due to their relatively low binding affinity and poor substrate selectivity when compared to biological macromolecules such as antibodies. Antibody-drug conjugates can, however, be difficult to characterise, are generally heterogeneous as it is difficult to control the number of drugs attached to one antibody, and the site at which these drugs bind to the antibody is very difficult to control. Small molecules, defined as low molecular weight organic compounds, allow for the attachment of a specified number of drugs to a targeting agent with tightly controlled chemistry, allowing for a clearer picture of the structure of the conjugate. Small molecules have been used as targeting moieties for the delivery of gold nanoparticles, as described in **section 1.4.6**, with folic acid by far the most explored. Folic acid is non-immunogenic, relatively inexpensive and highly stable in physiological conditions, which highlights it as an attractive targeting moiety.

4.1.2 Folic acid and its uptake in the human body

Folic acid, also known as folate or vitamin B9, is a small molecule (MW 441.40 g mol⁻¹) which, when reduced by dihydrofolate reductase to tetrahydrofolate, acts as a coenzyme for single-carbon transfers within a cell, allowing for the synthesis of nucleic acids and the metabolism of some amino acids.¹ Folic acid cannot be synthesised by the human body, so it is imperative that efficient uptake occurs into human cells. In healthy tissue, three methods of uptake are possible: the reduced folate carrier, the proton-coupled folate transporter and the folate receptors.

The reduced folate carrier is ubiquitously expressed throughout the body and is the major transport system for the uptake of reduced folates, such as 5-methyl tetrahydrofolate, at neutral pH.² It is a member of the organic anion transporter family and allows uptake of folates through a counter-transport mechanism. These proteins have a relatively low affinity for folate ($K_M \approx 1 \mu\text{M}$) but their ubiquity means they are the main pathway for the uptake of reduced folates, yet they will not transport folic acid itself.³

Proton-coupled folate transporter transports folic acid and reduced folates at acidic pH, optimally pH 5–5.5, encouraging the uptake of folate into the cell by producing an electrochemical gradient using a flow of protons out of the cell.⁴ The expression of the

proton-coupled folate transporter is mostly restricted to the kidneys, liver, spleen, placenta and small intestine, with limited levels expressed in other normal tissue.⁵ Notably, its levels are much lower than the reduced folate carrier. Reduced folate carriers and proton-coupled folate transporters are responsible for the majority of the folate uptake in healthy tissue in the human body.⁴

The third method by which folate can be absorbed into cells is the folate receptors. In humans, the folate receptors are a family of four proteins, known as folate receptor α (FR α or FOLR1), folate receptor β (FR β or FOLR2), folate receptor γ (FR γ or FOLR3) and folate receptor δ (FR δ or FOLR4), that take up folic acid *via* receptor-mediated endocytosis.⁶ This process involves the cell engulfing a cluster of the receptor with the bound ligand in an intracellular sorting compartment, which becomes an endosome and later a lysosome. These cellular structures contain an acidic environment and carry the ligand from the receptor into the cell, with the receptor itself being recycled back to the surface of the cell from the intracellular sorting compartment.⁷ FR α , FR β and FR δ are 38-40 kDa glycosylphosphatidylinositol-anchored membrane proteins whereas the FR γ protein is secreted.^{8,9} Little is known about the function or mechanism of FR γ , which is reported to be mainly secreted by hematopoietic tissue, but the other receptors are more widely studied.¹⁰ The folate receptors show a high affinity towards both folic acid and reduced folates ($K_D \approx 0.1$ nM),¹¹ but their expression is limited throughout the body. FR α is commonly expressed in epithelial cells, whereas FR β is expressed in hematopoietic tissue and by the placenta, and FR δ is expressed on T-cells.¹²⁻¹⁴

4.1.3 The significance of folic acid in NSCLC

As the lungs are primarily epithelial cells, the expression pattern of FR α is of note. In fact, the attractiveness of FR α for treatment of non-small cell lung cancer (NSCLC) goes even further; in healthy cells, epithelial cell walls are polarised and FR α is selectively expressed on the apical surface of these cells, meaning it is not accessible to blood-borne folate ligands.^{11,15} Upon mutation to cancerous cells, epithelial cells lose their polarity and FR α is expressed throughout the whole cell surface, as shown in **Figure 4.1**, accessible to any folate in the blood stream.¹⁶ This expression increases the ability of cancerous cells to uptake folic acid, which is vital for the aggressive proliferation of tumours.

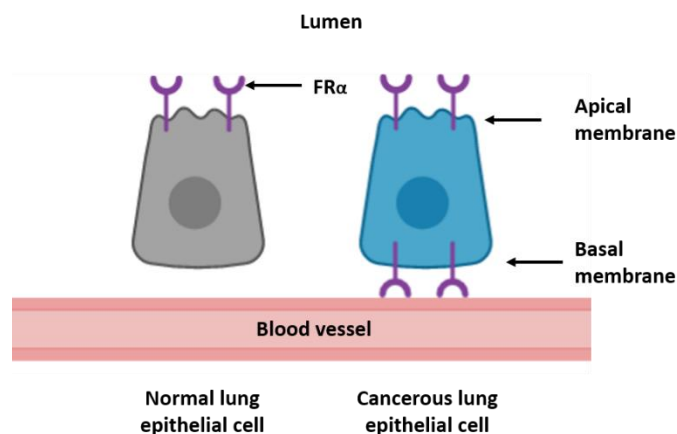


Figure 4.1: Expression of $FR\alpha$ on lung epithelial cells. Expression is limited to the apical membrane on normal epithelial cells (L), but mutation to cancerous cells (R) depolarises the membrane and leads to expression on the basal membrane which is accessible to blood borne folate

$FR\alpha$ has been found to be expressed on *ca.* 76%¹⁷ of lung adenocarcinomas and, more significantly, overexpressed on *ca.* 62%.¹⁸ The high level of overexpression of $FR\alpha$ in NSCLC highlights the appeal of this receptor as a target for treatments. The lack of this receptor on the basal surface of healthy lung cells enhances the selectivity of folate targeted drugs compared to other targets, which rely on an overexpression of the receptor, rather than an absence entirely.

4.1.4 Folic acid as a targeting agent

Folic acid (**Figure 4.2**) contains two carboxylic acids, one attached to the alpha carbon, and one to the gamma. These carboxylic acids can be used to conjugate folic acid to payloads and drug carriers, however, Low *et al.* demonstrated that the activity of folic acid towards the folate receptor is only maintained if conjugation occurs through the γ -conjugate,¹⁹ and therefore any folate-directed payloads need to be conjugated through this γ -position.

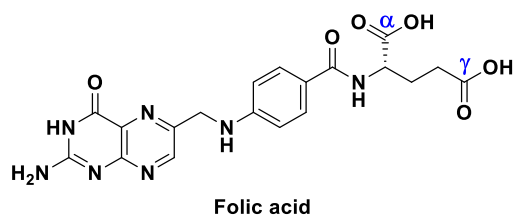


Figure 4.2: The structure of folic acid, highlighting the α and γ -carboxylic acids

4.1.4.1 Folic acid conjugated small molecule therapies

Since the discovery of folic acid as a targeting agent and the expression of FR α on malignant cells, folate has been widely investigated as a targeting ligand for therapies. Chemotherapeutics, immunotherapeutics, and loaded nanoparticles have been delivered by folic acid, alongside gene therapies and RNA. Notably, four folate targeted small molecule therapies have entered clinical trials for various cancers,²⁰ with Vintafolide (**Figure 4.3**, **4.1**) the most promising of these to date.

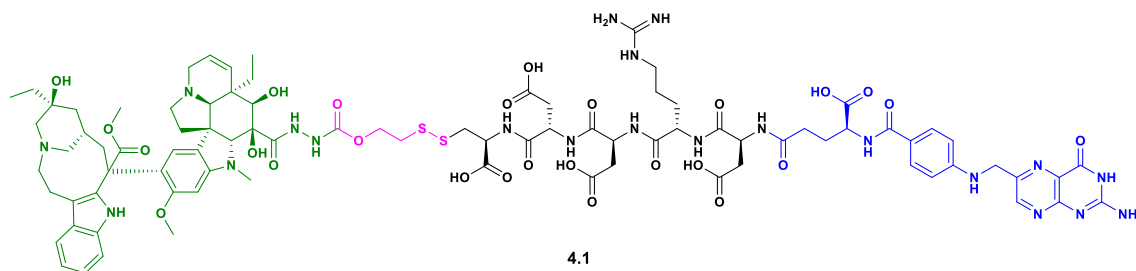
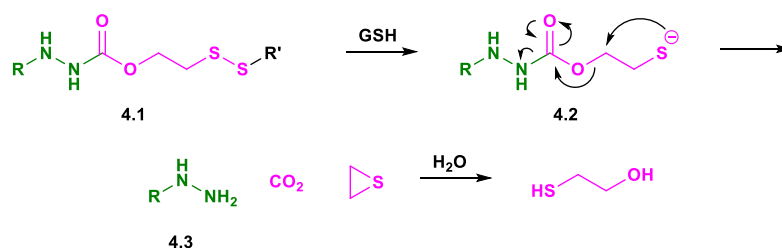


Figure 4.3: Structure of Vintafolide, consisting of DAVLBH (green), a self-immolative disulphide (pink), a water-soluble peptide chain (black) and folic acid (blue)

Vintafolide is a water-soluble conjugate of folic acid linked to desacetyl vinblastine monohydrazine (DAVLBH), a microtubule destabilising drug, through a water-soluble peptide linker and a self-immolative disulphide. Upon uptake into FR α expressing tumours, the reductive environment leads to the cleavage of the disulphide, and the self-immolation of the linker leads to the release of DAVLBH (**4.3**), as shown in **Scheme 4.1**. Phase IIb clinical trials in NSCLC and phase III trials in ovarian cancer using Vintafolide in combination with chemotherapeutic drugs showed promising results in FR α -positive tumours, with a phase III trial in NSCLC ongoing.^{21,22} Unfortunately, progression-free survival rates were not high enough in ovarian cancer for this trial to progress further, but this, and the ongoing phase III trial in NSCLC, highlights folic acid as a viable targeting ligand for cancer treatment.



Scheme 4.1: The reduction of the disulphide in Vintafolide leads to the self-immolation of the linker (pink) and the release of DAVLBH (green)

While it is agreed that only the γ -conjugate of folic acid is active, the activation of solely the γ -carboxylic acid is challenging. Most reports of folate conjugates use reagents such as *N,N'*-dicyclohexylcarbodiimide (DCC) and 2-(1H-Benzotriazole-1-yl)-1,1,3,3-tetramethylammonium tetrafluoroborate (TBTU) to couple folic acid, relying on the higher reactivity of the γ -carboxylic acid.^{23–26} However, few reports describe the production of solely the γ -conjugate. Many groups then separate these isomers using chromatographic techniques, but the two isomers are separated by less than one minute on reverse-phase HPLC which makes the separation process challenging.²⁷ Temperature control has been reported as a method for the selective formation of the γ -conjugate, but confusingly both cooling the reaction to 0 °C²⁸ and heating to 30 °C²⁹ have been reported to solely form the required isomer.

Few reports exist of the chemical manipulation of folate to selectively conjugate through the γ -conjugate. The structure of folic acid can be split into two constituent parts: pteronic acid (4.4) and glutamic acid (4.5, **Figure 4.4a**). Folic acid has been manipulated to remove the glutamic acid and to reintroduce γ -methyl glutamate, allowing for the selective manipulation of the γ -carboxylic acid. This γ -ester is reacted with ethylenediamine to selectively produce 2-aminoethylfolic acid (4.6, **Figure 4.4b**) which can be further conjugated without modifying the α -carboxylic acid.³⁰

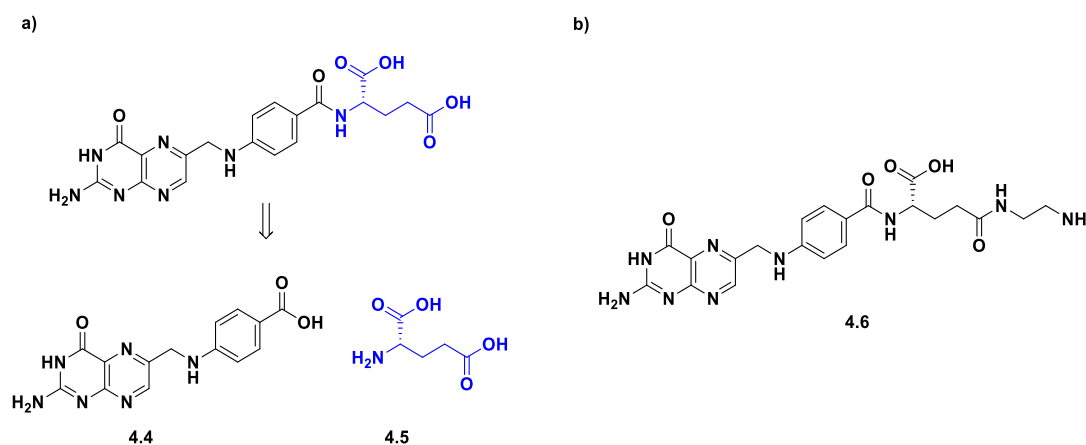


Figure 4.4: a) The structure of folic acid split and its retrosynthesis into its constituents, pteronic acid (black) and glutamic acid (blue) and b) the structure of 2-aminoethylfolic acid

A second method of selectively forming the γ -conjugate involves the use of solid phase peptide synthesis. Fmoc-protected glutamic acid with the C-terminus *t*Bu protected and a free side chain carboxylic acid (Fmoc-Glu-O*t*Bu, 4.7) forces the conjugation to be through the γ -carboxylic acid. Upon deprotection of the amine, N¹⁰-trifluoroacetyl pteronic

acid (N^{10} -TFA-pteronic acid, **4.8**) can be conjugated through HATU/DIPEA coupling to give protected γ -conjugated folic acid on resin.^{31,32} The reagents used in this solid phase synthesis are shown in **Figure 4.5**. The chemical manipulation of folic acid, while requiring more synthetic work, has the benefit of ensuring all the synthesised folic acid conjugate is through the γ -conjugate, while temperature control can easily still result in a mixture if not controlled tightly enough.

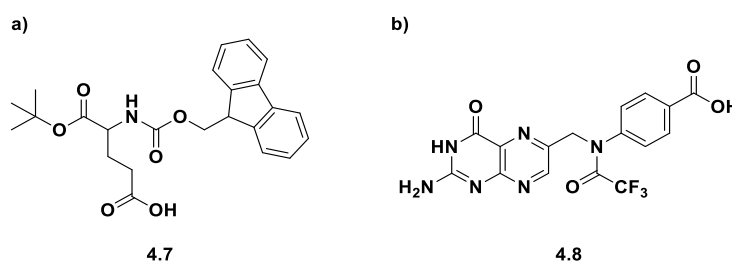


Figure 4.5: The structures of **a)** Fmoc-Glu-OtBu and **b)** N^{10} -TFA-pteronic acid for solid phase preparation of γ -conjugated folic acid

4.1.4.2 Folic acid and PDT

Folate has been employed as a targeting agent in PDT. The first report of folic acid as a targeting agent in PDT linked the photosensitiser tetraphenylporphyrin (TPP) to folic acid through alkyl and PEG linkers and selective uptake of the photosensitiser was observed in FR α overexpressing cells. The authors found that the nature of the linker changed the physical properties of the conjugate but not the affinity of folic acid to the receptor. The conjugates formed with a PEG linker displayed higher photodynamic activity than those synthesised with an alkyl linker, possibly due to the increased solubility that PEG provides to the structure.^{33,34} A range of porphyrins and chlorins have subsequently been conjugated to folic acid through PEG linkers.^{35,36} While PEG has a great benefit of increasing the water solubility of the conjugate, the direct conjugation of folic acid onto zinc phthalocyanines has also been shown to increase the water solubility of the photosensitiser.³⁷ All of these conjugates were synthesised using DCC as the coupling agent and the α - and γ -conjugates were not separated. Although selective activity was observed, this leads to the question of whether the same quantity of the γ -conjugate is formed in each batch of these photosensitiser-folate conjugates and therefore if the same amount of active drug is accessible.

While there have been some reports of small molecule photosensitiser-folic acid conjugates, the majority of the research has focussed on the use of folic acid to direct

nanoparticles carrying photosensitisers to tumours. The use of folic acid to deliver gold nanoparticles has been reviewed in **section 1.4.6**. Furthermore, folic acid has been used to deliver a range of other photosensitiser-nanoparticle conjugates to tumours, including quantum dots,³⁸ iron oxide,³⁹ chitosan,⁴⁰ silica,⁴¹ liposomes⁴² and polymeric⁴³ nanoparticles. In these nanoconjugates, the photosensitisers are either covalently bound to the nanoparticle surface, encapsulated in the nanoparticle, or trapped in the ligand corona. For the attachment of folic acid onto nanoparticle systems, most reports do not separate the α - and γ - conjugates, relying on the higher reactivity of the γ -conjugate to ensure there is active folic acid on the surface, but not quantifying exactly how much active folate is present.^{44,45} In fact, many groups use commercially available folate conjugates, which are purchased as a mixture of isomers.^{46,47} While using a mixture of folate isomers yields nanoparticles that show high selectivity towards FR α expressing cells, the inconsistency in the ratio of γ - to α -folate conjugates formed on the nanoparticle surface means these conjugates have questionable reproducibility, and thus use as drug candidates.

Efforts have been made by the scientific community to overcome this issue and, notably, N¹⁰-TFA-pteronic acid (**4.8**) has been used to prepare liposomes with γ -conjugated folic acid.⁴⁸ Folic acid has also been conjugated onto AuNPs through the aromatic amine on the pteronic acid section of folic acid.⁴⁹ However, the crystal structure of folic acid bound to FR α shows the pteronic acid deep inside the binding pocket^{50,51} (**Figure 4.6**) so it is questionable whether the folate is providing the targeting effect described *via* a folic acid-FR α mediated interaction.

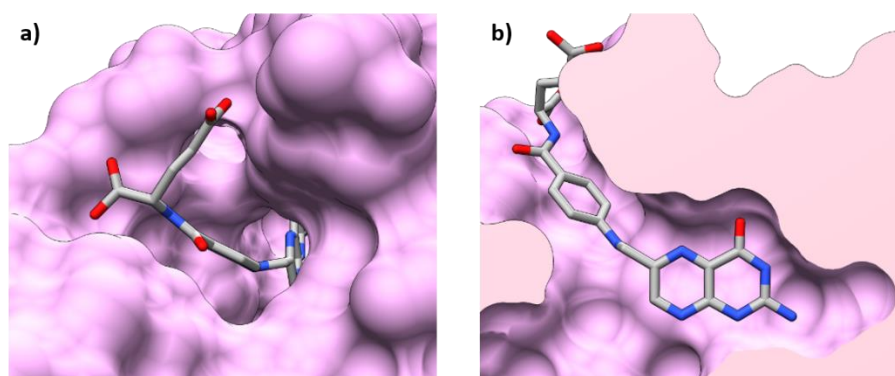


Figure 4.6: Orientation of folic acid in FR α showing the pteronic acid moiety deep inside the binding pocket and the γ -carboxylic acid protruding from the binding site (PBD: 4LRH). **a)** surface representation of folic acid in the FR α binding site and **b)** cross section of the binding pocket of FR α .

4.1.4.3 *Cleavable folate therapies*

While folate conjugates have shown selectivity towards FR α expressing cancers, it has been observed that the conjugation of folic acid to photosensitisers can cause a reduction in the singlet oxygen quantum yield, and in some cases complete quenching is observed.^{37,52} When folic acid has been used to deliver cytotoxic payloads, folate has been linked to payloads through pH,^{53–55} light,^{56,57} redox-active^{58,59} and enzymatically^{60,61} cleavable linkers with the aim of releasing the drug intracellularly.

pH labile linkers rely on the difference in pH between the blood (pH 7.4) and intracellular vesicles such as lysosomes (pH 4.5–5.0). The most common pH labile linker is a hydrazone, which undergoes acid hydrolysis at lysosomal pH. While this linker is appealing, some cleavage has been observed under physiological conditions (pH 7.4, 37 °C)⁶² and clinical trials of antibody drug conjugates linked through a hydrazone found off-target toxicity due to the lability of these linkers in circulation.⁶³

Disulphide linkers are cleaved by glutathione, which forms a reductive environment within cells. Glutathione is also found extracellularly so these cleavable linkers rely on the increased concentration of glutathione inside the cell to deliver the drug to the desired location.⁶⁴ Significantly, glutathione is also upregulated in lung cancers⁶⁵ so this can provide a second targeting effect towards disulphide linked folate-drug conjugates. For the work presented in this thesis, however, disulphides are not an ideal linker due to the affinity of gold for sulphur, meaning it is highly likely that the disulphide bond would be broken upon addition to gold nanoparticles, resulting in the folate moiety directly attached to the gold core and thus not accessible as a targeting ligand. Disulphide linkers also display lower plasma stability than hydrazones as they can exchange with low molecular weight thiols in circulation, which can lead to the loss of the targeting ligand and lead to off-target delivery of therapeutics.³¹

Light cleavable linkers depend on the use of UV radiation to supply enough energy to uncage the attached therapeutic from folic acid. UV radiation penetrates less than one millimetre through human skin⁶⁶ and therefore is a highly limited cleavage technique. Investigation into infrared-cleavable linkers may increase the applicability of light cleavable linkers as infrared penetrates much deeper into human tissue, but no infrared cleavable linkers are currently reported.

Enzymatically cleavable linkers are commonly targeted towards enzymes that are overexpressed in the cells of interest. Most notably, enzymes have been used to release

photosensitisers from folic acid. Peptidases have been shown to cleave a β -peptide spacer between folic acid and the protoporphyrin IX (PPIX) precursor 5-aminolevulinic acid methyl ester (MAL), targeting the formation of PPIX specifically to FR α expressing tumours.²⁹ The conjugation of folic acid and chlorin-e6 has been observed to quench the fluorescence and therefore singlet oxygen of the photosensitiser, and the design of a cathepsin B cleavable linker between folic acid and chlorin-e6 allowed the 'switch on' of singlet oxygen production in the targeted cells.⁵² Enzymatically cleavable sequences are the most appealing of these cleavable linkers due to their relative stability in circulation^{67,68} and the intracellular availability of the enzymes instigating selectivity.

4.1.5 Proteases and their significance in cancer

Proteases are a diverse group of enzymes that cause proteolysis of proteins, meaning they hydrolyse amide bonds and cause degradation. There are two classes of proteases; exopeptidases, which act on amide bonds at the N and C termini of proteins, and endopeptidases, which cleave internal amide bonds within proteins.⁶⁹ Proteases are ubiquitously produced in cells throughout the body and are vital for the function and regulation of healthy cells, however proteases can also be key markers for the mutation of healthy cells into cancerous cells.⁷⁰ There is a plethora of proteases found throughout the body, yet two classes are widely studied as both cancerous markers and as key targets for activating targeted therapies; these are matrix metalloproteinases and cathepsins.

Matrix metalloproteinases (MMPs) are a family of 20 proteases that degrade the extracellular matrix. These proteases have a dependence on metal ions, and in most cases this ion is zinc(II).⁷¹ In healthy cells, their role involves the release of growth factors and receptors from the cell surface. However, the mutation to cancerous cells can lead to the upregulation of MMPs, which are seen to have a role in tumour growth, progression and metastasis, along with an influence on increased rates of angiogenesis.⁷²

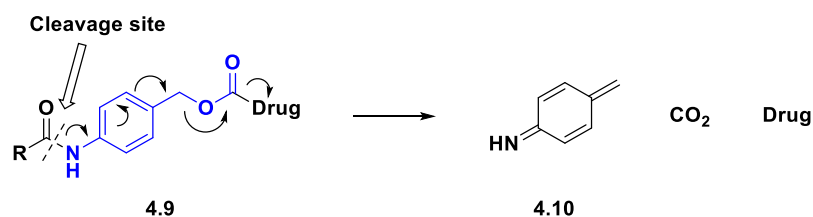
The cathepsin family comprises 11 lysosomal cysteine proteases, including cathepsin B (CatB). CatB is overexpressed in the majority of cancers and notably its upregulation is high in NSCLC.^{73,74} CatB is present in cells to degrade extracellular proteins that have entered the lysosomal compartments of a cell.⁷⁵ This protease acts as an endopeptidase, cleaving amide bonds between hydrophobic residues. CatB differs from other members of the cathepsin family as it can also accept an arginine in its sequence for degradation as it contains a glutamic acid in its binding pocket that acts as an acceptor for the positive

charge of arginine's side chain.⁷⁶ CatB has been seen to be overexpressed in a range of cancers, including lung, breast, colorectal and prostate, where it has been shown to be involved in tumour formation, proliferation and metastasis.^{75,77-79} In healthy cells a small amount (< 5%) of CatB is secreted, but the majority of CatB is found intracellularly. The localisation of CatB has been seen to be slightly altered by the transformation of cells from healthy to malignant, with an upregulation of CatB leading to its localisation in the cytoplasm.^{79,80}

Both MMPs⁸¹⁻⁸³ and CatB^{52,84,85} have been employed for the activation of photodynamic agents at the tumour, yet the localisation of CatB inside the lysosomes makes it a more interesting target. The release of drugs by MMPs could still lead to some off-target toxicity as the drug is not necessarily internalised when released extracellularly and could diffuse to surrounding healthy cells. CatB cleavage mainly occurs intracellularly, so the desired drug must be within the cell before it can be released, preventing this off-target effect.

4.1.6 Cathepsin B substrates and cleavable therapies

CatB does not have a specific substrate but is known to cleave amide bonds between hydrophobic residues, while also recognising arginine. As there is not a specific substrate, many amino acid sequences have been used as recognition sequences for CatB cleavage. Among the first reported sequences were the tetrapeptides Gly-Phe-Leu-Gly and Ala-Leu-Ala-Leu, yet these have been surpassed in the literature in favour of dipeptide sequences as they have unfavourable cleavage kinetics and are difficult to incorporate into peptide sequences due to their hydrophobicity.⁸⁶ A systematic review of dipeptide cleavable sequences determined that, for rapid cleavage by CatB, the second amino acid in a sequence needs to be a hydrophobic residue, with valine found to be the optimal amino acid.⁸⁷ It was also found that a spacer was required between the growing peptide chain and the cleavable sequence to prevent the overcrowding of the active site of CatB.⁸⁷ In fact, it was observed that without this spacer next to the cleavable sequence, CatB showed no activity towards cleavable sequences that were cleaved within minutes with the addition of a spacer.⁸⁷ The most widely utilised spacer is *para*-amino benzyl carbamate (PABC), as this restores the activity of CatB and is self-immolating, meaning upon cleavage any attached drug is restored without any attached amino acids from the cleavable sequence (**Scheme 4.2**).



Scheme 4.2: Self-immolation of PABC (blue) after cleavage (dotted line) gives the free drug

Many amino acids have been placed in the first position of these dipeptides, including alanine, lysine and citrulline (Cit), a non-essential amino acid that is isosteric and isoelectronic to arginine but is found to be more stable in circulation and is notably non-basic. Of the cleavable sequences trialled, Val-Lys was found to be the most rapidly cleaved sequence,⁸⁷ but the basicity of lysine adds complexity for the uptake of any cleavable drug into cells as the protonation of lysine can change its characteristics greatly. For the system reported in this thesis, the addition of a second lysine residue complicates the addition of the peptide onto PEG, following the method described in **section 2.3.2.1**. For these reasons, the cleavable dipeptide Val-Cit was investigated as a CatB substrate in this thesis. While PABC has been seen to be a very good spacer molecule, *para*-amino benzoic acid (PABA), which has the same characteristics as PABC, has been found to be a more stable building block for solid phase peptide synthesis due to the presence of a moderately electron withdrawing carboxylic acid.⁸⁸ PABA does not have the ability to self-immolate, but as this work aims to use this sequence (Val-Cit-PABA) to remove a quenching molecule, and not to release a drug, this is not a concern. The sequence Val-Cit-PABA (**4.11**, **Figure 4.7**) is commonly used in the literature for CatB release of molecules and drugs, and it is seen to be a very stable and efficiently cleaved linker.^{89,90}

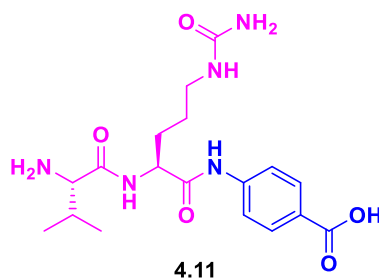


Figure 4.7: Structure of the Val-Cit-PABA cleavable sequence. The CatB cleavage sequence, valine and citrulline, is shown in pink and the PABA spacer is shown in blue

4.2 Summary and chapter aims

The expression patterns of FR α on cancerous epithelial cells, and most notably on lung adenocarcinomas, presents folic acid as a highly desirable targeting agent. Folate has been shown to selectively target drugs, photosensitisers and nanoparticles towards FR α expressing cells and clinical trials of folate-drug conjugates have indicated folic acid as a viable targeting moiety for drug candidates. Folic acid possesses two carboxylic acids, but it only remains active if the payload conjugation occurs through the γ -carboxylic acid. Most of the research into targeting nanoparticles towards FR α using folic acid does not discriminate between the α - and γ -isomers, using the higher reactivity of the γ -carboxylic acid to favour the formation of the γ -conjugate but not selectively forming it. This gives rise to questionable compositions and variable concentrations of the targeting moiety on the surface of these nanoconjugates. This variation between batches and lack of quantitation of targeting moiety on the nanoparticle surface makes these nanoparticle systems questionable drug candidates. Methods to selectively form the γ -conjugate have been reported and should be explored to form more uniform and reproducible nanocarriers.

Folic acid, while an attractive targeting moiety widely explored for targeted photodynamic therapy, has been shown to quench singlet oxygen production, and many conjugates formed show lower, or no, singlet oxygen production compared with the free photosensitiser. To overcome this, cleavable linkers have been explored to remove the targeting moiety once the photosensitiser, or other drug, has been internalised by cancerous cells. One of the most promising methods to remove folic acid intracellularly is the use of cathepsin B, a protease overexpressed in cancers. Many CatB cleavable linkers have been reported, with the sequence Val-Cit-PABA (4.11) the most widely utilised sequence due to its stability in circulation and relatively fast cleavage kinetics.

This chapter aims to explore the use of folic acid as a targeting agent for the delivery of phthalocyanine-gold nanocarriers towards non-small cell lung cancer cell lines. Firstly, methods to selectively conjugate folic acid to the nanocarriers were explored to ensure that all the folate present on these nanocarriers was active and to prevent any variation in targeting activity between batches. Once a method to selectively form γ -folate conjugates was determined, phthalocyanine-gold nanocarriers were synthesised, functionalised with this targeting moiety. The addition of CatB cleavable linkers between the folate moiety and the nanocarrier were explored to increase the production of singlet oxygen by the

nanocarriers. The addition of this cleavable sequence also provides a second level of selectivity to the nanocarriers as the nanocarriers would not be photodynamically active until the directing group was cleaved away by the CatB overexpressed in the target cancer cells.

4.3 Results and discussion

4.3.1 Folic acid conjugation

As folic acid is shown to only be active towards the folate receptor if conjugated through the γ -carboxylic acid, manipulation of its reactivity is required to optimise the conjugation and only attach the active form to the nanocarriers. As folic acid is a robust and inexpensive molecule possessing carboxylic acids, it can be used in solid phase peptide synthesis. To initially determine the effects of standard coupling conditions on the attachment of folic acid to a peptide, rink amide MBHA resin was loaded with lysine (Lys) and folic acid (FA) was coupled in DMSO overnight alongside HATU and DIPEA, to give FA-Lys (**4.12**, **Figure 4.8**). Upon cleavage, a crude HPLC (**Figure 4.9**) was obtained showing two prominent peaks at 10.1 and 10.5 minutes. These peaks were separated using preparative HPLC, and the mass obtained on a MALDI mass spectrometer showed both peaks had a m/z of 569, corresponding to the $[M+H]^+$ of **4.12** and therefore these peaks correspond to the α - and γ - conjugates. It has been found that upon random attachment, the ratio of α - to γ -conjugated products tends to be approximately 30:70 and that the γ -conjugate is slightly more polar so is eluted first on a reverse-phase column, and therefore it is assumed that the larger peak in the presented synthesis is that of the γ -conjugate.^{33,34,91,92}

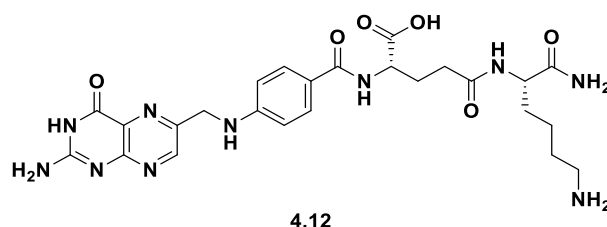


Figure 4.8: The structure of FA-Lys

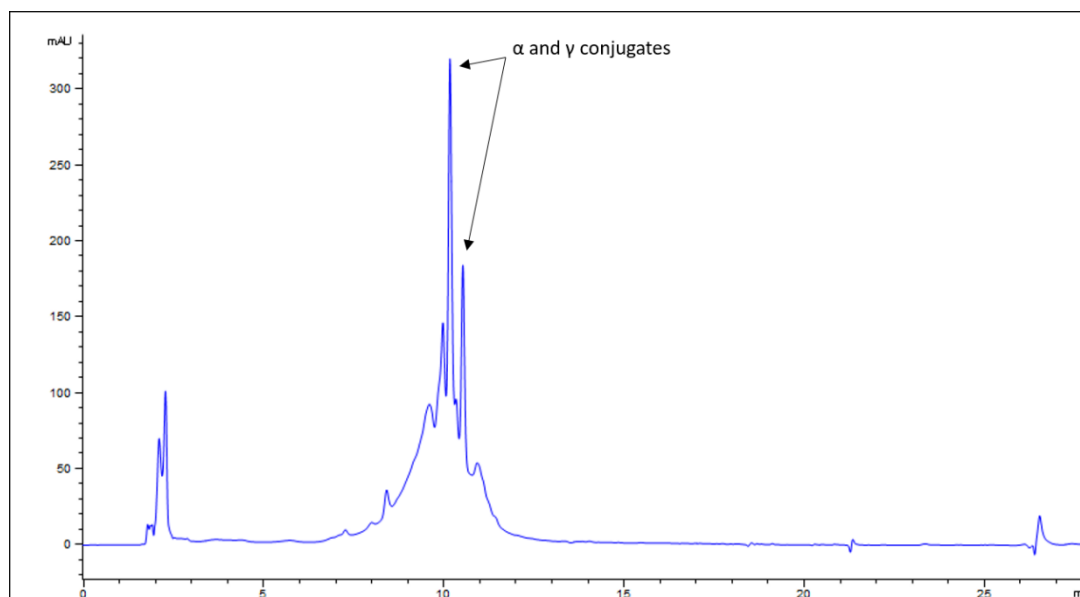


Figure 4.9: The analytical HPLC trace recorded at 214 nm of crude **4.12** formed using HATU/DIPEA at RT, showing the presence of the α and γ -conjugates

Guaragna *et al.* reported that dissolving folic acid in a solution of DIPEA in DMSO at 50 °C alongside PyBOP as a coupling agent, before shaking overnight at 30 °C, resulted in solely the γ -conjugate.²⁹ This simple method of controlling the selectivity of the coupling reaction was tested on the solid phase, again loading rink amide MBHA resin with lysine and attaching folic acid overnight in a water bath at 30 °C. The crude HPLC of this reaction post synthesis (**Figure 4.10**) presented two major peaks at retention times of 10.1 and 10.5 minutes, matching those of the synthesis without temperature control previously reported. Upon separation, the masses collected again showed a m/z of 569, corresponding to the $[M+H]^+$ of **4.12**, and therefore that this temperature-controlled reaction had no effect on the selectivity on the conjugation.

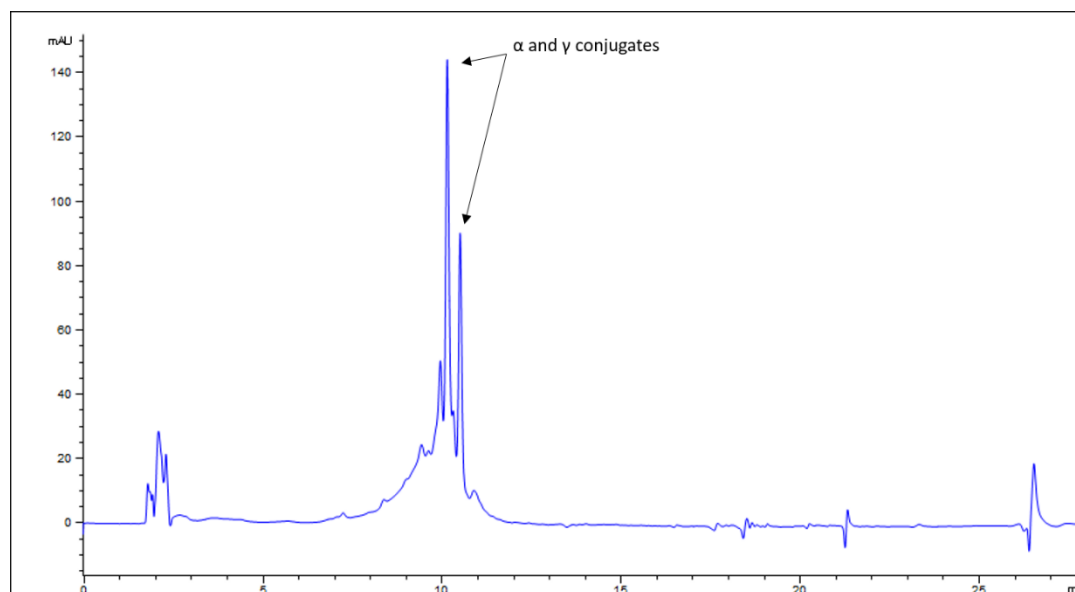


Figure 4.10: Analytical HPLC trace recorded at 214 nm of crude **4.12** synthesised using PyBOP/DIPEA at 30 °C, showing the presence of both the α and γ -conjugates

Further attempts to selectively conjugate through the γ -carboxylic acid were made in solution. Santos *et al.* reported that cooling a solution of folic acid alongside one equivalent of TBTU and *N*-methylmorpholine (NMM) to 0 °C, followed by the addition of an amine resulted in the γ -conjugate.²⁸ NMM acts as a base to activate folic acid and increases its reactivity towards TBTU. Cooling the mixture to 0 °C slowed the kinetics of the reaction and the steric bulk of TBTU as a coupling agent encouraged the activation of the γ -carboxylic acid in preference to the α -carbonyl. The presence of hydrogen bonding between the α -carbonyl and the neighbouring amide also increases the preferential activation of the γ -position.²⁸ In this thesis, 3-(dimethylamino)-1-propylamine was used as a model amine for this reaction, with the aim of selectively forming γ -3-dimethylaminopropylfolic acid (**4.13**, **Figure 4.11**).

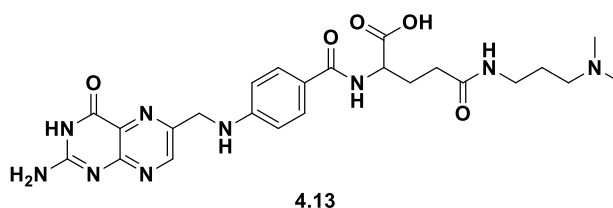


Figure 4.11: The structure of 3-dimethylaminopropylfolic acid

As steric bulk of the coupling agent is a major influence on the preferential activation of the γ -carbonyl, the bulkier coupling agent PyBOP was also trialled in parallel to TBTU.

PyBOP has a much higher steric bulk than TBTU, as shown in **Figure 4.12**, with its structure including three pyrrolidine rings, compared to the bulk of methylamines on TBTU.

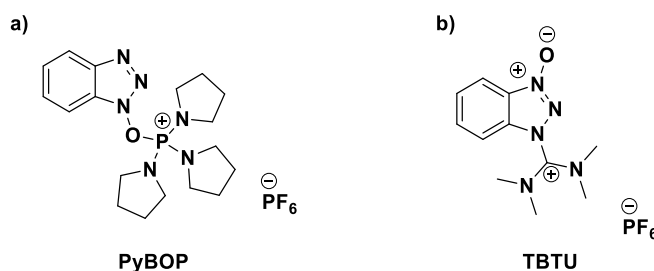


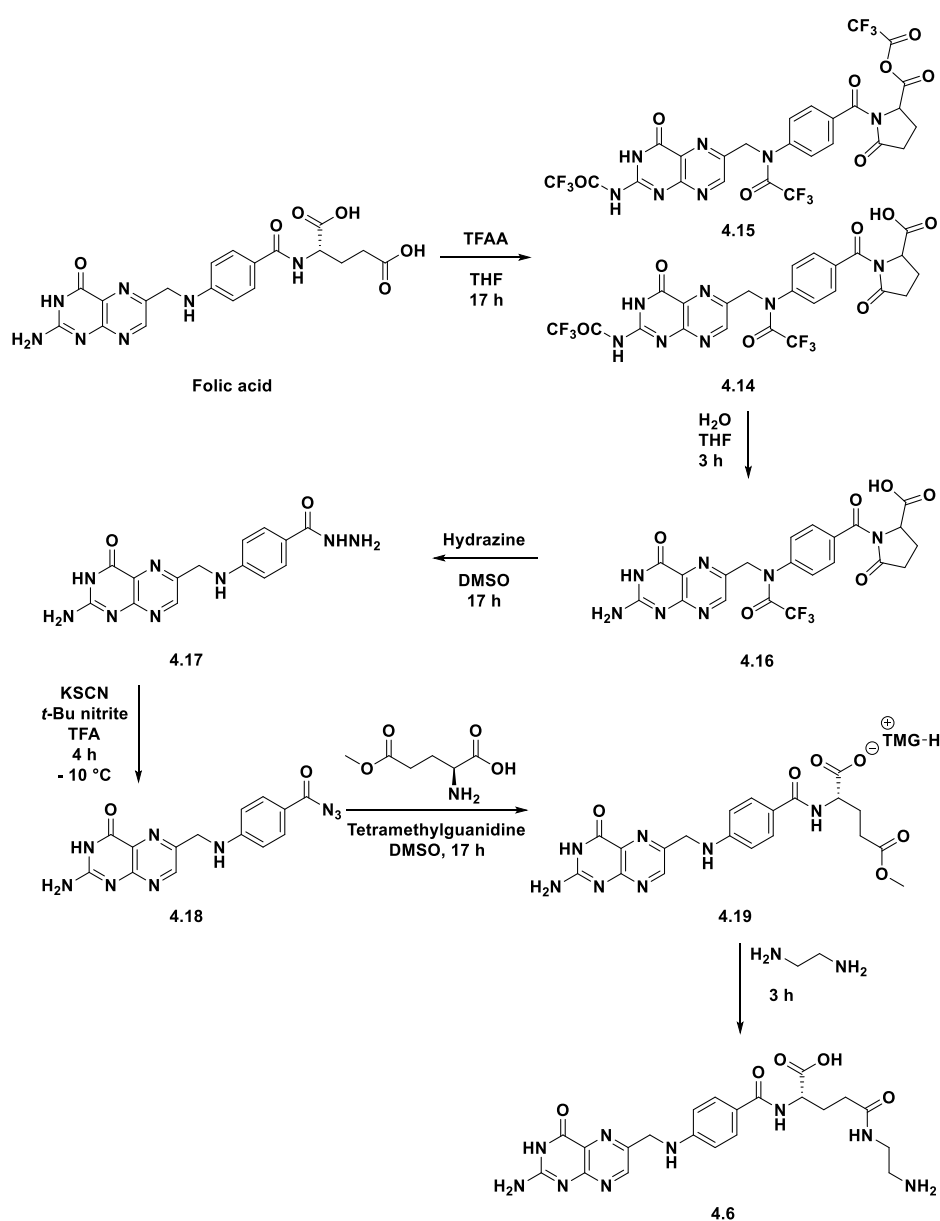
Figure 4.12: Structures of **a) PyBOP** and **b) TBTU**

The crude products of both these solution phase reactions were analysed by analytical RP-HPLC where three product peaks were observed at 10.15, 10.26, and 10.39 min for the PyBOP synthesis and 9.96, 10.14 and 10.37 min for the synthesis with TBTU. After separation of these peaks, the resulting products were analysed by MALDI mass spectrometry. Two of these product peaks showed a m/z of 526 and the third a m/z of 610, corresponding to $[\text{M}+\text{H}]^+$ of two products with the mass of mono-substituted folic acid and the mass of di-substituted folic acid respectively. As two peaks possess the mass of singly substituted folic acid, it is likely these are the α - and γ -conjugates, and no clear selection of the γ -conjugate has occurred.

It was also attempted to form the γ -conjugate of folic acid through an NHS ester, again hoping that the less hindered conjugate would be favoured. Folic acid was activated with one equivalent of DCC/NHS, then 3-(dimethylamino)-1-propylamine was added to react with the activated NHS ester. Analysis of the resulting product again showed the presence of two major products with retention times of 10.26 and 10.52 min. These products were separated, and both showed a m/z of 526, corresponding to the two isomers of 3-dimethylaminopropylfolic acid. Again, no selectivity was observed towards the γ -isomer of folic acid. As all attempts to use steric control for the conjugation of folic acid were unsuccessful, further manipulation of folic acid to encourage the selective γ -conjugation was explored.

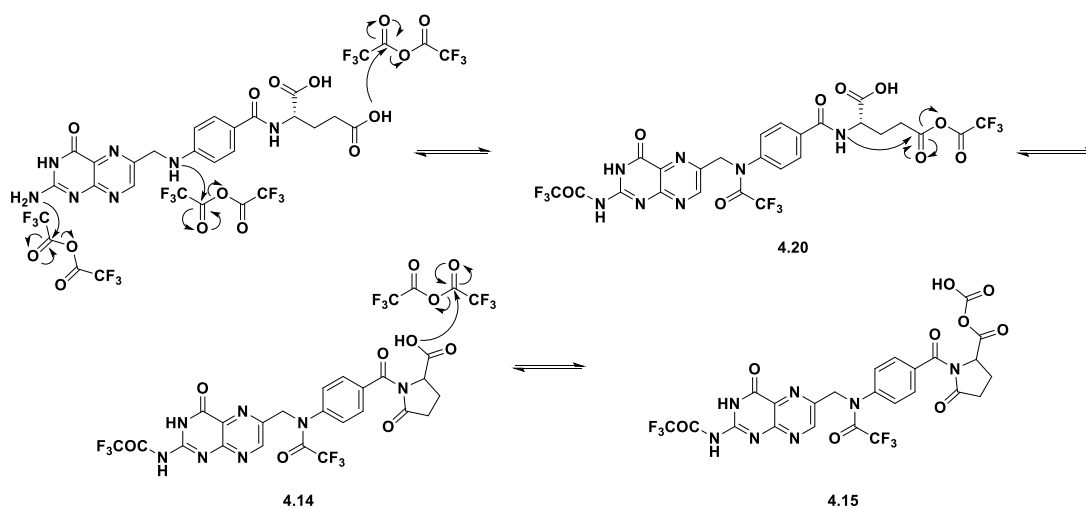
4.3.2 Synthesis of folate ligand 2-aminoethylfolic acid

Two chemical manipulations of folic acid to form solely the γ -conjugate have been reported; the use of N¹⁰-TFA-pteronic acid (**4.8**) on the solid phase^{31,32} and the solution phase manipulation to form 2-aminoethylfolic acid (**4.6**).^{30,93} While the solid phase manipulation involves less steps, **4.8** is expensive and the synthetic procedure is time consuming, with some steps taking over a week.⁹⁴ For these reasons, the synthesis of **4.6** was explored to form selective folate conjugates. **4.6** selectively adds a terminal amine onto the γ -carboxylic acid of folic acid, and this change of terminal functional group on the desired conjugation site provides an attractive way of controlling the conjugation.^{30,93} The synthesis of **4.6** involved a six-step manipulation of folic acid (**Scheme 4.3**).



Scheme 4.3: Synthesis of 2-aminoethylfolic acid (**4.6**)

Firstly, folic acid was reacted with trifluoroacetic anhydride to form a mixture of $N^{2,10}$ -bis(trifluoroacetyl)pyrofolate acid (**4.14**) and $N^{2,10}$ -bis(trifluoroacetyl)pyrofolate anhydride (**4.15**). All the amines present in folic acid can undergo nucleophilic attack on the trifluoroacetic anhydride to form amides, as shown in **Scheme 4.4**. The trifluoroacetic anhydride also reacts with both carboxylic acids in folic acid, forming mixed anhydrides (**4.20**). The amide nitrogen can then undergo nucleophilic addition to the γ -anhydride, causing a cyclisation to occur. The α -anhydride could also undergo this cyclisation, but the resulting three-membered ring would be highly strained, so this reaction is highly unfavourable. The formation of the mixed anhydride/acid was confirmed by the appearance of three peaks in the ^{19}F -NMR, corresponding to the two trifluoroacetate groups and the anhydride. This reaction yields a crude mix of the anhydride and acid that was taken straight forward into the next step of the synthesis, without further characterisation and purification.



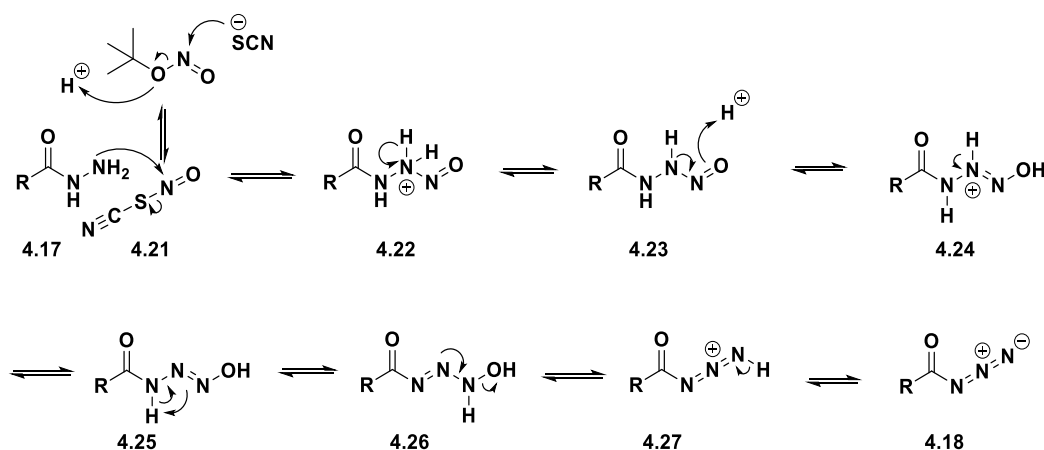
Scheme 4.4: The mechanism for the synthesis of **4.14** and **4.15** from folic acid and trifluoroacetic anhydride

The addition of ice to the crude mixture of **4.14** and **4.15** yielded N^{10} -bis(trifluoroacetyl)pyrofolate acid (**4.16**) through a hydrolysis, releasing trifluoroacetic acid. Both the anhydride and trifluoroacetate groups on secondary amides are hydrolysed but the higher nucleophilicity of the tertiary amide prevents the hydrolysis. It is possible that the hydrolysis of these groups is not complete as three fluoride peaks are still present in the ^{19}F -NMR, or that some of the eliminated TFA is forming salts with the product, and therefore still present in the product. To attempt to drive the reaction, the mixture was heated to 40 °C for three hours, yet this did not have any effect on the presence of these

fluorine peaks. The shift in the ppm of two of these peaks suggests that some alteration has occurred to their chemical environment, possibly suggesting they are now present as TFA salts. As the ^1H - and ^{13}C -NMRs showed accordance with the data provided by Luo *et al.*, and the next step of this reaction involved the addition of a strong base that would drive the hydrolysis to completion, no further alterations were made to the reported method to attempt to remove these peaks from the fluorine NMR.

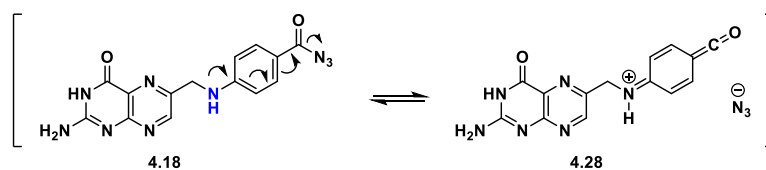
The next step of this manipulation involved the reaction of **4.16** with hydrazine monohydrate to form pteroyl hydrazide (**4.17**). Hydrazine monohydrate undergoes nucleophilic attack on the benzyl carbonyl, followed by elimination of the pyrrolidinone. The hydrazine also undergoes nucleophilic attack on the trifluoroacetate, with its removal giving the secondary amine. The success of this reaction could be determined by the loss of the four proton resonances between 2.70 and 2.00 ppm and a resonance at 4.77 ppm in the ^1H NMR spectra due to the elimination of the pyrrolidinone which contains these aliphatic protons. Additionally, a m/z of 327 was observed which corresponded to the desired product.

4.17 was next reacted with potassium thiocyanate and *tert*-butyl nitrite. Potassium thiocyanate acts catalytically as a potent nitrosating agent, reacting with *tert*-butyl nitrite to form nitrosyl thiocyanate (**4.21**). This highly reactive species can undergo electrophilic attack from the terminal amine of the hydrazine, leading to the elimination of thiocyanate and the formation of an *N*-nitrosamine (**4.23**).⁹⁵ The *N*-nitrosamine then undergoes a dehydration reaction, yielding the azide, as shown in **Scheme 4.5**. A mixture of pteroyl azide (**4.18**) and N^{10} -nitrosopteroyl azide is formed. Since the nitrosyl thiocyanate can also react with the secondary amine between the two aromatic groups in the same way, yet the primary amine is more reactive, and as one equivalent of *tert*-butyl nitrite is added, the major product is the terminal azide. N^{10} -nitrosopteroyl azide can be easily converted to pteroyl azide by the addition of sodium azide. The acidic conditions lead to the protonation of the nitrosamine, to which the azide is a strong nucleophile, resulting in the elimination of a nitrosated azide as the formation of secondary nitrosamines is reversible.⁹⁶ Again, this nitrosyl azide can act as a nitrosating agent, but the rate of the nitrosation of the azide is much faster than that of nitrosyl azide nitrosating another molecule, resulting in **4.18** as the main product.⁹⁷ The formation of **4.18** was confirmed by presence of a peak at 2137 nm in the IR spectrum, suggesting an azide moiety is present, and crude **4.18** was carried forward in this synthesis.



Scheme 4.5: The mechanism for the formation of pteroyl azide

The addition of *L*-glutamic acid 5-methyl ester and tetramethylguanidine resulted in a product of tetramethylguanidinium *L*-methyl folate (**4.19**). Pteroyl azide can undergo an imine/enamine tautomerisation, resulting in the elimination of the azide to give *p*-quinoketene monoamine (**4.28**), as shown in **Scheme 4.6**.³⁰



Scheme 4.6: Tautomerisation of **4.18**: pteroyl azide (**4.18**) and *p*-quinoketene monoamine (**4.28**), highlighting in blue the amine deprotonated by tetramethylguanidine to encourage the elimination of the azide.

The tetramethylguanidine can deprotonate the amine of the *p*-aminobenzoyl azide, highlighted in blue, leading to the elimination of the azide, encouraging the formation of the *p*-quinoketene tautomer. The amine of the protected glutamate is highly reactive towards this structure, leading to a high yield of **4.19**, which exists as a tetramethylguanidinium salt. The formation of **4.19** leads to the return of the general structure of folic acid, but notably with the alteration of a methyl ester selectively at the γ -conjugation site. The synthesis of **4.19** was confirmed by the appearance of eight resonances between 4.05-1.90 ppm in the ¹H-NMR spectra, corresponding to the aliphatic protons in the glutamate chain. These can be seen as a multiplet at 4.05 ppm with an integration corresponding to one hydrogen, due to the proton adjacent to the amide (1-CH, **Figure 4.13**), a singlet at 3.55 ppm with an integration corresponding to three hydrogens, due to the methyl ester, and a multiplet between 2.43 and 1.90 ppm with

an integration corresponding to 4 hydrogens, due to the adjacent methylenes in the glutamate chain (2-CH₂ and 3-CH₂). The tetramethylguanidinium salt can also be clearly observed in the ¹H NMR as a singlet at 2.90 ppm with an integration corresponding to the 12 methyl hydrogens. Further confirmation that this is due to the presence of **4.19**, not a mixture of the starting materials, was found by high resolution ion trap time of flight (IT-ToF) mass spectroscopy, with a m/z of 478.1452 observed, consistent with that of an **4.19** sodium adduct.

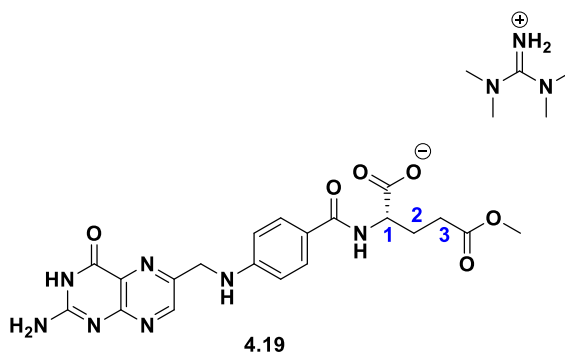


Figure 4.13: The structure of **4.19**, highlighting new ¹H-NMR resonances observed upon its synthesis

Finally, **4.19** was reacted with neat ethylenediamine, yielding **4.6** through a nucleophilic substitution of the γ -methyl ester. Using neat ethylenediamine drives the reaction to completion as a large excess is present. Following purification with water and acetone precipitations, **4.6** was further purified by preparative RP-HPLC to ensure high purity. The synthesis of **4.6** was confirmed by IT-ToF with a m/z of 484.2064 observed, matching the expected mass.

Once the synthesis of **4.6** was confirmed, it was important to determine whether cells could tolerate this ligand, or whether **4.6** itself would induce cytotoxicity. To test for the possible cytotoxicity of **4.6**, an FR α positive non-small cell lung cancer (NSCLC) cell line was required.

4.3.3 Determination of the presence of FR α and cytotoxicity of 4.6

NSCLC cell lines A549 and H292 were tested for the presence of FR α using flow cytometry, as described in **section 2.3.2**. A primary anti-FR α antibody and a goat anti-mouse FITC secondary antibody were incubated alongside H292 and A549 cells. **Figure 4.14** shows the flow cytometry histograms of fluorescence intensity for each sample. H292 cells displayed a large increase in fluorescence upon incubation with the anti-FR α

antibody, suggesting the presence of FR α on H292 cells. A549 cells showed no increase in fluorescence intensity upon incubation with the anti-FR α antibody, suggesting that A549 cells are negative for FR α . These results provide a cell line that can be targeted by folate-directed nanoparticles, and a control cell line to determine the selectivity of these nanoconjugates.

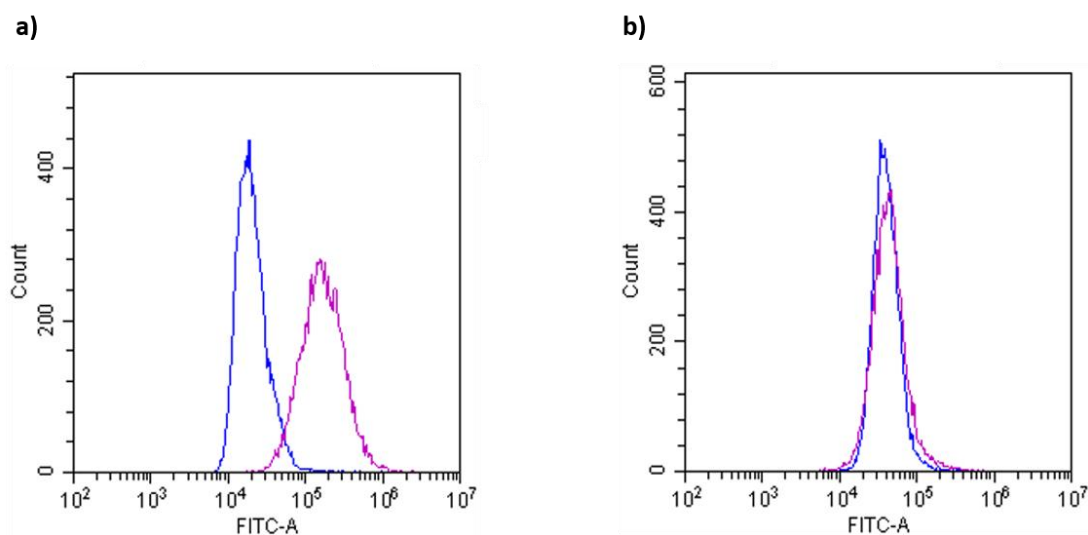


Figure 4.14: Flow cytometry histograms of **a)** H292 and **b)** A549 cells incubated with anti-FR α antibody then FITC-goat anti-mouse secondary antibody (purple) or just with the secondary antibody (blue).

As H292 cells were seen to be positive for FR α , these cells were used to assess **4.6** for any cytotoxicity towards FR α expressing cell lines using the cell proliferation assay 3-(4,5-dimethylthiazol-2-yl)-5-(3-carboxymethoxyphenyl)-2-(4-sulfophenyl)-2H-tetrazolium (MTS). H292 cells were seeded in 96 well plates and grown overnight at 37 °C, 5% CO₂. Following incubation with **4.6**, the cell viability was assessed with MTS. Negligible cytotoxicity was observed in H292 cells treated with up to 25 μ M, as seen in **Figure 4.15**, suggesting that **4.6** can be used as a targeting ligand without inducing cytotoxicity.

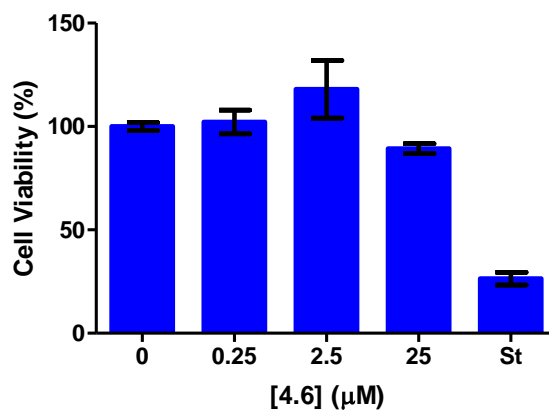


Figure 4.15: Cell viability of H292 cells incubated with **4.6** using an MTS assay. St = 30 μM staurosporine positive control

4.3.4 Functionalisation of C11Pc-PEG-AuNPs with 2-aminoethylfolic acid

4.6 provides the opportunity to now only conjugate through the γ -acid as the reactivity of the two termini are dramatically different. The presence of the free amine on **4.6** allows for its direct conjugation to HS-PEG-COOH. Due to the free carboxylic acid still present on **4.6**, the carboxylic acid terminus of HS-PEG-COOH was first activated with DCC/NHS/triethylamine to form an NHS ester, then the coupling agents removed to prevent activation of the carbonyl on **4.6**. After activation, **4.6** was added to the PEG-NHS ester in DMSO and stirred overnight. The low solubility of **4.6** in non-polar solvents allowed for the retrieval of the product by addition of diethyl ether, and any remaining DMSO was removed with multiple washes of diethyl ether. This **4.6**-PEG (**4.29**) was used to form **4.6**-C11Pc-PEG-AuNPs (**4.30**) in a 1:1 ratio with C11Pc. The synthesis was completed in a THF/H₂O mix and purified as described in **section 2.3.2.1**. The resulting nanocarriers were analysed by UV-vis spectroscopy, with the spectrum shown in **Figure 4.16**. The UV-vis spectrum shows the characteristic double peak of C11Pc, and the lack of surface plasmon resonance band confirms the gold core of these nanoconjugates is below 5 nm in size, as described in **section 2.3.2.1**.^{98,99} Unfortunately, as folic acid absorbs strongly at 280 nm, and at this wavelength the absorbance from the AuNPs is strong, this UV-vis spectrum cannot be used to estimate the concentration of folic acid on the nanocarriers.

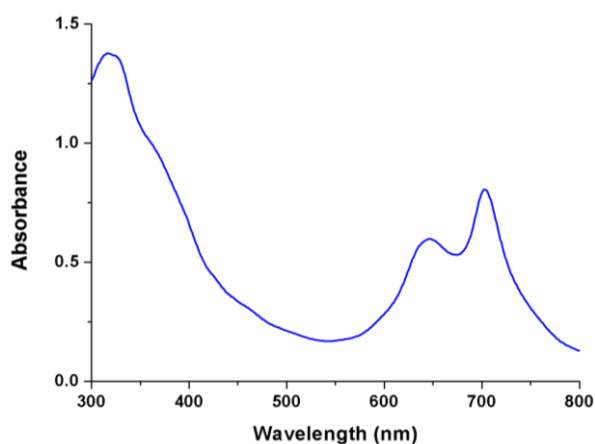


Figure 4.16: UV-vis spectrum of **4.30** in PBS

4.3.5 Singlet oxygen production

The ability of **4.30** to produce singlet oxygen was tested using the singlet oxygen probe ABMA in PBS, as described in **section 2.3.2.3**. Upon irradiation, these nanocarriers showed no singlet oxygen production over 30 minutes, as shown in **Figure 4.17a**. This is perhaps not surprising as folic acid is known to be an antioxidant¹⁰⁰ and to show the ability to quench singlet oxygen.^{101,102} It is possible that the folic acid is quenching the singlet oxygen that is produced before it has a chance to react with ABMA due to a much closer proximity to the phthalocyanine, with the folate reaction being intramolecular and the ABMA photobleaching intermolecular. However, many groups have reported the use of folic acid as a targeting ligand for photosensitisers, and so the ratio of PEG:**4.29** was varied to determine if there was an optimum point at which this antioxidant/quenching effect could be overcome but the targeting ability of the folic acid maintained. **4.6-C11Pc-PEG-AuNPs** were synthesised with ratios of PEG:**4.29** of 75:25 (**4.31**), 90:10 (**4.32**) and 95:5 (**4.33**). Singlet oxygen production studies were completed using ABMA on each of these **4.6**-conjugated nanocarrier systems with no significant singlet oxygen production observed for any ratio PEG:**4.29** (**Figure 4.17b**).

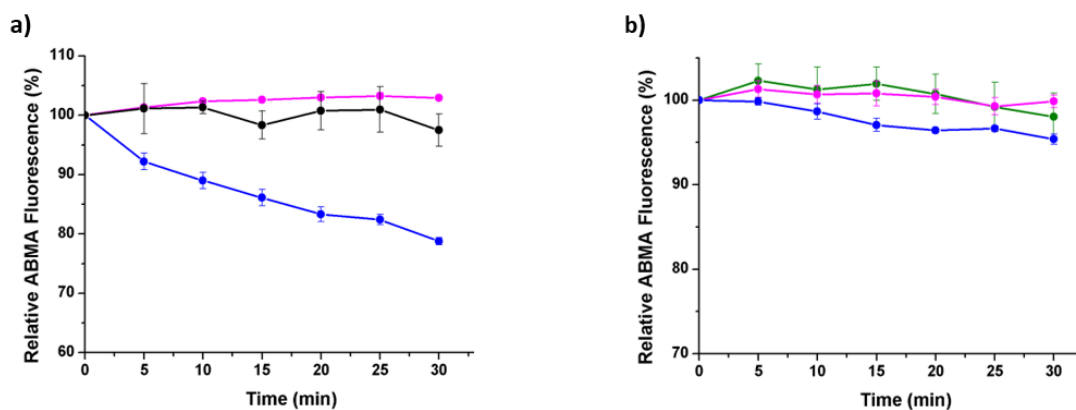


Figure 4.17: **a)** singlet oxygen production of **4.30** (pink), PEG-AuNPs (black) and C11Pc-PEG-AuNPs (blue). **b)** singlet oxygen production of, **4.31** (blue), **4.32** (pink) and **4.33** (green). All AuNPs were assessed in PBS at 1 μ M C11Pc and 1 μ M ABMA

4.3.6 Towards a cathepsin B cleavable linker

To overcome the lack of singlet oxygen production, the cathepsin B cleavable linker Val-Cit-PABA, described in **section 4.1.6**, can be employed. This allows for the cleavage of the folic acid from the nanoconjugates post cellular internalisation, with the aim of ‘switching on’ the activity of the C11Pc-PEG-AuNPs once delivered to the target tumour cells. This cleavable sequence can be built by solid phase peptide synthesis, but to attach **4.6** to the solid phase a linker is required that will link two amines. For this, glutaric acid (**4.34**, **Figure 4.18**) was employed.

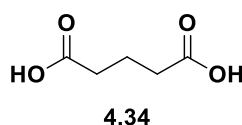


Figure 4.18: The structure of glutaric acid (**4.34**)

4.3.6.1 Development of an amine cross-linker for the solid phase

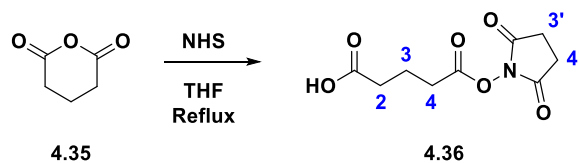
4.34 has been used as a linker in solution phase chemistry, often in excess to encourage mono-substitution, before the second component is added to the solution.^{103,104} Disuccinimidyl glutarate has also been employed in high excess in solution to allow the addition of a glutaric linker between peptides, forming amide bonds at each terminus of the glutaric acid.¹⁰⁵ Examples of more controlled substitution exist using glutaric anhydride (**4.35**) and various coupling agents or bases to form esters.^{106,107} The use of **4.35** means that only the mono-ester can be produced and prevents the formation of di-

substituted glutaric acid. While glutaric spacers are used readily in solution phase chemistry, there are few examples of its use on the solid phase.

On the solid phase, three synthetic pathways for the addition of a glutaric acid (**4.34**) spacer have been reported with increasing complexity. The first method involves the addition of **4.35** and *N*-methylmorpholine and results in the addition of **4.34** through an amide bond to the resin-bound peptide chain.¹⁰⁸ A second report uses mono-allyl protected glutaric acid for the addition to the solid phase, followed by an allyl ester deprotection using Pd(PPh₃)₄ and phenylsilane.¹⁰⁹ The third report involves the ring opening of a glutaric anhydride derivative with Fmoc-hydrazine to yield 5-(*N'*-Fmoc-hydrazyl)-5-oxo-3-pentanoic acids.¹¹⁰ These can then be Fmoc-deprotected leaving a hydrazine, but this technique leaves a free amine upon deprotection and is not suitable for reversing the reactivity on the solid phase.

In this thesis, we developed a fourth method for the addition of **4.34** to the solid phase. **4.35** reacts with NHS under reflux to form a mono-NHS ester, 5-(2,5-dioxopyrrolidin-1-yl)oxy-5-oxopentanoic acid (**4.36**, **Scheme 4.7**). Amines are highly reactive towards NHS esters, and the formation of a mono-NHS ester meant that there was no cross-linking of glutaric acid between two peptides on the solid phase. This synthetic pathway was followed as the activation of **4.35** could be confirmed and the high reactivity of the NHS-ester meant a highly efficient conjugation occurs. This was chosen over other protected glutaric acid residues due to ease of synthesis as no deprotection step was required. The synthesis of **4.36** was confirmed by ¹H-NMR. **4.35** shows a triplet at 2.75 ppm with an integration of four, suggesting the presence of four hydrogens, and a multiplet at 2.03 ppm with an integration of two, suggesting the presence of two hydrogens. NHS shows a singlet at 2.79 ppm with an integration of four. The resulting **4.36** showed a singlet at 2.82 ppm (4H) corresponding to the NHS protons (3'-CH₂, 4'-CH₂, **Scheme 4.7**), a triplet at 2.71 ppm (2H) corresponding to the protons on the α -carbon to the NHS-ester (4-CH₂), a triplet at 2.50 ppm (2H) corresponding to the protons on the α -carbon to the carboxylic acid (2-CH₂), and a multiplet at 2.04 ppm (2H) corresponding to the central carbon β to both moieties (3-CH₂). For all syntheses using **4.36**, a crude mixture was utilised as none of the starting materials were able to react with the free amine, and since the reagents are used in such high excess for solid phase peptide synthesis, a small amount of impurities will not affect the final product. **4.35** also contains a small amount of the hydrolysis product **4.34**, notable on the ¹H-NMR, but this cannot spontaneously react

with a free amine so does not present a concern for further use of the crude product mixture.

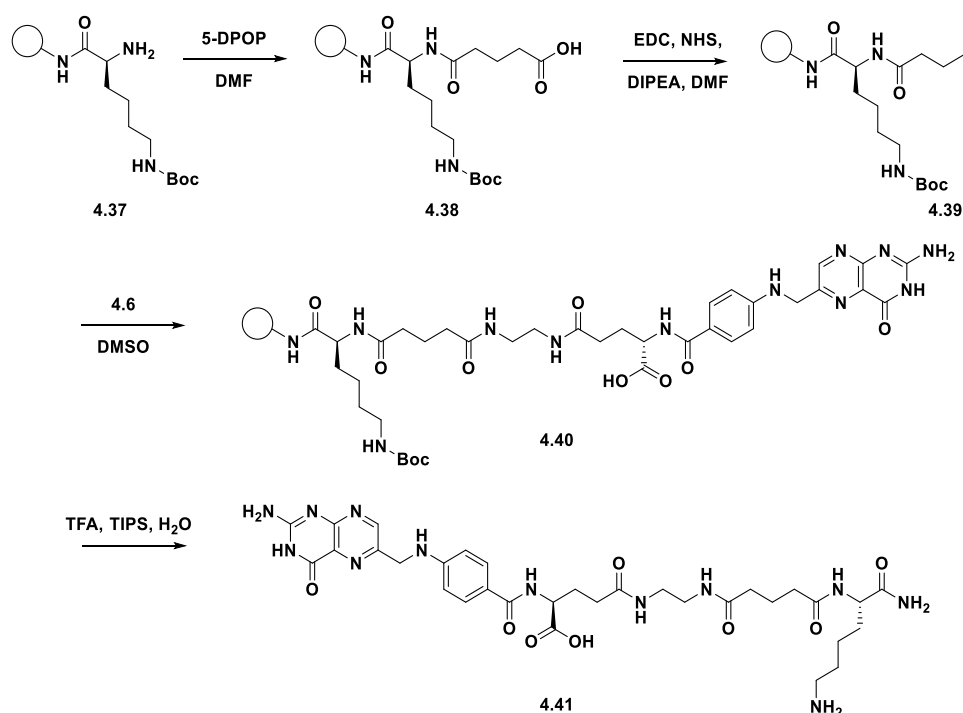


Scheme 4.7: The synthesis of 5-(2,5-dioxopyrrolidin-1-yl)oxy-5-oxopentanoic acid from glutaric anhydride

Addition of **4.36** to the free N-terminus of lysine on the solid phase allows for the efficient addition of the linker with the assurance that only one end of the linker will react with the solid phase. **4.36** was simply dissolved in DMF and mixed with the resin functionalised with lysine. This reaction was allowed to proceed overnight to ensure a high level of conjugation, and the addition of the NHS-ester provides no concerns for further reactions to produce unwanted byproducts. The addition of glutaric acid was assessed using malachite green oxalate after washing the resin with methanol. Malachite green oxalate (0.25% w/v in EtOH) and a single drop of trimethylamine can be mixed with the solid phase resin for three minutes, and if the resin possesses a free carboxylic acid, the malachite green will form a salt with the deprotonated acid. Washing of the resin with methanol removes excess dye and leaves a green resin if a carboxylic acid is present.¹¹¹ This was trialled with glutaric acid functionalised resin, which turned bright green on addition of malachite green. Rink amide MBHA resin and resin functionalised with lysine with the amine terminus free were tested as controls. Both these controls resulted in a colourless resin after washing, so malachite green oxalate was used throughout the rest of this chapter to routinely check for the presence of a carboxylic acid on the solid phase resin.

Once the coupling of the **4.36** to lysine was confirmed, **4.6** could be conjugated on to this growing peptide through its amine terminus. However, as there is still a free carboxylic acid on **4.6**, normal coupling conditions of HATU/DIPEA could not be utilised as this could lead to chains of polymerised **4.6**. Instead, the terminal carboxylic acid on the resin was activated by reaction with EDC/NHS, catalysed by DIPEA.¹¹² The reaction was left to proceed for two hours, then the excess EDC/NHS was washed away and **4.6** added to the solid phase in DMSO and shaken overnight. Upon cleavage from the resin in 95:2.5:2.5 TFA:TIPS:H₂O, the resulting glutaric linked peptide (**4.41**, **Scheme**

4.8), was obtained. The synthesis of this peptide was confirmed by high resolution IT-ToF mass spectrometry, with an m/z of 382.1554 observed, corresponding to the mass of a doubly charged potassium adduct of the peptide.



Scheme 4.8: The synthesis of **4.41** on the solid phase

4.3.6.2 Employment of **4.36** to synthesise a cathepsin B cleavable folate linker

Once the ability to use **4.36** to reverse the reactivity of the solid phase was confirmed, the cleavable sequence could be built. Rink amide MBHA resin was used to build the cleavable sequence, with lysine added to the C-terminus of the sequence to provide an amine side chain for conjugation to PEG. Once the peptide V-Cit-PABA-K (**4.42**) was built on the resin, **4.36** was reacted with the N-terminus of valine, allowing the addition of **4.6** as shown for peptide **4.41**, to give peptide CatB cleavable peptide **4.43** (Figure 4.19). While a small amount of peptide **4.43** was obtained in this synthesis, analysis by analytical RP-HPLC showed a large number of products upon the cleavage of this peptide, and peptide **4.43** was not the major product.

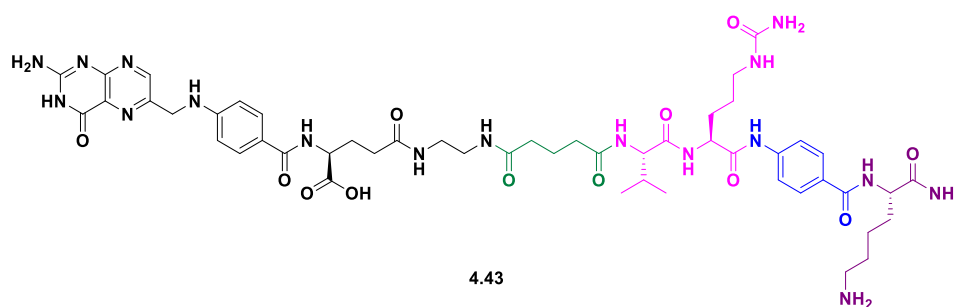


Figure 4.19: Structure of **4.6** cleavable sequence (**4.43**), showing **4.6** (black), glutamic linker (green), cleavable sequence (pink), PABA spacer (blue) and terminal lysine (purple) for coupling the peptide onto nanoparticles

To assess whether the peptide was being degraded under the harsh cleavage conditions used for peptide cleavage from rink amide resin (95:2.5:2.5 TFA:TIPS:H₂O, 3 h), peptide **4.43** was synthesised on rink amide MBHA resin, then the resulting resin split into three peptide columns. These were treated with three different cleavage cocktails to determine the effect of the TFA concentration on the resulting peptide. One column was treated with 95:2.5:2.5 TFA:TIPS:H₂O, the next with 65:30:2.5:2.5 TFA:DCM:TIPS:H₂O and the third with 47:48:2.5:2.5 TFA:DCM:TIPS:H₂O. Each cleavage was allowed to proceed for 3 hours, before the solvent was removed under vacuum and the resulting peptide washed with diethyl ether. The analytical HPLC traces obtained for each of these cleavage cocktails were near identical with a lot of peaks present in the trace, suggesting that the TFA concentration in the cleavage cocktail is not responsible for the mixture of products.

While the addition of **4.36** onto lysine on resin has been shown to be successful, it is possible that the differing steric bulk of valine could be less favourable for the addition of **4.36**, resulting in a lower conjugation efficiency and therefore a less clean reaction. To assess the versatility of **4.36** addition to amino acids on resin, a screen of amino acids was completed. A variety of amino acids were conjugated onto rink amide MBHA resin, and then coupled to **4.36** overnight. Valine provides a relatively high steric bulk near the N-terminus compared to most other amino acids. To assess whether this had any effect on **4.36** coupling, valine, leucine and alanine were tested. Leucine differs from valine due to a CH₂, which moves the steric bulk further away from the N-terminus amine, so if steric bulk is influencing this addition, more efficient coupling should be observed for leucine than valine. Alanine has the smallest side chain of the amino acids, with its side chain a single methyl group, and therefore has the lowest steric bulk. Again, if steric bulk is affecting this addition, alanine should display efficient conjugation if additions to leucine and valine are sterically hindered.

As lysine has been shown to conjugate to **4.36** on resin, arginine was also screened to determine the versatility of this coupling on aliphatic, basic residues. Phenylalanine and tryptophan were assessed to determine whether aromatic side chains had any influence on the conjugation and glutamic acid was tested to see the effect of acidic side chains. After conjugation, each resin was tested with malachite green for the presence of a carboxylic acid and therefore for the addition of **4.36**. As seen in **Figure 4.20**, each amino acid-**4.36** combination showed a positive result in the Malachite green test for the presence of a carboxylic acid.



Figure 4.20: Malachite green test for coupling of **4.36** on the solid phase to appropriately protected (L-R) arginine, tryptophan, phenylalanine, glutamic acid, valine, lysine, alanine and leucine. All reactions were completed on rink amide MBHA resin

The resulting peptides were cleaved from the resin using 95:2.5:2.5 TFA:TIPS:H₂O, then crude ¹H-NMR of each peptide collected. For each amino acid screened in this study, the crude ¹H-NMR showed the presence of the desired peptide. For each peptide there was no evidence of unreacted amino acid in the ¹H-NMR so it can be concluded that these couplings proceeded to near completion, as shown in **Figure 4.21** for Val-**4.36** (**4.44**), with the assignment provided to confirm its synthesis. Interestingly, in this spectrum the diastereotopic methyl groups on the valine residue appear as two overlapping doublets of 3H instead of the expected doublet of 6H, as seen at 0.97 and 0.96 ppm on the insert of **Figure 4.21**. Further 2D NMR spectra confirmed that this unexpected splitting pattern was indeed due to these methyl groups and that they are in some way inequivalent in this molecule, possibly due to hindered rotation. Due to the small size of these dipeptides, they have very low UV absorbance so their purity was hard to assess by other means. This result both highlighted the applicability of the use of **4.36** to reverse the reactivity on the solid phase and confirmed the reactivity of valine towards **4.36**, making a lack of reactivity at this point in the sequence of **4.43** a very unlikely reason for the impure product.

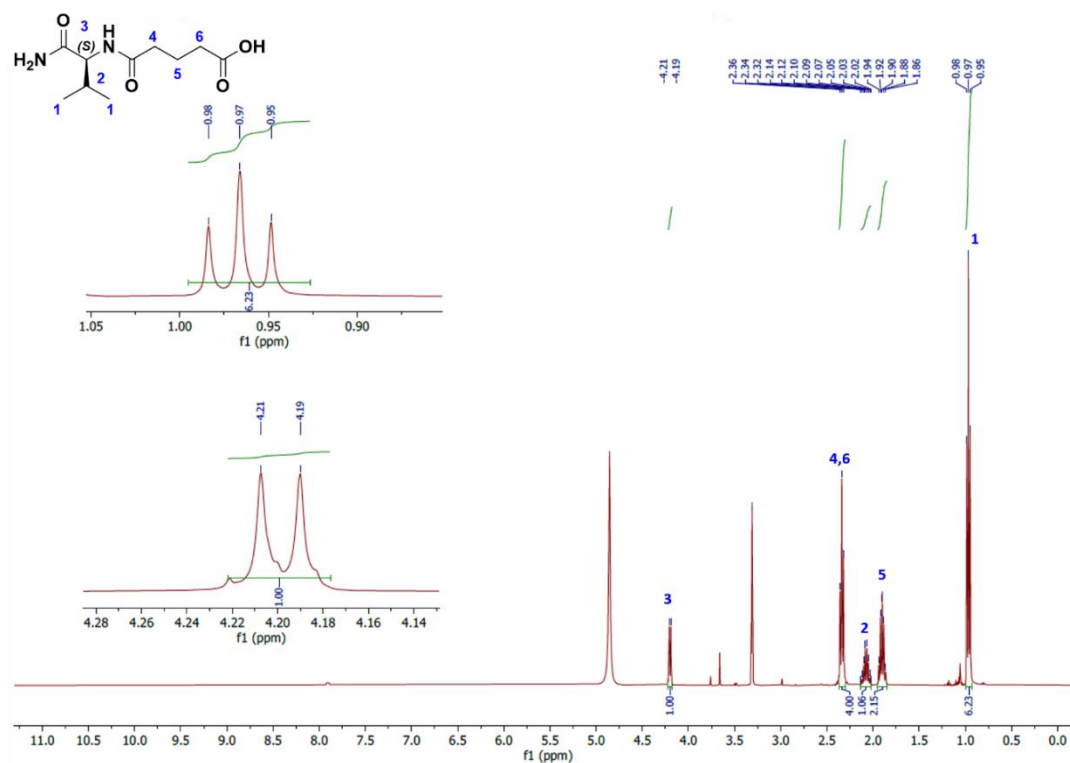


Figure 4.21: Structure and crude ^1H NMR of **4.44**. Inserts show magnifications of CH_3 (**1**) and CH (**3**) of valine, showing that there is no smaller peak of unconjugated valine present, suggesting this reaction has gone to completion

The activation of the resin-bound **4.36** by EDC/NHS was investigated to determine whether the initial conditions of five equivalents of coupling agent left to react for two hours was ideal. For this, resin functionalised with lysine-**4.36** was split into four reaction vessels. Two were treated with five equivalents of EDC/NHS/DIPEA and the other two with ten equivalents. Of these, one of each equivalence was allowed to proceed for two hours and the other for three. After this, the resin was washed with DMF, then 1.2 equivalents of **4.6** in DMSO was immediately added to each resin and shaken overnight. The resulting peptides were cleaved from the resin in 95:2.5:2.5 TFA:TIPS:H₂O and their purity assessed by analytical HPLC, with their traces shown in **Figure 4.22**. Two major peaks were seen in each spectrum, and each peak was isolated and the mass determined by MALD-ToF. The first peak ($t_R = 10.0$ mins) shows a m/z of 838, corresponding to the $[\text{M}+\text{Na}]^+$ of peptide **4.41** with the Boc protecting group still present on the lysine residue. The second peak ($t_R = 10.5$ mins) shows a m/z of 724, corresponding to the $[\text{M}+\text{H}]^+$ peak of peptide **4.41**. Most notably here, there does not appear to be an increase in side products upon longer EDC/NHS activation times, or with higher equivalents, so increasing the reaction time may allow for more efficient **4.6** coupling.

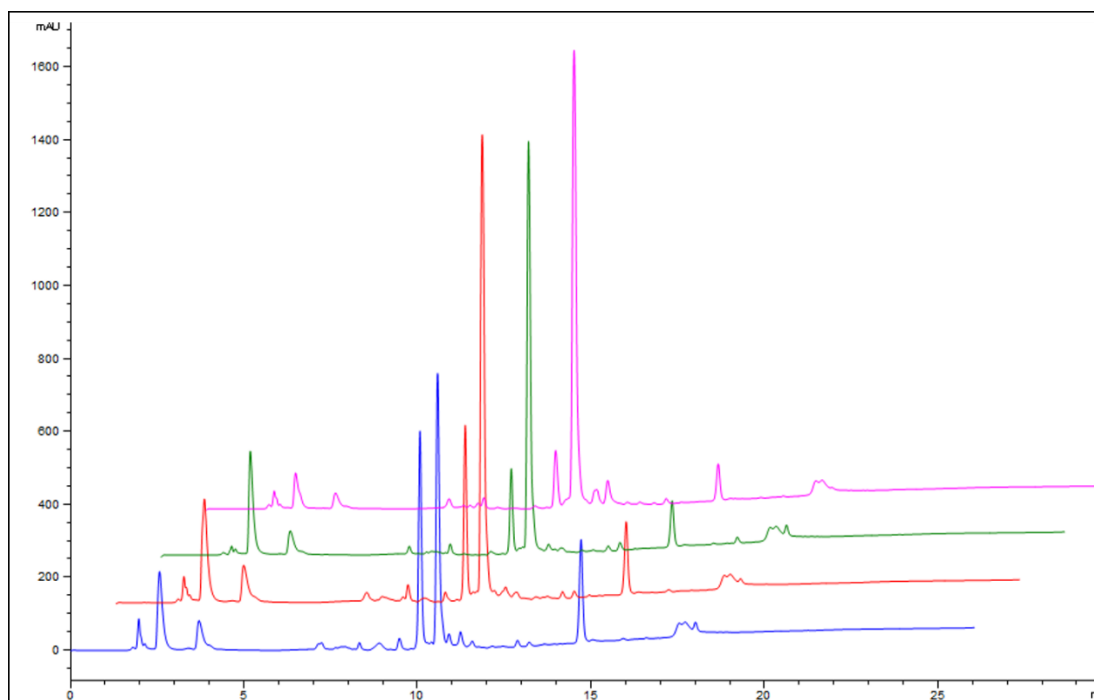


Figure 4.22: HPLC traces of peptide **4.41** following synthesis using different equivalents of EDC/NHS/DIPEA and different reaction times, recorded at 214 nm: 5 eq 2 h (blue), 5 eq 3 h (red), 10 eq 2 h (green), 10 eq 3 h (pink). Spectra are offset by 1.25 minutes to allow for easier comparison

To determine the efficiency of the synthesis of the cleavable sequence, the peptide was cleaved from the resin after the automatic synthesis of V-Cit-PABA-K (**4.42**) and after the addition of the **4.36** linker. The analytical RP-HPLC of the resulting peptide after the automated synthesis showed multiple peaks (**Figure 4.23**) suggesting the synthesis of **4.42** did not proceed as expected. To increase the yield of the desired peptide **4.43**, the synthesis of **4.42** must be improved to result in a single product after the automatic peptide synthesis. It is possible that the addition of spacers such as β -alanine or the use of a different resin may improve the purity of the resulting peptide. For example, NovaPEG rink amide resin could be used in the place of rink amide MBHA resin. NovaPEG resin swells more than MBHA, leading to more space between the growing peptide chains. Furthermore, NovaPEG resin has been shown to increase the yield of hydrophobic peptides and can increase the efficiency of the synthesis of difficult peptide sequences. A low loading rink amide resin could also be trialed to space out the growing peptide chains and to allow for more efficient couplings.

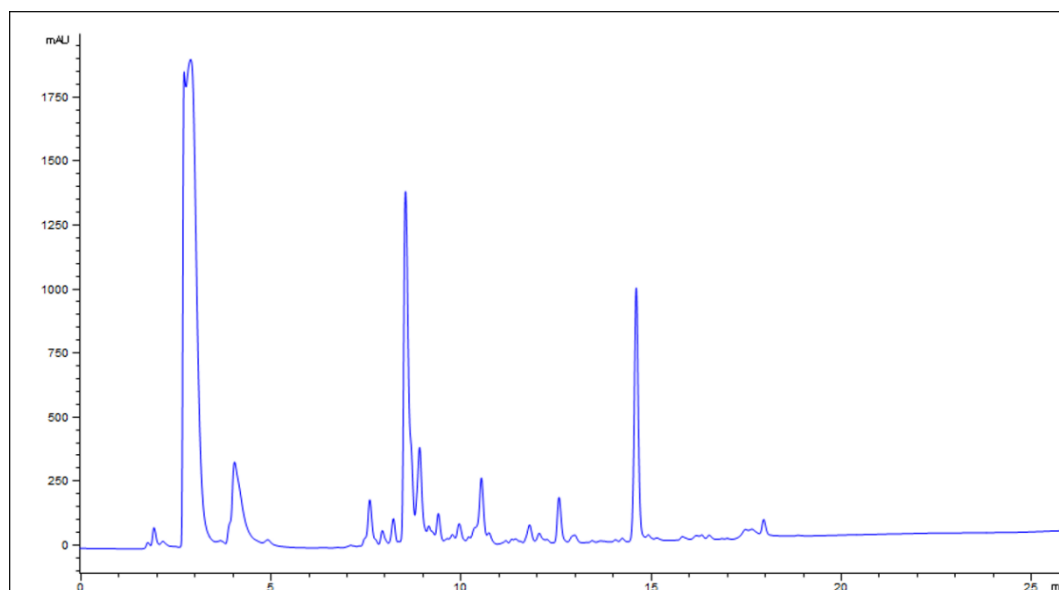


Figure 4.23: HPLC trace of cleavable sequence **4.42**, recorded at 214 nm

4.4 Conclusions and future work

Folic acid has been widely investigated as a targeting agent for AuNP-based therapeutics, but often very little consideration is taken towards the selectivity of the conjugation of folic acid to these AuNPs. Folic acid has been shown to only be active towards the FR α when conjugated to the nanocarrier through the γ -carboxylic acid. Most reports of folic acid addition use amide bond formation chemistry such as DCC/NHS which are not selective towards the γ -carbonyl. While reports have shown that these conjugations occur in a *ca.* 70:30 ratio in favour of the γ -conjugate, there is inactive α -conjugated folic acid present on these systems. This ratio varies from batch to batch so the number of active targeting moieties is not consistent between batches, raising variability in the delivered dose.

Interestingly, both cooling and heating folate coupling reactions has been reported to selectively produce the γ -conjugate. Heating folic acid to 30 °C upon the solid phase with PyBOP as a coupling agent and cooling folic acid to 0 °C in solution with TBTU and PyBOP coupling agents were trialled in this thesis. These reaction conditions, however, all resulted in a mixture of the α - and γ - conjugates, as observed by analytical RP-HPLC. In this thesis, the chemical manipulation of folic acid to produce 2-aminoethylfolic acid (**4.6**) has been reported for the selective conjugation of folic acid. The synthesis of **4.6** results in the addition of an amine functionality on the γ -carbonyl. This change in reactivity means that folic acid can be selectively conjugated through the γ -conjugate.

Once the formation of the γ -conjugate was confirmed and **4.6** had been confirmed to be non-toxic in H292 cells below 25 μ M, the folic acid derivative was conjugated onto PEG for use as a targeting agent for C11Pc-PEG-AuNPs. The synthesised AuNPs, **4.30**, were tested for singlet oxygen production, with **4.6** shown to quench the singlet oxygen production of these nanoconjugates entirely. While this may appear to be a disappointing result, this allows for the development of a nanoconjugate where singlet oxygen production is quenched until they are internalised into the target cells, adding another method of selectivity. Cathepsin B is a protease overexpressed in NSCLC, and the addition of a cathepsin B cleavable sequence between the AuNPs and the folate targeting moiety could lead to the 'switch on' of singlet oxygen production upon internalisation.

To conjugate **4.6** to the solid phase, 5-(2,5-dioxopyrrolidin-1-yl)oxy-5-oxopentanoic acid (**4.36**) was used for the first time to reverse the reactivity of the solid phase, adding a terminal carboxylic acid. This could be activated with an NHS-ester before the addition of **4.6** to form a solely γ -conjugated folate ligand. The synthesis of a cathepsin B cleavable folate peptide on the solid phase, **4.43**, was partially successful, with the peptide isolated, but the desired sequence was not the major product and the synthesis resulted in a mixture of products. Investigations into why this peptide was not produced in a high yield showed that the addition of **4.36** on the resin was efficient and could be applied to a wide range of amino acids. Variations in the acid content of the cleavage cocktail showed that the mixture of products was not due to peptide degradation on exposure to high concentrations of TFA. It was found that the synthesis of the cleavable sequence itself, **4.42**, was not clean and therefore steps towards the efficient synthesis of this sequence are needed to produce a higher yield of **4.43**. Cleavage after each amino acid addition in this sequence would allow for the determination of which additions are ineffective and therefore leading to an impure product. Once the synthesis of the cleavable sequence has been optimised, the addition of **4.36** and **4.6** can be completed.

Once synthesised, the cleavage of **4.43** by cathepsin B both by itself and upon conjugation onto AuNPs must be assessed to ensure that this sequence would cleave upon cell internalisation. Synthesis of AuNPs functionalised with the cleavage product, Lys-PABA, would confirm that these AuNPs can produce singlet oxygen upon folate cleavage and therefore that this protease cleavable sequence can lead to an additional targeting effect for the photodynamic therapy of FR α expressing NSCLC.

4.5 References

- (1) Stover, P. J. Physiology of Folate and Vitamin B₁₂ in Health and Disease. *Nutr. Rev.* **2004**, *62*, S3–S12.
- (2) Hou, Z.; Orr, S.; Matherly, L. H. Post-Transcriptional Regulation of the Human Reduced Folate Carrier as a Novel Adaptive Mechanism in Response to Folate Excess or Deficiency. *Biosci. Rep* **2014**, *34*, 457–468.
- (3) Hilgenbrink, A. R.; Low, P. S. Folate Receptor-Mediated Drug Targeting: From Therapeutics to Diagnostics. *J. Pharm. Sci.* **2005**, *94* (10), 2135–2146.
- (4) Desmoulin, S. K.; Hou, Z.; Gangjee, A.; Matherly, L. H. The Human Proton-Coupled Folate Transporter. *Cancer Biol. Ther.* **2012**, *13*, 1355–1373.
- (5) Qiu, A.; Jansen, M.; Sakaris, A.; Min, S. H.; Chattopadhyay, S.; Tsai, E.; Sandoval, C.; Zhao, R.; Akabas, M. H.; Goldman, I. D. Identification of an Intestinal Folate Transporter and the Molecular Basis for Hereditary Folate Malabsorption. *Cell* **2006**, *127* (5), 917–928.
- (6) Antony, A. C. The Biological Chemistry of Folate Receptors. *Blood* **1992**, *79* (11), 2807–2820.
- (7) Stahl, P.; Schwartz, A. L. Receptor-Mediated Endocytosis. *J. Clin. Invest.* **1986**, *77* (3), 657–662.
- (8) Leamon, C. P.; Low, P. S.; Reeder, K. M.; Carter, J. J.; Kovach, A. R.; Meng, W.; Ratnam, M.; Zhang, F.; Dann, C. E. Delivery of Macromolecules into Living Cells: A Method That Exploits Folate Receptor Endocytosis. *Proc. Natl. Acad. Sci. U. S. A.* **1991**, *88* (13), 5572–5576.
- (9) Sudimack, J.; Lee, R. J. Targeted Drug Delivery via the Folate Receptor. *Adv. Drug Deliv. Rev.* **2000**, *41*, 147–162.
- (10) Shen, F.; Wu, M.; Ross, J. F.; Miller, D.; Ratnam, M. Folate Receptor Type γ Is Primarily a Secretory Protein Due to Lack of an Efficient Signal for Glycosylphosphatidylinositol Modification: Protein Characterization and Cell Type Specificity. *Biochemistry* **1995**, *34*, 5660–5665.
- (11) Salazar, M. D.; Ratnam, M. The Folate Receptor: What Does It Promise in Tissue-Targeted Therapeutics? *Cancer Metastasis Rev.* **2007**, *26*, 141–152.
- (12) Weitman, S. D.; Weinberg, A. G.; Coney, L. R.; Zurawski, V. R.; Jennings, D. S.; Kamen, B. A. Cellular Localization of the Folate Receptor: Potential Role in Drug Toxicity and Folate Homeostasis. *Cancer Res.* **1992**, *52* (23), 6708–6711.
- (13) Ross, J. F.; Wang, H.; Behm, F. G.; Mathew, P.; Wu, M.; Booth, R.; Ratnam, M. Folate Receptor Type β Is a Neutrophilic Lineage Marker and Is Differentially Expressed in Myeloid Leukemia. *Cancer* **1999**, *85* (2), 348–357.
- (14) Yamaguchi, T.; Hirota, K.; Nagahama, K.; Ohkawa, K.; Takahashi, T.; Nomura, T.; Sakaguchi, S. Control of Immune Responses by Antigen-Specific Regulatory T Cells Expressing the Folate Receptor. *Immunity* **2007**, *27* (1), 145–159.
- (15) Low, P. S.; Kularatne, S. A. Folate-Targeted Therapeutic and Imaging Agents for Cancer. *Curr. Opin. Chem. Biol.* **2009**, *13* (3), 256–262.
- (16) Segal, E. I.; Low, P. S. Tumor Detection Using Folate Receptor-Targeted

- Imaging Agents. *Cancer Metastasis Rev.* **2008**, *27*, 655–664.
- (17) Shen, J.; Hu, Y.; Putt, K. S.; Singhal, S.; Han, H.; Visscher, D. W.; Murphy, L. M.; Low, P. S. Assessment of Folate Receptor Alpha and Beta Expression in Selection of Lung and Pancreatic Cancer Patients for Receptor Targeted Therapies. *Oncotarget* **2018**, *9* (4), 4485–4495.
- (18) Predina, J. D.; Newton, A. D.; Connolly, C.; Dunbar, A.; Baldassari, M.; Deshpande, C.; Cantu, E.; Stadanlick, J.; Kularatne, S. A.; Low, P. S.; et al. Identification of a Folate Receptor-Targeted Near-Infrared Molecular Contrast Agent to Localize Pulmonary Adenocarcinomas. *Mol. Ther.* **2018**, *26* (2), 390–403.
- (19) Wang, S.; Low, P. S. Folate-Mediated Targeting of Antineoplastic Drugs, Imaging Agents, and Nucleic Acids to Cancer Cells. *J. Control. Release* **1998**, *53* (1–3), 39–48.
- (20) Peethambaram, P. P.; Hartmann, L. C.; Jonker, D. J.; De Jonge, M.; Plummer, E. R.; Martin, L.; Konner, J.; Marshall, J.; Goss, G. D.; Teslenko, V.; et al. A Phase I Pharmacokinetic and Safety Analysis of Eपोthilone Folate (BMS-753493), a Folate Receptor Targeted Chemotherapeutic Agent in Humans with Advanced Solid Tumors. *Invest New Drugs* **2015**, *33*, 321–331.
- (21) Bartouskova, M.; Melichar, B.; Mohelnikova-Duchonova, B. Folate Receptor: A Potential Target in Ovarian Cancer. *Pteridines*. Walter de Gruyter GmbH March 1, 2015, pp 1–12.
- (22) Ledermann, J. A.; Canevari, S.; Thigpen, T. Targeting the Folate Receptor: Diagnostic and Therapeutic Approaches to Personalize Cancer Treatments. *Annals of Oncology*. Oxford University Press October 1, 2015, pp 2034–2043.
- (23) Yoo, H. S.; Park, T. G. Folate-Receptor-Targeted Delivery of Doxorubicin Nano-Aggregates Stabilized by Doxorubicin-PEG-Folate Conjugate. *J. Control. Release* **2004**, *100* (2), 247–256.
- (24) Boss, S. D.; Betzel, T.; Müller, C.; Fischer, C. R.; Haller, S.; Reber, J.; Groehn, V.; Schibli, R.; Ametamey, S. M. Comparative Studies of Three Pairs of α - And γ -Conjugated Folic Acid Derivatives Labeled with Fluorine-18. *Bioconjug. Chem.* **2016**, *27* (1), 74–86.
- (25) Zhang, Y.; Sun, Y.; Xu, X.; Zhang, X.; Zhu, H.; Huang, L.; Qi, Y.; Shen, Y.-M. Synthesis, Biodistribution, and Microsingle Photon Emission Computed Tomography (SPECT) Imaging Study of Technetium-99m Labeled PEGylated Dendrimer Poly(Amidoamine) (PAMAM)-Folic Acid Conjugates. *J. Med. Chem* **2010**, *53*, 3262–3272.
- (26) Pasut, G.; Canal, F.; Dalla Via, L.; Arpicco, S.; Veronese, F. M.; Schiavon, O. Antitumoral Activity of PEG-Gemcitabine Prodrugs Targeted by Folic Acid. *J. Control. Release* **2008**, *127* (3), 239–248.
- (27) Vortherms, A. R.; Doyle, R. P.; Gao, D.; Debrah, O.; Sinko, P. J. Synthesis, Characterisation, and in Vitro Assay of Folic Acid Conjugates of 3'-Azido-3'-Deoxythymidine (AZT): Toward Targeted AZT Nased Anticancer Therapeutics. *Nucleosides Nucleotides Nucleic Acids* **2008**, *27* (2), 173–185.
- (28) Santos, M. A.; Enyedy, E. A.; Nuti, E.; Rossello, A.; Krupenko, N. I.; Krupenko, S. A. Methotrexate γ -Hydroxamate Derivatives as Potential Dual Target

- Antitumor Drugs. *Bioorg. Med. Chem.* **2007**, *15* (3), 1266–1274.
- (29) Guaragna, A.; Roviello, G. N.; D'Errico, S.; Paoella, C.; Palumbo, G.; D'Alonzo, D. Solid Phase Synthesis of a Novel Folate-Conjugated 5-Aminolevulinic Acid Methyl Ester Based Photosensitizer for Selective Photodynamic Therapy. *Tetrahedron Lett.* **2015**, *56* (6), 775–778.
- (30) Luo, J.; Smith, M. D.; Lantrip, D. A.; Wang, S.; Fuchs, P. L. Efficient Syntheses of Pyrofolic Acid and Pteroyl Azide, Reagents for the Production of Carboxyl-Differentiated Derivatives of Folic Acid. *J. Am. Chem. Soc.* **1997**, *119*, 10004–10013.
- (31) Abu Ajaj, K.; El-Abadla, N.; Welker, P.; Azab, S.; Zeisig, R.; Fichtner, I.; Kratz, F. Comparative Evaluation of the Biological Properties of Reducible and Acid-Sensitive Folate Prodrugs of a Highly Potent Doxorubicin Derivative. *Eur. J. Cancer* **2012**, *48* (13), 2054–2065.
- (32) Chen, Q.; Meng, X.; Mcquade, P.; Rubins, D.; Lin, S.-A.; Zeng, Z.; Haley, H.; Miller, P.; Dinko González Trotter; Low, P. S. Folate-PEG-NOTA-Al 18 F: A New Folate Based Radiotracer for PET Imaging of Folate Receptor-Positive Tumors. *Mol. Pharm.* **2017**, *14*, 4353–4361.
- (33) Schneider, R.; Schmitt, F.; Frochot, C.; Fort, Y.; Lourette, N.; Guillemin, F.; Müller D, J.-F.; Barberi-Heyob, M. Design, Synthesis, and Biological Evaluation of Folic Acid Targeted Tetraphenylporphyrin as Novel Photosensitizers for Selective Photodynamic Therapy. *Bioorg. Med. Chem.* **2005**, *13*, 2799–2808.
- (34) Gravier, J.; Schneider, R.; Frochot, C.; Bastogne, T.; Schmitt, F.; Didelon, J.; Guillemin, F.; Barberi-Heyob, M. Improvement of Meta-Tetra(Hydroxyphenyl)Chlorin-Like Photosensitizer Selectivity with Folate-Based Targeted Delivery. Synthesis and in Vivo Delivery Studies. *J. Med. Chem.* **2008**, *51*, 3867–3877.
- (35) Stallivieri, A.; Colombeau, L.; Jetpisbayeva, G.; Moussaron, A.; Myrzakhmetov, B.; Arnoux, P.; Acherar, S.; Vanderesse, R.; Frochot, C. Folic Acid Conjugates with Photosensitizers for Cancer Targeting in Photodynamic Therapy: Synthesis and Photophysical Properties. *Bioorganic Med. Chem.* **2017**, *25* (1), 1–10.
- (36) Li, D.; Li, P.; Lin, H.; Jiang, Z.; Guo, L.; Li, B. A Novel Chlorin-PEG-Folate Conjugate with Higher Water Solubility, Lower Cytotoxicity, Better Tumor Targeting and Photodynamic Activity. *J. Photochem. Photobiol. B Biol.* **2013**, *127*, 28–37.
- (37) Khoza, P.; Antunes, E.; Chen, J. Y.; Nyokong, T. Synthesis and Photophysicochemical Studies of a Water Soluble Conjugate between Folic Acid and Zinc Tetraaminophthalocyanine. *J. Lumin.* **2013**, *134*, 784–790.
- (38) Morosini, V.; Bastogne, T.; Frochot, C.; Schneider, R.; Franois, A.; Guillemin, F.; Barberi-Heyob, M. Quantum Dot-Folic Acid Conjugates as Potential Photosensitizers in Photodynamic Therapy of Cancer. *Photochem. Photobiol. Sci.* **2011**, *10* (5), 842–851.
- (39) Wang, F.; Chen, X.; Zhao, Z.; Tang, S.; Huang, X.; Lin, C.; Cai, C.; Zheng, N. Synthesis of Magnetic, Fluorescent and Mesoporous Core-Shell-Structured Nanoparticles for Imaging, Targeting and Photodynamic Therapy. *J. Mater. Chem.* **2011**, *21* (30), 11244–11252.

-
- (40) Yang, S.-J.; Lin, F.-H.; Tsai, K.-C.; Wei, M.-F.; Tsai, H.-M.; Wong, J.-M.; Shieh, M.-J. Folic Acid-Conjugated Chitosan Nanoparticles Enhanced Protoporphyrin IX Accumulation in Colorectal Cancer Cells. *Bioconjug. Chem.* **2010**, *21* (4), 679–689.
- (41) Ma, X.; Qu, Q.; Zhao, Y. Targeted Delivery of 5-Aminolevulinic Acid by Multifunctional Hollow Mesoporous Silica Nanoparticles for Photodynamic Skin Cancer Therapy. *ACS Appl. Mater. Interfaces* **2015**, *7*, 10671–10676.
- (42) Kato, T.; Jin, C. S.; Ujii, H.; Lee, D.; Fujino, K.; Wada, H.; Hu, H. pei; Weersink, R. A.; Chen, J.; Kaji, M.; et al. Nanoparticle Targeted Folate Receptor 1-Enhanced Photodynamic Therapy for Lung Cancer. *Lung Cancer* **2017**, *113*, 59–68.
- (43) Ma, Y.; Sadoqi, M.; Shao, J. Biodistribution of Indocyanine Green-Loaded Nanoparticles with Surface Modifications of PEG and Folic Acid. *Int. J. Pharm.* **2012**, *436* (1–2), 25–31.
- (44) Wang, Y.; Li, P.; Chen, L.; Gao, W.; Zeng, F.; Kong, L. X. Drug Delivery Targeted Delivery of 5-Fluorouracil to HT-29 Cells Using High Efficient Folic Acid-Conjugated Nanoparticles. *Drug Deliv.* **2014**, *22* (2), 191–198.
- (45) Huang, Y.; Mao, K.; Zhang, B.; Zhao, Y. Superparamagnetic Iron Oxide Nanoparticles Conjugated with Folic Acid for Dual Target-Specific Drug Delivery and MRI in Cancer Theranostics. *Mater. Sci. Eng. C* **2017**, *70*, 763–771.
- (46) Moret, F.; Scheglmann, D.; Reddi, E. Folate-Targeted PEGylated Liposomes Improve the Selectivity of PDT with Meta-Tetra(Hydroxyphenyl)Chlorin (m-THPC). *Photochem. Photobiol. Sci.* **2013**, *12* (5), 823–834.
- (47) Son, J.; Yang, S. M.; Yi, G.; Roh, Y. J.; Park, H.; Park, J. M.; Choi, M. G.; Koo, H. Folate-Modified PLGA Nanoparticles for Tumor-Targeted Delivery of Pheophorbide a in Vivo. *Biochem. Biophys. Res. Commun.* **2018**, *498* (3), 523–528.
- (48) Zhang, Y.; Guo, L.; Roeske, R. W.; Antony, A. C.; Jayaram, H. N. Pteroyl- γ -Glutamate-Cysteine Synthesis and Its Application in Folate Receptor-Mediated Cancer Cell Targeting Using Folate-Tethered Liposomes. *Anal. Biochem.* **2004**, *332* (1), 168–177.
- (49) Nair, L. V.; Nazeer, S. S.; Jayasree, R. S.; Ajayaghosh, A. Fluorescence Imaging Assisted Photodynamic Therapy Using Photosensitizer-Linked Gold Quantum Clusters. *ACS Nano* **2015**, *9* (6), 5825–5832.
- (50) Chen, C.; Ke, J.; Edward Zhou, X.; Yi, W.; Brunzelle, J. S.; Li, J.; Yong, E. L.; Xu, H. E.; Melcher, K. Structural Basis for Molecular Recognition of Folic Acid by Folate Receptors. *Nature* **2013**, *500* (7463), 486–489.
- (51) Wibowo, A. S.; Singh, M.; Reeder, K. M.; Carter, J. J.; Kovach, A. R.; Meng, W.; Ratnam, M.; Zhang, F.; Dann, C. E. Structures of Human Folate Receptors Reveal Biological Trafficking States and Diversity in Folate and Antifolate Recognition. *Proc. Natl. Acad. Sci. U. S. A.* **2013**, *110* (38), 15180–15188.
- (52) Kim, J.; Tung, C.-H.; Choi, Y. Smart Dual-Functional Warhead for Folate Receptor-Specific Activatable Imaging and Photodynamic Therapy. *Chem. Commun.* **2014**, No. 50, 10600–10603.

-
- (53) Hu, X.; Wang, R.; Yue, J.; Liu, S.; Xie, Z.; Jing, X. Targeting and Anti-Tumor Effect of Folic Acid-Labeled Polymer-Doxorubicin Conjugates with PH-Sensitive Hydrazone Linker. *J. Mater. Chem.* **2012**, *22*, 13303–13310.
- (54) Du, C.; Deng, D.; Shan, L.; Wan, S.; Cao, J.; Tian, J.; Achilefu, S.; Gu, Y. A PH-Sensitive Doxorubicin Prodrug Based on Folate-Conjugated BSA for Tumor-Targeted Drug Delivery. *Biomaterials* **2013**, *34* (12), 3087–3097.
- (55) Cao, Y.; Yang, J. Development of a Folate Receptor (FR)-Targeted Indenoisoquinoline Using a PH-Sensitive N-Ethoxybenzylimidazole (NEBI) Bifunctional Cross-Linker. *Bioconjugate Chem* **2014**, *25*, 11.
- (56) Ki Choi, S.; Thomas, T.; Li, M.-H.; Kotlyar, A.; Desai, A.; Baker, J. R. Light-Controlled Release of Caged Doxorubicin from Folate Receptor-Targeting PAMAM Dendrimer Nanoconjugate. *Chem. Commun.* **2010**, *46*, 2632–2634.
- (57) Dcona, M. M.; Sheldon, J. E.; Mitra, D.; Hartman, M. C. T. Light Induced Drug Release from a Folic Acid-Drug Conjugate. *Bioorganic Med. Chem. Lett.* **2017**, *27* (3), 466–469.
- (58) Henne, W. A.; Doorneweerd, D. D.; Hilgenbrink, A. R.; Kularatne, S. A.; Low, P. S. Synthesis and Activity of a Folate Peptide Camptothecin Prodrug. *Bioorganic Med. Chem. Lett.* **2006**, *16* (20), 5350–5355.
- (59) Satyam, A. Design and Synthesis of Releasable Folate-Drug Conjugates Using a Novel Heterobifunctional Disulfide-Containing Linker. *Bioorganic Med. Chem. Lett.* **2008**, *18* (11), 3196–3199.
- (60) Gao, W.; Xiang, B.; Meng, T. T.; Liu, F.; Qi, X. R. Chemotherapeutic Drug Delivery to Cancer Cells Using a Combination of Folate Targeting and Tumor Microenvironment-Sensitive Polypeptides. *Biomaterials* **2013**, *34* (16), 4137–4149.
- (61) Warnecke, A.; Fichtner, I.; Saß, G.; Kratz, F. Synthesis, Cleavage Profile, and Antitumor Efficacy of an Albumin-Binding Prodrug of Methotrexate That Is Cleaved by Plasmin and Cathepsin B. *Arch. Pharm. Chem. Life Sci.* **2007**, *340* (8), 389–395.
- (62) Laguzza, B. C.; Nichols, C. L.; Briggs, S. L.; Cullinan, G. J.; Johnson, D. A.; Starling, J. J.; Baker, A. L.; Bumol, T. F.; Corvalan, J. R. F. New Antitumor Monoclonal Antibody-Vinca Conjugates LY203725 and Related Compounds: Design, Preparation, and Representative in Vivo Activity. *J. Med. Chem.* **1989**, *32* (3), 548–555.
- (63) Tsuchikama, K.; An, Z. Antibody-Drug Conjugates: Recent Advances in Conjugation and Linker Chemistries. *Protein Cell* **2018**, *9* (1), 33–46.
- (64) Wu, G.; Fang, Y.-Z.; Yang, S.; Lupton, J. R.; Turner, N. D. Glutathione Metabolism and Its Implications for Health. *J. Nutr.* **2004**, *134* (3), 489–492.
- (65) Oberli-Schrämml, A. E.; Joncourt, F.; Stadler, M.; Altermatt, H. -J.; Buser, K.; Ris, H. -B; Schmid, U.; Cerny, T. Parallel Assessment of Glutathione-based Detoxifying Enzymes, O6-alkylguanine-dna Alkyltransferase and P-glycoprotein as Indicators of Drug Resistance in Tumor and Normal Lung of Patients with Lung Cancer. *Int. J. Cancer* **1994**, *59* (5), 629–636.
- (66) Meinhardt, M.; Krebs, R.; Anders, A.; Heinrich, U.; Tronnier, H. Wavelength-

- Dependent Penetration Depths of Ultraviolet Radiation in Human Skin. *J. Biomed. Opt.* **2008**, *13* (4), 044030.
- (67) Doronina, S. O.; Toki, B. E.; Torgov, M. Y.; Mendelsohn, B. A.; Cervený, C. G.; Chace, D. F.; DeBlanc, R. L.; Gearing, R. P.; Bovee, T. D.; Siegall, C. B.; et al. Development of Potent Monoclonal Antibody Auristatin Conjugates for Cancer Therapy. *Nat. Biotechnol.* **2003**, *21* (7), 778–784.
- (68) Dorywalska, M.; Strop, P.; Melton-Witt, J. A.; Hasa-Moreno, A.; Farias, S. E.; Galindo Casas, M.; Delaria, K.; Lui, V.; Poulsen, K.; Loo, C.; et al. Effect of Attachment Site on Stability of Cleavable Antibody Drug Conjugates. *Bioconjugate Chem.* **2015**, *26*, 650–659.
- (69) López-Otín, C.; Bond, J. S. Proteases: Multifunctional Enzymes in Life and Disease. *J. Biol. Chem.* **2008**, *283* (45), 30433–30437.
- (70) Rakashandra, S.; Rana, F.; Rafiq, S.; Masood, A.; Amin, S. Role of Proteases in Cancer: A Review. *Biotechnol. Mol. Biol. Rev.* **2012**, *7* (4), 90–101.
- (71) Chang, C.; Werb, Z. *The Many Faces of Metalloproteases: Cell Growth, Invasion, Angiogenesis and Metastasis*; 2001; Vol. 11.
- (72) Egeblad, M.; Werb, Z. New Functions for the Matrix Metalloproteinases in Cancer Progression. *Nat. Rev. Cancer* **2002**, *2*, 161–174.
- (73) Olson, O. C.; Joyce, J. A. Cysteine Cathepsin Proteases: Regulators of Cancer Progression and Therapeutic Response. *Nat. Rev. Cancer* **2015**, *15* (12), 712–729.
- (74) Werle, B.; Lötterle, H.; Schanzenbächer, U.; Lah, T. T.; Kalman, E.; Kayser, K.; Bülzbruck, H.; Schirren, J.; Krasovec, M.; Kos, J.; et al. Immunochemical Analysis of Cathepsin B in Lung Tumours: An Independent Prognostic Factor for Squamous Cell Carcinoma Patients. *Br. J. Cancer* **1999**, *81* (3), 510–519.
- (75) Mohamed, M. M.; Sloane, B. F. Multifunctional Enzymes in Cancer. *Nat. Rev. Cancer* **2006**, *6* (10), 764–775.
- (76) Mort, J. S.; Buttle, D. J. Cathepsin B. *Int. J. Biochem. Cell Biol.* **1997**, *29* (5), 715–720.
- (77) Koblinski, J. E.; Ahram, M.; Sloane, B. F. Unraveling the Role of Proteases in Cancer. *Clin. Chim. Acta* **2000**, *291* (2), 113–135.
- (78) Sukoh, N.; Abe, S.; Ogura, S.; Isobe, H.; Takekawa, H.; Inoue, K.; Kawakami, Y. Immunohistochemical Study of Cathepsin B. Prognostic Significance in Human Lung Cancer. *Cancer* **1994**, *74* (1), 46–51.
- (79) Sloane, B. F.; Yan, S.; Podgorski, I.; Linebaugh, B. E.; Cher, M. L.; Mai, J.; Cavallo-Medved, D.; Sameni, M.; Dosescu, J.; Moin, K. Cathepsin B and Tumor Proteolysis: Contribution of the Tumor Microenvironment. *Semin. Cancer Biol.* **2005**, *15* (2), 149–157.
- (80) Roshly, S.; Sloane, B. F.; Moin, K. Pericellular Cathepsin B and Malignant Progression. *Cancer Metastasis Rev.* **2003**, *22*, 271–286.
- (81) Jang, B.; Choi, Y. Photosensitizer-Conjugated Gold Nanorods for Enzyme-Activatable Fluo-Rescence Imaging and Photodynamic Therapy. *Theranostics* **2012**, *2012* (2), 190–197.

- (82) Li, S.-Y.; Cheng, H.; Qiu, W.-X.; Liu, L.-H.; Chen, S.; Hu, Y.; Xie, B.-R.; Li, B.; Zhang, X.-Z. Protease-Activable Cell-Penetrating Peptide–Protoporphyrin Conjugate for Targeted Photodynamic Therapy in Vivo. *ACS Appl. Mater. Interfaces* **2015**, *7* (51), 28319–28329.
- (83) Zheng, G.; Chen, J.; Stefflova, K.; Jarvi, M.; Li, H.; Wilson, B. C. *Photodynamic Molecular Beacon as an Activatable Photosensitizer Based on Protease-Controlled Singlet Oxygen Quenching and Activation*; 2007; Vol. 104, pp 8989–8994.
- (84) Liu, J.; Zhang, L.; Lei, J.; Shen, H.; Ju, H. Multifunctional Metal–Organic Framework Nanoprobe for Cathepsin B-Activated Cancer Cell Imaging and Chemo-Photodynamic Therapy. *ACS Appl. Mater. Interfaces* **2017**, *9* (3), 2150–2158.
- (85) Choi, Y.; Weissleder, R.; Tung, C.-H. Selective Antitumor Effect of Novel Protease-Mediated Photodynamic Agent. *Cancer Res* **2006**, *66* (14), 7225–7229.
- (86) Bargh, J. D.; Isidro-Llobet, A.; Parker, J. S.; Spring, D. R. Cleavable Linkers in Antibody–Drug Conjugates. *Chem. Soc. Rev.* **2019**, *48* (16), 4361–4374.
- (87) Dubowchik, G. M.; Firestone, R. A. Cathepsin B-Sensitive Dipeptide Prodrugs. 1. A Model Study of Structural Requirements for Efficient Release of Doxorubicin. *Bioorg. Med. Chem. Lett.* **1998**, *8* (23), 3341–3346.
- (88) Acar, H.; Samaeekia, R.; Schnorenberg, M. R.; Sasmal, D. K.; Huang, J.; Tirrell, M. V.; LaBelle, J. L. Cathepsin-Mediated Cleavage of Peptides from Peptide Amphiphiles Leads to Enhanced Intracellular Peptide Accumulation. *Bioconjug. Chem.* **2017**, *28* (9), 2316–2326.
- (89) Klahn, P.; Fetz, V.; Ritter, A.; Collisi, W.; Hinkelmann, B.; Arnold, T.; Tegge, W.; Rox, K.; Hüttel, S.; Mohr, K. I.; et al. The Nuclear Export Inhibitor Aminorotjadone Is a Potent Effector in Extracellular-Targeted Drug Conjugates. *Chem. Sci.* **2019**, *10* (20), 5197–5210.
- (90) Zhang, X.; Tang, K.; Wang, H.; Liu, Y.; Bao, B.; Fang, Y.; Zhang, X.; Lu, W. Design, Synthesis, and Biological Evaluation of New Cathepsin B-Sensitive Camptothecin Nanoparticles Equipped with a Novel Multifunctional Linker. *Bioconjug. Chem.* **2016**, *27*, 1267–1275.
- (91) Wang, S.; Lee, R. J.; Mathias, C. J.; Green, M. A.; Low, P. S. Synthesis, Purification, and Tumor Cell Uptake of ^{67}Ga -Deferoxamine-Folate, a Potential Radiopharmaceutical for Tumor Imaging. *Bioconjug. Chem.* **1996**, *7*, 56–62.
- (92) Wei, W. H.; Fountain, M.; Magda, D.; Wang, Z.; Lecane, P.; Mesfin, M.; Miles, D.; Sessler, J. L. Gadolinium Texaphyrin-Methotrexate Conjugates. Towards Improved Cancer Chemotherapeutic Agents. *Org. Biomol. Chem.* **2005**, *3* (18), 3290–3296.
- (93) Wang, S.; Luo, J.; Lantrip, D. A.; Waters, D. J.; Mathias, C. J.; Green, M. A.; Fuchs, P. L.; Low, P. S. Design and Synthesis of [^{111}In]DTPA-Folate for Use as a Tumor-Targeted Radiopharmaceutical. *Bioconjug. Chem.* **1997**, *8*, 673–679.
- (94) Kularatne, S. A.; Low, P. S. Targeting of Nanoparticles: Folate Receptor. In *Cancer Nanotechnology Methods and Protocols*; Grobmeyer, S. R., Moudgil, B. M., Eds.; Humana Press: London, 2010; pp 249–265.

- (95) Meyer, T. A.; Williams, D. L. H. Catalysis of N-Nitrosation and Diazotisation by Thiourea and Thiocyanate Ion. *J. Chem. Soc. Perkin Trans. 2* **1981**, 361–365.
- (96) Challis, B. C.; Osborne, M. R. The Chemistry of Nitroso-Compounds. Part VI. Direct and Indirect Transnitrosation Reactions of N-Nitrosodiphenylamine. *J. Chem. Soc. Perkin Trans. 2* **1973**, 1526–1533.
- (97) Meyer, T. A.; Williams, D. L. H.; Bonnett, R.; Ooi, S. L. Denitrosation of N-Acetyl-N 1-Nitrosotryptophan in Acid Solution. *J. Chem. Soc. Perkin Trans. 2* **1982**, 1383–1387.
- (98) Tian, L.; Lee, P.; Singhana, B.; Chen, A.; Qiao, Y.; Lu, L.; Martinez, J. O.; Tasciotti, E.; Melancon, A.; Huang, S.; et al. Radiopaque Resorbable Inferior Vena Cava Filter Infused with Gold Nanoparticles. *Sci. Rep.* **2017**, 7 (1), 2147.
- (99) Hussain, I.; Graham, S.; Wang, Z.; Tan, B.; Sherrington, D. C.; Rannard, S.; Cooper, A. I.; Brust, M. Size-Controlled Synthesis of Near-Monodisperse Gold Nanoparticles in the 1–4 Nm Range Using Polymeric Stabilizers. *J. Am. Chem. Soc.* **2005**, 127, 16398–16399.
- (100) Joshi, R.; Adhikari, S.; Patro, B. S.; Chattopadhyay, S.; Mukherjee, T. Free Radical Scavenging Behavior of Folic Acid: Evidence for Possible Antioxidant Activity. *Free Radic. Biol. Med.* **2001**, 30 (12), 1390–1399.
- (101) Thomas, A. H.; Lorente, C.; Capparelli, A. L.; Martínez, C. G.; Braun, A. M.; Oliveros, E. Singlet Oxygen ($^1\Delta_g$) Production by Pterin Derivatives in Aqueous Solutions. *Photochem. Photobiol. Sci.* **2003**, 2 (3), 245–250.
- (102) Cabrerizo, F. M.; Laura Dántola, M.; Petroselli, G.; Capparelli, A. L.; Thomas, A. H.; Braun, A. M.; Lorente, C.; Oliveros, E. Reactivity of Conjugated and Unconjugated Pterins with Singlet Oxygen ($O_2(1\Delta_g)$): Physical Quenching and Chemical Reaction. *Photochem. Photobiol.* **2007**, 83 (3), 526–534.
- (103) Soudy, R.; Chen, C.; Kaur, K. Novel Peptide–Doxorubicin Conjugates for Targeting Breast Cancer Cells Including the Multidrug Resistant Cells. *J. Med. Chem.* **2013**, 56 (19), 7564–7573.
- (104) Perumal, O.; Khandare, J.; Kolhe, P.; Kannan, S.; Lieh-Lai, M.; Kannan, R. M. Effects of Branching Architecture and Linker on the Activity of Hyperbranched Polymer–Drug Conjugates. *Bioconjug. Chem.* **2009**, 20 (5), 842–846.
- (105) Pillai, R.; Marinelli, E. R.; Swenson, R. E. A Flexible Method for Preparation of Peptide Homo- and Heterodimers Functionalized with Affinity Probes, Chelating Ligands, and Latent Conjugating Groups. *Biopolymers* **2006**, 84 (6), 576–585.
- (106) Ndinguri, M. W.; Solipuram, R.; Gambrell, R. P.; Aggarwal, S.; Hammer, R. P. Peptide Targeting of Platinum Anti-Cancer Drugs. *Bioconjugate Chem.* **2009**, 20 (10), 1869–1878.
- (107) Safavy, A.; Georg, G. I.; Velde, D. Vander; Raisch, K. P.; Safavy, K.; Carpenter, M.; Wang, W.; Bonner, J. A.; Khazaeli, M. B.; Buchsbaum, D. J. Site-Specifically Traced Drug Release and Biodistribution of a Paclitaxel–Antibody Conjugate toward Improvement of the Linker Structure1. *Bioconjugate Chem.* **2004**, 15 (6), 1264–1274.

-
- (108) Elgendy, S.; Patel, G.; Green, D.; Goodwin, C. A.; Scully, M. F.; Husman, W.; Skordalakes, E.; Kakkar, V. V.; Deadman, J. J. Design of a Novel Class of Bifunctional Thrombin Inhibitors, Synthesised by the First Application of Peptide Boronates in Solid Phase Chemistry. *Tetrahedron Lett.* **1997**, *38* (18), 3305–3308.
- (109) Menegatti, S.; Hussain, M.; Naik, A. D.; Carbonell, R. G.; Rao, B. M. mRNA Display Selection and Solid-Phase Synthesis of Fc-Binding Cyclic Peptide Affinity Ligands. *Biotechnol. Bioeng.* **2013**, *110* (3), 857–870.
- (110) Sulyok, G. A. G.; Gibson, C.; Goodman, S. L.; Hölzemann, G.; Wiesner, M.; Kessler, H. Solid-Phase Synthesis of a Nonpeptide RGD Mimetic Library: New Selective $\text{Av}\beta 3$ Integrin Antagonists. *J. Med. Chem.* **2001**, *44* (12), 1938–1950.
- (111) Attardi, M. E.; Porcu, G.; Taddei, M. Malachite Green, a Valuable Reagent to Monitor the Presence of Free COOH on the Solid-Phase. *Tetrahedron Lett.* **2000**, *41* (38), 7391–7394.
- (112) Malmberg, J.; Perols, A.; Varasteh, Z.; Altai, M.; Braun, A.; Sandström, M.; Garske, U.; Tolmachev, V.; Orlova, A.; Karlström, A. E. Comparative Evaluation of Synthetic Anti-HER2 Affibody Molecules Site-Specifically Labelled with ^{111}In Using N-Terminal DOTA, NOTA and NODAGA Chelators in Mice Bearing Prostate Cancer Xenografts. *Eur. J. Nucl. Med. Mol. Imaging* **2012**, *39* (3), 481–492.

Chapter Five

Experimental

5.1 General procedures

5.1.1 Materials and solvents

All chemicals were purchased from Sigma Aldrich, Fisher Scientific or Fluorochem unless otherwise specified. Fmoc-amino acids and coupling agents were purchased from Novabiochem, Fluorochem or AGTC Bioproducts. Anhydrous solvents were purchased from Sigma Aldrich, used as purchased and assumed to conform to specification. α -Thio- ω -carboxy polyethylene glycol (3 kDa, PEG) was purchased from Iris Biotech GmbH (Germany). Vivaspin 500 (100 kDa MWCO, PES membrane) centrifuge columns were purchased from Sartorius Stedim Biotech (UK). Zeba spin desalting columns (7 kDa MWCO, 0.5 mL) were purchased from Fisher Scientific. Antibodies and secondary antibodies were purchased from Abcam or R&D Systems. White-walled clear-bottom 96 well plates for phototoxicity assays were purchased from Fisher Scientific. MTS was purchased from Promega. Pre-made NuPAGE™ 4-12% Bis-Tris Gels were purchased from Invitrogen. Cell lines were purchased from ATCC.

5.1.2 Instrumental techniques

^1H -, ^{13}C - and ^{19}F -NMR were collected using a Bruker spectrometer operating at 400 MHz (^1H), 100 MHz (^{13}C) or 376 MHz (^{19}F) using the specified deuterated solvent. Chemical shifts were recorded in ppm and were referenced to residual solvent peak of MeOH (3.31 ppm), DMSO (2.50 ppm), or chloroform (7.26 ppm). Multiplicities in the NMR spectra are described as s = singlet, d = doublet, t = triplet, q = quartet, m = multiplet, and combinations thereof. Coupling constants are reported in Hz.

Analytical RP-HPLC was performed using an Agilent 1200 HPLC, fitted with an Agilent eclipse XDB-C18 column (4.6 x 150 mm, 5 μm) and a flow rate of 1 mL/min. Spectra were run with a solvent gradient of 0-100% B over 20 min. Solvent A: H_2O , 0.05% TFA, solvent B: MeOH, 0.05% TFA. Detection wavelengths were 214 nm and 254 nm. Semi-preparative RP-HPLC was performed using an Agilent 1200 HPLC, fitted with an Agilent eclipse XDB-C18 column (9.4 x 250 mm, 5 μm) and a flow rate of 3 mL/min. Spectra were run with a solvent gradient of 0-100% B over 20 min. Solvents: A = H_2O , 0.05% TFA, B: MeOH, 0.05% TFA. Detection wavelengths were 214 nm and 254 nm. Preparative RP-HPLC was

performed using an Agilent 1200 HPLC, fitted with an Agilent eclipse XDB-C18 column (21.2 x 150 mm, 5 μ m) and a flow rate 20 mL/min. Spectra were run with a solvent gradient of 0-100% B over 15 min. Solvent A: 95% H₂O, 5% MeOH, 0.05% TFA, solvent B: 95% MeOH, 5% H₂O, 0.05% TFA. Detection wavelengths were 214 nm and 254 nm.

MALDI was performed on a Kratos Analytical Axima-CFR MALDI-ToF, using α -cyano-4-hydroxycinnamic acid (α -CHCA) as the matrix. High resolution masses were recorded at the John Innes Centre, Norwich Research Park, using an ESI Shimadzu ion-trap ToF mass spectrometer with Shimadzu Prominence/Nexera UHPLC system, providing a solvent flow of 0.4 mL/min 50% MeOH, 50% H₂O.

UV-vis spectra were recorded on an Agilent Cary 60 spectrometer, using quartz cuvettes with 1 cm pathlength. Fluorescence spectra were recorded on a Horiba Jobin Yvon Fluorolog spectrometer, using quartz cuvettes with a 1 cm pathlength. Infrared spectra were recorded on a PerkinElmer BX with an ATR attachment.

Centrifugation was performed in either an Eppendorf 5415D or, for temperature controlled centrifugation, a HERMLE Z 326 K centrifuge.

Flow cytometry was performed using a Beckman Coulter CytoFLEX, with a flow rate of 10 μ L/min.

Automated peptide synthesis was performed using a Biotage Syro I.

Irradiation of samples for singlet oxygen and phototoxicity studies was performed using a JDS Uniphase 10 mW 633 nm HeNe laser (1125P) fitted with biconvex diverging lens.

UV irradiation was performed using a UVP Spot Lite SCL2-6 UV wand.

Fluorescence microscopy was performed using an inverted Leica DMIL fluorescent microscope with an associated Leica DFC420 camera at 10x magnification.

Cell viability assays were analysed using a BMG Labtech PolarStar Optima microplate reader at 492 nm. Microplate fluorescence spectral scans were recorded on a CLARIOstar (BMG Labtech) microplate reader.

SDS-PAGE was performed in an Invitrogen Novex mini-cell chamber and analysed for fluorescence in an ImageQuant LAS 4000 imager.

5.1.3 Solid phase peptide synthesis

All peptides synthesised in this thesis were synthesised via Fmoc-solid phase peptide synthesis. Rink amide MBHA resin was swelled for 30 minutes in DMF.

For manual peptide synthesis the resin was deprotected with 40% piperidine in DMF for ten minutes, then 20% piperidine in DMF for five minutes twice, followed by washing the resin five times with DMF. Fmoc-protected amino acids (5 eq) were coupled using HATU (5 eq) and DIPEA (10 eq) in DMF and shaken for one hour on the resin. Each peptide coupling was repeated and the resin washed five times with DMF. After each peptide coupling, the growing peptide chain was deprotected with piperidine.

For automated peptide synthesis the resin was deprotected with 20% piperidine in DMF for 20 minutes twice, followed by washing the resin three times with DMF. The coupling of Fmoc-protected amino acids (4 eq) was completed with HOBt/HBTU (4 eq) and DIPEA (8 eq) and shaken for 45 minutes. Each peptide coupling was repeated, then the resin washed three times with DMF. After each peptide coupling, the growing peptide chain was deprotected with piperidine.

Once the peptide was completed, the resin was washed six times with methanol. Cleavage of the peptide from the resin was completed in 95:2.5:2.5 TFA:TIPS:H₂O with shaking for three hours. The resulting solution was evaporated to dryness and washed with cold ether. Peptides were purified by preparative HPLC and their purity confirmed by analytical HPLC.

5.1.4 Cell culture, passage and count

A549 and H292 cells were cultured in phenol red free RPMI 1640 and HEK293 cells were cultured in phenol red free DMEM/F12. They were routinely subcultured 1 in 12 every 4 days. The culture medium was removed and the cells were washed with PBS (5 mL). TrypLE express (2 mL) was added to the flask and cells were incubated at 37 °C, 5% CO₂ until they lifted away from the culture flask (1 minute for HEK293, 5 minutes for A549 and H292). Media (10 mL) was added to the flask to deactivate the TrypLE express, then all but 1 mL of this cell suspension removed from the flask. Media (9 mL) was added to the flask and the cells returned to the incubator.

To seed for experiments, cells were counted in a haemocytometer. Cells (20 μL) were mixed with PBS (20 μL) then pipetted onto the haemocytometer (20 μL). Cells within a 5 by 4 grid were counted with a hand tally counter and repeated three times. The average cell count was multiplied by 10^4 . Cells were diluted in media to reach the desired cell count, then seeded into cell culture treated 96 well plates (100 μL).

5.1.5 Flow cytometry

A549, H292 or HEK293 cells (1×10^6) were centrifuged at 350 g, 4 °C for 5 minutes and the supernatant removed. Anti-EGFR or anti-FR α antibody (5 μL , 1 mg/mL) was diluted in PBS 0.5% BSA (500 μL). The cell pellet was resuspended in this antibody solution (100 μL), then the cells incubated on ice for one hour. A second tube of cells was incubated with PBS 0.5% BSA (100 μL) on ice for one hour. PBS 0.5% BSA (1 mL) was added to each tube and then centrifuged at 350 g, 4 °C for 5 minutes. The supernatant was removed, the pellet resuspended in FITC-goat anti-mouse secondary antibody (1 μL , 2 mg/mL in 100 μL PBS 0.5% BSA) and the cells incubated on ice for one hour in the dark. PBS 0.5% BSA (1 mL) was added to each tube then centrifuged 350 g, 4 °C for 5 minutes. The supernatant was removed and the pellet resuspended in PBS 0.5% BSA (300 μL) and transferred into a flow cytometry tube. Cells were analysed in a Beckman Coulter CytoFLEX flow cytometer. Live cells were gated and cells run at a flow rate of 10 $\mu\text{L}/\text{min}$ with 10,000 events recorded.

5.1.6 Preparation of buffers

Phosphate buffered saline (PBS) was prepared by addition of NaCl (150 mM) and $\text{CaCl}_2 \cdot 2\text{H}_2\text{O}$ (100 μM) to 10 mM sodium phosphate buffer. 10 mM sodium phosphate buffer was prepared using stock solutions of $\text{NaH}_2\text{PO}_4 \cdot 2\text{H}_2\text{O}$ (200 mM) and $\text{Na}_2\text{HPO}_4 \cdot 2\text{H}_2\text{O}$ (200 mM) in H_2O , with the pH adjusted to 7.4.

MES buffer was prepared by addition of Tween-20 (0.05%) to an aqueous solution of 2-(*N*-morpholino)ethanesulphonic acid (50 mM), and the pH was adjusted to pH 5.5 .

Sodium phosphate buffer was prepared by adjusting the pH of an aqueous solution of $\text{NaH}_2\text{PO}_4 \cdot 2\text{H}_2\text{O}$ (0.1 mM) and $\text{Na}_2\text{HPO}_4 \cdot 2\text{H}_2\text{O}$ (0.1 mM) to 8.0.

Triethanolamine buffer was prepared by adjusting the pH of an aqueous solution of triethanolamine (0.2 M) to 8.2.

Ethanolamine buffer was prepared by adjusting the pH of an aqueous solution of ethanolamine (0.1 M) to 8.2.

Histidine acetate buffer was prepared by adjusting the pH of an aqueous solution of L-histidine (20 mM) to 5.5 with acetic acid.

Prior to use, all buffers were filtered through syringe filters (0.45 μ m) and stored at 4 °C.

5.2 Design, synthesis and biological evaluation of peptide directed phthalocyanine-gold nanocarriers

5.2.1 Synthesis of FITC- β AAEYLRK (2.16)

2.16 was synthesised following the general procedure described in **section 5.1.3**. Once the peptide was built, FITC was coupled onto the free N-terminus. FITC (1.2 eq) was dissolved in 12:7:5 pyridine:DMF:DCM, added to the resin and shaken overnight in the dark. Excess FITC was washed off the resin by washing six times with DMF, then the resin was washed six times with methanol and the peptide cleaved from the resin and purified as described in **section 5.1.3** to collect the peptide as a yellow solid (54 mg, 43.6 μ mol, 84%). RP-HPLC: t_R = 13.90 min. MALDI-ToF ($[M+H]^+$): $C_{59}H_{75}N_{13}O_{15}S$ calculated 1238.52, found 1238.50. HRMS (ESI-): calculated 1236.5148, found 1236.4804.

5.2.2 Synthesis of FITC- β ALARLLTK (2.17)

2.17 was synthesised following the general procedure described in **section 5.1.3**, then the peptide was FITC-tagged as described in **section 5.2.1**. After purification by preparative-RPHPLC the peptide was collected as a yellow solid (30 mg, 23.6 μ mol, 45%). RP-HPLC: t_R = 15.48 min. MALDI-ToF ($[M+H]^+$): $C_{61}H_{88}N_{14}O_{14}S$ calculated 1273.63, found 1273.29. HRMS (IT-ToF) ($[M+2H]^{2+}$): calculated 673.3235, found 637.3260.

5.2.3 Fluorescence microscopy for peptide binding determination

A549 cells were seeded at 1×10^5 cells/ mL, 100 μ L per well in a 96 well plate and incubated overnight at 37 °C, 5% CO₂. **2.16** (1 μ L, 10 mM), **2.17** (1 μ L, 10 mM), fluorescein (1 μ L, 10 mM) in DMSO were added to separate wells alongside a control well of DMSO (100 μ L). These cells were incubated for one hour at 37 °C, 5% CO₂, then washed three times with cold PBS. The cells were imaged using a Lieca fluorescent microscope at x10 magnification.

5.2.4 Flow cytometry

A549 and HEK293 cells were analysed for EGFR expression as described in **section 5.1.5**, using an anti-EGFR antibody.

5.2.5 Assessment of peptide cytotoxicity

A549 or HEK293 cells were seeded in 96 well plated (100 μ L, 1×10^5 cells/ mL) then incubated overnight at 37 °C, 5% CO₂. **2.16** or **2.17** (10 mM in DMSO) were diluted in a serial dilution then added to wells in triplicate (1 μ L). Cells were incubated for 72 hours at 37 °C, 5% CO₂ before the media was removed and fresh media added to each well (100 μ L). MTS (10 μ L) was added to each well then the cells incubated for three hours. The absorbance was recorded at 492 nm and corrected for background absorbance by subtracting the absorbance of media treated with MTS. Cell viability was calculated as a percentage of non-treated cells.

5.2.6 Synthesis of FITC- β ARALELK (2.26)

2.26 was synthesised following the general procedure described in **section 5.1.3**, then the peptide was FITC-tagged as described in **section 5.2.1**. After purification by preparative RP-HPLC the peptide was collected as a yellow solid (35 mg, 29.5 μ mol, 57%). Analytical HPLC: t_R = 14.20 min. MALDI-ToF: ($[M+H]^+$) C₅₆H₇₇N₁₃O₁₄S calculated 1188.54, found 1188.50. HRMS (IT-ToF) ($[M+3H]^{3+}$): calculated 396.8551, found 396.8570.

5.2.7 Synthesis of HS-PEG-peptides (2.27 and 2.28)

α -Thio- ω -carboxy-poly(ethylene glycol) (HS-PEG-COOH) (7.5 mg, 2.44 μ mol) was mixed with HATU (1.1 mg, 2.93 μ mol, 1.2 eq) and DIPEA (0.8 μ L, 4.88 μ mol, 2 eq) in DMF (300 μ L). **2.16** (4.53 mg, 3.66 μ mol, 1.5 eq) or **2.17** (4.66 mg, 3.66 μ mol, 1.5 eq) in DMF (50 μ L) was added to the solution and stirred overnight. The solution was evaporated to dryness and the crude peptide-PEG carried forward for nanoparticle synthesis.

5.2.8 Synthesis of peptide-C11Pc-PEG-AuNPs (2.29 and 2.30)

C11Pc (2.4 mg, 0.94 μ mol) was dissolved in anhydrous THF (1 mL) and stirred in the dark. **2.27** (5.24 mg, 1.22 μ mol) or **2.28** (5.30 mg, 1.22 μ mol) was dissolved in anhydrous THF (1 mL) and added to the solution alongside PEG (3.75 mg, 1.22 μ mol) in anhydrous THF (1 mL). HAuCl₄·3H₂O (1.2 mg, 3.05 μ mol) was dissolved in anhydrous THF (1.2 mL) and added to the solution. Sodium borohydride (1.5 mg, 39.65 μ mol) was dissolved in dH₂O (1.2 mL) and added under vigorous stirring. This solution was stirred for *ca.* 17 hrs in the dark. THF (5.4 mL) was added to the solution, then the solution was centrifuged at 1,400 rpm for 2 minutes. The supernatant was removed and evaporated to dryness. The nanoparticles were resuspended in PBS (2 mL) then centrifuged at 8,000 rpm for 20 minutes. The resulting supernatant was filtered, then purified through Vivaspin 500 columns, centrifuging at 8,000 rpm for 10 minutes, washing with PBS and repeating the purification. The resulting pellet was resuspended in PBS or RPMI 1640 without phenol red (2 mL) and stored at 4 °C in the dark. These peptide-C11Pc-PEG-AuNPs were characterised by UV-vis between 200-800 nm. The fluorescence excitation spectrum of C11Pc was recorded between 550-750 nm with an emission wavelength of 780 nm. The emission spectrum of C11Pc was recorded between 653-850 nm with an excitation wavelength of 633 nm. The excitation spectrum of FITC was recorded between 400-520 nm with an emission wavelength of 525 nm. The emission spectrum of FITC was recorded between 500-650 nm with an excitation wavelength of 490 nm.

5.2.9 Synthesis of C11Pc-PEG-AuNPs

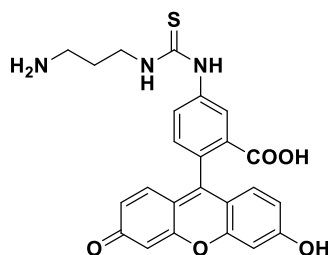
This synthesis followed the procedure of Garcia Calavia *et al.*¹ C11Pc (2.4 mg, 0.94 μ mol) was dissolved in anhydrous THF (1 mL) and stirred in the dark. PEG (7.5 mg, 2.44 μ mol) in

anhydrous THF (1 mL) was added to the solution, followed by H₂AuCl₄·3H₂O (1.2 mg, 3.05 μmol) dissolved in anhydrous THF (1.2 mL). Sodium borohydride (1.5 mg, 39.65 μmol) was dissolved in dH₂O (1.2 mL) and added under vigorous stirring. This solution was stirred for *ca.* 17 hrs in the dark. THF (5.4 mL) was added to the solution, then the solution centrifuged at 1,400 rpm for 2 minutes. The supernatant was removed and evaporated to dryness. The nanoparticles were resuspended in PBS or RPMI 1640 without phenol red (2 mL) then centrifuged at 8,000 rpm for 20 minutes. The resulting supernatant was filtered and stored at 4 °C in the dark. These C11Pc-PEG-AuNPs were characterised by UV-vis between 200-800 nm. The fluorescence excitation spectrum was recorded between 550-750 nm with an emission wavelength of 780 nm. The emission spectrum was recorded between 653-850 nm with an excitation wavelength of 633 nm.

5.2.10 Synthesis of PEG-AuNPs

PEG (15.2 mg, 5.1 μmol) was dissolved in dH₂O (15 mL). H₂AuCl₄·3H₂O (1.2 mg, 3.0 μmol) was dissolved in anhydrous THF (1.2 mL) and stirred with the PEG solution for five minutes. Sodium borohydride (1.5 mg, 39.7 μmol) was dissolved in dH₂O (0.5 mL) and added to the solution under rapid stirring. The solution was stirred for four hours at room temperature. Purification of these PEG-AuNPs was completed by centrifugation in Vivaspin 500 columns at 8,000 rpm for 10 minutes. The brown pellet was re-suspended in PBS buffer (10 mL), filtered through a syringe driven filter (0.22 μm) and stored at 4 °C. The UV-vis spectrum was recorded between 200-800 nm.

5.2.11 Synthesis of 5-(3-(3-aminopropyl)thioureido)-2-(6-hydroxy-3-oxo-3H-xanthen-9-yl) benzoic acid (2.34)



This synthesis followed the method of Trévisiol *et al.* with modifications.² FITC (6.00 mg, 15.41 μmol) was dissolved in methanol (1 mL) alongside 1,3-diaminopropane (2.60 μL, 31.15

μmol) and stirred for three hours. The methanol was removed under vacuum and the resulting orange solid purified by preparative HPLC, giving the product as an orange powder (6.35 mg, 13.70 μmol , 89%). $^1\text{H-NMR}$ (400 MHz, CD_3OD): 8.22 (d, 2H, $J = 1.8$ Hz), 7.81 (dd, 1H, $J = 2.0$ and 8.2 Hz), 7.25 (d, 1H, $J = 8.2$ Hz), 6.91 (d, 2H, $J = 8.3$ Hz), 6.86 (d, 2H, $J = 1.6$ Hz), 6.72 (d, 2H, $J = 8.8$ Hz), 3.80 (t, 2H, $J = 6.6$ Hz), 3.06 (t, 2H, $J = 7.3$ Hz), 2.02 (tt, 2H, $J = 7.0$ and 7.0 Hz). RP-HPLC $t_R = 13.12$ min. MALDI-ToF: ($[\text{M}+\text{H}]^+$) $\text{C}_{24}\text{H}_{21}\text{N}_3\text{O}_5\text{S}$ calculated 464.12, found 464.31. HRMS (IT-ToF) ($[\text{M}+\text{H}]^+$): calculated 464.1275, found 464.1284.

5.2.12 Synthesis of FITC-PEG

α -Thio- ω -carboxy-poly(ethylene glycol) (HS-PEG-COOH) (7.5 mg, 2.44 μmol) was mixed with HATU (1.4 mg, 3.68 μmol , 1.5 eq) and DIPEA (0.8 μL , 4.88 μmol , 2 eq) in DMF (100 μL). **2.34** (1.3 mg, 2.80 μmol , 1.1 eq) in DMF (50 μL) was added to the solution and stirred overnight. The solution was evaporated to dryness and the crude peptide-PEG carried forward for nanoparticle synthesis.

5.2.13 Synthesis of FITC-PEG-AuNPs (2.31)

PEG (3.75 mg, 1.27 μmol) and FITC-PEG (4.47 mg, 1.27 μmol) were dissolved in dH_2O (7.5 mL). $\text{HAuCl}_4 \cdot 3\text{H}_2\text{O}$ (0.6 mg, 1.5 μmol) was dissolved in anhydrous THF (0.6 mL) and stirred with the PEG solution for five min. Sodium borohydride (0.75 mg, 19.9 μmol) was dissolved in dH_2O (0.25 mL) and added to the solution under rapid stirring. The solution was stirred for four hours at room temperature. Purification of these FITC-PEG-AuNPs was completed by centrifugation in Vivaspin 500 columns at 8,000 rpm for 10 minutes. The pellet was re-suspended in PBS buffer (4 mL), filtered through a syringe driven filter (0.22 μm) and stored at 4 $^\circ\text{C}$. The UV-vis spectrum was recorded between 800-300 nm.

5.2.14 Synthesis of FITC-C11Pc-PEG-AuNPs (2.33)

C11Pc (2.4 mg, 0.94 μmol) was dissolved in anhydrous THF (1 mL) and stirred in the dark. FITC-PEG (4.29 mg, 1.22 μmol) was dissolved in anhydrous THF (1 mL) and added to the solution alongside PEG (3.75 mg, 1.22 μmol) in anhydrous THF (1 mL). $\text{HAuCl}_4 \cdot 3\text{H}_2\text{O}$ (1.2

mg, 3.05 μmol) was dissolved in anhydrous THF (1.2 mL) and added to the solution. Sodium borohydride (1.5 mg, 39.65 μmol) was dissolved in dH_2O (1.2 mL) and added under vigorous stirring. This solution was stirred for *ca.* 17 hrs in the dark. THF (5.4 mL) was added to the solution, then the solution centrifuged at 1,400 rpm for 2 minutes. The supernatant was removed and evaporated to dryness. The nanoparticles were resuspended in PBS (2 mL) then centrifuged at 8,000 rpm for 20 minutes. The resulting supernatant was filtered, then purified through Vivaspin 500 columns, centrifuging at 8,000 rpm for 10 minutes, washing with PBS and repeating the purification. The resulting pellet was resuspended in PBS (2 mL) and stored at 4 °C in the dark. These FITC-C11Pc-PEG-AuNPs were characterised by UV-vis between 200-800 nm.

5.2.15 Singlet oxygen production

2.29, 2.30, C11Pc-PEG-AuNPs or PEG-AuNPs in PBS or methanol (1 μM , 511 μL) were added to a quartz cuvette alongside ABMA (1 μL , 0.512 mM in MeOH). This cuvette was stoppered and irradiated with a 10 mW HeNe laser at 633 nm, with the laser placed 50 cm away. Every five minutes the fluorescence emission spectrum of ABMA was recorded between 390-600 nm, with an excitation wavelength of 380 nm. A control of PBS or methanol and ABMA (1 μL , 0.512 mM in MeOH) was also irradiated and the ABMA fluorescence emission spectrum recorded every five minutes.

5.2.16 Optimised solvent system for peptide-nanoparticle synthesis

HS-PEG-COOH (3.75 mg, 1.22 μmol) was mixed with HATU (4.63 mg, 1.22 μmol , 1 eq) and DIPEA (2.12 μL , 1.22 μmol , 1 eq) in DMF (100 μL), then stirred for five minutes. **2.16** (1.51 mg, 1.22 μmol , 1 eq) in DMF (150 μL) was added to the solution and stirred for 15 minutes. The solution was evaporated to dryness and the crude peptide-PEG carried forward for nanoparticle synthesis.

C11Pc (2.4 mg, 0.94 μmol) was dissolved in anhydrous THF (1 mL) and stirred in the dark. **2.27** (5.24 mg, 1.22 μmol) was dissolved in anhydrous DMF (1 mL) and added to the solution alongside PEG (3.75 mg, 1.22 μmol) in anhydrous THF (1 mL). $\text{HAuCl}_4 \cdot 3\text{H}_2\text{O}$ (1.2 mg, 3.05 μmol) was dissolved in anhydrous THF (1.2 mL) and added to the solution. Sodium borohydride (1.5 mg, 39.65 μmol) was dissolved in dH_2O (1.2 mL) and added under vigorous

stirring. This solution was stirred for *ca.* 17 hrs in the dark. THF (5.4 mL) was added to the solution, then the solution centrifuged at 1,400 rpm for 2 minutes. The supernatant was removed and evaporated to dryness. The nanoparticles were resuspended in PBS then centrifuged at 8,000 rpm for 20 minutes. The resulting supernatant was filtered, then purified through Vivaspin 500 columns, centrifuging at 8,000 rpm for 10 minutes, washing with PBS and repeating the purification. The resulting pellet was resuspended in PBS (1 mL) and stored at 4 °C in the dark. The resulting nanoparticles were characterised by UV-vis spectroscopy between 200-800 nm.

5.2.17 Variation of coupling agent

PEG (1.88 mg, 61.28 μ mol) was dissolved in DMF (150 μ L) alongside the coupling agents listed in **Table 5.1** (1 eq) and DIPEA (0.11 μ L, 1 eq).

Table 5.1: A summary of the coupling agents trialled for the synthesis of **2.29**

Entry	Coupling agent	Mass (mg)
1	(Benzotriazol-1-yloxy)tripyrrolidinophosphonium hexafluorophosphate (PyBOP)	0.32
2	<i>N</i> -[(Dimethylamino)-1 <i>H</i> -1,2,3-triazolo-[4,5- <i>b</i>]pyridin-1-ylmethylene]- <i>N</i> -methylmethanaminium hexafluorophosphate <i>N</i> -oxide (HATU)	0.23
3	2-(1 <i>H</i> -Benzotriazole-1-yl)-1,1,3,3-tetramethylaminium tetrafluoroborate (TBTU)	0.20
4	(1-cyano-2-ethoxy-2-oxoethylidenaminoxy)dimethylamino-morpholinocarbenium hexafluorophosphate (COMU)	0.26
5	<i>N</i> -(3-dimethylaminopropyl)- <i>N</i> '-ethylcarbodiimide hydrochloride (EDC)	0.12
	<i>N</i> -hydroxysuccinimide (NHS)	0.07
6	<i>N,N</i> '-diisopropylcarbodiimide (DIC)	0.08 (0.1 μ L)
	Ethyl cyano(hydroximino)acetate (Oxyma)	1.10
7	Carbonyldiimidazole (CDI)	0.10

This solution was stirred for 5 min, then **2.16** (0.76 mg, 1 eq) in DMF (10 μ L) was added to the solution and stirred in the dark for 15 min. The solvent was removed under vacuum and the crude mixture used in the synthesis of **2.29** as described in **section 5.2.16**.

5.2.18 Phototoxicity of 2.29

A549 or HEK293 cells were seeded at 1×10^5 cells/mL, 100 μ L per well in 96 well plates, then incubated for 24 hours. The media was removed and **2.29** (50 μ L) were added in FCS free RPMI and incubated for three hours. Staurosporine (3 μ L, 1 mM in DMSO) was used as a positive control. The wells were washed three times with PBS, then complete phenol red free media (100 μ L) added to each well. For each experiment two identical plates were prepared, then one plate irradiated with a 633 nm 10 mW HeNe laser, 6 minutes per well with the laser secured 50 cm above the plate. The other plate was kept in the dark. After irradiation, both plates were incubated a further 48 hours. MTS (10 μ L) was added to each well and the plates incubated for three hours before measurement of the absorption at 492 nm on a BMG Labtech PolarStar Optima plate reader.

5.2.19 Phototoxicity of control AuNPs

2.16 (200 nM), PEG-AuNPs (20 nM), **2.31** (200 nM), **2.32** (200 nM), **2.33** (200 nM) and C11Pc-PEG-AuNPs (200 nM) were tested for phototoxicity as described in **section 5.2.18**.

5.3 Investigations into antibody conjugation for the development of antibody directed phthalocyanine-gold nanocarriers

5.3.1 Synthesis of C11Pc-PEG-AuNPs

C11Pc-PEG-AuNPs were synthesised as described in **section 5.2.9**.

5.3.2 FITC-tagging of antibodies (3.7)

FITC (1 μ L, 10.2 mM in DMSO) and anti-EGFR antibody (5 μ L, 1 mg/mL) were mixed in PBS (20 μ L) and incubated in the dark for seven hours. PBS (15 μ L) was added to the solution, then the antibody purified through Zeba spin desalting columns (7,000 MWCO). The resulting antibody was diluted to 50 μ L total volume in PBS. The emission spectrum was

recorded between 500-600 nm with an excitation wavelength of 472 nm. The excitation spectrum was recorded between 420-520 nm with an emission wavelength of 548 nm.

5.3.3 Conjugation of 5-FAM to antibody (3.8)

5-carboxyfluorescein (5-FAM, 6.5 mg, 17.27 μmol) was dissolved in 2:1 DMSO:MES buffer (1.6 mL), then mixed with EDC (3.4 mg, 17.74 μmol) and NHS (3.6 mg, 31.28 μmol) and stirred for 30 minutes. The resulting activated 5-FAM (1 μL) was added to anti-EGFR antibody (5 μL , 1 mg/mL) in PBS (50 μL) and the solution was incubated for six hours. The antibody was purified through Zeba spin desalting columns (7,000 MWCO). The emission spectrum was recorded between 500-600 nm with an excitation wavelength of 472 nm. The excitation spectrum was recorded between 420-520 nm with an emission wavelength of 548 nm.

5.3.4 Conjugation of 2.34 to C11Pc-PEG-AuNPs (3.9)

EDC (1 mg, 5.22 μmol) and NHS (1.2 mg, 10.43 μmol) were mixed with C11Pc-PEG-AuNPs in MES buffer (1 mL, 3 μM) and stirred in the dark for 30 minutes. The excess EDC/NHS was removed by centrifugation through Vivaspin 500 columns (8,000 rpm, 10 min). **2.34** (0.15 mg, 0.32 μmol) was dissolved in PBS (1 mL) and the AuNP pellets resuspended in this solution. The AuNPs were stirred overnight in the dark, then purified by centrifugation in Vivapsin 500 columns (8,000 rpm, 20 min), washing six times with PBS. The resulting FITC-C11Pc-PEG-AuNPs were resuspended in PBS and analysed by UV-vis spectroscopy between 300-800 nm.

5.3.5 Antibody functionalisation of C11Pc-PEG-AuNPs via EDC/NHS (3.10 and 3.15)

C11Pc-PEG-AuNPs in MES buffer (1 mL, 4 μM), EDC (1 mg, 5.22 μmol) and NHS (1.2 mg, 10.43 μmol) were stirred in the dark for 30 minutes. Excess EDC/NHS was removed by centrifugation in Vivaspin 500 columns, 8,000 rpm, 15 minutes. Anti-EGFR antibody (5 μL , 1 mg/mL) was diluted in PBS (1 mL) and stirred slowly overnight in the dark with the AuNPs. The resulting nanoconjugates were purified through Vivaspin 500 columns, washing

the pellet three times, then resuspended in PBS. The UV-spectrum was recorded between 300-800 nm.

5.3.6 Functionalisation of C11Pc-PEG-AuNPs with PDEA

C11Pc-PEG-AuNPs in MES buffer (1 mL, 4 μ M), EDC (1 mg, 5.22 μ mol) and NHS (1.2 mg, 10.43 μ mol) were stirred in the dark for 30 minutes. Excess EDC/NHS was removed by centrifugation in Vivaspin 500 columns (8,000 rpm, 15 min). Pyridine dithioethylamine hydrochloride (PDEA, 1.33 mg, 5.97 μ mol) was dissolved in PBS (1 mL), added to the AuNPs, and the resulting solution stirred overnight in the dark. The resulting nanocarriers were purified in Vivaspin 500 columns (8,000 rpm, 15 min) and washed three times with PBS, then the nanoparticles resuspended in PBS (1 mL). UV-vis spectra were recorded of the washings and PDEA-C11Pc-PEG-AuNPs between 300-800 nm.

5.3.7 Antibody functionalisation of C11Pc-PEG-AuNPs via maleimide (3.12, 3.13, 3.16)

C11Pc-PEG-AuNPs in MES buffer (1 mL, 4 μ M), EDC (1 mg, 5.22 μ mol) and NHS (1.2 mg, 10.43 μ mol) were stirred in the dark for 30 minutes. Excess EDC/NHS was removed by centrifugation in Vivaspin 500 columns, 8,000 rpm, 15 minutes. 1-(2-aminoethyl)maleimide hydrochloride (3 mg, 16.99 μ mol) was dissolved in PBS (1 mL) and the collected AuNP pellets were added to this solution. This solution was stirred in the dark for 30 minutes, then centrifuged at 8,000 rpm, 15 minutes in Vivaspin 500 columns to give **3.12**. Anti-EGFR antibody (5 μ L, 1 mg/mL) was diluted in PBS (1 mL) and stirred slowly overnight with the AuNPs. The resulting nanoparticles were purified through Vivaspin 500 columns, washing the pellet three times, then resuspended in PBS. The UV-spectrum was recorded between 300-800 nm.

5.3.8 Reduction of antibody disulphides and functionalisation of 3.12 (3.14 and 3.17)

3.12 were synthesised as described in **section 5.3.7**. Anti-EGFR antibody (5 μ L, 1 mg/mL) was mixed with TCEP (4×10^{-11} mol, 1.2 eq) in PBS (200 μ L). The solution was incubated at

37°C for 30 minutes, then purified in Zeba spin desalting columns (7,000 MWCO). The purified antibody was immediately added to maleimide-functionalised C11Pc-PEG-AuNPs and stirred overnight. The resulting nanocarriers were purified as described in **section 5.3.7**, and analysed by UV-vis spectroscopy between 300-800 nm.

5.3.9 Flow cytometry

The binding of the Abcam anti-EGFR antibody and the R&D Systems anti-EGFR antibody to EGFR on A549 and H292 cells was analysed by flow cytometry as described in **section 5.1.5**.

5.3.10 Singlet oxygen production

3.10, **3.13**, and **3.14** (1 µL) in PBS were tested for singlet oxygen production as described in **section 5.2.15**.

5.3.11 SDS-PAGE for determining antibody binding to AuNPs

This method followed the method of van der Heide *et al.* with modifications.³ AuNPs (1 mL) were concentrated in Vivaspin columns by centrifugation (8,000 rpm, 10 min). The resulting pellet (20 µL) was mixed with tris-glycine SDS sample buffer (20 µL) and DTT (4 µL, 2 M in H₂O). Antibody controls were prepared by diluting in PBS (5 µL in 15 µL PBS, 0.25 mg/mL), then mixing with tris-glycine SDS sample buffer (20 µL) and DTT (4 µL, 2 M in H₂O). The solutions were incubated at 100 °C for 10 mins, then cooled before 20 µL of AuNPs and 10 µL of Ab was loaded onto a 4-12% SDS-polyacrylamide gel alongside Thermo Scientific PageRuler prestained protein ladder (3 µL). Electrophoresis was performed at a constant voltage of 170 V for 75 minutes in MOPS SDS running buffer.

The resulting gel was washed with H₂O, stained with Coomassie stain under rocking until the gel maintained a bright blue colour. The gel was then destained with destaining solution under rocking until the background was colourless again. Coomassie stain was prepared by dissolving Coomassie Brilliant blue R250 (1.00 g, 1.21 mmol) in 1:5:4 glacial acetic acid:water:methanol (1 L), before filtering to remove particulates. Destaining solution was prepared by mixing glacial acetic acid (100 mL) with water (700 mL) and methanol (200 mL).

5.3.12 Anti-EGFR antibody functionalisation of 2.31

2.31 were functionalised with an anti-EGFR antibody, as described in **sections 5.3.5, 5.3.7** and **5.3.8**.

5.3.13 Fluorescence microscopy for the internalisation of antibody-AuNPs

A549 cells were seeded at 1×10^5 cells/ mL, 2 mL per well in a 6 well plate and incubated overnight at 37 °C, 5% CO₂. Ab-FITC-PEG-AuNPs (1 mL, 5 μM) in serum free RPMI were added to separate wells. These cells were incubated for one hour at 37 °C, 5% CO₂, then washed three times with cold PBS. The cells were imaged using a Lieca fluorescent microscope at x10 magnification.

5.3.14 Synthesis of PEG-AuNPs

PEG-AuNPs were synthesised as described in **section 5.2.10**.

5.3.15 Synthesis of protein G-PEG-AuNPs (3.19)

PEG-AuNPs in MES buffer (1 mL, 120 nM) were mixed with EDC (1 mg, 5.22 μmol) and NHS (1.2 mg, 10.43 μmol) and stirred in the dark for 30 minutes. The excess EDC/NHS was removed by centrifugation at 8,000 rpm for 15 minutes in Vivaspin 500 columns. Protein G (5 μL, 1 mg/mL in PBS) was diluted in PBS (1 mL), then stirred overnight with the activated AuNPs. The resulting protein G-C11Pc-PEG-AuNPs (**3.9**) were purified by centrifugation at 8,000 rpm, 15 minutes in Vivaspin 500 columns, washing the pellet three times with PBS buffer. The pellet was resuspended in PBS.

5.3.16 Non-covalent binding of anti-HER2 antibody to 3.19 (3.20)

3.19 (1 mL) were prepared as described in **section 5.3.15** and dispersed in sodium phosphate buffer, pH 8.0. Anti-HER2 antibody (5 μL, 1 mg/mL) was stirred slowly alongside these nanocarriers for one hour. The resulting nanocarriers were purified through Vivaspin 500 columns (8,000 rpm, 15 minutes, 4 °C), washing three times with sodium phosphate buffer.

5.3.17 Cross-linking of anti-HER2 antibody to 3.19 (3.21)

3.19 (500 μL) were prepared as described in **section 5.3.15** and dispersed in phosphate buffer, pH 8.0. Anti-HER2 antibody (2.5 μL , 1 mg/mL) was stirred slowly alongside these nanocarriers for one hour. The resulting nanocarriers were purified through Vivaspin 500 columns (8,000 rpm, 15 minutes, 4 $^{\circ}\text{C}$) and resuspended in triethanolamine buffer (1 mL) alongside dimethylpimelimidate dihydrochloride (DMP, 3.3 mg, 12.73 μmol). The solution was stirred slowly for *ca.* 45 minutes, then purified by centrifugation in Vivaspin 500 columns (14,000 rpm, 15 min, 4 $^{\circ}\text{C}$). The resulting nanoparticle pellet was resuspended in ethanolamine buffer and incubated for one hour with slow stirring, before purification by centrifugation in Vivaspin 500 columns (14,000 rpm, 15 min, 4 $^{\circ}\text{C}$). The nanoparticle pellet was washed three times with sodium phosphate buffer.

5.3.18 SDS-PAGE of protein G-AuNPs

3.9, **3.10** and **3.11** were analysed by SDS-PAGE as described in **section 5.3.11**.

5.3.19 Gly-Fc-III-Bpa (3.22) and FITC-Fc-III-Bpa (3.23) synthesis

3.22 (GDCAWHLGELBpaWCT) and **3.23** (FITC- β ADCAWHLGELBpaWCT) were synthesised by solid phase peptide synthesis, as described in **section 5.1.3**. FITC was added to the peptide as described in **section 5.2.1**. The peptides were cleaved from the resin using 92.5:2.5:2.5:2.5 TFA:EDT:TIPS:H₂O and shaking for three hours. The solvent was removed under vacuum and the resulting peptide washed with cold diethyl ether. Gly-Fc-III-Bpa and FITC-Fc-III-Bpa were stirred overnight in 0.1 M sodium phosphate buffer (15 mL, pH 8.0) at 35 $^{\circ}\text{C}$, then the solvent removed under vacuum. The resulting peptides were purified by preparative RP-HPLC, giving the pure peptides **3.22** (4.04 mg, 2.32 μmol , 4.5%) and **3.23** (4.50 mg, 2.10 μmol , 4%).

3.22: MALDI-ToF ($[\text{M}+\text{H}]^+$): C₈₂H₁₀₃N₁₉O₂₀S₂ calculated 1738.70, found 1738.60. RP-HPLC t_{R} = 15.75 min.

3.23: MALDI-ToF ($[\text{M}+\text{H}]^+$): C₁₀₄H₁₁₆N₂₀O₂₅S₃ calculated 2141.76, found 2141.66. RP-HPLC t_{R} = 17.62 min.

5.3.20 UV crosslinking of 3.22 to an anti-EGFR antibody

Photo-crosslinking reactions were completed in Eppendorf tubes with a final volume of 20 μL . Samples were prepared in PBS, with final concentrations of 1.67 μM (0.25 mg/mL) of anti-EGFR antibody, 16 μM **3.22**, and 5% v/v DMSO. Samples were irradiated for 4 h in the dark.

5.3.21 SDS-PAGE for 3.22 binding to an anti-EGFR antibody

Conjugated anti-EGFR antibody (10 μL , 0.25 mg/mL), anti-EGFR antibody (10 μL , 0.5 mg/mL) and a 10:1 peptide:Ab solution in PBS (10 μL) were analysed by SDS-PAGE. Samples were mixed with tris-glycine SDS sample buffer (10 μL) and DTT (2 μL). The solutions were incubated at 100 $^{\circ}\text{C}$ for 10 mins, then cooled before 20 μL each sample was loaded onto a 4-12% SDS-polyacrylamide gel alongside Thermo Scientific PageRuler prestained protein ladder (3 μL). Electrophoresis was performed at a constant voltage of 170 V for 75 minutes in MOPS SDS running buffer.

The resulting gel was washed with H_2O , stained with Coomassie stain under rocking until the gel maintained a bright blue colour. The gel was then destained with destaining solution under rocking until the background was colourless. Coomassie stain and destaining solution were prepared as described in **section 5.3.11**.

5.3.22 UV crosslinking of 3.23 to an anti-EGFR antibody

This method followed the method of Vance *et al.* with modification.⁴ Photo-crosslinking reactions were performed in a clear, 96-well plate with a final reaction volume of 100 μL . The reaction was performed in either histidine acetate buffer or PBS, with final concentrations of 6.67 μM (1mg/mL) of anti-EGFR antibody, 66.67 μM **3.23**, 66.67 μM 5-hydroxyindole and 10% v/v DMSO. Samples were irradiated for 4 h in the dark with the plate resting on an ice pack. Samples were collected after 2 h (25 μL) and 4 h (75 μL), then precipitated in cold acetone (500 μL) and left in a cooling bath at -20 $^{\circ}\text{C}$ for 1 h. The antibody was collected by centrifugation and resuspended in PBS (5 μL).

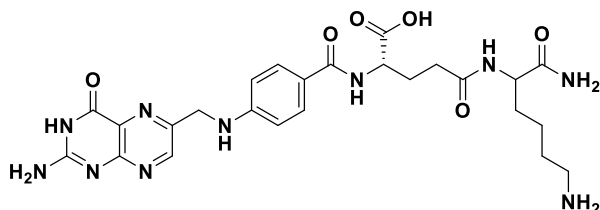
5.3.23 SDS-PAGE for 3.23 binding to an anti-EGFR antibody

Conjugated anti-EGFR antibody samples (5 μ L), anti-EGFR antibody (5 μ L, 1 mg/mL) and FITC goat anti-mouse secondary antibody (5 μ L, 2 mg/mL) were mixed with tris-glycine SDS sample buffer (5 μ L) and DTT (2 μ L, 2 M in H₂O). The solutions were incubated at 100 °C for 10 mins, then cooled before 10 μ L of each sample was loaded onto a 4-12% SDS-polyacrylamide gel alongside Thermo Scientific PageRuler prestained protein ladder (3 μ L). Electrophoresis was performed at a constant voltage of 190 V for 40 minutes in MOPS SDS running buffer.

The resulting gel was washed with H₂O, then imaged in an ImageQuant LAS 4000 imager. The gel was then stained with Coomassie stain under rocking until the gel maintained a bright blue colour. The gel was then destained with destaining solution under rocking until the background was colourless. Coomassie stain and destaining solution were prepared as described in **section 5.3.11**.

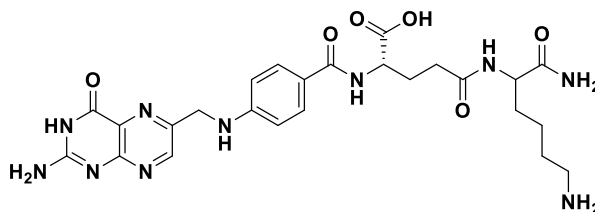
5.4 Towards protease cleavable sequences to ‘turn on’ the photodynamic activity of folate directed phthalocyanine-gold nanocarriers

5.4.1 Synthesis of FA-Lys (4.12) on the solid phase



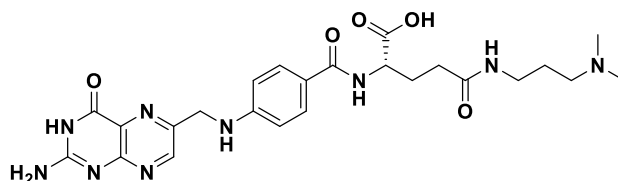
Rink amide MBHA resin (30 mg, 0.016 mg) was swelled for 30 minutes in DMF then loaded with appropriately protected lysine, as described in **section 5.1.3**. Folic acid (8.3 mg, 18.80 μ mol, 1.2 eq) in DMSO was added to the resin and shaken overnight. The resin was washed with DMSO (x2), DMF (x6) and DCM (x6), then cleavage of the peptide from the resin was completed in 95:2.5:2.5 TFA:TIPS:H₂O, 3 h. The solvent was removed under vacuum, the peptide isolated with cold ether precipitation. The peptide was purified by semi-preparative RP-HPLC, giving the peptide (4.11 mg, 46%). RP-HPLC: t_R = 10.05 and 10.41 mins, MALDI-ToF: C₂₅H₃₂N₁₀O₆ ([M+H]⁺) calculated 569.26, found 569.13.

5.4.2 Temperature controlled synthesis of 4.12 on the solid phase



This synthesis followed the method of Guaragna *et al.* with modifications.⁵ Rink amide MBHA resin (30 mg, 0.0156 mmol) loaded with appropriated protected lysine, as described in **section 5.1.3**. DMSO (2 mL) and DIPEA (3.9 μ L, 22.56 μ mol, 1.44 eq) were heated to 50 $^{\circ}$ C, then folic acid (8.3 mg, 18.80 μ mol 1.2 eq) was slowly added. Once dissolved, PyBOP (9.8 mg, 18.80 μ mol, 1.2 eq) was added and the resulting solution added to the resin and shaken overnight at 30 $^{\circ}$ C in a peptide column. The resin was washed with DMSO (x2), DMF (x6) and DCM (x6), then cleavage of the peptide from the resin was completed in 95:2.5:2.5 TFA:TIPS:H₂O. The solvent was removed under vacuum, the peptide isolated with cold ether precipitation, then purified by semi-preparative HPLC, giving the peptide (3.09 mg, 35%). RP-HPLC: t_R = 10.01 and 10.36 min. MALDI-ToF: C₂₅H₃₂N₁₀O₆ [(M+H)⁺] calculated 569.26, found 569.32, 569.31.

5.4.3 Synthesis of 3-dimethylaminopropylfolic acid (4.13) via temperature control

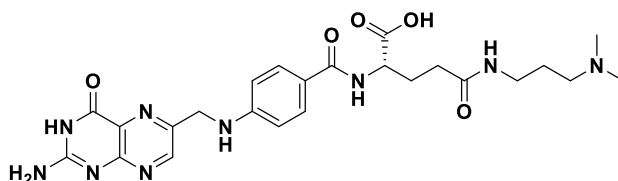


This synthesis followed the method of Santos *et al.* with modifications.⁶ Folic acid (88 mg, 0.2 mmol) was dissolved in DMF (1 mL) alongside N-methylmorpholine (45 μ L, 0.4 mmol) and either TBTU (64 mg, 0.2 mmol) or PyBOP (104 mg, 0.2 mmol) and stirred at 0 $^{\circ}$ C for 45 minutes. 3-(dimethylamino)-1-propylamine (25 μ L, 0.2 mmol) was added to the solution and stirred for two hours at 0 $^{\circ}$ C. The DMF was removed under vacuum, yielding the crude product.

TBTU coupling: RP-HPLC: $t_R = 9.96, 10.14, 10.37$ mins. MALDI-ToF ($[M+H]^+$): $C_{24}H_{32}N_9O_5$ calculated 526.25, found 526.36 and 526.45. For the di-substituted product ($[M+H]^+$): $C_{29}H_{43}N_{10}O_5$ calculated 611.34, found 611.78.

PyBOP coupling: RP-HPLC: $t_R = 10.15, 10.26$ and 10.39 mins. MALDI-ToF ($[M+H]^+$): $C_{24}H_{31}N_9O_5$ calculated 526.25, found 526.77 and 526.64. For the di-substituted product ($[M+H]^+$): $C_{29}H_{43}N_{10}O_5$ calculated 611.34, found 610.99.

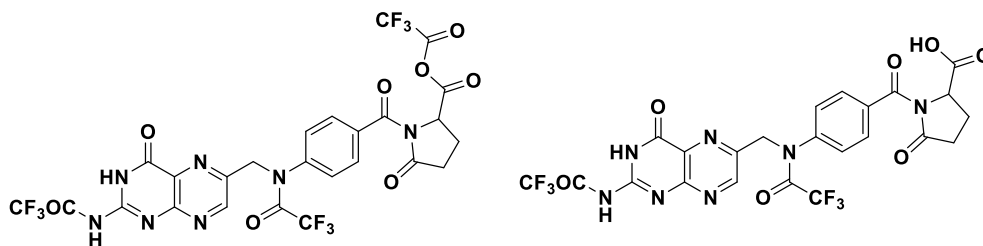
5.4.4 Synthesis of 4.13 via NHS-ester



Folic acid (0.47 g, 1.06 mmol) was dissolved in DMSO (10 mL) alongside DCC (0.49 g, 2.37 mmol), NHS (0.16 g, 1.39 mmol) and triethylamine (0.25 mL, 1.79 mmol). The reaction was stirred overnight, filtered and precipitated with diethyl ether. The resulting orange precipitate was filtered under vacuum and washed with diethyl ether, yielding crude folate-NHS ester (0.64 g).

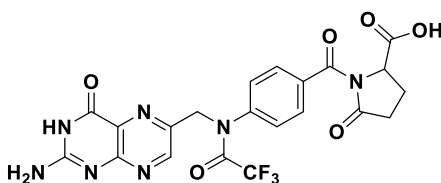
Crude folate NHS ester (0.27 g) was dissolved in DMSO (5 mL). 3-(dimethylamino)-1-propylamine (63.1 μ L, 0.50 mmol) was added to the solution and stirred overnight. The product was precipitated with acetone, filtered under vacuum and washed with acetone to give the crude product (0.23 g, 0.44 mmol). No further purification was undertaken. RP-HPLC: $t_R = 10.26$ and 10.52 mins. MALDI-ToF: $C_{24}H_{31}N_9O_5$ ($[M+H]^+$) calculated 526.25, found 526.32 & 526.31.

5.4.5 Synthesis of N^{2,10}-Bis(trifluoroacetyl)pyrofolic acid/anhydride (4.14 and 4.15)



This synthesis followed the procedure of Luo *et al.* with modifications.⁷ Folic acid (5.00 g, 11.32 mmol) was suspended in anhydrous THF (40 mL) and cooled to 0 °C. Trifluoroacetic anhydride (13 mL, 93.52 mmol) was added dropwise to the suspension, causing a colour change from orange-yellow to dark brown. Once the trifluoroacetic anhydride was all added, the reaction was warmed to RT and stirred for *ca.* 17 h. The solution was filtered to remove any solid residue and concentrated under reduced pressure. The solution was transferred with the aid of THF into well-stirred diethyl ether and the precipitated yellow solid collected by filtration then washed with diethyl ether to yield a crude product (4.13 g). ¹H-NMR; some peaks appear as atropisomers and are reported as their most abundant peak (400 MHz, DMSO-*d*₆): 8.75 (s, 1 H), 7.77-7.66 (m, 4 H), 5.20 (s, 2 H), 4.77 (dd, 1 H, *J* = 4.0 and 8.9 Hz), 2.63-2.00 (overlap, 4 H). ¹⁹F-NMR (376 MHz, DMSO-*d*₆): -66.11, -74.66, -80.90 (integration ratio 0.67:1.00:0.12).

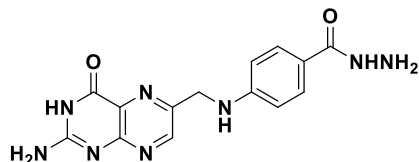
5.4.6 Synthesis of N¹⁰-(trifluoroacetyl)pyrofolic acid (4.16)



This synthesis followed the procedure of Luo *et al.*⁷ Crude **4.14/4.15** (4.12 g) was dissolved in THF (15 mL) and ice (3.01 g) was added. The solution immediately darkened in colour and was stirred for 3 h. The gel was precipitated in diethyl ether then the orange solid collected by filtration and triturated in diethyl ether. The final product was dried under vacuum for 18 h giving **4.16** (3.35 g, 6.82 mmol, 60% over two steps) ¹H-NMR; some peaks appear as atropisomers and are reported as their most abundant peak (400 MHz, DMSO-*d*₆):

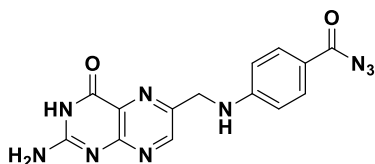
8.69 (s, 1 H), 7.78-7.65 (m, 4 H), 5.17 (s, 2 H), 4.77 (dd, 1 H, $J = 3.9$ and 8.9 Hz), 2.70-2.00 (overlap, 4 H). ^{13}C -NMR (100 MHz, $\text{DMSO-}d_6$): 175.9, 174.5, 172.8, 169.1, 156.1, 155.7, 154.4, 149.4, 144.6, 142.1, 135.0, 130.0, 128.4, 117.7, 114.9, 58.8, 54.1, 31.5, 21.6 ^{19}F -NMR (376 MHz, $\text{DMSO-}d_6$): -62.24, -66.07, -80.89 (integration ratio 0.04:1.00:0.13).

5.4.7 Synthesis of pteroyl hydrazide (4.17)



This synthesis followed the procedure of Luo *et al.* with modifications.⁷ **4.16** (0.50 g, 1.02 mmol) was dissolved in DMSO (10 mL) and hydrazine monohydrate (0.3 mL, 6.18 mmol) slowly added while the temperature was maintained at 25 °C. The solution was stirred for *ca.* 17 h then the product precipitated from solution using methanol. The yellowish solid was collected by filtration, washed with diethyl ether and dried under vacuum for 18 h, giving **4.17** (0.30 g, 0.92 mmol, 90%). ^1H -NMR (400 MHz, $\text{DMSO-}d_6$): 8.64 (s, 1 H), 7.62 (d, 2 H, $J = 8.7$), 6.64 (d, 2 H, $J = 8.7$ Hz), 4.48 (d, 2 H, $J = 6.0$ Hz). ^{13}C -NMR (100 MHz, $\text{DMSO-}d_6$): 171.1, 165.2, 160.0, 155.2, 150.5, 147.6, 147.4, 128.1, 127.0, 117.5, 110.4, 44.8. MALDI-ToF ($[\text{M}+\text{H}]^+$): $\text{C}_{14}\text{H}_{14}\text{N}_8\text{O}_2$ calculated 327.12, found 327.42. RP-HPLC: $t_R = 9.95$ mins.

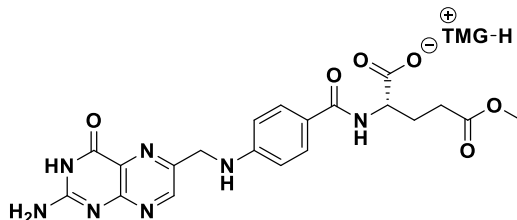
5.4.8 Synthesis of pteroyl azide (4.18)



This synthesis followed the procedure of Luo *et al.*⁷ **4.17** (1.88 g, 5.76 mmol) was stirred with potassium thiocyanate (27 mg, 0.28 mmol). Ice-cold trifluoroacetic acid (14.5 mL, 189.36 mmol) was added and stirred until the solid dissolved. The solution was cooled to -5 °C, *tert*-butyl nitrite (0.67 mL, 5.63 mmol) added and stirred for 4 h at -5 °C. The solution was warmed to RT and sodium azide (0.19 g, 2.92 mmol, 0.5 eq) was added to the solution and stirred for 10 mins. The solution was precipitated with 2-propanol. the resulting yellow

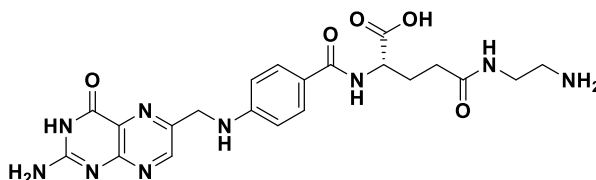
powder was purified by centrifugation, washing with water (3 x), acetonitrile (1 x) and diethyl ether (3 x) then dried under vacuum for 18 h, resulting in **4.18** (1.16 g, 3.44 mmol, 60%). The formation of the azide was confirmed using IR spectroscopy, then the crude mixture used in the next step. ν_{max} : 2137 (N_3), 1708 (C=O), 1592 (C=O).

5.4.9 Synthesis of tetramethylguanadinium L-methyl folate (4.19)



This synthesis followed the procedure of Luo *et al.*⁷ Crude **4.18** (0.53 g, 1.57 mmol) was dissolved in DMSO (5 mL). *L*-glutamic acid 5-methyl ester (0.48 g, 2.97 mmol) and tetramethylguanidine (313.5 μL , 2.50 mmol) was added to the solution and stirred overnight. The solution was precipitated in acetone, collected by filtration and washed with diethyl ether. The resulting yellow powder was dried under vacuum overnight, yielding the product (0.73 g, 1.27 mmol, 81%). ¹H-NMR (400 MHz, DMSO-*d*₆): 8.62 (s, 1 H), 7.59 (d, 2 H, *J* = 8.6 Hz), 6.92 (t, 1 H, *J* = 5.7 Hz), 6.69 (d, 2 H, *J* = 8.8 Hz), 4.49 (d, 2 H, *J* = 5.6 Hz), 4.05 (m, 1 H), 3.55 (s, 3 H), 2.90 (s, 12 H), 2.43-1.90 (m, 4 H). ¹³C-NMR (100 MHz, DMSO-*d*₆): 177.0, 174.9, 173.6, 173.1, 165.4, 163.1, 161.2, 156.5, 156.2, 150.7, 148.2, 147.7, 128.5, 128.0, 122.2, 111.4, 53.6, 51.2, 46.1, 39.4, 30.3, 28.1. HRMS (IT-ToF): C₂₀H₂₁N₇O₆ ([M+Na]⁺) calculated 478.1446, found 478.1452

5.4.10 Synthesis of 2-aminoethylfolic acid (4.6)



This synthesis followed the procedure of Luo *et al.* with modifications.⁷ **4.19** (50 mg, 87.63 μmol) was stirred with ethylenediamine (0.36 mL) for 3 h. As the reaction proceeded the **4.19**

dissolved (*ca.* 5 mins to dissolve). The product was precipitated using 1:1 diethyl ether:acetonitrile and the resulting sol centrifuged to collect an orange oil. This oil was dissolved in water, precipitated in acetone, collected via filtration and washed with diethyl ether to give an orange-brown product (36 mg, 74.46 μmol , 85%). $^1\text{H-NMR}$ (400 MHz, $\text{DMSO-}d_6$): 8.62 (s, 1 H), 7.92 (s, 1 H), 7.56 (d, 2 H, $J = 8.7$ Hz), 7.21 (s, 2 H), 6.91 (s, 1 H), 6.64 (d, 2 H, $J = 8.6$ Hz), 4.46 (s, 2 H), 4.01 (m, 1 H), 3.13-3.01 (m, 2 H), 2.83-2.71 (m, 2 H), 2.69 (s, 1 H), 2.18-1.91 (m, 4 H). RP-HPLC $t_R = 9.40$ min. HRMS (IT-ToF): $\text{C}_{21}\text{H}_{25}\text{N}_9\text{O}_5$ ($[\text{M}+\text{H}]^+$) calculated 484.2051, found 484.2064.

5.4.11 4.6 cytotoxicity assessment

H292 cells were seeded in 96 well plated (100 μL , 1×10^5 cells/ mL) then incubated overnight at 37 $^\circ\text{C}$, 5% CO_2 . **4.6** (14 mM in DMSO) was diluted in a serial dilution then added to wells in triplicate (1 μL). Cells were incubated for 24 hours at 37 $^\circ\text{C}$, 5% CO_2 before MTS (10 μL) was added to each well then the cells incubated for three hours. The absorbance was recorded at 492 nm and corrected for background absorbance by subtracting the absorbance of media treated with MTS. Cell viability was calculated as a percentage of non-treated cells.

5.4.12 Synthesis of polyethylene Glycol-2-aminoethylfolic acid (4.29)

HS-PEG-COOH (15 mg, 4.88 μmol) was dissolved in dry DMF (0.60 mL). NHS (0.84 mg, 7.3 μmol), dicyclohexylcarbodiimide (DCC, 1.50 mg, 7.3 μmol) and triethylamine (0.53 μL , 3.8 μmol) were added to the solution and stirred overnight. The solution was filtered and the solvent removed under vacuum. **4.6** (5 mg, 10.34 μmol , 2 eq) was dissolved in DMSO (0.6 mL), added to the dry PEG-NHS and stirred overnight. The solution was precipitated in diethyl ether and washed with diethyl ether 5 times, decanting off the solvent each time. The solid was dried under vacuum then resuspended in THF and centrifuged. The supernatant was collected, and the solvent removed under vacuum, giving the product. No further purification was undertaken.

5.4.13 Synthesis of 4.6 functionalised C11Pc-PEG-AuNPs (4.30)

C11Pc (2.4 mg, 0.94 μmol) was dissolved in anhydrous THF (1 mL) and left to stir in the dark at room temperature. **4.29** (8.6 mg, 2.41 μmol) was dissolved in anhydrous THF (2 mL), added to the solution and stirred for five minutes. $\text{HAuCl}_4 \cdot 3\text{H}_2\text{O}$ (1.2 mg, 3.05 μmol) was dissolved in anhydrous THF (1.2 mL), added to the solution and stirred for a further five minutes. Sodium borohydride (1.5 mg, 39.65 μmol) was dissolved in dH_2O (1.2 mL) and added rapidly to the solution under vigorous stirring. This solution was left stirring in the dark for *ca.* 17 h at room temperature. THF (5.4 mL) was added to the solution then the solution was centrifuged at 1,400 rpm for 2 mins. The supernatant was collected and evaporated to dryness under reduced pressure. The nanoparticles were resuspended in PBS or RPMI 1640 without phenol red (2 mL) then centrifuged at 8,000 rpm for 20 minutes. The resulting supernatant was filtered and stored at 4 °C in the dark. These **4.6**-C11Pc-PEG-AuNPs were characterised by UV-vis between 200-800 nm. The fluorescence excitation spectrum was recorded between 550-750 nm with an emission wavelength of 780 nm. The emission spectrum was recorded between 653-850 nm with an excitation wavelength of 633 nm.

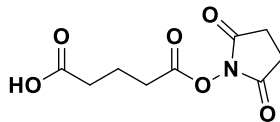
5.4.14 Variation of 4.29 concentration on AuNPs (4.31, 4.32 and 4.33)

4.6-C11Pc-PEG-AuNPs were synthesis as described in **section 5.4.13**, with the ratio of **4.29**:PEG of either 25:75 (**4.31**), 10:90 (**4.32**) or 5:95 (**4.33**) used in the place of 100:0 **4.29**:PEG.

5.4.15 Singlet oxygen production

4.30, **4.31**, **4.32**, **4.33**, C11Pc-PEG-AuNPs and PEG-AuNPs in PBS (1 μM) were tested for singlet oxygen production as described in **section 5.2.15**.

5.4.16 Synthesis of 5-(2,5-dioxopyrrolidin-1-yl)oxy-5-oxopentanoic acid (4.36)

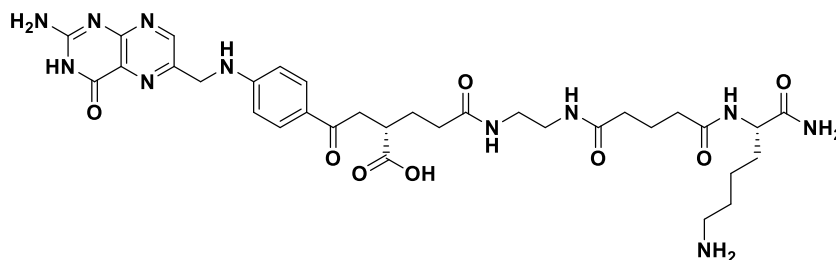


This synthesis followed the procedure of Li *et al.* with modifications.⁸ Glutaric anhydride (500 mg, 4.38 mmol) and NHS (504 mg, 4.38 mmol, 1 eq) were dissolved in THF (20 mL) and heated to reflux for two hours. The solvent was removed under vacuum to yield the crude product as an oil in quantitative yield. ¹H-NMR (400 MHz, CDCl₃): 2.82 (s, 4 H), 2.71 (t, 2 H, *J* = 7.32 Hz), 2.50 (t, 2 H, *J* = 7.24 Hz), 2.04 (m, 2H).

5.4.17 Malachite green test for carboxylic acids on resin

A few beads of resin were washed with methanol, then malachite green oxalate in ethanol (0.25% w/v, *ca.* 1 mL) was added to the beads. Triethylamine (10 μL) was added to the solution and the beads left to stand for three minutes. The beads were washed with methanol until the solution was clear and a positive test for the presence of a carboxylic acid was confirmed by the beads remaining green.

5.4.18 Synthesis of peptide 4.41 (4.6-4.36-Lys)



Rink amide MBHA resin (30 mg, 0.0156 mmol) was loaded with Fmoc-L-Lys(Boc)-OH as described in **section 5.1.3**. After Fmoc deprotection, crude **4.36** (36 mg, 0.17 mmol, 10 eq) was dissolved in DMF and overnight, then the resin washed with DMF (x6). EDC (15.0 mg, 0.078 mmol, 5 eq), NHS (9.0 mg, 0.078 mmol, 5 eq) and DIPEA (27 μL, 0.156 mmol, 10 eq) were dissolved in DMF, added to the resin and shaken for three hours. The resin was washed with DMF (x6) and **4.6** (9 mg, 0.019 mmol, 1.2 eq) in DMSO was shaken with the resin

overnight. The resin was washed with DMSO (x2), DMF (x6) and DCM (x6), then cleavage of the peptide from the resin was completed in 95:2.5:2.5 TFA:TIPS:H₂O. The solvent was removed under vacuum, the peptide isolated with cold ether precipitation, then purified by preparative RP-HPLC, giving the peptide (1.54 mg, 14%). RP-HPLC: $t_R = 9.69$ mins. MALDI-ToF: C₃₂H₄₄N₁₂O₈ [(M+H)⁺] calculated 725.34, found 725.36. HRMS (IT-ToF): [M+H+K]²⁺ calculated 382.1554, found 382.1579.

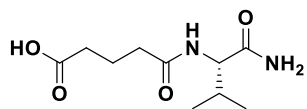
5.4.19 Synthesis of peptide 4.43 (4.6-4.36-V-Cit-PABA-K)

4.43 was synthesised via Fmoc-solid phase peptide synthesis. Briefly, rink amide MBHA was functionalised with V-Cit-PABA-K as described in **section 5.1.3**, before **4.36** and **4.6** were added to the growing peptide sequence as described in **section 5.4.18**. The resulting peptide was cleaved from the resin in 95:2.5:2.5 TFA:TIPS:H₂O for three hours, then the solvent removed under vacuum. The resulting peptide was washed with cold diethyl ether, then purified by preparative RP-HPLC, giving the product as an orange solid (4.63 mg, 4.59 μ mol, 8.8%). RP-HPLC: $t_R = 11.90$ min. MALDI-ToF [(M+H)⁺]: C₅₀H₆₉N₁₇O₁₂ calculated 1100.53, found 1100.39.

5.4.20 4.36 addition screen

Rink amide MBHA (100 mg, 0.052 mmol) was loaded with appropriately protected Fmoc-amino acids (5 eq), as described in **section 5.1.3**. After Fmoc-deprotection, **4.36** (20 eq, 1.04 mmol) in DMF was shaken overnight alongside the resin. The resin was washed with DMF (x6) then methanol (x6). The resulting peptide was cleaved from the resin with 95:2.5:2.5 TFA:TIPS:H₂O, shaking for three hours. The solvent was removed under reduced pressure and the resulting peptide washed with cold diethyl ether.

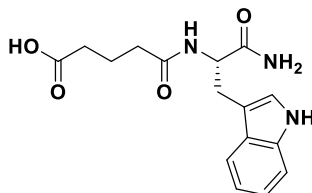
5.4.20.1 4.36-Val (4.44)



Crude **4.44** was prepared as described in **section 5.4.20**. ¹H-NMR (400 MHz, CH₃OD): 4.20 (d, 1 H, $J = 6.9$ Hz), 2.34 (t, 2 H, $J = 7.3$ Hz), 2.34 (t, 2 H, $J = 7.3$ Hz), 2.07 (dq, 1 H, $J =$

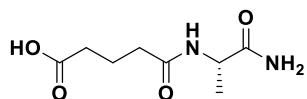
6.9, 7.1 and 7.0 Hz), 1.90 (dt, 2 H, $J = 7.3$ and 7.3 Hz), 0.97 (d, 3 H, $J = 7.1$ Hz), 0.96 (d, 2 H, $J = 7.0$ Hz).

5.4.20.2 **4.36-Trp**



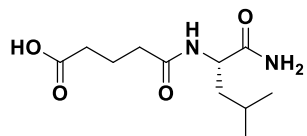
Crude **4.36-Trp** was prepared as described in **section 5.4.20**. $^1\text{H-NMR}$ (400 MHz, CH_3OD): 7.62 (d, 1 H, $J = 7.8$ Hz), 3.31 (d, 1 H, $J = 8.0$ Hz), 7.10-6.99 (m, 3 H), 4.73-4.68 (m, 1H), 2.99 (d, 2 H, $J = 3.6$ Hz), 2.22-2.14 (m, 4 H), 1.81-1.72 (m, 2 H).

5.4.20.3 **4.36-Ala**



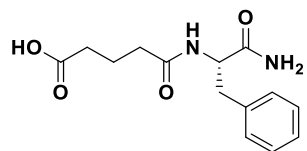
Crude **4.36-Ala** was prepared as described in **section 5.4.20**. $^1\text{H-NMR}$ (400 MHz, CH_3OD): 4.33 (q, 1 H, $J = 7.2$ Hz), 2.34 (t, 2 H, $J = 7.4$ Hz), 2.30 (t, 2 H, $J = 7.7$ Hz), 1.90 (dt, 2 H, $J = 7.4$ and 7.7 Hz), 1.35 (d, 3 H, $J = 7.2$ Hz).

5.4.20.4 **4.36-Leu**



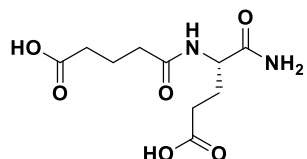
Crude **4.36-Leu** was prepared as described in **section 5.4.20**. $^1\text{H-NMR}$ (400 MHz, CH_3OD): 4.39 (t, 1 H, $J = 7.5$ Hz), 2.33 (t, 2 H, $J = 7.5$ Hz) 2.32 (t, 2 H, $J = 7.9$ Hz), 1.9 (dt, 2 H $J = 7.5$ and 7.9 Hz), 1.73-1.62 (m, 1 H), 1.60-1.56 (m, 2 H), 0.96 (d, 3 H, $J = 6.5$ Hz), 0.93 (d, 3 H, $J = 6.5$ Hz).

5.4.20.5 **4.36-Phe**



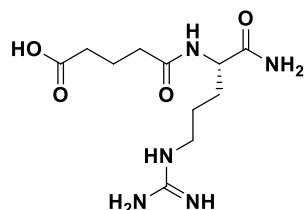
Crude **4.36-Phe** was prepared as described in **section 5.4.20**. $^1\text{H-NMR}$ (400 MHz, CH_3OD): 7.29-7.17 (m, 5 H), 4.66 (dd, 1 H, $J = 5.4$ and 4.2 Hz), 3.19-1.16 (m, 1 H), 2.88-2.82 (m, 1 H), 2.21 (t, 2 H, $J = 7.5$ Hz), 2.16 (t, 2 H, $J = 7.4$ Hz), 1.76 (dt, 2 H, $J = 7.5$ and 7.4 Hz).

5.4.20.6 **4.36-Glu**



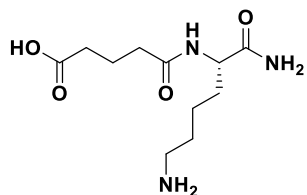
Crude **4.36-Glu** was prepared as described in **section 5.4.20**. $^1\text{H-NMR}$ (400 MHz, CH_3OD): 4.38 (dd, 1 H, $J = 5.0$ and 4.0 Hz), 2.44-2.29 (m, 6 H), 2.15-2.07 (m, 1 H), 1.95-1.86 (m, 3 H).

5.4.20.7 **4.36-Arg**



Crude **4.36-Arg** was prepared as described in **section 5.4.20**. $^1\text{H-NMR}$ (400 MHz, CH_3OD): 4.23 (dd, 1 H, $J = 4.9$ and 2.9 Hz), 3.10-3.06 (m, 2 H), 2.22 (t, 2 H, $J = 2.8$ Hz), 2.19 (t, 2 H, $J = 3.0$ Hz), 1.77 (dt, 2 H, $J = 2.8$ and 3.0 Hz), 1.72-1.71 (m, 1 H), 1.60-1.44 (m, 3 H).

5.4.20.8 **4.36-Lys**



Crude **4.36-Lys** was prepared as described in **section 5.4.20**. $^1\text{H-NMR}$ (400 MHz, CH_3OD): 4.37 (dd, 1 H, $J = 5.1$ and 3.9 Hz), 2.97-2.94 (m, 2 H), 2.37 (t, 2 H, $J = 7.4$ Hz), 2.36 (t, 2 H, $J = 7.5$ Hz), 1.93 (dt, 2 H, $J = 7.5$ and 7.4 Hz), 1.88-1.84 (m, 1 H), 1.77-1.67 (m, 3 H), 1.58-1.40 (m, 2 H).

5.5 References

- (1) García Calavia, P.; Marín, M. J.; Chambrier, I.; Cook, M. J.; Russell, D. A. Towards Optimisation of Surface Enhanced Photodynamic Therapy of Breast Cancer Cells Using Gold Nanoparticle–photosensitiser Conjugates. *Photochem. Photobiol. Sci.* **2018**, *17*, 281–289.
- (2) Trévisiol, E. T.; Defrancq, E. D.; Lhomme, J. L.; Laayoun, A. L.; Cros, P. C. Synthesis of Methylketone Containing Nucleoside Triphosphates for RNA Labelling. *Tetrahedron* **2000**, *56* (35), 6501–6510.
- (3) van der Heide, S.; Russell, D. A. Optimisation of Immuno-Gold Nanoparticle Complexes for Antigen Detection. *J. Colloid Interface Sci.* **2016**, *471*, 127–135.
- (4) Vance, N.; Zacharias, N.; Ultsch, M.; Li, G.; Fourie, A.; Liu, P.; LaFrance-Vanasse, J.; Ernst, J. A.; Sandoval, W.; Kozak, K. R.; et al. Development, Optimization, and Structural Characterization of an Efficient Peptide-Based Photoaffinity Cross-Linking Reaction for Generation of Homogeneous Conjugates from Wild-Type Antibodies. *Bioconjug. Chem.* **2019**, *30*, 148–160.
- (5) Guaragna, A.; Roviello, G. N.; D’Errico, S.; Paoella, C.; Palumbo, G.; D’Alonzo, D. Solid Phase Synthesis of a Novel Folate-Conjugated 5-Aminolevulinic Acid Methyl Ester Based Photosensitizer for Selective Photodynamic Therapy. *Tetrahedron Lett.* **2015**, *56* (6), 775–778.
- (6) Santos, M. A.; Enyedy, E. A.; Nuti, E.; Rossello, A.; Krupenko, N. I.; Krupenko, S. A. Methotrexate γ -Hydroxamate Derivatives as Potential Dual Target Antitumor Drugs. *Bioorg. Med. Chem.* **2007**, *15* (3), 1266–1274.
- (7) Luo, J.; Smith, M. D.; Lantrip, D. A.; Wang, S.; Fuchs, P. L. Efficient Syntheses of Pyrofollic Acid and Pteroyl Azide, Reagents for the Production of Carboxyl-Differentiated Derivatives of Folic Acid. *J. Am. Chem. Soc.* **1997**, *119*, 10004–10013.
- (8) Li, M.; Wu, R. S.; Tsai, J. S. C. Water Soluble Derivatives of Lipophilic Drugs. WO 03/062819 A2, 2003.